TUM

Technische Universität München
TUM School of Natural Sciences

Investigation of innovative cofactor-based antimicrobial strategies against bacteria and parasites by chemical proteomics

Dissertation zur Erlangung des akademischen Grades eines Doktors der Naturwissenschaften von

Jan-Niklas Dienemann

München 2023

Technische Universität München
TUM School of Natural Sciences

Investigation of innovative cofactor-based antimicrobial strategies against bacteria and parasites by chemical proteomics

Jan-Niklas Dienemann

Vollständiger Abdruck der von der TUM School of Natural Sciences
der Technischen Universität München zur Erlangung des akademischen Grades
eines

Doktors der Naturwissenschaften (Dr. rer. nat.)

genehmigten Dissertation.

Vorsitz: Prof. Dr. Cathleen Zeymer
Prüfer*innen der Dissertation: 1. Prof. Dr. Stephan A. Sieber
2. Prof. Dr. Michael Groll

Die Dissertation wurde am 13.06.2023 bei der Technischen Universität München
eingereicht und durch die TUM School of Natural Sciences
am 03.07.2023 angenommen.

"Covid was like a tsunami. It hit massively. It hit violently, and it washed over the world, but it will pass. AMR [antimicrobial resistance] is like rising sea levels. It will keep rising. It will not stop, and suddenly we'll be standing there with water around our knees."

– Robert Bowers (Leader antibiotic commercialization, GSK)

FOR MY FAMILY

FOR MY FRIENDS

Abstract

Antimicrobial resistance (AMR) poses a significant global health threat, demanding for the development of new strategies to combat this impending crisis. Failure of not taking immediate action against AMR could lead to estimated 10 Mio deaths annually by 2050, surpassing the cancer-related death toll.

The focus of this thesis is on investigating novel antimicrobial concepts by manipulating the cofactor-dependent metabolism of pathogens. Pathogens of critical concern, such as *Plasmodium falciparum*, *Mycobacterium tuberculosis*, and *Enterococci* spp., are analyzed with priority to discuss potential targets suitable for drug development.

In particular, the study introduces activity-based protein profiling (ABPP) probe molecules for lipoic acid-dependent metabolism and explores the development of lipoate protein ligase (LPL) inhibitors. LPL is essential for global energy metabolism and metabolic flux of lipoate-auxotroph strains, including *P. falciparum* and *Listeria monocytogenes*. A herein developed probe molecule successfully monitors LPL activity by fluorescent SDS-PAGE and mass spectrometry, enabling the screening of a library of potential LPL inhibitors. Two rational designed hits as intermediate mimics (**LAMe** and **C3**) were characterized as LPL inhibitors by competitive profiling, exhibiting significant antimalarial activity against *P. falciparum* while displaying low to moderate toxicity in human cells, respectively. Further lead structure optimization is required for pre-clinical development.

Furthermore, this thesis also investigates homologous PLK and ThiD proteins involved in vitamin B6 (**PLP**) salvage and vitamin B1 (**TPP**) biosynthesis within bacterial pathogens, respectively. Both cofactors catalyze decarboxylation reactions in lipoic acid-dependent enzyme complexes, and thus, are also important for central metabolism. Therefore, depletion of **PLP** or **TPP** supply might result in antibiotic effects against *Enterococci* spp. or mycobacteria due to their unique pathways. Interestingly, certain subclasses of PLK and ThiD enzymes contain a conserved lid-cysteine in the active pockets. Tailored B-vitamin cofactor probes containing cysteine-reactive warheads were synthesized to engage with these signature residues covalently, which would ultimately result in blocking of substrate binding in the active pocket. Indeed, fluorescent SDS-PAGE binding studies with recombinant wild type PLK and ThiD proteins as well as their respective alanine mutants validated probe binding to the desired lid-cysteine, which enabled us to study their relevance for catalysis. While no probe exhibited antibiotic activity, the compounds could serve as reporter molecules that allow for competitive screenings of PLK or ThiD inhibitors in the active pockets in future studies.

Overall, the development of cofactor-based probes contributes to the urgent quest for innovative antimicrobial strategies to combat the approaching global AMR crisis.

Kurzfassung

Die antimikrobielle Resistenz (AMR) stellt eine erhebliche globale Gesundheitsbedrohung dar und erfordert die Entwicklung neuer Strategien, um dieser bevorstehenden Krise entgegenzuwirken. Das Unterlassen sofortiger Maßnahmen gegen AMR könnte bis zum Jahr 2050 zu geschätzten 10 Millionen Todesfällen jährlich führen und die Anzahl der krebsbedingten Todesfälle übertreffen.

Der Schwerpunkt dieser Arbeit liegt auf der Untersuchung neuartiger antimikrobieller Konzepte durch Manipulation des kofaktorabhängigen Stoffwechsels von Krankheitserregern. Besonderes Augenmerk gilt Krankheitserregern von kritischer Bedeutung wie *Plasmodium falciparum*, *Mycobacterium tuberculosis* und *Enterococci* spp., um potenzielle Ziele für die Arzneimittelentwicklung zu diskutieren.

Insbesondere führt die Studie Sondenmoleküle ein, um liponsäureabhängigen Stoffwechsel mittels aktivitätsbasiertem Protein Profiling (ABPP) zu visualisieren, was die Entwicklung von Lipoat Protein Ligase (LPL)-Inhibitoren ermöglicht. LPL ist essentiell für den globalen Energiestoffwechsel und den metabolischen Fluss in Lipoat auxotrophen Stämmen wie *P. falciparum* und *Listeria monocytogenes*. Ein hier entwickeltes Sondenmolekül überwacht erfolgreich die LPL-Aktivität mittels fluoreszierender SDS-PAGE und Massenspektrometrie und ermöglicht so das Screening einer Substanzbibliothek potenzieller LPL-Inhibitoren. Zwei rational entworfene Moleküle als Übergangszustandsmimetika (**LAMe** und **C3**) wurden durch kompetitive Selektion als LPL-Inhibitoren charakterisiert und zeigten signifikante Aktivität gegen den Malariaerreger *P. falciparum*, während sie in menschlichen Zellen eine geringe bis moderate Toxizität aufwiesen. Eine weitere Optimierung der Leitstrukturen ist für die präklinische Entwicklung erforderlich.

Darüber hinaus untersucht diese Arbeit auch homologe PLK und ThiD Proteine, die an der Vitamin B6 (**PLP**) Wiederverwertung bzw. der Vitamin B1 (**TPP**) Biosynthese bei bakteriellen Krankheitserregern beteiligt sind. Beide Kofaktoren katalysieren Decarboxylierungsreaktionen in liponsäureabhängigen Enzymkomplexen und sind somit auch für den zentralen Stoffwechsel wichtig. Daher könnte eine **PLP**- oder **TPP**-Unterversorgung zu antibiotischen Wirkungen gegen *Enterococci* spp. oder Mykobakterien aufgrund ihrer einzigartigen Stoffwechselwege führen. Interessanterweise enthalten bestimmte Unterklassen von PLK und ThiD Enzymen ein konserviertes Deckel-Cystein in den aktiven Taschen. Maßgeschneiderte B-Vitamin-Kofaktor-Sondenmoleküle mit cysteinreaktiven Kopfgruppen wurden synthetisiert, um mit diesen charakteristischen Aminosäuren kovalent zu reagieren, was letztendlich zur Blockierung der Substratbindung in der aktiven Tasche führt. Tatsächlich bestätigten fluoreszierende SDS-PAGE-Bindungsstudien mit rekombinanten Wildtyp PLK und ThiD Proteinen sowie ihren jeweiligen Alanin-Mutanten die Sondenbindung an das gewünschte Deckel-Cystein und ermöglichten so die Untersuchung ihrer Bedeutung für die Katalyse. Während keine der Sonden antibiotische Aktivitäten zeigten, könnten die Verbindungen in zukünftigen Studien als Reporter-Moleküle dienen, welche die Identifizierung von PLK oder ThiD Inhibitoren in den aktiven Taschen durch kompetetive Selektion ermöglichen.

Insgesamt trägt die Entwicklung kofaktorbasierter Sonden zur dringenden Suche nach innovativen antimikrobiellen Strategien bei, um der herannahenden globalen AMR-Krise entgegenzuwirken.

Parts of this thesis have been published in peer-reviewed journals as listed below:

A chemical proteomic strategy reveals inhibitors of lipoate salvage in bacteria and parasites

Jan-Niklas Dienemann, Shu-Yu Chen, Manuel Hitzenberger, Montana L. Sievert, Stephan M. Hacker, Sean T. Prigge, Martin Zacharias, Michael Groll, Stephan A. Sieber

Tailored cofactor traps for the in situ detection of hemithioacetal-forming pyridoxal kinases

Ines Hübner*, **Jan-Niklas Dienemann***, Julia Friederich, Sabine Schneider, Stephan A. Sieber

* These authors contributed equally to this work.

Parts of this thesis have been presented at conferences and workshops:

Interact 2023 - Science & Translation

30th – 31st March 2023, Munich, Germany

oral and poster presentation

264th American Chemical Society (ACS) National Fall Meeting and Exposition

21st – 25th August 2022, Chicago, IL, US

poster presentation

138th BASF International Summer Course

22nd – 28th August 2021, Ludwigshafen, Germany

digital poster presentation

Contents

Part I - Scientific Background

Part II - Research

Contents

Contents

PART I

SCIENTIFIC BACKGROUND

1|
Introduction

## 1.1 Drug resistance against current antimicrobial strategies as major health threat

Evolution is the process through which living organisms adapt to their environment, ensuring their fitness by natural selection.[1] As an example, fungi[2] and plants[3] have developed a repertoire of natural compounds that exhibit activity against pathogens. Humans have recognized the immense potential of these compounds as a valuable resource for drugs, including those with efficacy against bacteria and parasites.[4] However, the widespread and partially irresponsible use of antimicrobial compounds has extensively threatened pathogen survival over the last century, leading to accelerated evolution by selective pressure,[5] and the emergence of diverse biochemical adaptations that confer drug resistance.[5-6] In recent decades, this inevitable however controllable drug resistance development process has outpaced the invention of new drugs to combat bacteria[7] and malaria parasites,[8] posing a global risk to human health. In 2019, a predicitive statistical model attributed already 1.3 Mio deaths to antimicrobial resistance.[9] Future projections indicate that without immediate preventive action, annual deaths from drug-resistant infections could increase to 10 Mio cases by 2050.[10] This prediction even surpasses the current annual death toll from cancer (8.2 Mio),[10] highlighting the alarming possibility of a post-antibiotic era for the 21th century.[11] This resembles ancient times when millions of deaths occurred due to diseases like the plague caused by *Yersinia pestis* in the 14th century (estimated 25 Mio deaths)[12] at a time when antibiotics were not yet available.

In recent decades, scientists have raised public awareness to prevent such a disaster.[13] The COVID-19 pandemic, caused by the SARS-CoV-2 coronavirus (approximately 6 Mio deaths from January 2020 to December 2021),[14] has demonstrated that global collaboration can lead to significant success in rapidly developing new pharmaceuticals.[15] This serves as a powerful reminder to take immediate action in finding innovative solutions to address the 'silent pandemic' of antimicrobial resistance and prevent catastrophic outcomes.[16]

The following sections of this thesis will present current anti-infective compounds targeting bacteria and malaria-causing parasites, as well as discuss economical, regulatory, and societal challenges that hinder research and development of innovative antimicrobials. Encouraging solutions involving global key stakeholders will be summarized. This thesis will also introduce and discuss three novel anti-infective strategies based on cofactor-dependent metabolism and explore their applicability by theoretical and experimental assessment, aiming to contribute to the fight against this dire prospect.

1.2 Antibiotics for treating bacterial infections

In 1928, FLEMING made a groundbreaking discovery when he found that a mold contamination on a petri dish inhibited the growth of bacteria in the surrounding area. This discovery led to the identification of the antibiotic compound known as penicillin (Fig. 1.1).[2b] Over the course of the next decade, this β-lactam derivative underwent successful development and was subsequently used as a broad-spectrum antibiotic drug during the Second World War, resulting in the saving of millions of lives.[17]
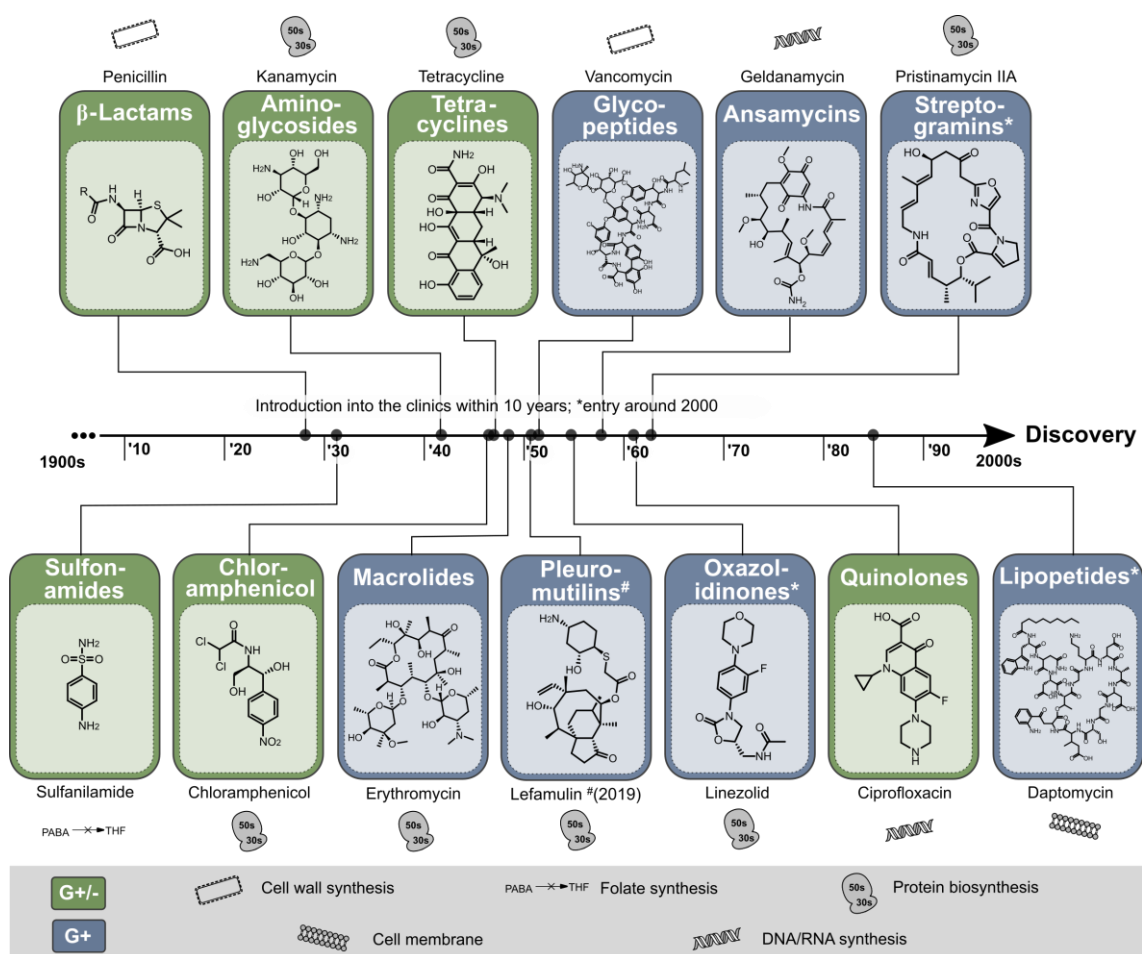
Fig. 1.1. Discovery timeline of antibiotic classes with approval for clinical use. The data have been compiled and adapted from LEWIS.[18] Thirteen different classes of antibiotics are currently available (by 2020) for clinical use, and one derivative of each class is depicted exemplarily. The majority of these compounds were discovered in the 1940s to 1960s and successfully went through the development and approval process within a span of 10 years with a few exceptions marked by * and #. Overall, five different modes of actions are covered by the thirteen compound classes,[19] whereas increasing antimicrobial resistance challenges their effectiveness.[6, 19] In particular, Gram-negative bacteria are becoming more difficult to treat due to increasing antimicrobial resistance[20] as recently introduced antibiotics (*, #) only showed activity against Gram-positive bacteria (blue).

The discovery of penicillin marked the beginning of a remarkable era known as 'the golden age of antibiotic discovery'.[21] This success story, along with the urgent medical need for effective treatment of bacterial infections, fueled extensive research and development efforts focused on natural products (NP) during the mid-20th century (Fig. 1.1). Currently, there are thirteen

antibiotic classes approved for clinical use[18] that exhibit modes of actions based on interference with cell wall synthesis, folate synthesis, protein biosynthesis, DNA/RNA synthesis and cell membrane integrity.[19] However, the efficacy of these antibiotics is constantly challenged by the emergence of resistance mechanisms, including compound inactivation (*e.g.* by β-lactamases), enhanced efflux, target modification or overexpression, and activation of bypass-pathway.[6, 19]

In the 1940s, FLEMING already drew attention to the possibility of resistance formation and stressed the importance of investigating new structures.[22] The depletion of NP-derived compounds and the limited success of screening synthetic chemical libraries have made the discovery of new scaffolds exceedingly difficult.[23] Recent strategies have focused on modifying existing antibiotics to extend their lifespan, or directly targeting the resistance mechanisms itself (*e.g.* through β-lactamase inhibitors).[24] However, bacterial resistance has quickly emerged against these modified derivatives, having lead to the development of several generations of popular β-lactams, such as cephalosporins and carbapenems,[24] but also of macrolides[25] or quinolones.[26] Within the last two decades, previously discovered antibacterial classes (pleuromutilins, oxazolidinones, streptogramins and lipopeptides) against Gram-positive bacteria were successfully launched for clinical use after their discovery about 40 to 70 years ago. However, quinolones remain the most recent antibiotic class with activity against Gram-negative bacteria, which were already introduced into the clinics about 60 years ago.[18]

Considering that the current antibacterial therapeutics only address the five aforementioned cellular targets, there is a pressing need to explore a wide range of novel strategies for their antimicrobial potential, such as phage therapy or vaccine development.[27] Antimetabolites of cofactors,[28] exemplified by clinically approved sulfonamides as antifolates,[29] are particularly intriguing. Many of their biosynthesis pathways are unique to bacteria, while mammals most often rely on uptake, making cofactors promising candidates for selective pathogen targeting with a potentially favorable safety profile.[30] In this thesis, the investigation and discussion revolve around lipoic acid (**LA**), vitamin B6 (**PLP**) and vitamin B1 (**TPP**) as potential cofactor-based strategies against microbes.

The World Health Organization (WHO) has identified a subset of bacterial species that require immediate attention and should be addressed with priority over other bacterial pathogens. These species, which are the focus of investigation in this thesis, include *M. tuberculosis*, *P. aeruginosa* and *E. coli* (Gram-negative) as well as *Enterococci* spp. and *S. aureus* (Gram-positive).[31]

1.3 Antimalarials for treatment of malaria caused by parasites

Malaria is a disease caused by *Plasmodium* spp. parasites that are transmitted to humans through the bites of infected female *Anopheles* mosquitoes as vector. After transmission, a dozen sporozoites migrate to liver cells, where they multiply before releasing thousands of merozoites from the matured schizont into the bloodstream. The parasites then invade erythrocytes for maturation into ring stage trophozoites prior to release of merozoites upon rapture of the schizont. The destruction of red blood cells, accompanied with fever flares, is responsible for the clinical manifestations of malaria, which occur periodically depending on the developmental stage of the parasites.[32]

Several classes of substances (Fig. 1.2) have been discovered and clinically approved for the treatment of malaria.
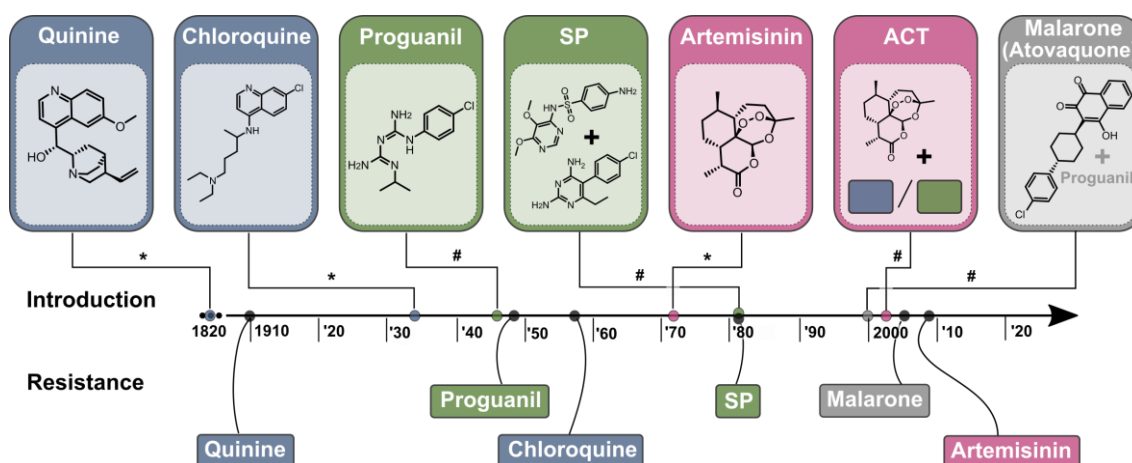
Fig. 1.2. Timeline representing the introduction (*discovery or #application) and development of resistance to antimalaial compounds in clinical use. The blue boxes exemplify quinoline derivatives that interfere with hemoglobin degradation.[33] The green boxes depict pyrimidine derivatives as antifolates, which inhibit folate synthesis similar to sulfonamides, which is why SP (sulfadoxin/pyrimethamine) was administered as combination therapy.[34] The pink boxes depict the NP artemisinin, which contains an essential endoperoxide moiety for its antimalarial activity. It is believed that this peroxide bridge is cleaved by intraparasitic heme-iron, leading to subsequent alkylation and poisoning of parasite proteins.[35] Artemisinin-based combination therapy (ACT) was employed to reduce resistance development and enhance its lifespan, combining multiple target approaches synergistically with previously reported antimalarial drugs.[36] Lastly, atovaquone was identified as an antimetabolite of ubiquinone (coenzyme Q10) and leads to disruption of parasitic mitochondrial membrane potential that is crucial for ATP production.[37] It is commonly used in combination with the prodrug proguanil as Malarone® (grey box) to prevent resistance formation.[38] Overall, successful malaria treatments in the past have employed two natural compounds (quinine and artemisinin) and two cofactor-dependent strategies (folate and ubiquinone). In the meantime, resistance has been observed for all classes of compounds.

Quinine, an alkaloid compound (blue box), was isolated in 1820 by PELLETIER and CAVENTOU from the bark of *Cinchona calisaya* as NP and became the first chemically purified drug for effective malaria treatment.[39] The first case of resistance to quinine was reported in 1910.[40] In 1934, synthetic analogues of quinine, including Resochin (chloroquine, blue box), were synthesized by ANDERSAG and coworkers in 1934 and introduced to the market in 1947 after the Second World War.[41] A decade later, resistance to chloroquine emerged in South East Asia in 1957.[42]

In parallel, antifolates, a second class of antimalarial compounds (pyrimidine derivatives, green), were developed as inhibitors of dihydrofolate reductase, a crucial enzyme in the biosynthesis of the cofactor folic acid.[34] Monotherapy with the prodrug proguanil in 1946 quickly led to resistance within two years.[43] To prevent rapid resistance development, pyrimethamine was introduced as combination therapy (sulfadoxin/pyrimethamine, SP) in 1981, along with a sulfonamide (sulfadoxin) as a second inhibitor of folate synthesis.[44] Resistance to this combination therapy emerged in the same year of introduction[45] and spread rapidly throughout South-East Asia, although it remained broadly effective in Africa until the end of the 20th century.[46]

In response to increasing resistance to chloroquine in the late 1950s,[42] the Chinese government initiated efforts to screen ancient traditional Chinese medicine books to identify new antimalarial agents. Indeed, the NP artemisinin was successfully isolated from *Artemisia annua* in 1972 and demonstrated strong efficacy against *Plasmodium* spp. parasites.[47] Its discovery by YOUYOU was recognized with the Nobel Prize in 2015 for its breakthrough to combat malaria.[48] Artemisinin and its derivatives have been applied as frontline therapeutics, particularly as artemisinin-based combination therapies (ACT) since the early 2000s. These combinations involve previously developed drugs to synergistically kill malaria parasites more efficiently.[49] However, resistance to artemisinin, characterized by mutations in the Kelch13 protein, has re-emerged in South-East Asia in 2009,[50] posing a risk to malaria eradication efforts.[51]

Atovaquone is primarily used as a prophylaxis drug for malaria by travelers visiting endemic regions. It is used in a fixed combination with proguanil, known as Malarone® (FDA approved in 2000), and resistance has been reported since 2005.[52] Malarone® is also considered for use in combination with artemisinin as triple ACT in cases of uncomplicated malaria caused by *P. falciparum* when first-line ACT are ineffective.[53]

Overall, only four different classes of compounds have been developed for the treatment of malaria, mostly used in combination therapies. Therefore, there is an urgent need to invent a more diverse chemoprotective strategy to effectively combat malaria, especially when considering the threat of artemisinin resistance to recent successes in malaria eradication.[51] Thus, the interference of lipoic acid metabolism in the most deadly species *P. falciparum* will be presented as an innovative cofactor-based approach and experimentally assessed within this thesis.

1.4 Societal, regulatory, and economic aspects in the context of antimicrobial resistance

Despite the development of a diverse set of antibiotics and antimalarials during the past century, new anti-infective strategies are urgently needed in the near future due to rising antimicrobial resistance to current therapies, posing a global health threat.[54] Societal, regulatory, and economic aspects influence the research and development of new entities and are discussed in more detail.[10, 55]

With the initial discovery of antibacterial compounds, concerns regarding the evolution of antimicrobial resistances mechanisms were raised.[22] Despite their early detection, the number of critical medical cases remained low, and a wide range of treatment options were available.[56] However, misuse and overuse in humans, as well as agricultural applications, along with poor infection control, have facilitated the spread of resistance.[57] Hence, scientists have significantly raised awareness in policy and society about the escalating challenge of resistance mechansims against current therapies for bacteria and parasites.[58]

Enforcing global public awareness campaigns on emerging antimicrobial resistance is of utmost importance to reduce unnecessary use of anti-infectives in mammals.[59] At an early stage, improvement of sanitation and prevention of spread could render the use of antimicrobials obsolete, extending the effectiveness of current therapies.[60] Further, global surveillance of resistance development, antimicrobial consumption, and the use of rapid diagnostic tools could help to restrict and specify the appropriate use of drugs.[61] Additionally, the promotion of alternative antimicrobial approaches, such as phage therapy against bacteria[62] or vaccine development,[63] offers novel strategies even against drug-resistant microbes.[10]

Throughout the historical development of new pharmaceuticals, scandals have led to stricter safety profiles for drug use in humans, as regulated in Good Manufacturing Practice (GMP) guidelines.[64] While these changes ensure patient safety, they have also increased the costs of development and market applications over the past decades,[65] posing economic burdens for small enterprises that struggle to attract investors.[66] This is particularly true in the field of antimicrobial development, as markets for novel antibiotics are currently unattractive.[67]

The success rate of a new pharmaceutical compound is below five percent with expenses reaching several 100 Mio US Dollars,[55a] which classifies the biopharmaceutical industry as a high-risk sector for investors. However, the expectation of a large sales margin still makes investments in this sector attractive and profitable.[68]

In case of malaria, artemisinin-based combination therapies (ACT) are currently the most effective choice of treatment against *P. falciparum.* However, resistance has emerged in South-East Asia,[69] and its global spread is reminiscent of the previous scenario with chloroquine, which rendered the compound ineffective in monotherapies. Consequently, WHO closely monitors the spread of resistance and highlights the importance of novel antimalarial strategies.[70] As the application of the stand-alone-therapy is threatened and will be ineffective due to increasing cases of resistance in the future, the development of a novel drug for artemisinin-resistant parasite eradication is urgent.[51] Several compounds with new modes of actions are currently in clinical trials, *e.g.*, phosphoinositide lipid kinase inhibitors.[32b, 71]

While the clinical development of innovative antimalarial therapies looks promising, current antibiotics in clinical trials seem less innovative and are mainly based on previous antibiotic classes.[72] Furthermore, their market profitability is a major concern, which is why pharmaceutical companies currently show only little interest in this research field.[73] New antibiotic compounds are planned to be used very conservatively as last resort options when other therapies fail, as defined by the WHO AWaRe (access, watch, reserve) classification as a stewardship tool.[74] Hence, sales revenues for new antibiotics will be minimal at the time of invention compared to the high developmental costs, such as post-approval requirements for pediatric use, global registration and commercialization infrastructure. Small enterprises attempting to tackle the challenge of antimicrobial resistance face financial pressure without the support of established pharmaceutical companies.[67] For instance, Achaogen, a small enterprise that successfully launched the aminoglycoside plazomicin, went bankrupt in 2019 due to lack of financial support. This unfortunate event has further deterred investors and highlighted the current lack of economic attractiveness in the field of innovative antibacterial research.[67, 75]

Therefore, there has been a rethinking of the antibiotic business in recent years, with a priority on global health over commercial interest. Policymakers have presented strategies to address this issue in autumn 2009, categorized into "push" and "pull" incentives.[55a]

Push incentives aim to raise public investments. Global collaborative organizations, such as the "Combating Antibiotic Resistant Bacteria Biopharmaceutical Accelerator" (CARB-X) and the "Joint Programming Initiative on Antimicrobial Resistance" (JPIAMR), have joint forces to collaborate with small enterprises developing innovative approaches against antimicrobial resistance. Furthermore, financial support is provided by publicly funded organizations like the European Research Council (ERC) and private funds, such as the the Bill & Melinda Gates foundation.

Pull incentives aim to increase attractiveness of innovative antibiotics. The most important criterion is delinking the revenue of antibiotics from their sales, which could be achieved through a pilot incentive known as the "Netflix" model, proposed by Sweden and the UK. This strategy is based on an annual fixed fee paied by governments for access to new antibiotics. However, there are current uncertainties regarding the subscription rate, qualifying criteria, and scalability of this model. Its implementation is expected to enhance political and economic attractiveness, stabilize the market, and attract investors.

Overall, these initial politically driven incentives are intened to inspire a transformation in the antimicrobial business, deploying a new business model in the real world while ensuring the appropriate and responsible use of newly discovered antimicrobial entities.

1.5 References

[1]   R. E. Lenski, *PLOS Genetics* **2017**, *13*, e1006668.
[2]   a) J. M. Boysen, N. Saeed, F. Hillmann, *Beilstein Journal of Organic Chemistry* **2021**, *17*, 1814-1827; b) A. Fleming, *British Medical Bulletin* **1944**, *2*, 4-5.
[3]   K. D. Gwinn, in *Studies in Natural Products Chemistry, Vol. 56*, Elsevier, **2018**, pp. 229-246.
[4]   L. Luo, J. Yang, C. Wang, J. Wu, Y. Li, X. Zhang, H. Li, H. Zhang, Y. Zhou, A. Lu, S. Chen, *Science China Life Sciences* **2022**, *65*, 1123-1145.
[5]   a) L. Serwecińska, *Water* **2020**, *12*, 3313; b) A. Tello, B. Austin, C. Telfer Trevor, *Environmental Health Perspectives* **2012**, *120*, 1100-1106.
[6]   M. Munita Jose, A. Arias Cesar, *Microbiology Spectrum* **2016**, *4*, 4.2.15.
[7]   N. Sabtu, D. A. Enoch, N. M. Brown, *British Medical Bulletin* **2015**, *116*, 105-113.
[8]   L. Cui, S. Mharakurwa, D. Ndiaye, P. K. Rathod, P. J. Rosenthal, *American Journal of Tropical Medicine and Hygiene* **2015**, *93*, 57-68.
[9]   C. J. L. Murray, K. S. Ikuta, F. Sharara, L. Swetschinski, G. Robles Aguilar, A. Gray, C. Han, C. Bisignano, P. Rao, E. Wool, S. C. Johnson, A. J. Browne, M. G. Chipeta, F. Fell, S. Hackett, G. Haines-Woodhouse, B. H. Kashef Hamadani, E. A. P. Kumaran, B. McManigal, S. Achalapong, R. Agarwal, S. Akech, S. Albertson, J. Amuasi, J. Andrews, A. Aravkin, E. Ashley, F.-X. Babin, F. Bailey, S. Baker, B. Basnyat, A. Bekker, R. Bender, J. A. Berkley, A. Bethou, J. Bielicki, S. Boonkasidecha, J. Bukosia, C. Carvalheiro, C. Castañeda-Orjuela, V. Chansamouth, S. Chaurasia, S. Chiurchiù, F. Chowdhury, R. Clotaire Donatien, A. J. Cook, B. Cooper, T. R. Cressey, E. Criollo-Mora, M. Cunningham, S. Darboe, N. P. J. Day, M. De Luca, K. Dokova, A. Dramowski, S. J. Dunachie, T. Duong Bich, T. Eckmanns, D. Eibach, A. Emami, N. Feasey, N. Fisher-Pearson, K. Forrest, C. Garcia, D. Garrett, P. Gastmeier, A. Z. Giref, R. C. Greer, V. Gupta, S. Haller, A. Haselbeck, S. I. Hay, M. Holm, S. Hopkins, Y. Hsia, K. C. Iregbu, J. Jacobs, D. Jarovsky, F. Javanmardi, A. W. J. Jenney, M. Khorana, S. Khusuwan, N. Kissoon, E. Kobeissi, T. Kostyanev, F. Krapp, R. Krumkamp, A. Kumar, H. H. Kyu, C. Lim, K. Lim, D. Limmathurotsakul, M. J. Loftus, M. Lunn, J. Ma, A. Manoharan, F. Marks, J. May, M. Mayxay, N. Mturi, et al., *The Lancet* **2022**, *399*, 629-655.
[10]   J. O'Neill, **2016**, The Review on Antimicrobial Resistance, Tackling drug-resistant infections globally: final report and recommendations.
[11]   WHO, **2014**, Antimicrobial resistance – global report on surveillance.
[12]   K. A. Glatter, P. Finkelman, *The American Journal of Medicine* **2021**, *134*, 176-181.
[13]   M. Davis, *Journal of Pharmacy Practice and Research* **2020**, *50*, 463-464.
[14]   H. Wang, K. R. Paulson, S. A. Pease, S. Watson, H. Comfort, P. Zheng, A. Y. Aravkin, C. Bisignano, R. M. Barber, T. Alam, J. E. Fuller, E. A. May, D. P. Jones, M. E. Frisch, C. Abbafati, C. Adolph, A. Allorant, J. O. Amlag, B. Bang-Jensen, G. J. Bertolacci, S. S. Bloom, A. Carter, E. Castro, S. Chakrabarti, J. Chattopadhyay, R. M. Cogen, J. K. Collins, K. Cooperrider, X. Dai, W. J. Dangel, F. Daoud, C. Dapper, A. Deen, B. B. Duncan, M. Erickson, S. B. Ewald, T. Fedosseeva, A. J. Ferrari, J. J. Frostad, N. Fullman, J. Gallagher, A. Gamkrelidze, G. Guo, J. He, M. Helak, N. J. Henry, E. N. Hulland, B. M. Huntley, M. Kereselidze, A. Lazzar-Atwood, K. E. LeGrand, A. Lindstrom, E. Linebarger, P. A. Lotufo, R. Lozano, B. Magistro, D. C. Malta, J. Månsson, A. M. Mantilla Herrera, F. Marinho, A. H. Mirkuzie, A. T. Misganaw, L. Monasta, P. Naik, S. Nomura, E. G. O'Brien, J. K. O'Halloran, L. T. Olana, S. M. Ostroff, L. Penberthy, R. C. Reiner Jr, G. Reinke, A. L. P. Ribeiro, D. F. Santomauro, M. I. Schmidt, D. H. Shaw, B. S. Sheena, A. Sholokhov, N. Skhvitaridze, R. J. D. Sorensen, E. E. Spurlock, R. Syailendrawati, R. Topor-Madry, C. E. Troeger, R. Walcott, A. Walker, C. S. Wiysonge, N. A. Worku, B. Zigler, D. M. Pigott, M. Naghavi, A. H. Mokdad, S. S. Lim, S. I. Hay, E. Gakidou, C. J. L. Murray, *The Lancet* **2022**, *399*, 1513-1536.

[15] O. Sharma, A. A. Sultan, H. Ding, C. R. Triggle, *Frontiers in Immunology* **2020**, *11*, 585354.

[16] R. A. Rayan, *World Journal of Clinical Cases* **2023**, *11*, 1267-1274.

[17] R. Gaynes, *Emerging Infectious Diseases* **2017**, *23*, 849-853.

[18] K. Lewis, *Biochemistry (Moscow)* **2020**, *85*, 1469-1483.

[19] G. Kapoor, S. Saigal, A. Elongavan, *Journal of Anaesthesiology Clinical Pharmacology* **2017**, *33*, 300-305.

[20] H. Giamarellou, I. Karaiskos, *Antibiotics* **2022**, *11*, 1009.

[21] P. S. Hoffman, *Antibiotics* **2020**, *9*, 213.

[22] N. Rosenblatt-Farrell, *Environmental Health Perspectives* **2009**, *117*, A244-250.

[23] K. Lewis, *Nature Reviews Drug Discovery* **2013**, *12*, 371-387.

[24] K. Bush, P. A. Bradford, *Cold Spring Harbor Perspectives in Medicine* **2016**, *6*, a025247.

[25] G. P. Dinos, *British Journal of Pharmacology* **2017**, *174*, 2967-2983.

[26] T. D. M. Pham, Z. M. Ziora, M. A. T. Blaskovich, *MedChemComm* **2019**, *10*, 1719-1739.

[27] T. M. Belete, *Human Microbiome Journal* **2019**, *11*, 100052.

[28] a) C. Spry, K. Kirk, K. J. Saliba, *FEMS Microbiology Reviews* **2008**, *32*, 56-106; b) N. Farah, V. K. Chin, P. P. Chong, W. F. Lim, C. W. Lim, R. Basir, S. K. Chang, T. Y. Lee, *Current Research in Microbial Sciences* **2022**, *3*, 100111; c) S. Shapiro, *Journal of Antibiotics* **2013**, *66*, 371-386.

[29] K. Gruenberg, B. J. Guglielmo, in *Current Medical Diagnosis and Treatment 2022*, McGraw-Hill Education, New York, **2022**.

[30] A. L. C. Barra, L. O. C. Dantas, L. G. Morão, R. F. Gutierrez, I. Polikarpov, C. Wrenger, A. S. Nascimento, *Frontiers in Public Health* **2020**, *8*, 26.

[31] a) G. Mancuso, A. Midiri, E. Gerace, C. Biondo, *Pathogens* **2021**, *10*, 1310; b) E. L.-H. MacLean, P. Miotto, L. González Angulo, M. Chiacchiaretta, T. M. Walker, M. Casenghi, C. Rodrigues, T. C. Rodwell, P. Supply, E. André, M. Kohli, M. Ruhwald, D. M. Cirillo, N. Ismail, M. Zignol, *PLOS Global Public Health* **2023**, *3*, e0001754.

[32] a) A. F. Cowman, J. Healer, D. Marapana, K. Marsh, *Cell* **2016**, *167*, 610-624; b) M. A. Phillips, J. N. Burrows, C. Manyando, R. H. van Huijsduijnen, W. C. Van Voorhis, T. N. C. Wells, *Nature Reviews Disease Primers* **2017**, *3*, 17050.

[33] S. Kapishnikov, T. Staalsø, Y. Yang, J. Lee, A. J. Pérez-Berná, E. Pereiro, Y. Yang, S. Werner, P. Guttmann, L. Leiserowitz, J. Als-Nielsen, *Proceedings of the National Academy of Sciences of the United States of America* **2019**, *116*, 22946-22952.

[34] A. Nzila, *Journal of Antimicrobial Chemotherapy* **2006**, *57*, 1043-1054.

[35] S. R. Meshnick, *International Journal for Parasitology* **2002**, *32*, 1655-1660.

[36] R. T. Eastman, D. A. Fidock, *Nature Reviews Microbiology* **2009**, *7*, 864-874.

[37] I. K. Srivastava, H. Rottenberg, A. B. Vaidya, *Journal of Biological Chemistry* **1997**, *272*, 3961-3966.

[38] S. Looareesuwan, J. D. Chulay, C. J. Canfield, D. B. Hutchinson, *American Journal of Tropical Medicine and Hygiene* **1999**, *60*, 533-541.

[39] A. R. Renslo, *ACS Medicinal Chemistry Letters* **2013**, *4*, 1126-1128.

[40] A. F. da Silva, J. L. Benchimol, *Medical History* **2014**, *58*, 1-26.

[41] V. R. Solomon, H. Lee, *European Journal of Pharmacology* **2009**, *625*, 220-233.

[42] J. E. Hyde, *FEBS Journal* **2007**, *274*, 4688-4698.

[43] D. G. Davey, G. I. Robertson, *Transactions of The Royal Society of Tropical Medicine and Hygiene* **1957**, *51*, 463-466.

[44] S. Saini, R. Kumar, R. K. Tyagi, in *Plasmodium Species and Drug Resistance*, IntechOpen, Rijeka, **2021**.

[45] R. Abdul-Ghani, H. F. Farag, A. F. Allam, *Acta Tropica* **2013**, *125*, 163-190.

[46] C. H. Sibley, J. E. Hyde, P. F. G. Sims, C. V. Plowe, J. G. Kublin, E. K. Mberu, A. F. Cowman, P. A. Winstanley, W. M. Watkins, A. M. Nzila, *Trends in Parasitology* **2001**, *17*, 582-588.

[47] Louis H. Miller, X. Su, *Cell* **2011**, *146*, 855-858.

[48]   W. Liu, Y. Liu, *Cardiovascular Diagnosis and Therapy* **2016**, *6*, 1-2.

[49]   N. J. White, *Journal of Clinical Investigation* **2004**, *113*, 1084-1092.

[50]   L. Zhu, R. W. van der Pluijm, M. Kucharski, S. Nayak, J. Tripathi, N. J. White, N. P. J. Day, A. Faiz, A. P. Phyo, C. Amaratunga, D. Lek, E. A. Ashley, F. Nosten, F. Smithuis, H. Ginsburg, L. von Seidlein, K. Lin, M. Imwong, K. Chotivanich, M. Mayxay, M. Dhorda, H. C. Nguyen, T. N. T. Nguyen, O. Miotto, P. N. Newton, P. Jittamala, R. Tripura, S. Pukrittayakamee, T. J. Peto, T. T. Hien, A. M. Dondorp, Z. Bozdech, *Communications Biology* **2022**, *5*, 274.

[51]   A. M. Dondorp, R. M. Fairhurst, L. Slutsker, J. R. MacArthur, J. G. B. M.D, P. J. Guerin, T. E. Wellems, P. Ringwald, R. D. Newman, C. V. Plowe, *New England Journal of Medicine* **2011**, *365*, 1073-1075.

[52]   S. Kuhn, M. J. Gill, K. C. Kain, *American Journal of Tropical Medicine and Hygiene* **2005**, *72*, 407-409.

[53]   a) A. Blanshard, P. Hine, *Cochrane Database Systematic Reviews* **2021**, *1*, Cd004529; b) I. Chen, M. S. Hsiang, *The Lancet Infectious Diseases* **2022**, *22*, 751-753.

[54]   Editorial, *EClinicalMedicine* **2021**, *41*, 101221.

[55]   a) C. Årdal, M. Balasegaram, R. Laxminarayan, D. McAdams, K. Outterson, J. H. Rex, N. Sumpradit, *Nature Reviews Microbiology* **2020**, *18*, 267-274; b) T. Minssen, K. Outterson, S. Rogers Van Katwyk, P. H. D. Batista, C. I. R. Chandler, F. Ciabuschi, S. Harbarth, A. S. Kesselheim, R. Laxminarayan, K. Liddell, M. T. Osterholm, L. Price, S. J. Hoffman, *Bulletin of the World Health Organization* **2020**, *98*, 823-823a; c) J. F. Hayes, *Antibiotics* **2022**, *11*, 644.

[56]   M. I. Hutchings, A. W. Truman, B. Wilkinson, *Current Opinion in Microbiology* **2019**, *51*, 72-80.

[57]   S. Harbarth, H. H. Balkhy, H. Goossens, V. Jarlier, J. Kluytmans, R. Laxminarayan, M. Saam, A. Van Belkum, D. Pittet, p. for the World Healthcare-Associated Infections Resistance Forum, *Antimicrobial Resistance and Infection Control* **2015**, *4*, 49.

[58]   a) S. Rogers Van Katwyk, S. J. Hoffman, M. Mendelson, M. Taljaard, J. M. Grimshaw, *Health Research Policy and Systems* **2020**, *18*, 60; b) V. Tangcharoensathien, S. Chanvatik, H. Kosiyaporn, S. Kirivan, W. Kaewkhankhaeng, A. Thunyahan, A. Lekagul, *BMC Public Health* **2021**, *21*, 2188.

[59]   C. Llor, L. Bjerrum, *Therapeutic Advances in Drug Safety* **2014**, *5*, 229-241.

[60]   P. J. Collignon, S. A. McEwen, *Tropical Medicine and Infectious Disease* **2019**, *4*, 22.

[61]   P. K. Goyal, A. Semwal, A. Prakash, B. Medhi, *Indian Journal of Pharmacology* **2019**, *51*, 291-295.

[62]   C. Ghosh, P. Sarkar, R. Issa, J. Haldar, *Trends in Microbiology* **2019**, *27*, 323-338.

[63]   a) F. Micoli, F. Bagnoli, R. Rappuoli, D. Serruto, *Nature Reviews Microbiology* **2021**, *19*, 287-302; b) I. Frost, H. Sati, P. Garcia-Vello, M. Hasso-Agopsowicz, C. Lienhardt, V. Gigante, P. Beyer, *The Lancet Microbe* **2023**, *4*, e113-e125; c) R. M. Mariano, A. A. Gonçalves, D. S. Oliveira, H. S. Ribeiro, D. F. Pereira, I. S. Santos, D. F. Lair, A. V. Silva, A. S. Galdino, M. A. Chávez-Fumagalli, D. D. Silveira-Lemos, W. O. Dutra, R. C. Giunchetti, *Pathogens* **2023**, *12*, 247.

[64]   K. T. Patel, N. P. Chotai, *Pharmazie* **2008**, *63*, 251-255.

[65]   S. Kumariya, R. Mehra, R. Kumariya, in *Emerging Modalities in Mitigation of Antimicrobial Resistance*, Springer International Publishing, Cham, **2022**, pp. 159-177.

[66]   C. Årdal, E. Baraldi, U. Theuretzbacher, K. Outterson, J. Plahte, F. Ciabuschi, J.-A. Røttingen, *Journal of Pharmaceutical Policy and Practice* **2018**, *11*, 8.

[67]   D. M. Klug, F. I. M. Idiris, M. A. T. Blaskovich, F. von Delft, C. G. Dowson, C. Kirchhelle, A. P. Roberts, A. C. Singer, M. H. Todd, *Wellcome Open Research* **2021**, *6*, 146.

[68]   C. Popa, K. Holvoet, T. Van Montfort, F. Groeneveld, S. Simoens, *Frontiers in Pharmacology* **2018**, *9*, 1108.

[69]   R. W. van der Pluijm, C. Amaratunga, M. Dhorda, A. M. Dondorp, *Trends in Parasitology* **2021**, *37*, 15-24.

[70]   C. Rasmussen, P. Alonso, P. Ringwald, *Expert Review of Anti-infective Therapy* **2022**, *20*, 353-372.

[71]   T. M. Belete, *Drug Design, Development and Therapy* **2020**, *14*, 3875-3889.

[72]   WHO, **2021**, 2021 Antibacterial agents in clinical and preclinical development: an overview and analysis.

[73]   M. Miethke, M. Pieroni, T. Weber, M. Brönstrup, P. Hammann, L. Halby, P. B. Arimondo, P. Glaser, B. Aigle, H. B. Bode, R. Moreira, Y. Li, A. Luzhetskyy, M. H. Medema, J.-L. Pernodet, M. Stadler, J. R. Tormo, O. Genilloud, A. W. Truman, K. J. Weissman, E. Takano, S. Sabatini, E. Stegmann, H. Brötz-Oesterhelt, W. Wohlleben, M. Seemann, M. Empting, A. K. H. Hirsch, B. Loretz, C.-M. Lehr, A. Titz, J. Herrmann, T. Jaeger, S. Alt, T. Hesterkamp, M. Winterhalter, A. Schiefer, K. Pfarr, A. Hoerauf, H. Graz, M. Graz, M. Lindvall, S. Ramurthy, A. Karlén, M. van Dongen, H. Petkovic, A. Keller, F. Peyrane, S. Donadio, L. Fraisse, L. J. V. Piddock, I. H. Gilbert, H. E. Moser, R. Müller, *Nature Reviews Chemistry* **2021**, *5*, 726-749.

[74]   M. Sharland, V. Zanichelli, L. A. Ombajo, J. Bazira, B. Cappello, R. Chitatanga, P. Chuki, S. Gandra, H. Getahun, S. Harbarth, M. Loeb, M. Mendelson, L. Moja, C. Pulcini, H. Sati, E. Tacconelli, M. Zeng, B. Huttner, *Clinical Microbiology and Infection* **2022**, *28*, 1533-1535.

[75]   A. Mullard, *Nature Reviews Drug Discovery* **2019**, *18*, 411.

2|
# Cofactor metabolism as antimicrobial strategy

2.1 Lipoic acid metabolism

R-Lipoic acid (*R*-**LA**) is an ubiquitous redox-active cofactor that is covalently bound *via* its carboxylate to conserved lysine residues of respective dependent enzymes as lipoamide, and plays a crucial role in various enzymatic reactions.[1] It is mainly involved in oxidation reactions of large enzyme complex assemblies (Fig. 2.1).
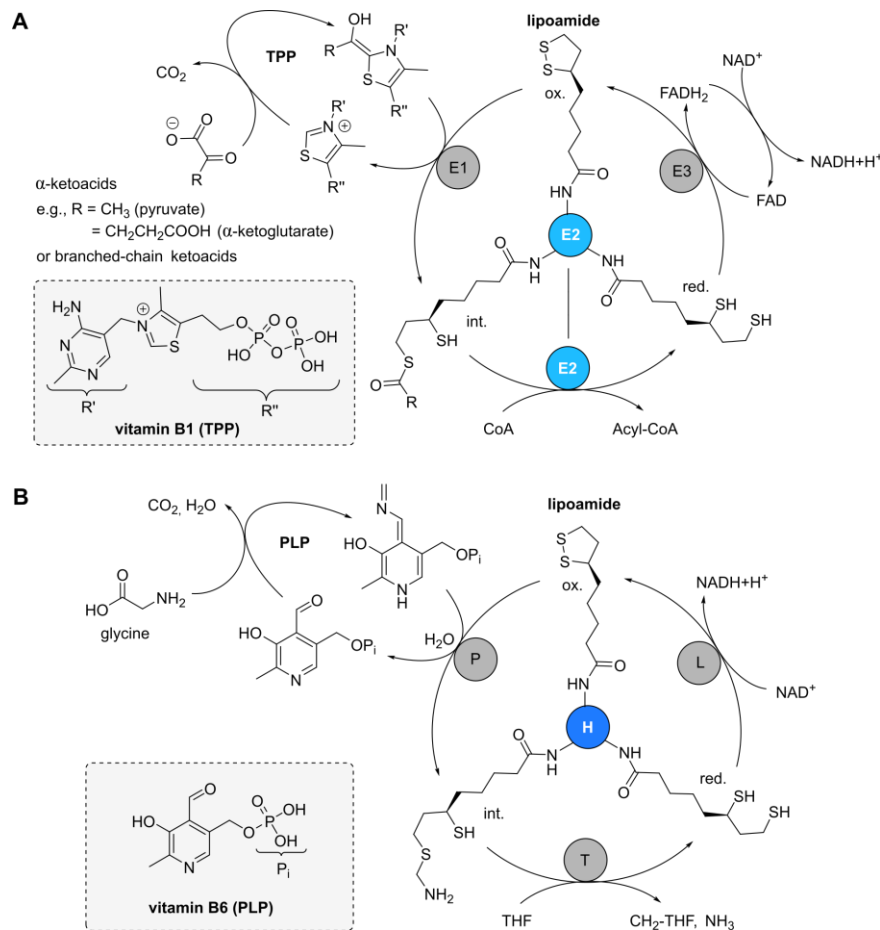
Fig. 2.1. Schematic representation of catalytic cycles that involve *R*-lipoic acid covalently bound as lipoamide on lysines as central cofactor in (A) dehydrogenase complexes (E2 subunit, bright blue) and (B) the glycine cleavage system (H-protein, dark blue).[2] In the initial substrate decarboxylation reactions, dehydrogenase complexes (A) additionally use **TPP** as cofactor in the E1 subunit whereas the glycine cleavage system uses **PLP** as cofactor in the P-protein. In both cycles, lipoamide then catalyzes substrate oxidations with its redox-active dithiolane ring while it transiently binds substrates for subsequent transfer onto CoA (A) or tetrahydrofolate (THF, B). In the last step, the reduced dihydrolipoyl moiety is re-oxidized by redox-equivalents within the E3 subunit or the L-protein, respectively. Importantly, the pyruvate dehydrogenase or α-ketoglutarate dehydrogenase complexes are located at central biochemical pathways relevant for energy metabolism and metabolic flux, which renders each cofactor essential for their individual contribution to centrally placed enzymatic catalysis.[3]

LA transiently binds substrates released from vitamin B1 (thiamine pyrophosphate, **TPP**) or vitamin B6 (pyridoxal phosphate, **PLP**) cofactors, facilitating their oxidation into acyl-CoA species in case of α-ketoacid dehydrogenase complexes (*e.g.,* pyruvate or α-ketoglutarate dehydrogenases) or THF-bound methylene in glycine cleavage systems (GCS), respectively.[1, 4] The E2 (dehydrogenases) or H (GCS) subunit bound to lipoate is of particular importance, as it not only participates in the oxidation process but also acts as an elongated swinging arm,

transferring substrates between enzymatic subunits.[5] In the final step, the reduced dihydrolipoyl moiety is regenerated to its dithiolane ring by oxidation catalyzed by the third subunit (E3 in dehydrogenases, L in GCS) and supported by FAD and NAD+ as cofactors, respectively (Fig. 2.1).[2]
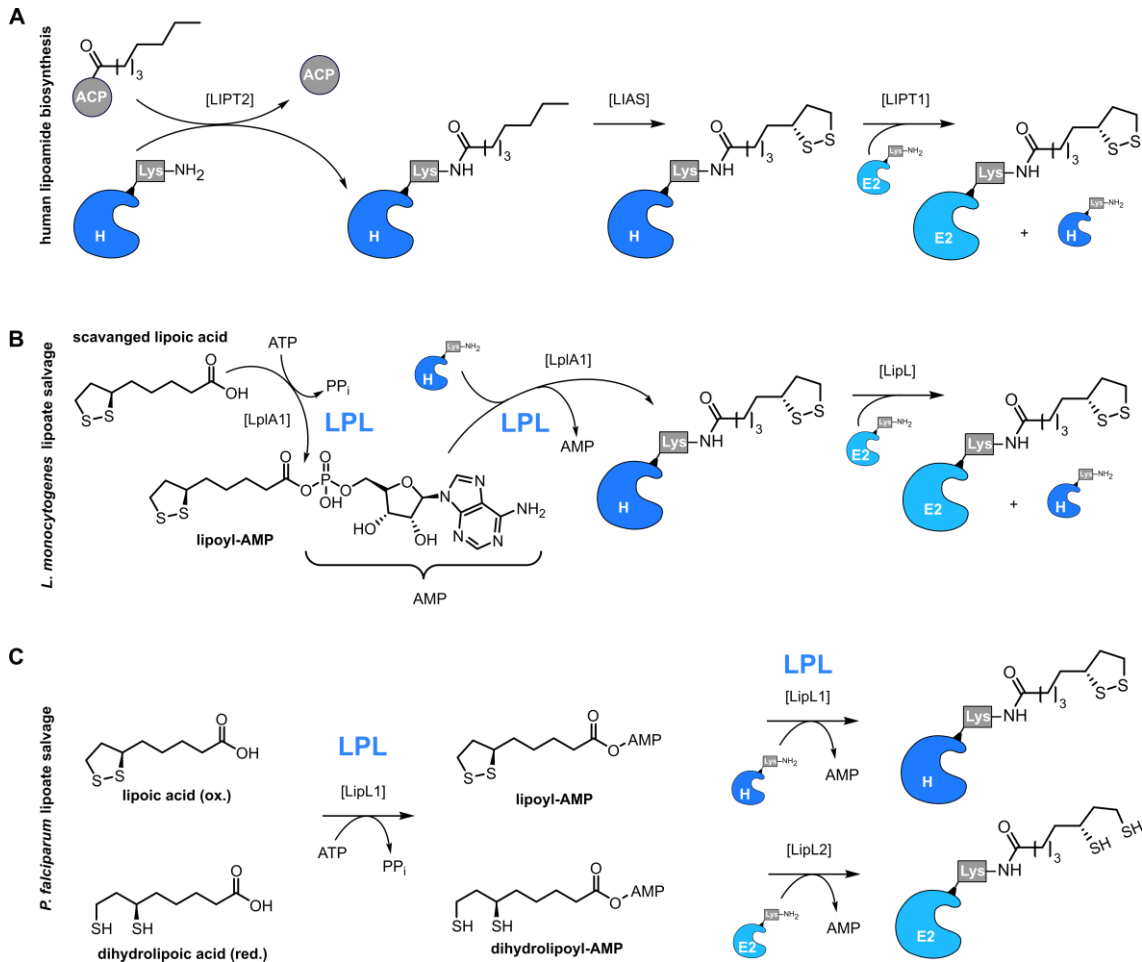
Fig. 2.2. Comparison in biochemical decoration of lipoate-dependent proteins with lipoamide during biosynthesis in human and salvage in auxotrophic microbes. (A) Humans rely on lipoate biosynthesis starting from octanoyl-ACP, as generated during fatty acid biosynthesis inside mitochondria. LIPT2 transfers octanoyl onto H-proteins (dark blue) where LIAS additionally installs the dithiolane ring. LIPT1 then transfers lipoamide onto cognate E2 enzymes (bright blue).[6] Lipoate cannot be salvaged in humans by lipoate protein ligase (LPL) as they lack such an enzyme.[6] By contrast, it is the only pathway with that auxotrophic microbes, such as *L. monocytogenes*[7] and *P. falciparum* (inside mitochondria),[8] can acquire lipoate. (B) *L. monocytogenes* uses its LPL (LplA1, *lplA1*) to first active **LA** by ATP to lipoyl-AMP, and secondly, to transfer it onto the H-protein as lipoamide. The transferase LipL subsequently distributes the lipoyl-domain to other E2 subunits.[7a] (C) Similarly, *P. falciparum* scavenges lipoic acid or dihydrolipoic acid inside its mitochondria with its LPL (LipL1, *lipL1*) to activate the compounds into their AMP-derivatives. While LipL1 can only transfer the oxidized species onto solely H-proteins, the second LipL2 (*lipL2*) enzyme accepts the released dihydrolipoyl-AMP compound to transfer it onto E2 subunits.[9] Although *P. falciparum* additionally possesses a **LA** biosynthesis pathway inside its apicoplast (not shown), it relies on salvage of **LA** from the host into its mitochondria.[8, 10]

These complex catalytic cycles are present across species, including bacteria, parasites, and mammals, as they contribute to central energy metabolism and metabolic flux.[4] For instance, they are located as link between glycolysis and the tricarboxylic acid (TCA) cycle (pyruvate dehydrogenase)[3a] or inside the TCA itself (α-ketoglutarate dehydrogenase).[3b] However,

decoration of the lipoate-dependent subunit differs vastly in species, rendering this enzymatic attachment process as a potentially selective antimicrobial strategy (Fig. 2.2).

Humans are able to synthesize the cofactor *de novo* inside mitochondria.[6] Starting with acyl-carrier-protein-(ACP)-bound octanoyl that originated from the fatty acid biosynthesis, LIPT2 transfers octanoate onto a conserved lysine residue of the H protein of the GCS. Next, LIAS subsequently installs the dithiolane ring on the H protein prior to distribution of **LA** to other lipoate-dependent enzymes by LIPT1. Bacteria and parasites use similar but distinct pathways for **LA** biosynthesis.[4a, 4c, 10-11] Several microbes, such as *E. coli*, possess an additional salvage pathway to activate and transfer scavenged **LA** from the exterior environment by so called lipoate protein ligases (LPL), which class is absent in humans.[4a, 6] Interestingly, some bacteria, such as *L. monocytogenes*[7] and *E. faecalis*,[7a] and *Plasmodium* spp. parasites,[8, 12] *e.g. P. falciparum*,[8] are lipoate auxotroph (*Plasmodium* spp. in their mitochondria), and hence, exclusively rely on lipoate salvage by LPL. In the following, the recycling pathway is presented in detail for *L. monocytogenes* and *P. falciparum,* as these microbes will be investigated in this thesis.

In *L. monocytogenes*, ATP activates scavenged **LA** inside the active pocket of LPL (LplA1, *lplA1*), which process creates pyrophosphate (PP$_i$) and a hydrolysis sensitive lipoyl-AMP species. In a second step, LPL further catalyzes the transfer of the lipoyl-domain onto a specific lysine residue of the H-protein (GcvH, *gcvH*, UniProt ID: Q8Y2L2) of the GCS as lipoate-dependent protein.[7a] Of note, a second LPL enzyme exists (LplA2, *lplA2*) which was previously reported to show only very low activity.[7c] Subsequently, LipL (*lipL*) recognizes the modification and further distributes the lipoyl-domain after cleavage from the H-protein to other lipoate-dependent enzymes (E2) as part of pyruvate dehydrogenase (*pdhC*, UniProt ID: Q8Y863) and branched-chain ketoacid dehydrogenase (*lmo1374*, UniProt ID: Q8Y7B2) complexes.[7a]

Similarly, LPL (LipL1, *lipL1*) in *P. falciparum* activates scavenged **LA** to lipoyl-AMP solely inside the mitochondrion, which is again transferred onto the H-protein of the GCS. Interestingly, only the reduced **LA** form, dihydrolipoate, can be used as substrate for lipoylation of other lipoate-dependent enzymes. After dihydrolipoyl-AMP was released by LipL1, LipL2 recognizes the activated species to ligate the reduced lipoyl-domain onto lysines of the E2 subunits of branched-chain ketoacid dehydrogenase and α-ketoglutarate dehydrogenase.[9]

Overall, this **LA** auxotrophy observed in certain pathogens provides a promising opportunity to disrupt **LA** salvage, which is essential for central metabolism, and presents a novel approach for the development of antimicrobial agents.[11a, 11b, 13] Previous studies have demonstrated the significance of **LA** salvage pathways by investigating the effects of LPL knockouts in

L. monocytogenes (Δ*lplA1*), which resulted in the inability of the mutant to grow in macrophages.[7b, 7c] Additionally, the use of 8-bromo octanoic acid (**BrO**) as a redox-inactive **LA** surrogate showed promising results as it was transferred in place of **LA** onto mitochondrial lipoate-dependent proteins in *Plasmodium* spp.,[9] leading to parasite killing, albeit at high concentrations (up to the millimolar range).[8, 12, 14] Furthermore, a recent study delved deeper into the role of these mitochondrial enzymes in *P. falciparum* and demonstrated that impaired LPL function impedes global cellular acetyl-CoA supply through mitochondrial dehydrogenase activity, ultimately resulting in parasite death.[13c] These initial results support the idea of addressing LPL as an innovative antimicrobial drug target. The discovery of stable lipoyl-AMP mimics holds great potential in this regard,[11c] and hence, this thesis will investigate the development of active site inhibitors for LPL in chapter 3.

2.2 Vitamin B6 metabolism

Pyridoxal phosphate (**PLP**), commonly known as vitamin B6, represents another conserved cofactor facilitating chemical transformations in **PLP**-dependent enzymes.[15] During catalysis, this vitamin serves as electronic sink,[16] enabling almost 4% of all reported enzymatic reactions known to date.[17] Often, the aldehyde of **PLP** binds to active site lysines to form an internal aldimine,[18] which is then displaced to an external aldimine with a substrate amino group.[19] The resulting quinoid-like structures are resonance stabilized and allow for manifold reactions.[20] For example, decarboxylation in lipoate-dependent glycine cleavage systems (GCS) is catalyzed by **PLP**, associated to the P-protein (Fig. 2.1, B).[21] More broadly, **PLP** contributes to amino acid, glucose and lipid metabolism next to heme, nucleotide and neurotransmitter formation by catalyzing not only decarboxylations but also side-chain cleavages, racemization and transaminations.[20, 22]
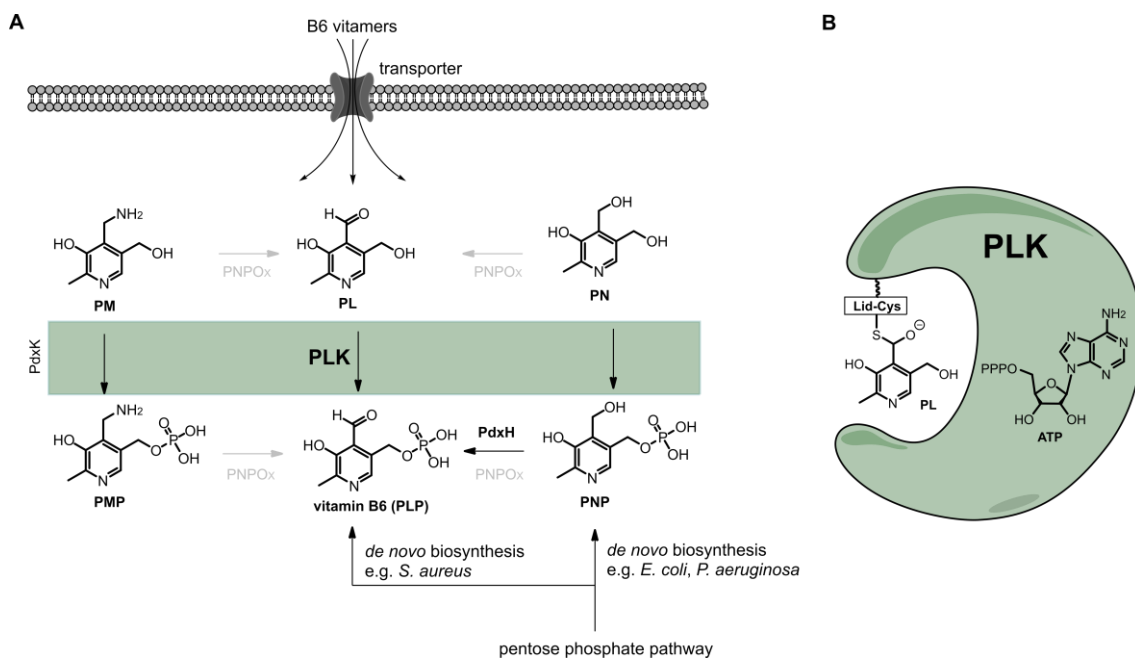
Fig. 2.3. Simplified overview of salvage and biosynthesis pathways of pyridoxal phosphate (**PLP**, vitamin B6) across species. (A) Humans are **PLP** auxotroph and rely on B6 vitamer uptake (**PM**, **PL**, **PN**) *via* transporters with subsequent conversion into **PLP** by PdxK (green box) and PNPOx (grey).[23] Some bacteria, such as *E. coli* and *P. aeruginosa* or *S. aureus,* possess diverse *de novo* biosynthesis pathways with precursors of the pentose phosphate pathway.[24] Additionally, they possess enzymes with B6 vitamer kinase activity (green box), *e.g.* PdxK or PdxY.[25] The latter subclass from Gram-negative bacteria uses a lid-cysteine for transient covalent binding of **PL** during phosphorylation (hemithioacetal), and hence, was named pyridoxal kinase (PLK, B), *e.g. E. coli* PLK (*Ec*PLK, PdxY, PDBID: 1TD2).[25b] Similarly, respective enzymes were identified in Gram-positive species that were shown to also phosphorylate HMP (hydroxymethylpyrimidine) to a minor extend, such as *S. aureus* PLK (*Sa*PLK, UniProt ID: A0A0H2XGZ0, PDBID: 4C5L).[26]

Humans are **PLP** auxotroph, *i.e.* they cannot synthesize this cofactor themselves, and hence, rely on uptake from external sources like the diet.[23] They inherited a kinase, PdxK, which allows for phosphorylation of salvaged B6 vitamers, comprising pyridoxal (**PL**), pyridoxine (**PN**) and pyridoxamine (**PM**).[23] Phosphorylation of **PL** by PdxK directly results in **PLP** as the active

cofactor. Additionally, **PNP** and **PMP** are converted into **PLP**, or **PN** and **PM** into **PL** by human PNPO$_X$ (grey), respectively.[23] By contrast, bacteria contain a *de novo* biosynthesis pathway which is different across species, and hence, rather complex. For instance, *E. coli* and *P. aeruginosa* or *S. aureus* are capable of synthesizing **PLP** based on two different strategies using pentose phosphate pathway precursors.[24] By contrast, *Enterococci* spp., such as *E. faecalis*, are **PLP** auxotroph, and therefore, exclusively rely on salvage.[27] However, all mentioned bacteria inherited at least enzymatic pyridoxal kinase (PLK) activity, which proteins are homologues of the human PdxK.[25a, 26, 27b, 28]

Interestingly, in some bacteria, more than one of these homologues were identified. For example, an *E. coli* strain, containing an inactive PdxK enzyme and an inactive *de novo* biosynthesis, was found to still grow upon **PL** supplementation.[29] This led to the discovery of a second PLK encoded by *pdxY* as a subclass,[25b] which only showed low **PL** phosphorylation activity compared to PdxK.[25a] Studies with the recombinant enzyme could demonstrate that **PL** bound covalently as hemithioacetal to PdxY *via* the lid-cysteine 122 which residue is absent in PdxK.[25] Subsequently, the same transient covalent mode of catalysis was found for PdxY (*pdxY*) of *P. aeruginosa*[28a] and the protein product of *sav0580* of *S. aureus* Mu50 at C110.[26] Activity experiments with the latter recombinant enzyme as well as metabolome analysis of respective transposon mutant cells suggested an essential role for this enzyme in terms of **PL** phosphorylation, which is why it was classified as PLK.[26] Interestingly, in the **PLP** auxotrophic strain *E. faecalis*,[27a] only one enzyme (UniProt ID: Q839G7)[27b, 30] could be identified as pyridoxal kinase based on sequence alignment[31] that even carries the signature lid-cysteine.

Overall, the absence of a lid-cysteine inside the active pocket of PdxK in humans[28b] but its presence in certain bacterial PLKs[25b, 26, 28a] renders this amino acid residue as an interesting handle for a potential antibiotic strategy. Especially *Enterococci* spp. might be potential targets as they are **PLP** auxotroph and, *e.g.*, as in case of *E. faecalis*, possibly contain only one PLK that carries the catalytically active signature lid-cysteine.[27, 31] Cysteine targeting warheads, such as acrylamides or chloroacetamides, can be incorporated into the pyridoxal core structure to irreversibly bind inside of the bacterial active pocket to potentially inhibit the enzymatic function, and hence, disturb bacterial **PLP** supply of auxotroph strains.[32] This strategic idea will be discussed in more detail in chapter 2.4 and experimentally investigated and discussed in chapter 4 of this thesis.

2.3 Vitamin B1 metabolism

Thiamine pyrophosphate (**TPP**), commonly referred to as vitamin B1, is an essential, non-covalently bound cofactor in ubiquitous organisms. It contributes to central energy metabolism and metabolic flux.[33] For instance, it catalyzes the oxidative decarboxylation from pyruvate to acetyl-CoA and from α-ketoglutarate to succinyl-CoA in conjunction with the cofactor **LA** in aforementioned dehydrogenase complexes (Fig. 2.1 A).[34]
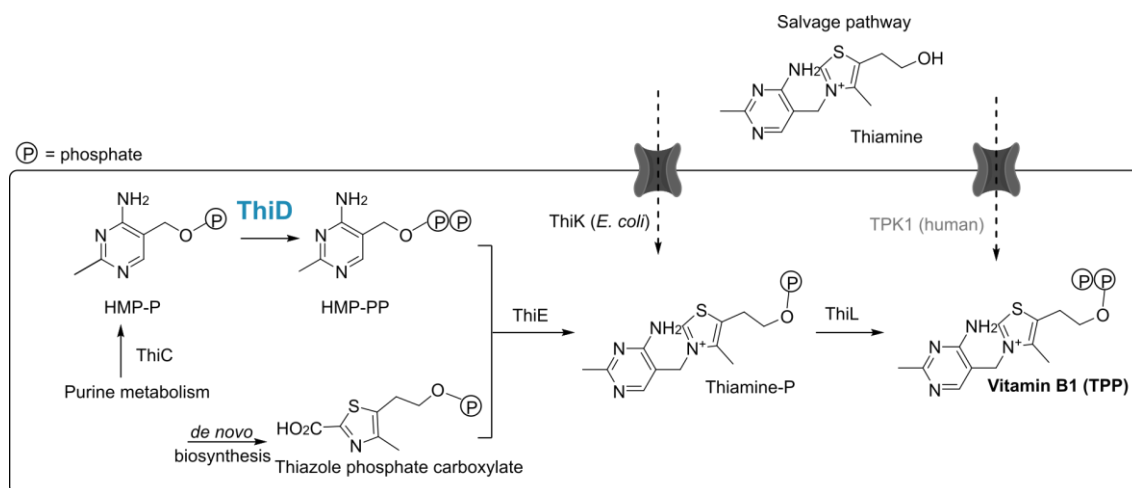
Fig. 2.4. Simplified schematic overview of the *de novo* biosynthesis and salvage of thiamine pyrophosphate (**TPP**, vitamin B1) of *E. coli* and humans.[35] Similarly to **PLP**, humans are auxotroph and exclusively rely on uptake of thiamine *via* transporters and subsequent activation by TPK1 (grey).[35d] *M. tuberculosis* possesses a **TPP** biosynthesis comparable to *E. coli* but notably, fully relies on biosynthesis due to a lack of thiamine transporters for salvage.[27b, 36] This renders the ThiD kinase (blue) as an interesting antimycobacterial drug-target.

The pathways by which bacteria and humans acquire the essential **TPP** cofactor exhibit notable differences. Of note, humans are **TPP** auxotroph, meaning they cannot synthesize this vitamin themselves and rely on uptake of thiamine with the diet. After transport into cells with transporter proteins, thiamine pyrophosphokinase (TPK1, Fig. 2.4, grey) subsequently activates thiamine to its active form **TPP**.[35d] By contrast, bacteria like *E. coli*, synthesize **TPP** *de novo*[35a, 35b] and additionally possess thiamine salvage enzymes, such as thiamine kinase (ThiK).[35c] The mycobacterial thiamine biosynthesis pathway is comparable to *E. coli*.[27b] Notably, mycobacteria such as *M. tuberculosis* fully rely on the *de novo* biosynthesis with ThiD as centrally placed enzyme as depicted in Fig. 2.4. With a lack of thiamine transporters, they cannot salvage thiamine.[36] Previous studies found growth defects of ThiD transposon mutants (*Rv0422c*),[37] and as such a hydroxymethylpyrimidine (**HMP**) / phosphomethylpyrimidine (**HMP**-P) kinase is absent in humans, the ThiD protein was classified as high-confident drug target for development of antimycobacterials.[30, 38]
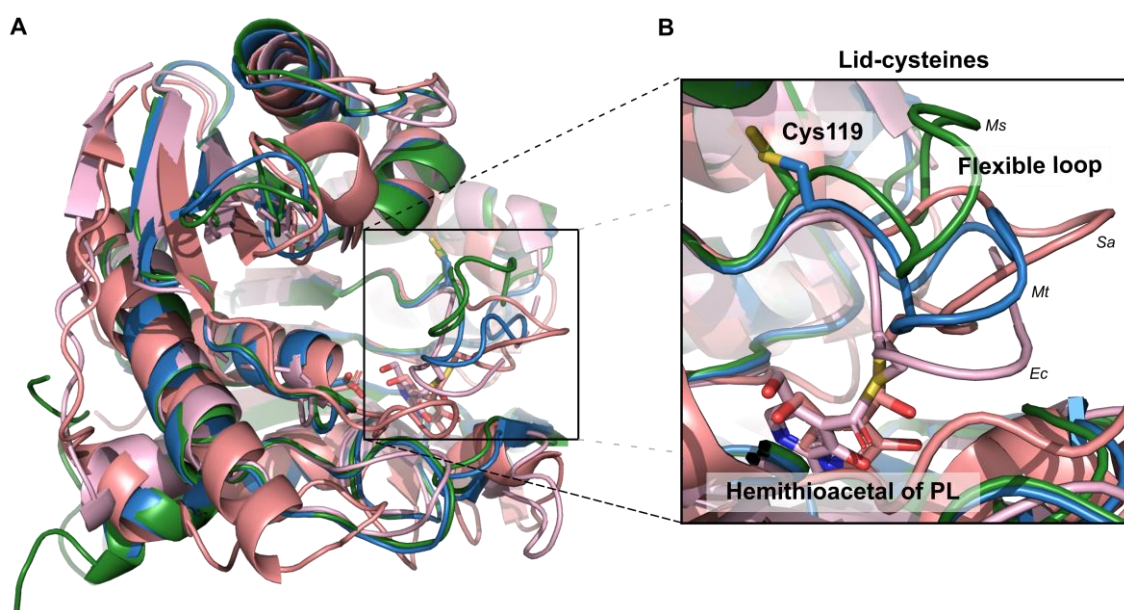
Fig. 2.5. Overlay of computationally predicted mycobacterial ThiD protein structures and co-crystallized bacterial PLK enzymes. (A) The overlay of AlphaFold2-predicted *M. smegmatis* (*Ms*, UniProt ID: I7G2G7, green)[30] and *M. tuberculosis* (*Mt*, UniProt ID: P9WG77, blue)[30] ThiD enzymes reveals a similar three-dimensional fold compared to crystallized *Ec*PLK (PDB ID: 1TD2, C122, bright salmon)[25b] and *Sa*PLK (PDB ID: 4C5L, C110, dark salmon).[26] (B) The close-up representation of the flexible loop region shows covalent binding of **PL** with lid-cysteines of bacterial PLKs and reveals that mycobacterial ThiD enzymes also contain a conserved lid-cysteine (C119) despite its irrelevance for HMP-P phosphorylation.

Alignment of AlphaFold2-predicted mycobacterial ThiD protein structures (*M. tuberculosis* H37Rv, UniProt ID: P9WG77, blue; *M. smegmatis* mc(2)155, Uniprot ID: I7G2G7, green)[30] indicate a conserved but catalytically irrelevant lid-cysteine inside of the active pocket (Fig. 2.5) which resembles homologous pyridoxal kinases (PLK, bright (*Ec*PLK)[25b] and dark (*Sa*PLK)[26] salmon) with covalently bound **PL** as hemithioacetal. Similarly, as presented for PLK in the previous chapter, compounds based on the hydroxymethylpyrimidine (**HMP**) scaffold could be equipped with warheads that irreversibly bind this residue covalently to occupy the active pocket, and hence, to potentially inhibit enzymatic activity with overall antimycobacterial activity. This idea will be strategically introduced in more detail in the following subchapter and experimentally investigated and discussed in chapter 5 of this thesis.

2.4 Concept of affinity-based protein profiling to study cofactor-related proteins

To study and monitor the activities of previously discussed pathways in microbes, appropriate bioorganic tools need to be developed. The concept of bioorthogonal click-chemistry, which was recognized with the Nobel prize in chemistry in 2022, is suitable for such an approach.[39] Cofactor mimics, bearing a characteristic scaffold with an additional modifiable chemical entity, such as alkynes or azides, can be synthesized and used within a workflow entitled "Activity-based protein profiling" (ABPP).[40] Cravatt[41] and Bogyo[42] pioneered this technique to study hydrolases and proteases in complex biological samples, respectively (Fig. 2.6).
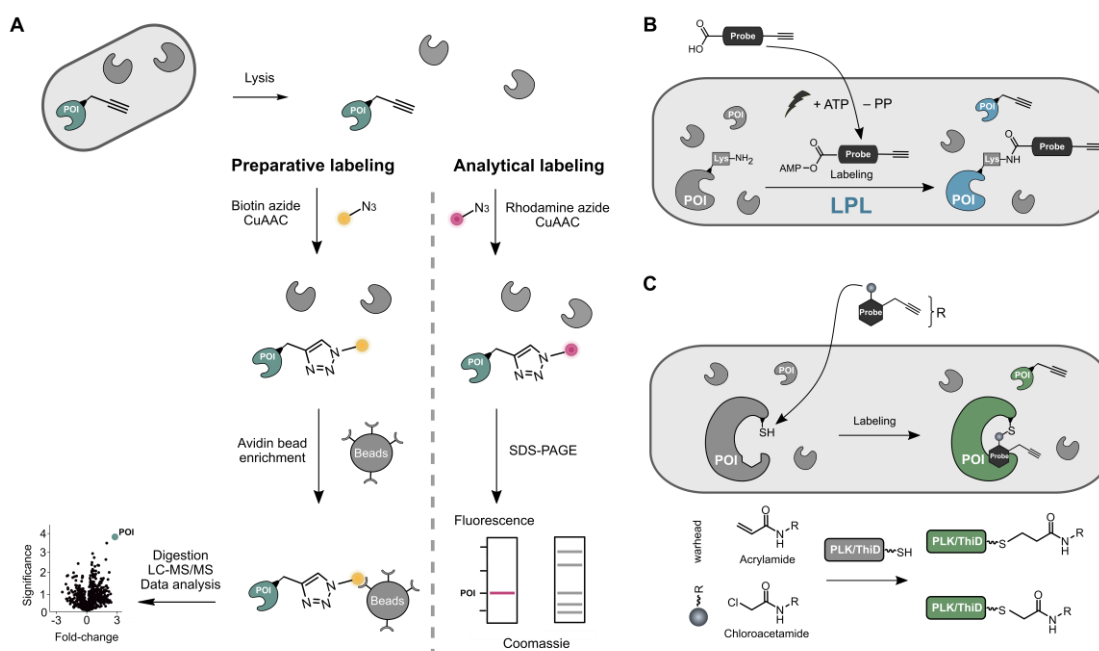
Fig. 2.6. Schematic representation of ABPP strategies (A) used in this thesis to investigate the cofactor metabolism of lipoic acid (B) and vitamin B6 and B1 (C). (A) When proteins of interest (POI) were addressed covalently with small molecules that carry an additional bioorthogonal handle (probe), such as alkynes (shown in A) or azides, the respective proteins can be detected in two different down-stream workflows after lysis: During the analytical labeling protocol, the bioorthogonal handle is conjugated to a fluorescent dye, *e.g.* rhodamine, by copper-catalyzed azide-alkyne cycloaddition (CuAAC), and subsequently the whole proteome can be separated by protein sizes on SDS-PAGE. Visualization of fluorescent bands indicates the masses of previously labeled proteins in comparison to marker proteins. Alternatively, labeled proteins can be conjugated to biotin for enrichment on avidin beads within the preparative labeling procedure. This step eliminates unlabeled proteins by washing steps and after digestion, LC-MS/MS measurement and comparison to a DMSO treated sample, enriched (previously labeled) proteins can be identified and quantified.[43] (B) In order to survey the activity of LPL in **LA** auxotrophic microbes, a probe molecule mimicking **LA** with a free carboxylate and an alkyne handle[44] could be installed alternatively on lipoate-dependent enzymes (blue). This strategy not only allows for detection of **LA**-dependent enzymes but also for screening of LPL inhibitors that would block probe transfer. The respective readout can be performed either *via* gel-based visualization of vanishing fluorescent bands of **LA**-dependent proteins or by LC-MS/MS detection. (C) As certain PLK and ThiD proteins carry a conserved lid-cysteine in the flexible lid region close to where binding of the natural substrate occurs,[25b, 26, 28a, 30-31] this nucleophilic handle could be trapped covalently by cysteine-reactive warheads (sphere), such as acrylamides (Michael-acceptors) or chloroacetamides.[32] In order to fine-tune for respective desired proteins (green), the warheads can be attached to respective vitamin B6 and B1 cofactor scaffolds (hexagon) to block the active pocket irreversibly. The addition of a bioorthogonal handle (alkyne for vitamin B6, azide for **HMP**) allows for down-stream analysis by fluorescence visualization and LC-MS/MS detection.[43a]

After covalent attachment of probe molecules to proteins of interest (POI), copper-catalyzed alkyne-azide cycloaddition (click-chemistry tool) can be used for downstream analysis.[45] This concept will be adapted in this thesis to chemically modify previously introduced protein amino acid residues with novel probe molecules.

In general, the probe molecules can label respective protein residues covalently so that stable interactions can be analyzed in the whole proteome in two similar approaches (Fig. 2.6, A). The qualitative analysis, referred as analytical labeling, visualizes probe-modified proteins on SDS-PAGE after conjugation to a fluorescent tag by click-chemistry, allowing for rough estimation of the labeled protein size. Liquid chromatography-coupled mass spectrometry (LC-MS/MS) serves as quantification method during the preparative labeling procedure. Labeled proteins are ligated to a biotin-tag for subsequent enrichment on avidin-beads. Then, unmodified proteins can be washed away which allows for LC-MS/MS identification of mainly trapped proteins by analyzing respective peptide intensities after proteolytic digest.[43]

In the context of lipoic acid metabolism, two recent chemical proteomic methods were demonstrated to enrich **LA**-dependent enzymes in bacterial and human lysates by chemical modification of the thiolane ring.[46] However, these technologies can only be used in lysates and lack the possibility to survey LPL activity for inhibitor development. Instead, a cell permeable lipoic acid-like probe molecule with an alkyne tag as a substrate of LPL could be transferred covalently onto lysines of **LA**-dependent proteins in place of **LA** (Fig. 2.6, B), similarly as previously demonstrated with fatty-acid based probes for cell surface labeling of engineered fusion-proteins.[44] The concept would allow for intracellular monitoring of LPL's activity by ABPP in order to identify cell permeable potential inhibitors of this enzyme, which presents a potential candidate for an innovative drug-target against **LA** auxotroph microorganisms, such as *L. monocytogenes*[7b, 7c, 11c] and *P. falciparum.*[8] This approach will be investigated in chapter 3.

Cysteines in the active pockets of structural homologous bacterial PLK[25b, 26, 28a] and mycobacterial ThiD[30-31] as part of vitamin B6 (**PLP**) and vitamin B1 (**TPP**) metabolism, respectively, could be covalently addressed with nucleophilic warheads, such as acrylamides or chloroacetamides,[32] bearing the respective cofactor scaffold. This irreversible modification could occupy the active pocket so that the native substrate would not bind anymore, leading to possible alterations in the metabolism of the respective vitamins. To visualize such interactions by ABPP experiments, an additional bioorthogonal tag, alkyne or azide, respectively, can be installed additionally which also allows for mining of diverse bacterial proteomes for respective yet undiscovered proteins (Fig. 2.6, C).[43a, 47] The approaches will be discussed in chapter 4 and chapter 5 for vitamin B6 and vitamin B1, respectively.

Of note, no homologous LPL or ThiD proteins are present in human cells,[6, 35d] and the human **PL** kinase PdxK does not contain a cysteine in the lid,[28b] rendering all these three proteins as potential antimicrobial targets due to their important metabolic function and uniqueness in microbes. The next research chapters 3-5 will apply the described ideas and assess the individual suitability of each cofactor as novel antimicrobial strategies against parasites and bacteria.

2.5 References

[1]   A. Solmonson, R. J. DeBerardinis, *Journal of Biological Chemistry* **2018**, *293*, 7522-7530.

[2]   R. Ramachanderan, B. Schaefer, *ChemTexts* **2019**, *5*, 18.

[3]   a) M. S. Patel, N. S. Nemeria, W. Furey, F. Jordan, *Journal of Biological Chemistry* **2014**, *289*, 16615-16623; b) L. Tretter, V. Adam-Vizi, *Philosophical Transactions of the Royal Society of London. Series B, Biological Sciences* **2005**, *360*, 2335-2345.

[4]   a) M. D. Spalding, S. T. Prigge, *Microbiology and Molecular Biology Reviews* **2010**, *74*, 200-228; b) E. A. Rowland, C. K. Snowden, I. M. Cristea, *Current Opinion in Chemical Biology* **2018**, *42*, 76-85; c) E. Cronan John, *Microbiology and Molecular Biology Reviews* **2016**, *80*, 429-450.

[5]   R. N. Perham, *Annual Review of Biochemistry* **2000**, *69*, 961-1004.

[6]   J. E. Cronan, *Frontiers in Genetics* **2020**, *11*, 510.

[7]   a) Q. H. Christensen, J. A. Hagar, M. X. D. O'Riordan, J. E. Cronan, *Journal of Biological Chemistry* **2011**, *286*, 31447-31456; b) M. O'Riordan, M. A. Moors, D. A. Portnoy, *Science* **2003**, *302*, 462-464; c) K. M. Keeney, J. A. Stuckey, M. X. D. O'Riordan, *Molecular Microbiology* **2007**, *66*, 758-770; d) J.-D. Sauer, A. A. Herskovits, M. X. D. O'Riordan, *Microbiology Spectrum* **2019**, *7*, 7.4.26.

[8]   M. Allary, J. Z. Lu, L. Zhu, S. T. Prigge, *Molecular Microbiology* **2007**, *63*, 1331-1344.

[9]   G. A. Afanador, K. A. Matthews, D. Bartee, J. E. Gisselberg, M. S. Walters, C. L. Freel Meyers, S. T. Prigge, *Molecular Microbiology* **2014**, *94*, 156-171.

[10]   S. Günther, L. Wallace, E. M. Patzewitz, P. J. McMillan, J. Storm, C. Wrenger, R. Bissett, T. K. Smith, S. Müller, *PLOS Pathogens* **2007**, *3*, e189.

[11]   a) J. Storm, S. Müller, *Current Pharmaceutical Design* **2012**, *18*, 3480-3489; b) C. Wrenger, S. Müller, *Molecular Microbiology* **2004**, *53*, 103-113; c) S. Shapiro, *Journal of Antibiotics* **2013**, *66*, 371-386.

[12]   C. Deschermeier, L.-S. Hecht, F. Bach, K. Rützel, R. R. Stanway, A. Nagel, F. Seeber, V. T. Heussler, *Cellular Microbiology* **2012**, *14*, 416-430.

[13]   a) S. L. Rei Yan, F. Wakasuqui, X. Du, M. R. Groves, C. Wrenger, *Frontiers in Chemistry* **2021**, *9*, 742175-742175; b) S. Günther, K. Matuschewski, S. Müller, *PLOS One* **2009**, *4*, e5510; c) S. C. Nair, J. T. Munro, A. Mann, M. Llinás, S. T. Prigge, *Proceedings of the National Academy of Sciences of the United States of America* **2023**, *120*, e2210929120.

[14]   a) B. Falkard, T. R. S. Kumar, L.-S. Hecht, K. A. Matthews, P. P. Henrich, S. Gulati, R. E. Lewis, M. J. Manary, E. A. Winzeler, P. Sinnis, S. T. Prigge, V. Heussler, C. Deschermeier, D. Fidock, *Cellular Microbiology* **2013**, *15*, 1585-1604; b) M. J. Crawford, N. Thomsen-Zieger, M. Ray, J. Schachtner, D. S. Roos, F. Seeber, *The EMBO Journal* **2006**, *25*, 3214-3222.

[15]   a) Y.-L. Du, K. S. Ryan, *Natural Product Reports* **2019**, *36*, 430-457; b) J. Liang, Q. Han, Y. Tan, H. Ding, J. Li, *Frontiers in Molecular Biosciences* **2019**, *6*, 4.

[16]   G. Schneider, H. Käck, Y. Lindqvist, *Structure* **2000**, *8*, R1-R6.

[17]   R. Percudani, A. Peracchi, *EMBO reports* **2003**, *4*, 850-854.

[18]   E. F. Oliveira, N. M. F. S. A. Cerqueira, P. A. Fernandes, M. J. Ramos, *Journal of the American Chemical Society* **2011**, *133*, 15496-15505.

[19]   R. Nakamura, M. Hikita, S. Ogawa, Y. Takahashi, T. Fujishiro, *FEBS Journal* **2020**, *287*, 1138-1154.

[20]   M. D. Toney, *Biochimica et Biophysica Acta* **2011**, *1814*, 1407-1418.

[21]   T. Nakai, N. Nakagawa, N. Maoka, R. Masui, S. Kuramitsu, N. Kamiya, *The EMBO Journal* **2005**, *24*, 1523-1536.

[22]   a) R. A. John, *Biochimica et Biophysica Acta* **1995**, *1248*, 81-96; b) A. C. Eliot, J. F. Kirsch, *Annual Review of Biochemistry* **2004**, *73*, 383-415.

[23]   M. L. di Salvo, R. Contestabile, M. K. Safo, *Biochimica et Biophysica Acta* **2011**, *1814*, 1597-1608.

[24]   T. Mukherjee, J. Hanes, I. Tews, S. E. Ealick, T. P. Begley, *Biochimica et Biophysica Acta* **2011**, *1814*, 1585-1596.

[25]   a) M. K. Safo, F. N. Musayev, M. L. di Salvo, S. Hunt, J. B. Claude, V. Schirch, *Journal of Bacteriology* **2006**, *188*, 4542-4552; b) M. K. Safo, F. N. Musayev, S. Hunt, M. L. di Salvo, N. Scarsdale, V. Schirch, *Journal of Bacteriology* **2004**, *186*, 8074-8082.

[26]   M. B. Nodwell, M. F. Koch, F. Alte, S. Schneider, S. A. Sieber, *Journal of the American Chemical Society* **2014**, *136*, 4992-4999.

[27]   a) A. L. C. Barra, L. O. C. Dantas, L. G. Morão, R. F. Gutierrez, I. Polikarpov, C. Wrenger, A. S. Nascimento, *Frontiers in Public Health* **2020**, *8*, 26; b) M. Kanehisa, S. Goto, *Nucleic Acids Research* **2000**, *28*, 27-30.

[28]   a) M. I. Kim, M. Hong, *Biochemical and Biophysical Research Communications* **2016**, *478*, 300-306; b) A. K. Gandhi, J. V. Desai, M. S. Ghatge, M. L. di Salvo, S. Di Biase, R. Danso-Danquah, F. N. Musayev, R. Contestabile, V. Schirch, M. K. Safo, *PLOS ONE* **2012**, *7*, e40954.

[29]   Y. Yang, H. C. Tsui, T. K. Man, M. E. Winkler, *Journal of Bacteriology* **1998**, *180*, 1814-1821.

[30]   UniProtConsortium, *Nucleic Acids Research* **2023**, *51*, D523-D531.

[31]   S. F. Altschul, W. Gish, W. Miller, E. W. Myers, D. J. Lipman, *Journal of Molecular Biology* **1990**, *215*, 403-410.

[32]   F. Huang, X. Han, X. Xiao, J. Zhou, *Molecules* **2022**, *27*, 7728.

[33]   S. Manzetti, J. Zhang, D. van der Spoel, *Biochemistry* **2014**, *53*, 821-835.

[34]   M. L. Das, M. Koike, L. J. Reed, *Proceedings of the National Academy of Sciences* **1961**, *47*, 753-759.

[35]   a) C. T. Jurgenson, T. P. Begley, S. E. Ealick, *Annual Review of Biochemistry* **2009**, *78*, 569-603; b) C. T. Jurgenson, S. E. Ealick, T. P. Begley, *EcoSal Plus* **2009**, *3*, 3.6.3.7; c) J. Melnick, E. Lis, J. H. Park, C. Kinsland, H. Mori, T. Baba, J. Perkins, G. Schyns, O. Vassieva, A. Osterman, T. P. Begley, *Journal of Bacteriology* **2004**, *186*, 3660-3662; d) A. Marcé-Grau, L. Martí-Sánchez, H. Baide-Mairena, J. D. Ortigoza-Escobar, B. Pérez-Dueñas, *Journal of Inherited Metabolic Disease* **2019**, *42*, 581-597.

[36]   Q. Du, H. Wang, J. Xie, *International Journal of Biological Sciences* **2011**, *7*, 41-52.

[37]   a) M. A. DeJesus, E. R. Gerrick, W. Xu, S. W. Park, J. E. Long, C. C. Boutte, E. J. Rubin, D. Schnappinger, S. Ehrt, S. M. Fortune, C. M. Sassetti, T. R. Ioerger, *mBio* **2017**, *8*, e02133-02116; b) C. M. Sassetti, D. H. Boyd, E. J. Rubin, *Molecular Microbiology* **2003**, *48*, 77-84.

[38]   K. Raman, K. Yeturu, N. Chandra, *BMC Systems Biology* **2008**, *2*, 109.

[39]   N. K. Devaraj, M. G. Finn, *Chemical Reviews* **2021**, *121*, 6697-6698.

[40]   H. J. Benns, C. J. Wincott, E. W. Tate, M. A. Child, *Current Opinion in Chemical Biology* **2021**, *60*, 20-29.

[41]   a) A. E. Speers, G. C. Adam, B. F. Cravatt, *Journal of the American Chemical Society* **2003**, *125*, 4686-4687; b) A. E. Speers, B. F. Cravatt, *Chemistry & Biology* **2004**, *11*, 535-546; c) Y. Liu, M. P. Patricelli, B. F. Cravatt, *Proceedings of the National Academy of Sciences* **1999**, *96*, 14694-14699.

[42]   a) D. Greenbaum, K. F. Medzihradszky, A. Burlingame, M. Bogyo, *Chemistry & Biology* **2000**, *7*, 569-581; b) L. E. Sanman, M. Bogyo, *Annual Review of Biochemistry* **2014**, *83*, 249-273.

[43]   a) J. Martell, E. Weerapana, *Molecules* **2014**, *19*, 1378-1393; b) S. Wang, Y. Tian, M. Wang, M. Wang, G.-b. Sun, X.-b. Sun, *Frontiers in Pharmacology* **2018**, *9*, 353.

[44]   M. Fernández-Suárez, H. Baruah, L. Martínez-Hernández, K. T. Xie, J. M. Baskin, C. R. Bertozzi, A. Y. Ting, *Nature Biotechnology* **2007**, *25*, 1483-1487.

[45]   E. Haldón, M. C. Nicasio, P. J. Pérez, *Organic & Biomolecular Chemistry* **2015**, *13*, 9528-9550.

[46]   a) Q. Tang, Y. Guo, L. Meng, X. Chen, *Angewandte Chemie International Edition* **2021**, *60*, 4028-4033; b) S. Lai, Y. Chen, F. Yang, W. Xiao, Y. Liu, C. Wang, *Journal of the American Chemical Society* **2022**, *144*, 10320-10329.

[47]   I. V. L. Wilkinson, M. Pfanzelt, S. A. Sieber, *Angewandte Chemie International Edition* **2022**, *61*, e202201136.

PART II

RESEARCH

3|
A chemical proteomic strategy reveals inhibitors of lipoate salvage in bacteria and parasites

by **Jan-Niklas Dienemann**, Shu-Yu Chen, Manuel Hitzenberger, Montana L. Sievert, Stephan M. Hacker, Sean T. Prigge, Martin Zacharias, Michael Groll & Stephan A. Sieber.

Synopsis

In the quest to identify active site inhibitors of lipoate protein ligases (LPL) that can impede the salvage of lipoic acid (**LA**) in lipoate-auxotroph pathogens, a chemoproteomic tool was developed to monitor LPL activity. Mimics of **LA**, carrying an alkyne tag, serve as probe molecules, and computational docking into a previously crystallized LPL from *E. coli* with subsequent molecular dynamics simulations discerned suitable chemical structures. After successful synthesis of all racemic probe molecules, their ability in labeling lipoate-dependent enzymes *via* LPL was assessed intracellularly in Gram-negative *E. coli* Δ*lipB* and Gram-positive *L. monocytogenes* wild type bacterial strains, using the concept of ABPP. Interestingly, probe **2** expelled an exceptional selectivity for all three known lipoate-dependent proteins in both bacteria during LC-MS/MS along with resolution of respective lysine binding sites. Furthermore, in fluorescent SDS-PAGE analysis of probe-labeled proteins, three selective bands could be visualized which were competed with pre-treatment of **LA** or 8-bromo octanoic acid (**BrO**) as a previously established weak inhibitor of lipoate salvage.[1] This intracellular proof of concept makes this facile gel-based technique attractive for identification of more potent and cell-permeable LPL inhibitors. Therefore, a small compound library as mimics of the intermediate lipoyl-adenosine monophosphate (lipoyl-AMP) was compiled by means of rational design as well as *in-silico* screens of the ZINC database, which contains commercially available small molecules. After computational assessment of promising binding affinities and stabilities of **C3** ad **LAMe** (the rationally designed compounds) in LPLs of two **LA** auxotrophic pathogens, *L. monocytogenes* and *P. falciparum*, the molecules were synthesized by amide coupling, while the ten most promising hits from the digital screen were purchased. Subsequently, all twelve compounds were applied to *L. monocytogenes* cells and screened with fluorescent SDS-PAGE for competition upon co-incubation with probe **2**, revealing **C3** and **LAMe** as LPL inhibitors with intracellular EC_{50} values of 210 nM and 330 nM, respectively, compared to **LA** (100 nM) and **BrO** (2.3 µM). Further, compound binding was validated to both recombinant LPLs in ITC in the low micromolar range and co-crystallography with the bacterial LPL revealed binding in the active pocket as a mimic of lipoyl-AMP. Finally, both LPL inhibitors were examined for their antimicrobial effect in *L. monocytogenes* and *P. falciparum* as representative **LA** auxotrophic strains, relying on **LA** salvage for survival. Whereas no antibiotic effect could be demonstrated, most likely as the native cofactor binds stronger to LPL, the malaria-causing parasite was killed by **LAMe** and **C3** effectively with EC_{50} values of 15 and 27 µM, while only low to moderate toxicity was observed in human HeLa cells, respectively.

Taken together, the study demonstrates the successful establishment of a chemoproteomic tool for monitoring intracellular lipoylation by LPL which allows for competitive profiling of respective inhibitors. The approach of addressing LPL as an alternate antimicrobial target was demonstrated with promising eradication effects against the malaria-causing parasite *P. falciparum*, even better than the

previously reported inhibitor **BrO**.[1] In the future, the newly discovered LPL inhibitors could be refined to further improve their potency by crystal-structure-aided rational drug design along with analysis of their pharmacodynamics.

Author contributions

Jan-Niklas Dienemann and Stephan A. Sieber conceived the project. Shu-Yu Chen and Manuel Hitzenberger ran molecular docking studies as well as molecular dynamics simulations for which Martin Zacharias provided equipment. Manuel Hitzenberger screened the ZINC database for potential inhibitors. Jan-Niklas Dienemann synthesized probes and inhibitors, tested their antibacterial properties and performed *in situ* labeling with gel-based and LC-MS/MS-based detection. Stephan M. Hacker provided the heavy and light isoDTB tags and assisted during the evaluation process of binding site identification. Jan-Niklas Dienemann identified and characterized inhibitors experimentally with regards of binding affinity in intracellular competitive ABPP and ITC experiments. Sean T. Prigge provided the expression strain for *P. falciparum* LPL and helped with trouble shooting during ITC experiments. Jan-Niklas Dienemann expressed and purified recombinant proteins and Michael Groll carried out subsequent co-crystallography with help of Jan-Niklas Dienemann. Montana L. Sievert conducted assays with *P. falciparum* parasites in erythrocytes while Jan-Niklas Dienemann performed macrophage infection assays with *L. monocytogenes* as well as toxicity studies in HeLa cells. Stephan A. Sieber, Jan-Niklas Dienemann and Shu-Yu Chen wrote the manuscript with input of all authors.

WILEY-VCH

RESEARCH ARTICLE

A Chemical Proteomic Strategy Reveals Inhibitors of Lipoate Salvage in Bacteria and Parasites

Jan-Niklas Dienemann,[a] Shu-Yu Chen,[a] Manuel Hitzenberger,[a] Montana L. Sievert,[b] Stephan M. Hacker,[c] Sean T. Prigge,[b] Martin Zacharias,[a] Michael Groll[a] & Stephan A. Sieber*[a]

[a] Technical University of Munich, TUM School of Natural Sciences
     Department of Bioscience, Center for Functional Protein Assemblies (CPA)
     Ernst-Otto-Fischer Strasse 8, 85748 Garching bei München, Germany
     E-mail: stephan.sieber@tum.de
[b] Department of Molecular Microbiology and Immunology
     Johns Hopkins Bloomberg School of Public Health
     615 N. Wolfe Street, E5132 Baltimore, MD 21205, USA
[c] Leiden Institute of Chemistry, Leiden University
     Einsteinweg 55, 2333 CC Leiden, The Netherlands

Supporting information for this article is given via a link at the end of the document.

Abstract: The development of novel anti-infectives requires unprecedented strategies targeting pathways which are solely present in pathogens but absent in humans. Following this principle, we developed inhibitors of lipoic acid (**LA**) salvage, a crucial pathway for the survival of **LA** auxotrophic bacteria and parasites but non-essential in human cells. An **LA**-based probe was selectively transferred onto substrate proteins via lipoate protein ligase (LPL) in intact cells, and their binding sites were determined by mass spectrometry. Probe labeling served as a proxy of LPL activity, enabling in-situ screenings for cell-permeable LPL inhibitors. Profiling a focused compound library revealed two substrate analogs (**LAMe** and **C3**) as inhibitors, which were further validated by binding studies and co-crystallography. Importantly, **LAMe** exhibited low toxicity in human cells and achieved killing of *Plasmodium falciparum* in erythrocytes with an EC_{50} value of 15 µM, making it the most effective LPL inhibitor reported to date.

Introduction

Cofactors enhance the scope of chemical transformations in enzymes beyond the limited diversity provided by the 20 canonical amino acids.[1] They play crucial roles in many cellular processes and are thus attractive drug targets.[2] Recently, several chemical proteomic strategies utilized small molecule cofactor mimics, e.g. pyridoxal phosphate[3] and heme,[4] to infiltrate the cellular metabolic machinery and facilitate their incorporation in cofactor-dependent enzymes. A small bioorthogonal handle (alkyne or azide) is clicked to an affinity tag (e.g., biotin) for enrichment on avidin beads and subsequent identification by mass spectrometry (MS).[5] In addition to the discovery of previously unknown cofactor-dependent enzymes, the methodology identified inhibitors against selected targets via competitive profiling.[6]

Lipoic acid (**LA**) is a promising candidate for this strategy as it contributes to central metabolism in various organisms.[7] **LA** is covalently bound to particular lysine residues where it catalyzes reactions such as acyl-CoA formation in dehydrogenase complexes, e.g., pyruvate dehydrogenase (oxidative decarboxylation).[8] Bacteria and parasites exhibit a highly diverse machinery to synthesize or acquire the cofactor compared to humans. In *Escherichia coli*, the biosynthesis pathway consists of

the enzymes LipB (octanoyl transferase) and LipA (lipoyl synthase). These enzymes assemble the **LA** cofactor directly ('on-site') on specific lysine residues of conserved domains of **LA**-dependent proteins via octanoylation (LipB) and subsequent introduction of the redox-active dithiolane moiety (LipA, Fig. 1A).[7a, 7b, 7d] In addition, salvage of **LA** is an alternate strategy by which organisms lipoylate proteins with the scavenged cofactor from the exterior environment (Fig. 1A). This process is catalyzed by ATP-dependent lipoate protein ligases (LPL).[7a, 7b, 7d, 9] By contrast, no homologous **LA** salvage pathway is known in mammalian cells, which instead rely on **LA** biosynthesis in the mitochondrion.[7a, 7d, 10] Some bacteria and parasites, such as *Listeria monocytogenes*[11] and *Plasmodium* spp.,[12] respectively, are **LA** auxotroph organisms, i.e., they rely on the uptake and salvage of **LA** for survival (in case of *P. falciparum* and *P. berghei* into the mitochondrion). Thus, these organisms represent a unique opportunity for the development of selective LPL inhibitors in order to block **LA**-dependent central metabolism pathways and, thereby, growth.[13] Despite this intriguing opportunity and the urgent need for novel anti-infectives, the development of such inhibitors has not been significantly exploited. One example is the redox-inactive small molecule mimic of **LA**, 8-bromo octanoic acid (**BrO**), which is transferred via LPL to substrate proteins, but cannot further support enzymatic catalysis.[14] **BrO** was shown to reduce growth of *P. falciparum* in erythrocytes,[12a] *P. berghei* in HepG2 cells[12b] and mice,[15] and *Toxoplasma gondii* in fibroblasts,[16] but high concentrations up to the millimolar range were needed for parasite killing.[12, 15] Thus, novel chemical tools are required to decipher more potent LPL inhibitors. Recently, two methods have been introduced to chemically modify endogenous lipoylated proteins exclusively in lysates via iodoacetamide-assisted lipoate-cyclooctyne ligation (iLCL)[17] or reduction of the dithiolane ring followed by thioacetalization with an alkynylated aldehyde.[18] These methods enriched lipoylated proteins in lysates and determined their lipoylation sites on lysines. However, because they do not involve the transfer of **LA** via LPL catalysis in intact cells, they are unsuitable for direct inhibitor discovery via competitive profiling.

Here, we introduce novel **LA** probes, which infiltrate the cellular salvage pathway in intact cells and get incorporated in cognate lipoate-dependent proteins (Fig. 1B).

RESEARCH ARTICLE

Chemical proteomics of intact *E. coli* and *L. monocytogenes* cells show selective enrichment of **LA**-dependent proteins and resolution of their modified lysine sites. Computational design, *in-situ* profiling, and co-crystallization revealed two effective LPL inhibitors (**C3** and **LAMe**). These compounds killed *P. falciparum* in erythrocytes with EC$_{50}$ values of 27 μM and 15 μM, respectively, highlighting the value of this approach in uncovering novel anti-infectives.

Results and Discussion

Design and Synthesis of Probes to Monitor Protein Lipoylation

As benchmarks, we started our studies with the C8-fatty acid probes **1a** (8-azido octanoic acid) and **1b** (7-octynoic acid) as previously confirmed LPL substrates (Fig. 1C).[19] First, we determined their toxicity in *E. coli* and identified up to 50% growth reduction with probe **1a**, while probe **1b** showed no effect (Fig. S1A). Next, wild-type *E. coli* and ΔlipB cells, bearing a mutation in the *de novo* biosynthesis pathway to maximize probe

uptake, were treated with various concentrations of the non-toxic probe **1b** for 2h in the stationary and exponential phase. Cells were lysed and click-chemistry was used to link any proteins modified by probe **1b** to rhodamine azide for fluorescent SDS-PAGE analysis (Fig. 1B). Interestingly, a distinct labeling pattern was only observed in the stationary phase of ΔlipB cells at a probe concentration of 50 μM or higher (Fig. 1D, S1B). A similar fluorescence pattern with higher background labeling was observed for the azide-bearing probe **1a** after linking modified proteins to rhodamine alkyne by click-chemistry.[20] From these results, we selected optimal conditions to perform quantitative MS analysis of covalently-labeled proteins. Therefore, we treated stationary cells for 2h with 100 μM of the non-toxic probe **1b**, followed by lysis, click to biotin azide, enrichment, digestion, and analysis *via* LC-MS/MS (Fig. 1B). Notably, one of the three **LA**-dependent proteins known in *E. coli*, ODP2 (*aceF*), was 3-fold enriched (Fig. 1E).[17-18] Moreover, numerous proteins belonging to fatty acid biosynthesis were among the top hits [−log$_{10}$ (*P* value) 6 − 8, log$_2$ (fold-change) 2 − 8]. These initial results demonstrated the infiltration of bacterial **LA** metabolism. However, the relatively simple probe design prevented the desired specificity for **LA**-dependent proteins with fatty acid biosynthesis enzymes as predominant off-targets.
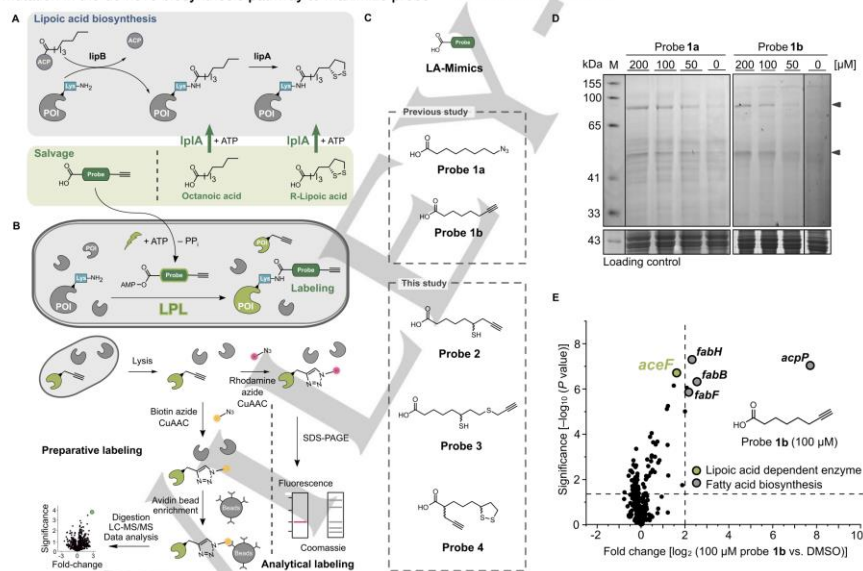

Figure 1. *In-situ* chemical proteomic strategy to investigate lipoylation *via* LPL-mediated activation and transfer. (A) The biosynthesis (grey box) and salvage of **LA** (green box) *via* the LPL enzyme lplA in *E. coli*. ACP − acyl carrier protein, POI − protein of interest. (B) Intracellular probe-based infiltration strategy *via* ATP-dependent LPL as **LA** salvage enzyme with subsequent downstream analysis of labeled proteins by click-chemistry (CuAAC − copper-catalyzed azide-alkyne cycloaddition) using either gel-based rhodamine fluorescence readout by SDS-PAGE (magenta, analytical labeling) or mass spectrometry-based detection after biotin conjugation and enrichment on avidin beads (yellow, preparative labeling). (C) Probe structures as **LA** salvage mimics used in this study. (D) Analytical labeling of intact *E. coli* ΔlipB cells with probes **1a** and **1b** (2h) in stationary phase revealed a similar pattern of concentration-dependently labeled fluorescent bands (grey box). The procedure with the azide-bearing C8-fatty acid probe **1a** showed higher background labeling than the alkyne-based derivative **1b**.[20] 'M' represents a marker as a protein size reference. Coomassie staining served as loading control. (E) The volcano plot shows enrichment of mainly fatty acid biosynthesis proteins (grey) on a log$_2$ scale after treatment of intact *E. coli* ΔlipB cells in stationary phase with the alkyne-bearing probe **1b** (100 μM, 2h). Of note, the **LA**-dependent protein product of the gene *aceF* (green) could be 3-fold enriched. The threshold lines indicate 4-fold enrichment compared to DMSO and a −log$_{10}$ *P* value of 1.3 (two-sided two-sample *t*-test, n = 4 independent experiments per group). Gene names of proteins are shown in italic.

2

RESEARCH ARTICLE

In order to enhance the fidelity in detection of enzyme lipoylation, we designed a suite of **LA** mimics as probes that are attainable by chemical synthesis (Fig. 1C). Starting from probe **1b**, we incrementally increased the structural complexity to more closely mimic **LA**. In a first step, we placed a free thiol at position 6 of 8-nonynoic acid to obtain probe **2**. The synthesis started with propargylating cyclohexanone (**5**), followed by a *Baeyer-Villiger* oxidation as a key step to introduce the lactone moiety (Scheme 1).[21] After ring opening by transesterification, the hydroxyl group at position 6 could be transformed into thioester **10** by tosylation and substitution with thioacetate. Saponification as final step generated probe **2** as a racemic mixture in six steps (5% overall yield).
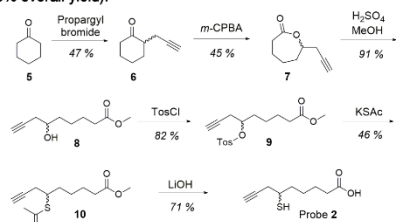
Scheme 1. Synthesis of probe **2**. The propargylated lactone **7** was synthesized as previously reported[21] prior to transesterification (**8**), tosylation (**9**), and nucleophilic substitution by thioacetate. Global saponification of **10** yielded probe **2** as racemate.

Next, the propargyl tag was linked to the thiol at position 8 of the reduced **LA** moiety as a thioether (probe **3**). Probe **4** presents the most similar mimic to **LA** after functionalization at position 2 with a propargyl handle. For probes **3** and **4**, **LA** was protected by esterification, followed by reduction to open the dithiolane ring. To obtain probe **3**, the thiol group at position 8 was selectively propargylated, followed by saponification to liberate the carboxylic acid as racemate. By contrast, for probe **4**, both thiols were protected by tritylation to install a propargyl tag at position 2, followed by global deprotection and oxidation to yield the desired probe as a mixture of all diastereoisomers (Scheme S1).

Probe 2 Labels LA-dependent Proteins in *E. coli* and *L. monocytogenes*

With a panel of probes (**2 – 4**) in hand, we first tested their impact on bacterial growth under labeling conditions (Fig. S2A). At high concentrations of 500 µM, only probe **2** slightly reduced the growth of *E. coli* Δ*lipB* by 20%. Secondly, we examined their labeling performance in intact *E. coli* Δ*lipB* cells in both fluorescent gel-based and LC-MS/MS experiments. Labeling with probes **4** and **3** revealed high background without competition upon **LA** treatment (Fig. S2B-C). However, probe **2** showed distinct bands on the fluorescent gel that could be competed with **LA** and **BrO** pre-treatment, indicating that **LA**-dependent proteins were labeled *via* LPL (Fig. 2A). Additionally, application of probe **2** in wild-type *E. coli* cells showed no labeling indicating that it cannot compete with the *de novo* biosynthesis (Fig. S2D). Subsequent quantitative LC-MS/MS profiling exclusively revealed all three known **LA**-dependent enzymes in the *E. coli* Δ*lipB* cells (ODP2 – *aceF*, 66 kDa; ODO2 – *sucB*, 44 kDa; GCSH – *gcvH*,

14 kDa) without any background (Fig. S3A).[17-18] Moreover, labeling was competed by addition of **LA** or **BrO** in 10-fold excess, demonstrating improved specificity of probe **2** (Fig. 2B, S3B).

To rationalize the diverging labeling properties, we applied computational methods to predict how **LA** and the probe stereoisomers bind into the crystal structure of *E. coli* LPL (lplA – *lplA*, PDBID 1x2h).[22] The structures were docked into the active site (Fig. S4A) and subjected to molecular dynamics (MD) simulations to investigate their binding behavior, including binding free energies ($\Delta\Delta G_{Bind}$), root-square deviation ($RMSD_{Lig}$), and root-mean-square fluctuation ($RMSF_{Lig}$). Different binding modes were observed across these compounds. The *S*-enantiomer of probe **2** exhibited similar binding stability as **LA**, shown by $RMSD_{Lig}$ and $RMSF_{Lig}$ (Fig. S4B), and both compounds remain in a binding pose forming hydrogen bonds with R70, H149, and S72 (Fig. 2C, S4C). By contrast, probe **1b** and enantiomers and diastereomers of probes **3** and **4**, respectively, were occasionally attracted by neighboring R140 and deviated from their initial binding locations (Fig. 2C, S4B-D), which may prevent their activation by ATP for subsequent transfer to **LA**-dependent proteins (Fig. 1B).

With probe **2** as ideal lipoylation tool in hand, we deciphered the modified lysines in whole *E. coli* proteomes. Enrichment of the labeled peptides *via* tailored desthiobiotin (isoDTB) linkers[23] and subsequent MS analysis revealed K44 of ODO2 (*sucB*) and K41/K144/K245 of ODP2 (*aceF*) as modified lipoylation sites, which is in line with literature data (Fig. 2D).[17-18]

The high fidelity of our method was also retained when we switched from the Gram-negative *E. coli* mutant to the labeling of a wild-type Gram-positive *L. monocytogenes* bacterial strain, which relies solely on an **LA** salvage pathway consisting of two LPL orthologs (lplA1 – *lmo0931*; lplA2 – *lmo0764*) to lipoylate GcvH. In a next step, the lipoyl group is transferred by LipL from GcvH to other **LA**-dependent proteins.[9] Again, direct labeling of intact cells with probe **2** and competition with **LA** or **BrO** revealed three hits, comprising all known **LA**-dependent enzymes in *Listeria* (Q8Y863 – *pdhC*, 58 kDa; Q8Y7B2 – *lmo1374*, 45 kDa; GcvH – *gcvH*, 14 kDa; Fig. 2E-F, S3C-D).[24] Additionally, the corresponding modified lysines were identified *via* the isoDTB technology (Fig. 2D).[23] Of note, the binding sites – K63 of GcvH (*gcvH*), K44 of Q8Y7B2 (*lmo1374*) and K43/K153 of Q8Y863 (*pdhC*) – have been determined experimentally for the first time in *Listeria* and match theoretical predictions.[24]

Computational Design and Screen of Novel Active Site LPL Inhibitors

The versatility of our novel labeling technology for different strains and its selectivity for the detection of lipoylated proteins represents a unique opportunity for identifying chemical compounds that lead to the manipulation of cellular lipoylation and putative therapeutic applications. Specifically, probe **2** is activated and transferred onto the cognate substrate proteins by LPL, facilitating a direct readout of its activity. The lack of an LPL-mediated salvage pathway in human cells makes this enzyme attractive for selective pathogen targeting.[9-10, 12a] Since there are no active site LPL inhibitors reported, we performed computational studies to design a suite of potential candidates for subsequent validation *via* our competitive profiling approach

3

RESEARCH ARTICLE
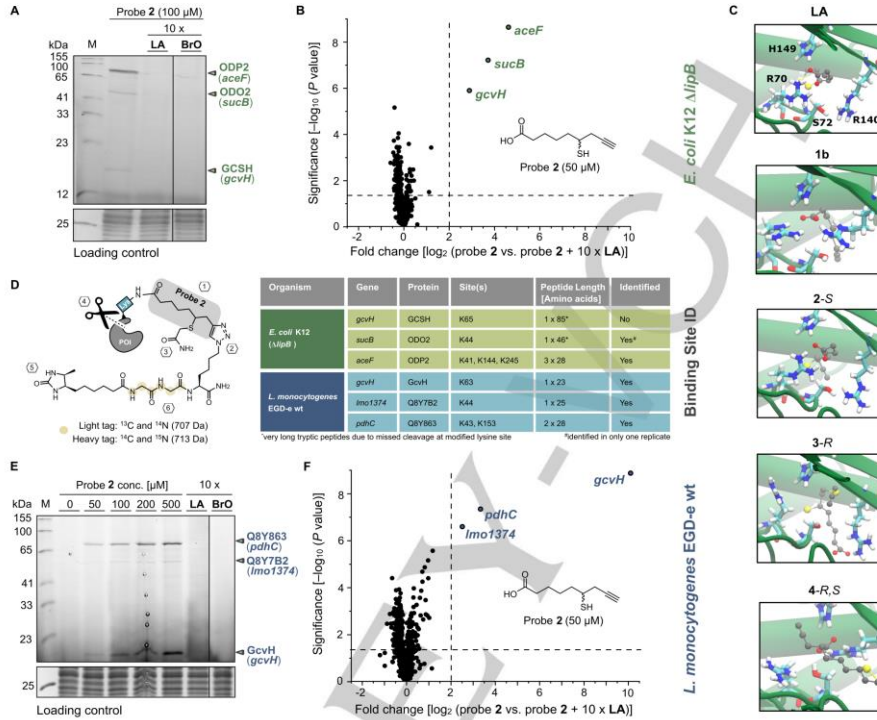
Figure 2. In-situ profiling of lipoylation in *E. coli* ΔlipB (Gram-negative) and *L. monocytogenes* wild type (Gram-positive) with binding site identification. Gene names of corresponding protein products are presented in italic. 'M' represents a marker as a protein size reference, and Coomassie staining served as loading control during analytical labeling. Of note, the protein products might show reduced migration on SDS-PAGE after rhodamine modification. The threshold lines in volcano plots indicate a $-\log_{10} P$ value of 1.3 (two-sided two-sample *t*-test, $n = 4$ independent experiments per group) and 4-fold enrichment. (A) Analytical labeling of intact *E. coli* ΔlipB cells with probe **2** (100 μM, 2h) and in competition with 10-fold excess (1 mM) of **LA** or **BrO** indicated infiltration of **LA** salvage *via* LPL. The green arrows mark the expected size of ODP2 (*aceF*, 66 kDa), ODO2 (*sucB*, 44 kDa), and GCSH (*gcvH*, 14 kDa) as known lipoylated proteins.[17-18] (B) The volcano plot presents preparative labeling results of intact *E. coli* ΔlipB cells with probe **2** (50 μM, 2h) in comparison to probe **2** (50 μM) in competition with 10-fold excess **LA** (500 μM), indicating selective enrichment of **LA**-dependent enzymes.[17-18] (C) Representative snapshots of the native *R*-enantiomer of **LA** and computationally predicted best-performing probe candidates **1b**, **2-S**, **3-R** and **4-R,S** in *E. coli* lplA (PDBID 1x2h) are depicted at the end of molecular dynamics simulations (400 ns), highlighting comparable binding orientations of **LA** and **2-S** in contrast to **1b**, **3** and **4** (Fig. S4B-D). (D) The methodology of isoDTB tags[23] was applied to identify the binding sites of probe **2** on lysine residues in *E. coli* ΔlipB and *L. monocytogenes* that corresponded to protein lipoylation sites. After labeling respective lysines in intact bacterial cells with probe **2** (1), the labeled proteome was clicked to a heavy and a light isoDTB tag as a technical replicate (2), followed by capping of free thiols with iodoacetamide (3). Proteins were digested by trypsin (4) to release the modified desthiobiotinylated peptides with one missed cleavage at the modified lysine. Tryptic peptides were enriched on avidin beads (5) and eluted to be identified by mass spectrometry. Mass shifts of 707 Da and 713 Da revealed isoDTB-tagged peptides (6). Peptides up to 28 amino acids were detected without problems in contrast to longer tryptic peptides with missed cleavage at the modified lysine, as indicated by asterisks.[18] Peptides that were only identified in one replicate were marked with #. (E) Concentration-dependent analytical labeling of intact *L. monocytogenes* wild type cells with probe **2** (0 μM – 500 μM, 2h) and in competition with 10-fold excess (2 mM) of **LA** or **BrO** compared to probe **2** (200 μM) revealed infiltration of **LA** salvage *via* LPL and lipoyl transferase LipL. The blue arrows mark the expected size of Q8Y863 (*pdhC*, 58 kDa), Q8Y7B2 (*lmo1374*, 45 kDa), and GcvH (*gcvH*, 14 kDa) as known **LA**-dependent proteins.[24] (F) The volcano plot presents preparative labeling results of intact *L. monocytogenes* wild type cells with probe **2** (50 μM, 2h) in comparison to probe **2** (50 μM) in competition with 10-fold excess **LA** (500 μM), indicating selective enrichment of **LA**-dependent enzymes.[24]

using probe **2**. We initiated the inhibitor development by a structural overlay of three representative LPL enzymes, lplA from *E. coli* (Gram-negative bacterium) and LipL1 (*lipL1*) from *P. falciparum* (parasite), for which crystal structures are available,[22, 25] and lplA1 from *L. monocytogenes* (Gram-positive bacterium) from a structural AlphaFold2 (AF2) prediction.[26] The overlay of all enzymes revealed a high structural similarity of the active sites as indicated by particular lysine and histidine residues
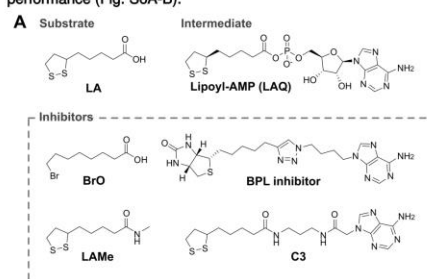
(Fig. S5), suggesting that inhibitors may be effective across different organisms. Three ligand binding pockets (A, B, and C, Fig. S5) could be identified depending on the enzyme's catalytic state. The comparison between the **LA** bound crystal structure (*E. coli*, PDBID 1x2h, loading state)[22] and the lipoyl-AMP (**LAQ**) bound structure (*E. coli*, PDBID 3a7r, intermediate state)[25a] indicates that **LA** binds first to the initial loading pocket A (as demonstrated for the probe simulations, Fig. S4) and is
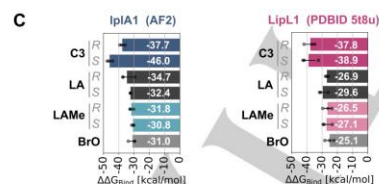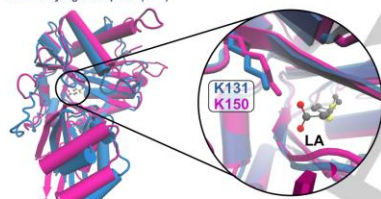
4

WILEY-VCH

RESEARCH ARTICLE

subsequently found in pocket B after adenylation by ATP, while the adenine motif of **LAQ** resides in pocket C. In the search for LPL active site inhibitors, we followed a two-tiered strategy by targeting pockets B and C. In the first approach, we virtually screened the ZINC database[27] by a pharmacophore-guided[28] search against the LPL active site, revealing 126 putative hits which were subsequently docked into LPL enzymes. The top 50 compounds of each ligase, selected by their docking score, were screened for overlapping compounds. The resulting 29 molecules were sorted by their averaged ranking position to identify ten commercially available compounds with the best-predicted performance (Fig. S6A-B).

In a second approach, we made use of the similar catalytic activity between LPL and biotin protein ligase (BPL), for which a potent BPL inhibitor with antibacterial activity was previously reported.[29-30] This molecule, mimicking biotin-AMP as native substrate, is composed of the signature biotin moiety linked *via* a triazole linker to an adenine heterocycle group (Fig. 3A). Both biotin and adenine bind to distinct pockets of BPL, of which the latter adenine pocket is also present in LPL (pocket C, Fig. S5). We thus tailored the molecule towards LPL to mimic **LAQ** by replacing the biotin with **LA** and the triazole with a more flexible but chemically stable amide linker while preserving the same linker length (**C3**, Fig. 3A). **C3** and its cropped version, lipoic acid monomethyl amide (**LAMe,** Fig. 3A), were docked into the active sites of LPL from *L. monocytogenes* and *P. falciparum* in comparison to the native ligand **LA** and **BrO** (Fig. 3B, S7A) to calculate and compare their binding affinities ($\Delta\Delta G_{Bind}$, Fig. 3C) and stabilities (RMSD$_{Lig}$, RMSF$_{Lig}$, Fig.S7B) *in-silico* by MD simulations. Overall, the same trend of predicted binding affinities for the compounds was observed in both enzymes as follows: **C3** > **LA** ~ **LAMe** = **BrO**. Interestingly, **LA**, **LAMe**, and **BrO** were predicted to bind stronger and more stably to pocket B of *L. monocytogenes* lplA1 (approximately -32 kcal/mol) compared to *P. falciparum* LipL1 (roughly -26 kcal/mol), whereas **C3** showed the strongest binding free energy with around -38 kcal/mol for both ligases (Fig. 3C). Remarkably, the adenine motif of **C3** in pocket C of LipL1 contributed significantly to the binding free energy (-12 kcal/mol), compared to the truncated **LAMe** solely residing in pocket B. As expected, this finding underlines a significant affinity enhancement for the introduction of the adenine-linker group in addressing both pockets. Based on these promising calculations, we synthesized **C3** and **LAMe** by amide coupling for experimental comparison to **BrO** and **LA** (Scheme S2).

Figure 3. Docking and MD simulations of rational-designed potential inhibitors of LPL in *L. monocytogenes* (blue) and *P. falciparum* (magenta) as substrate and intermediate mimics. (A) The inspiration for compound design was driven by mimicking the intermediate lipoyl-AMP (**LAQ**) with chemically stable amide bonds in analogy to a previously reported inhibitor of the biotin protein ligase (BPL).[29] The simple **LAMe** molecule carries a monomethyl amide function that would not allow the **LA** moiety to be activated by ATP. **C3** presents an extended version with an additional amide linker-adenine moiety. **BrO** was described as an inhibitor of cognate lipoylation sites as it is activated and transferred by LPL.[14] **LA** as the native substrate and **BrO** as an established inhibitor serve as benchmarks. **LA** and all stereoisomers of potential inhibitors were docked into the active sites of *L. monocytogenes* lplA1 (AF2), and *P. falciparum* LipL1 (PDBID 5t8u), and representative binding modes of *R*-enantiomers are depicted exemplarily (Fig. S7A). (C) MD simulations in *L. monocytogenes* and *P. falciparum* predict all stereoisomers' LPL binding affinities ($\Delta\Delta G_{Bind}$, mean value in white). The calculations were run in $n = 3$ independent attempts, and error bars represent SEM.

Biochemical and Crystallographic Studies Reveal C3 and LAMe as Active Site Inhibitors of LPL in Bacteria and Parasites

With a suite of twelve potential LPL inhibitors at hand, we tested their performance *via* competitive profiling with probe **2**. For this, we focused on *L. monocytogenes* as a representative example of an **LA**-auxotrophic wild-type strain and treated cells with a 10-fold excess of competitor (1 mM) compared to the amount of probe **2** (100 µM) and analyzed the band intensity of signature protein Q8Y863 (*pdhC*, Fig. 4A) *via* fluorescent SDS-PAGE analysis. While the ten compounds (**16 – 25**) derived from the virtual ZINC database screen largely lacked significant competition with the probe, the rationally designed **C3** and **LAMe** compounds turned out to be potent with a gel-based EC$_{50}$ value of about 210 nM and 330 nM, respectively (calculated for the residual in-gel modification of Q8Y863 – *pdhC*; Fig. 4B, S8A). This value is in the same range as competition with **LA** (100 nM) and 10-fold more potent than competition with the substrate analog **BrO** (2.3 µM). In addition, to verify that **C3** is an LPL inhibitor and not metabolized to release **LA** after possible enzymatic amide cleavage in the cell, we demonstrated its stability in lysate over time with an HPLC-MS-based assay (Fig. S8B). In line with the lack of LPL enzymes in humans,[10a] MTT studies in HeLa cells indicate low to moderate toxicity for **LAMe** and **C3**, respectively (Fig. S9A).

5

RESEARCH ARTICLE
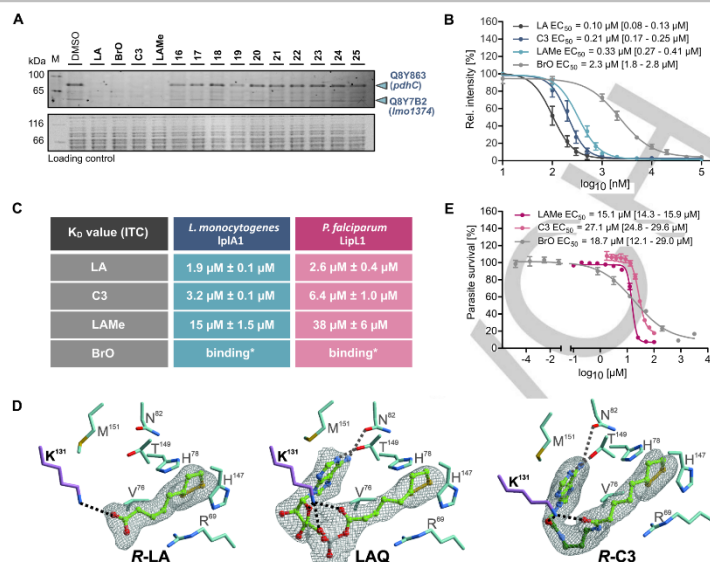
Figure 4. Identification and validation of LPL inhibitors in *L. monocytogenes* (blue) and *P. falciparum* (magenta). (A) A competitive screen of the 12 selected potential inhibitors in 10-fold excess (1 mM) compared to probe **2** (100 μM, 2h) was performed in intact *L. monocytogenes* cells to identify cell-permeable LPL inhibitors by measuring the decreased fluorescent signals of reporter proteins. SDS-PAGE with fluorescent analysis was performed, and blue arrows indicate reporter proteins Q8Y863 (*pdhC*) and Q8Y7B2 (*lmo1374*). Coomassie stain served as loading control, and 'M' indicates a protein marker. (B) EC₅₀ value determination of corresponding gel-based *in-situ* competitive labeling studies in *L. monocytogenes* cells with identified inhibitors **C3** and **LAMe** versus probe **2** (100 μM, 2h). Fluorescent signal intensities for Q8Y863 (Fig. S8A) were analyzed by ImageJ. The analysis, plotted with mean values and error bars indicating SEM, was performed in n = 3 independent experiments, and competition with **LA** and **BrO** served as benchmarks. The error range is shown as 95% confidence interval. (C) Recombinant *L. monocytogenes* lplA1 and *P. falciparum* LipL1 proteins were analyzed by ITC to separately verify the binding trends of inhibitors **C3** and **LAMe** towards LPL compared to **LA** and **BrO**. The experiments were measured at least in duplicates (n ≥ 2). Asterisk marks indicate qualitative ligand binding as low enthalpy change prevented quantification. (D) Co-crystallization studies with *L. monocytogenes* lplA1 and ligands (*R*-LA, PDBID 8crl, left; **LAQ**, PDBID 8crj, middle; *R*-C3, PDBID 8crl, right) with respective 2Fo-Fc electron density maps (grey mesh, contoured to 1.0 σ) and amino acid interactions are depicted as a close-up of the active pocket. The analysis shows binding of *R*-C3 as intermediate mimic with Lys131 (plume) as a key interaction for coordination of the lipoyl-domain and adenine unit. (E) Blood-stage *P. falciparum* parasites were incubated in presence of **LAMe, C3**, and **BrO** concentration-dependently to measure parasite growth inhibition. Growth experiments were performed in quadruplicates (n = 4) in two individual experiments. Mean values were plotted, and error bars represent SEM. The error range is shown as 95% confidence interval.

Accordingly, labeling with the non-toxic probe **2** (Fig. S9A) in mammalian HeLa cells revealed no characteristic hits (Fig. S9B). We independently confirmed a high affinity for **C3** and **LAMe** with K_D values of 3.2 μM and 15 μM, respectively, which is again similar to the value of **LA** (K_D = 1.9 μM). By contrast, the affinity of **BrO** was very low, and hence, binding could not be quantified (Fig. 4C, S10A).

Based on these results, we aimed to better rationalize the binding mode of **C3** in *L. monocytogenes* lplA1 and performed x-ray crystallography. So far, no experimental structural information of *L. monocytogenes* lplA1 is available, and we thus attempted to co-crystallize **LAQ** as the native intermediate. We noted that the C-terminus is flipped in the lplA1:**LAQ** complex (PDBID 8crj) in comparison to the predicted apo-AF2 structure (Fig. S11A-B), which is in agreement with a previously co-crystallized homologous enzyme.[25a] However, the AF2 structure perfectly aligns with the co-crystals of **C3** (PDBID 8crl) and **LA** (PDBID 8cri), which confirms previous computational analysis (Fig. S11B). Of note, we were able to co-crystallize **LA, LAQ,** and **C3** solely as *R*-enantiomers and demonstrate inhibitor binding in the active pocket as a chemically stable **LAQ** analog (Fig. 4D). Interestingly,

C3 as an **LAQ** mimic could not induce the flip of the C-terminal domain (Fig. S11B) as, *e.g.*, crucial interactions with the phosphate and Lys131 are lacking, which offers a potential avenue for inhibitor refinement (Fig. 4D).

Due to the structurally conserved binding pocket of *L. monocytogenes* lplA1 and *P. falciparum* LipL1 (Fig. 3B, S5), we performed ITC studies with the recombinant ligase of the parasite, demonstrating a comparably high binding affinity of **LA** (K_D = 2.6 μM) and **C3** (K_D = 6.4 μM) followed by **LAMe** (K_D = 38 μM, Fig. 4C, S10B). To evaluate the effects of **C3** and **LAMe** on the growth of **LA** auxotroph organisms, we tested the compounds against *L. monocytogenes* and *P. falciparum*. While we did not observe any effects on the growth of the bacterial strain, even in macrophage infection assays (Fig. S12), **LAMe** and **C3** killed blood-stage *P. falciparum* with EC₅₀ values of 15 μM and 27 μM, respectively (Fig. 4E). Although the benchmark inhibitor **BrO** achieved a similar EC₅₀ value, effective parasite eradication required millimolar concentrations, corroborating previous literature reports.[12a] Thus, these novel compounds represent the most potent LPL inhibitors reported to date.

6

RESEARCH ARTICLE

Conclusion

Lipoylation is a crucial post-translational modification which enables the catalysis of essential cellular processes, such as the oxidative decarboxylation of pyruvate to acetyl-CoA (pyruvate dehydrogenase).[8] As human and pathogenic cells differ in the salvage pathways for **LA**, selective inhibitors of pathogenic lipoate protein ligase represent an attractive strategy to develop anti-infective therapies.[13d] However, tools to directly monitor LPL activity in living cells have been elusive so far.

We developed a cell-permeable lipoylation-probe (probe **2**) that utilizes LPL to modify **LA**-dependent enzymes covalently and thus serves as proxy for its activity. This *in-situ* labeling strategy exhibits several benefits over screens against recombinant LPL, including the direct readout of cell permeability and sufficient *in-situ* target engagement. Mass spectrometry confirmed the specificity of probe **2** for intracellular lysine residues in **LA**-dependent proteins. Based on this proof-of-concept, we designed a small virtual compound library by computational methods and identified two cell-permeable and potent active site LPL inhibitors, namely **C3** and **LAMe**. Co-crystallization of **C3** provided intriguing insights into LPL inhibition as the compound forms strong bonds with Lys131 in *L. monocytogenes* lplA1. However, no antibiotic activity was observed in *L. monocytogenes*, even though previous work showed that lplA1 is essential for the growth of bacteria in macrophages.[11a, 11b] We confirmed uptake and stability of **C3** in *L. monocytogenes*, raising the possibility that the lack of antibiotic activity could be due to strong competition with **LA** during salvage. Further modification of the inhibitor (*e.g.,* mimicking the interaction of **LAQ** phosphate with Lys131 as observed in crystal structures) could improve competition with **LA**. Based on the conserved three-dimensional fold and active site pockets, we tested **C3** and **LAMe** against *P. falciparum* to see if these molecules may inhibit LPLs across species. Indeed, we saw killing of blood-stage parasites with both inhibitors, validating our approach.

Overall, we showcase LPL-dependent probes as ideal tools for identifying **LA** salvage pathway inhibitors with effective *in-situ* activity against the malaria-causing parasite *P. falciparum*. As an outlook, iterative cycles of pre-selected computational compounds followed by intracellular LPL profiling will minimize the overall experimental effort and enhance the chances of cell-permeable hit molecules with high potency.

Acknowledgments

Author Contributions

JND and SAS conceived and designed the project. JND performed synthesis, labeling, mass spectrometry, protein purifications, ITC studies, and biological assays. SYC and MH ran docking studies and molecular dynamics simulations. MG performed crystallography with help of JND. MS conducted assays with parasites in cell culture. SMH provided isoDTB tags and assisted with the evaluation of binding site identification. SAS, JND, and SYC wrote the manuscript with input of all authors.

Conflict of Interest

The authors declare no conflict of interest.

Data Availability Statement

The proteomics data have been deposited to the ProteomeXchange Consortium[31] *via* the PRIDE[32] partner repository, which can be accessed with the identifier PXD040359. All new crystal structures have been deposited in the RCSB Protein Data Bank (PDB) with the depository numbers 8cri, 8crj, 8crl.[33] Analyzed proteomics data and comprehensive ZINC database[27] screen hits are presented in supplementary files.

Keywords: anti-infectives · cofactors · drug discovery · lipoic acid · proteomics

[1] A. Kirschning, *Angewandte Chemie International Edition* **2021**, *60*, 6242-6269.
[2] A. Ganesan, *Philosophical Transactions of the Royal Society B: Biological Sciences* **2018**, *373*, 20170069.
[3] a) A. Hoegl, M. B. Nodwell, V. C. Kirsch, N. C. Bach, M. Pfanzelt, M. Stahl, S. Schneider, S. A. Sieber, *Nature Chemistry* **2018**, *10*, 1234-1245; b) M. Pfanzelt, T. E. Maher, R. M. Absmeier, M. Schwarz, S. A. Sieber, *Angewandte Chemie International Edition* **2022**, *61*, e202117724.
[4] a) I. V. L. Wilkinson, M. Bottlinger, Y. El Harraoui, S. A. Sieber, *Angewandte Chemie International Edition* **2022**, *62*, e202212111; b) R. A. Homan, A. M. Jadhav, L. P. Conway, C. G. Parker, *J Am Chem Soc* **2022**, *144*, 15013-15019.
[5] a) M. J. Evans, B. F. Cravatt, *Chem Rev* **2006**, *106*, 3279-3301; b) B. F. Cravatt, A. T. Wright, J. W. Kozarich, *Annu Rev Biochem* **2008**, *77*, 383-414; c) M. G. Paulick, M. Bogyo, *Current Opinion in Genetics & Development* **2008**, *18*, 97-106.
[6] I. V. L. Wilkinson, M. Pfanzelt, S. A. Sieber, *Angewandte Chemie International Edition* **2022**, *61*, e202201136.
[7] a) A. Solmonson, R. J. DeBerardinis, *Journal of Biological Chemistry* **2018**, *293*, 7522-7530; b) M. D. Spalding, S. T. Prigge, *Microbiol Mol Biol Rev* **2010**, *74*, 200-228; c) E. A. Rowland, C. K. Snowden, I. M. Cristea, *Curr Opin Chem Biol* **2018**, *42*, 76-85; d) J. E. Cronan, *Microbiology and Molecular Biology Reviews* **2016**, *80*, 429-450.
[8] R. N. Perham, *Annu Rev Biochem* **2000**, *69*, 961-1004.
[9] Q. H. Christensen, J. A. Hagar, M. X. D. O'Riordan, J. E. Cronan, *Journal of Biological Chemistry* **2011**, *286*, 31447-31456.

7

RESEARCH ARTICLE

[10] a) J. E. Cronan, *Front Genet* **2020**, *11*, 510; b) X. Cao, L. Zhu, X. Song, Z. Hu, J. E. Cronan, *Proceedings of the National Academy of Sciences* **2018**, *115*, E7063-E7072.

[11] a) M. O'Riordan, M. A. Moors, D. A. Portnoy, *Science* **2003**, *302*, 462-464; b) K. M. Keeney, J. A. Stuckey, M. X. D. O'Riordan, *Molecular Microbiology* **2007**, *66*, 758-770; c) K. Keeney, L. Colosi, W. Weber, M. O'Riordan, *J Bacteriol* **2009**, *191*, 2187-2196; d) J.-D. Sauer, A. A. Herskovits, M. X. D. O'Riordan, *Microbiol Spectr* **2019**, *7*, 7.4.26; e) R. J. Premaratne, W. J. Lin, E. A. Johnson, *Appl Environ Microbiol* **1991**, *57*, 3046-3048.

[12] a) M. Allary, J. Z. Lu, L. Zhu, S. T. Prigge, *Molecular microbiology* **2007**, *63*, 1331-1344; b) C. Deschermeier, L.-S. Hecht, F. Bach, K. Rützel, R. R. Stanway, A. Nagel, F. Seeber, V. T. Heussler, *Cellular Microbiology* **2012**, *14*, 416-430.

[13] a) S. L. Rei Yan, F. Wakasuqui, X. Du, M. R. Groves, C. Wrenger, *Front Chem* **2021**, *9*, 742175-742175; b) S. Günther, K. Matuschewski, S. Müller, *PLoS One* **2009**, *4*, e5510; c) J. Storm, S. Müller, *Curr Pharm Des* **2012**, *18*, 3480-3489; d) C. Wrenger, S. Müller, *Molecular Microbiology* **2004**, *53*, 103-113; e) S. C. Nair, J. T. Munro, A. Mann, M. Llinás, S. T. Prigge, *Proceedings of the National Academy of Sciences* **2023**, *120*, e2210929120.

[14] G. A. Afanador, K. A. Matthews, D. Bartee, J. E. Gisselberg, M. S. Walters, C. L. Freel Meyers, S. T. Prigge, *Molecular Microbiology* **2014**, *94*, 156-171.

[15] B. Falkard, T. R. S. Kumar, L.-S. Hecht, K. A. Matthews, P. P. Henrich, S. Gulati, R. E. Lewis, M. J. Manary, E. A. Winzeler, P. Sinnis, S. T. Prigge, V. Heussler, C. Deschermeier, D. Fidock, *Cellular Microbiology* **2013**, *15*, 1585-1604.

[16] M. J. Crawford, N. Thomsen-Zieger, M. Ray, J. Schachtner, D. S. Roos, F. Seeber, *The EMBO Journal* **2006**, *25*, 3214-3222.

[17] Q. Tang, Y. Guo, L. Meng, X. Chen, *Angewandte Chemie International Edition* **2021**, *60*, 4028-4033.

[18] S. Lai, Y. Chen, F. Yang, W. Xiao, Y. Liu, C. Wang, *J Am Chem Soc* **2022**, *144*, 10320-10329.

[19] M. Fernández-Suárez, H. Baruah, L. Martínez-Hernández, K. T. Xie, J. M. Baskin, C. R. Bertozzi, A. Y. Ting, *Nat Biotechnol* **2007**, *25*, 1483-1487.

[20] W. Zhong, B. Sun, C. Lu, H. Yu, C. Wang, L. He, J. Gu, S. Chen, Y. Liu, X. Jing, Z. Bi, G. Yang, H. Zhou, T. Sun, C. Yang, *Sci Rep* **2016**, *6*, 35579.

[21] L. Tan, S. Maji, C. Mattheis, Y. Chen, S. Agarwal, *Macromolecular Bioscience* **2012**, *12*, 1721-1730.

[22] K. Fujiwara, S. Toma, K. Okamura-Ikeda, Y. Motokawa, A. Nakagawa, H. Taniguchi, *Journal of Biological Chemistry* **2005**, *280*, 33645-33651.

[23] P. R. A. Zanon, L. Lewald, S. M. Hacker, *Angewandte Chemie International Edition* **2020**, *59*, 2829-2836.

[24] UniProt Consortium, *Nucleic Acids Research* **2023**, *51*, D523-D531.

[25] a) K. Fujiwara, N. Maita, H. Hosaka, K. Okamura-Ikeda, A. Nakagawa, H. Taniguchi, *Journal of Biological Chemistry* **2010**, *285*, 9971-9980; b) A. J. Guerra, G. A. Afanador, S. T. Prigge, *Proteins: Structure, Function, and Bioinformatics* **2017**, *85*, 1777-1783.

[26] M. Mirdita, K. Schütze, Y. Moriwaki, L. Heo, S. Ovchinnikov, M. Steinegger, *Nat Methods* **2022**, *19*, 679-682.

[27] J. J. Irwin, T. Sterling, M. M. Mysinger, E. S. Bolstad, R. G. Coleman, *Journal of Chemical Information and Modeling* **2012**, *52*, 1757-1768.

[28] D. R. Koes, C. J. Camacho, *Nucleic Acids Research* **2012**, *40*, W409-W414.

[29] J. Feng, A. S. Paparella, G. W. Booker, S. W. Polyak, A. D. Abell, *Antibiotics* **2016**, *5*, 26.

[30] J. Feng, A. S. Paparella, W. Tieu, D. Heim, S. Clark, A. Hayes, G. W. Booker, S. W. Polyak, A. D. Abell, *ACS Med Chem Lett* **2016**, *7*, 1068-1072.

[31] J. A. Vizcaíno, E. W. Deutsch, R. Wang, A. Csordas, F. Reisinger, D. Ríos, J. A. Dianes, Z. Sun, T. Farrah, N. Bandeira, P.-A. Binz, I. Xenarios, M. Eisenacher, G.

Mayer, L. Gatto, A. Campos, R. J. Chalkley, H.-J. Kraus, J. P. Albar, S. Martinez-Bartolomé, R. Apweiler, G. S. Omenn, L. Martens, A. R. Jones, H. Hermjakob, *Nat Biotechnol* **2014**, *32*, 223-226.

[32] Y. Perez-Riverol, A. Csordas, J. Bai, M. Bernal-Llinares, S. Hewapathirana, D. J. Kundu, A. Inuganti, J. Griss, G. Mayer, M. Eisenacher, E. Pérez, J. Uszkoreit, J. Pfeuffer, T. Sachsenberg, Ş. Yılmaz, S. Tiwary, J. Cox, E. Audain, M. Walzer, A. F. Jarnuczak, T. Ternent, A. Brazma, J. A. Vizcaíno, *Nucleic Acids Research* **2019**, *47*, D442-D450.

[33] H. M. Berman, J. Westbrook, Z. Feng, G. Gilliland, T. N. Bhat, H. Weissig, I. N. Shindyalov, P. E. Bourne, *Nucleic Acids Research* **2000**, *28*, 235-242.

8

RESEARCH ARTICLE

Entry for the Table of Contents
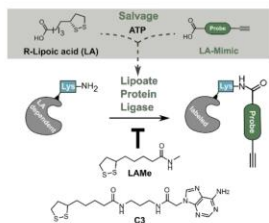
Distinct from humans, lipoic acid (**LA**) salvage by lipoate protein ligase (LPL) is an essential scavenging pathway for auxotrophic bacteria and parasites. Probes as **LA**-mimics were designed and shown to label **LA**-dependent proteins in living cells on lysines. This tool enabled us to perform competitive screens in order to identify two cell-permeable LPL inhibitors with activity against *P. falciparum* in erythrocytes.

Institute and/or researcher Twitter usernames: @SieberLab, @StephanHacker2

WG: Copyright Agreement for Dissertation Thesis

Rights DE <RIGHTS-and-LICENCES@wiley-vch.de>

Fr 02.06.2023 12:00

An:Jan-Niklas Dienemann <jan-niklas.dienemann@tum.de>;

Dear Jan-Niklas Dienemann,

The requested material is from an Open Access article, please see copyright holder below. You may re-use the material provided re-use is accordance with the conditions of the license (we have included the link to the CC-license below):

Kind regards

Bettina Loycke
Senior Rights Manager
Rights & Licenses

Wiley-VCH GmbH
Boschstraße 12
69469 Weinheim
Germany
www.wiley-vch.de

T   +(49) 6201 606-280
F   +(49) 6201 606-332
rightsDE@wiley.com

WILEY

Von: Jan-Niklas Dienemann <jan-niklas.dienemann@tum.de>
Gesendet: Freitag, 2. Juni 2023 09:11
An: Angewandte <angewandte@wiley-vch.de>
Betreff: Copyright Agreement for Dissertation Thesis

🚫 This is an external email.

Dear Sir or Madam,

in order to finish my PhD after my paper (https://doi.org/10.1002/anie.202304533) got accepted on 30th May by you as open access article, I would need an official statement for re-use of the article in my dissertation/thesis for "electronic and print" use.

Could you please provide me with such a statement as soon as possible, as it is the only document missing prior to submit my thesis?

Thank you very much for your understanding and for your help.

Best,

Jan-Niklas Dienemann

3.1 Supporting figures and schemes
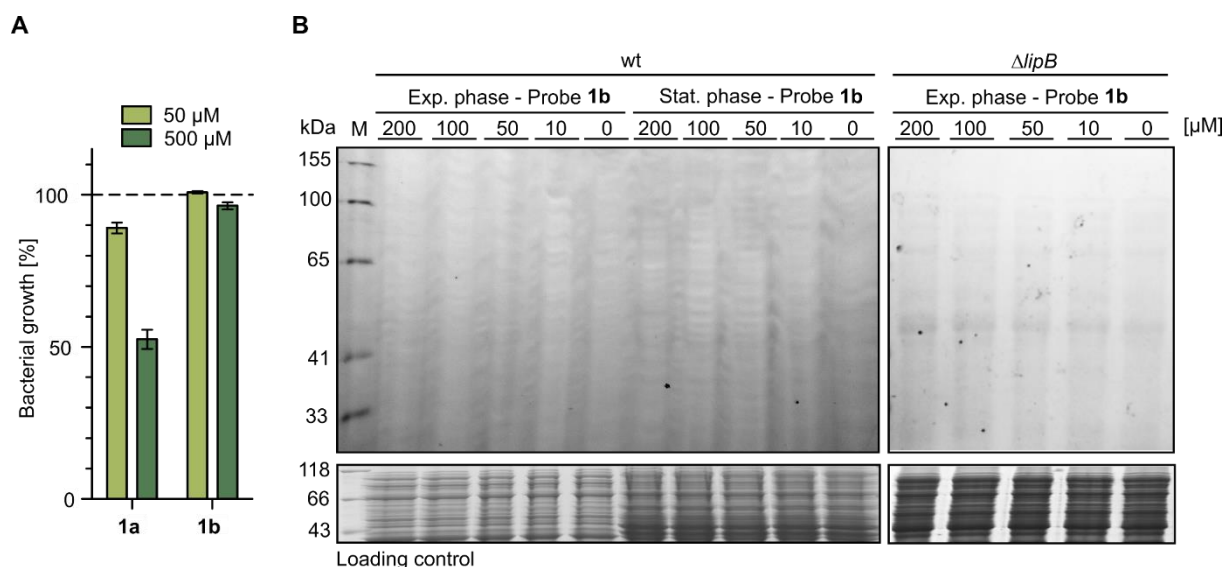
Supporting Figure S1. Application of the C8-fatty acid-based probes **1a** and **1b** in *E. coli*. (A) The growth of *E. coli* Δ*lipB* at 37 °C in presence of 50 µM and 500 µM probe **1a** and **1b** was referenced to DMSO treatment (100%). The azide probe **1a** impaired the bacterial growth, indicating toxicity. The measurements were performed in triplicates in two independent experiments and error bars represent SEM. (B) Analytical labeling with probe **1b** (2h, 0 – 200 µM) of intact *E. coli* wild type (wt) cells in exponential and stationary phase as well as Δ*lipB* mutant cells in exponential phase. No concentration-dependent fluorescent labeling was observed. 'M' represents a marker as a protein size reference. Coomassie staining served as loading control.
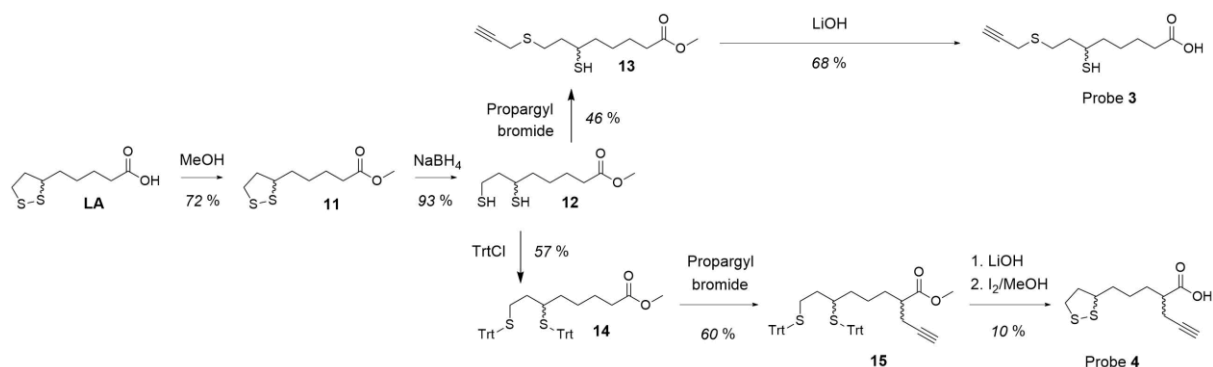

Supporting Scheme S1. Synthesis of probe **3** and probe **4**. **LA** was protected as methyl ester (**11**) and reduced to open the dithiolane ring.[2] This oxidation sensitive key intermediate **12** was either selectively propargylated to compound **13** and further deprotected to obtain probe **3**, or both thiol groups were protected by tritylation (**14**) prior to installation of the propargyl-handle at position 2 (**15**). Global deprotection by saponification and oxidation yielded probe **4**.
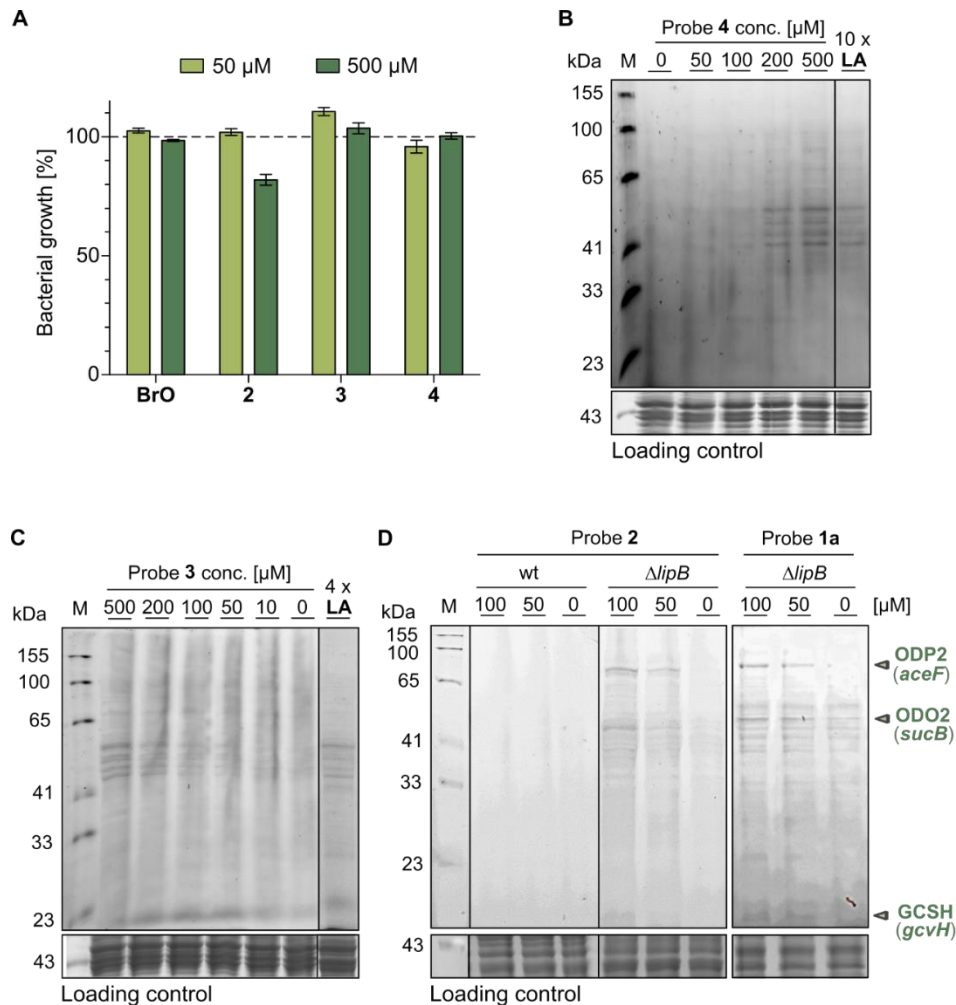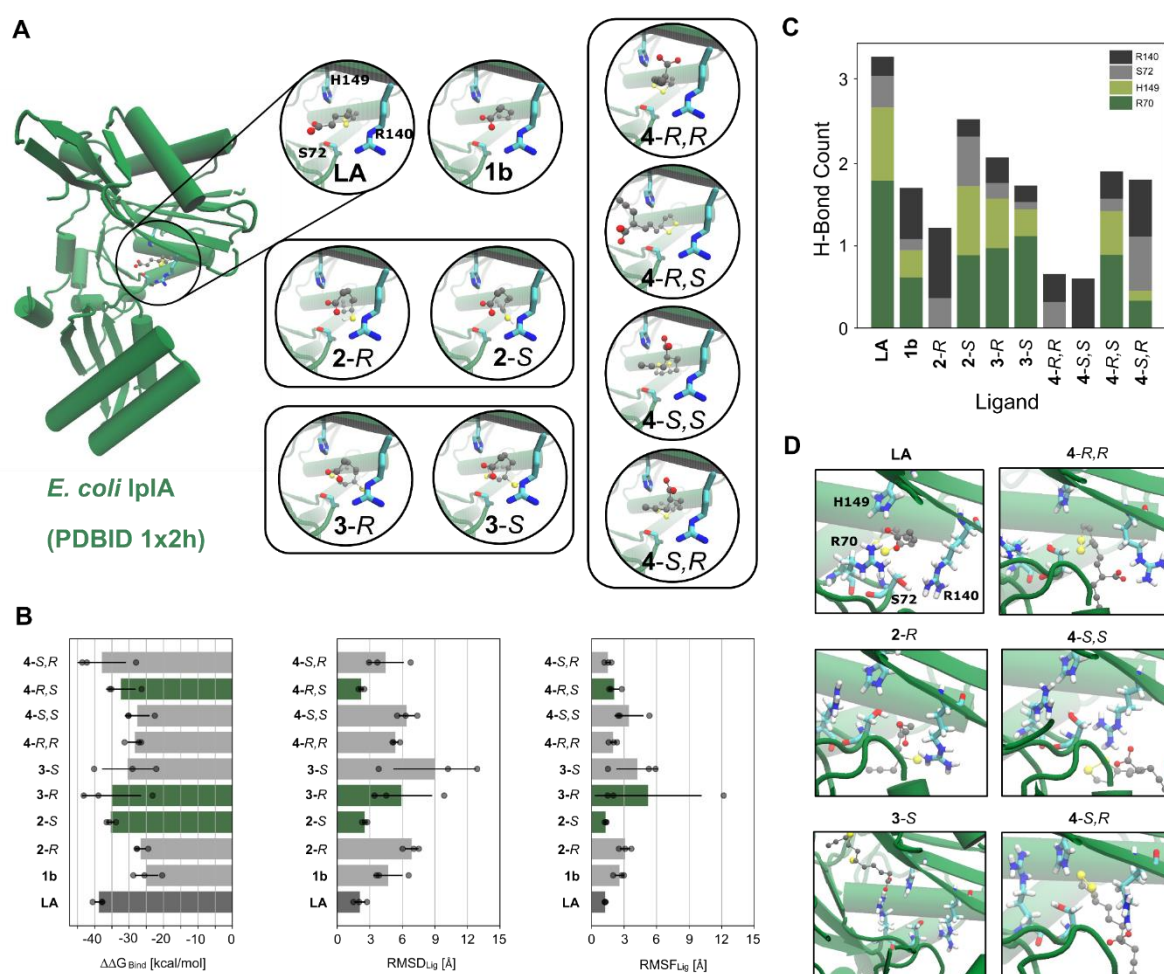
Supporting Figure S2. Determination of the probes' bacterial toxicity and their labeling properties in *E. coli*. (A) *E. coli* Δ*lipB* cells were grown at 37 °C in presence of probes **2** – **4** and **BrO** as benchmark (50 µM, 500 µM) to determine the effect on bacterial growth as a measure of cytotoxicity. Values were referenced to DMSO treatment, and experiments were carried out in two independent experiments in triplicates. Error bars represent SEM. (B+C) Analytical concentration-dependent labeling of intact *E. coli* Δ*lipB* cells with probe **4** (0 µM – 500 µM, 2h; B) and probe **3** (0 µM – 500 µM, 2h; C) showed high background labeling with similar pattern. No fluorescence bands could be competed with excess treatment of **LA** (2 mM **LA** versus 200 µM probe **4**, 10-fold excess; 2 mM **LA** versus 500 µM probe **3**), indicating unspecific protein binding unrelated to lipoylation metabolism. (D) Analytical concentration-dependent labeling (0 µM – 100 µM, 2h) of intact *E. coli* wild type (wt) and Δ*lipB* cells with probe **2** showed that labeling of lipoate-dependent proteins *via* LPL could not compete with the *de novo* biosynthesis of lipoate. However, probe **2** showed more specific labeling of lipoate-dependent proteins in comparison to the azide-containing fatty acid probe **1a** which was demonstrated as partially toxic (Fig. S1A) and to label more background. Coomassie staining as loading control indicates equal protein amounts, and 'M' indicates markers as protein size references.
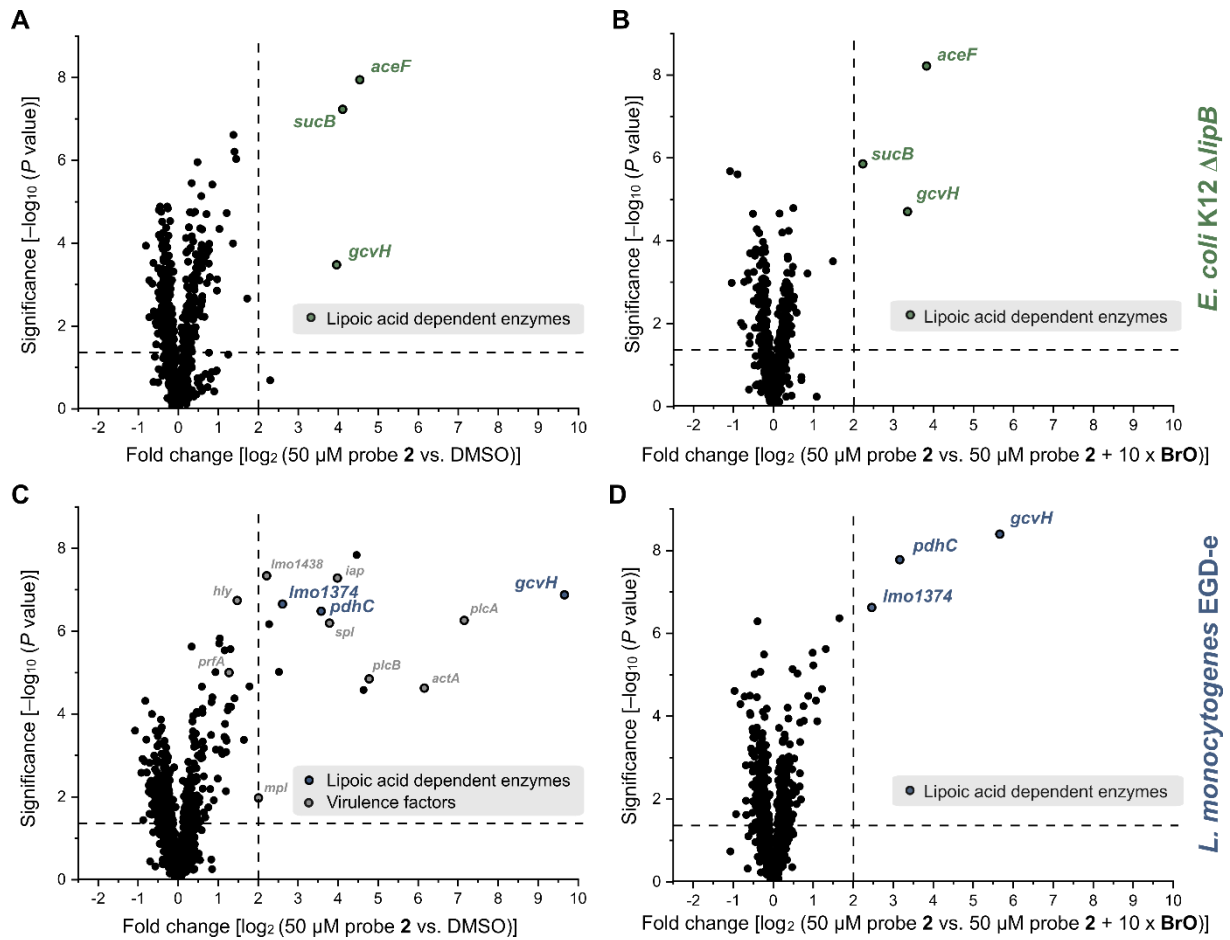
Supporting Figure S3. *In-situ* preparative labeling results of *E. coli* Δ*lipB* cells and *L. monocytogenes* wild type cells with probe **2** (50 µM, 2h) are depicted in volcano plots. Gene names of corresponding protein products are presented in italic. The threshold lines in volcano plots indicate 4-fold enrichment and a –log$_{10}$ *P* value of 1.3 (two-sided two-sample *t*-test, *n* = 4 independent experiments per group). The volcano plots for *E. coli* Δ*lipB* (green) present high specificity for **LA**-dependent proteins compared to DMSO treatment (A) as well as in a competition experiment with probe **2** (50 µM) and 10-fold **BrO** treatment (500 µM, B). The volcano plots for *L. monocytogenes* (blue) show labeling of **LA**-dependent proteins with virulence factors as off-targets (grey) compared to DMSO treatment (C) and shows high selectivity for solely **LA**-dependent enzymes in a competition experiment with probe **2** (50 µM) and 10-fold **BrO** treatment (500 µM, D). Further information of all hits can be found online in the Supporting_Excel_1_Mass_Spectrometry file.
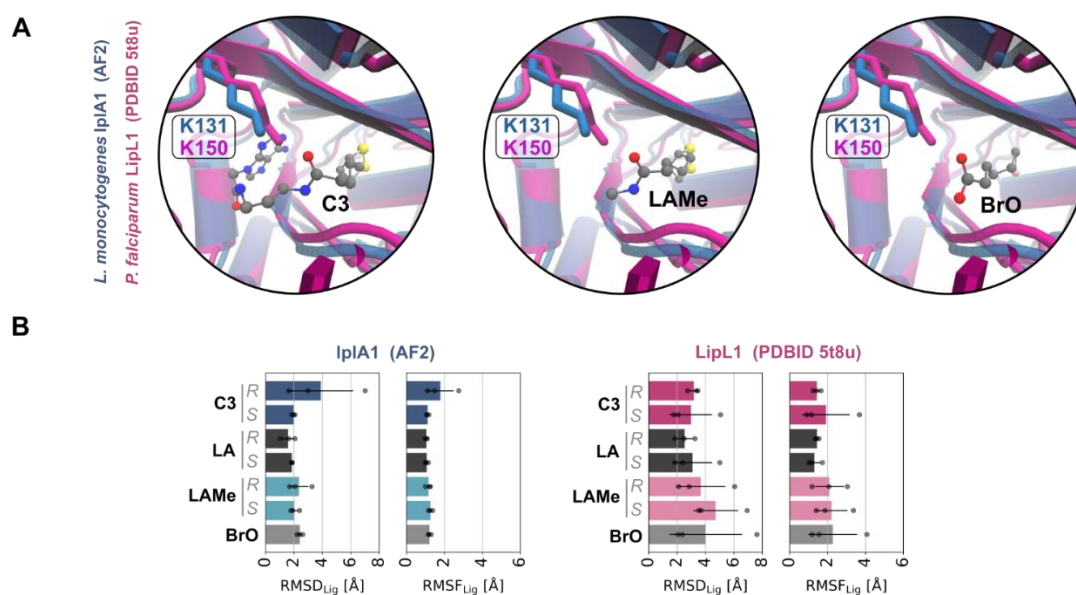
Supporting Figure S4. Molecular docking and molecular dynamics simulations on the native *R*-enantiomer of **LA** and the corresponding stereoisomers of the probes. (A) The *E. coli* lplA crystal structure (PDBID 1x2h, dark green)[3] is presented with its co-crystallized ligand **LA** as well as with the obtained docking poses of the 9 probe stereoisomers (**1b** – **4**). In case of probe **4**, the first given stereochemical information describes position 2 and the second one position 6. The interacting residues H149, S72 and R140 inside the pocket are highlighted in cyan. (B) The evaluation of molecular dynamics simulations of **LA** (dark grey) and the nine probe candidates bound to *E. coli* lplA (PDBID 1x2h),[3] including calculated binding free energies ($\Delta\Delta G_{Bind}$, left), root-mean square deviation (RMSD$_{Lig}$, middle), and root-mean square fluctuation (RMSF$_{Lig}$, right). The calculations were run in *n* = 3 independent attempts and error bars represent SEM. Results that predict overall good performance for ligands are marked in dark green. (C) The average number of hydrogen bond formations between probe candidates with R70 (dark green), H149 (bright green), S72 (bright grey) and R140 (dark grey) around the **LA** binding site in the last quarter of three simulations are shown. (D) Representative snapshots of **LA** and probe candidates **2**-*R*, **3**-*S*, **4**-*R,R*, **4**-*S,S* and **4**-*S,R* at the end of molecular dynamics simulations (400 ns) are depicted, highlighting deviated binding orientations in comparison to **LA**.
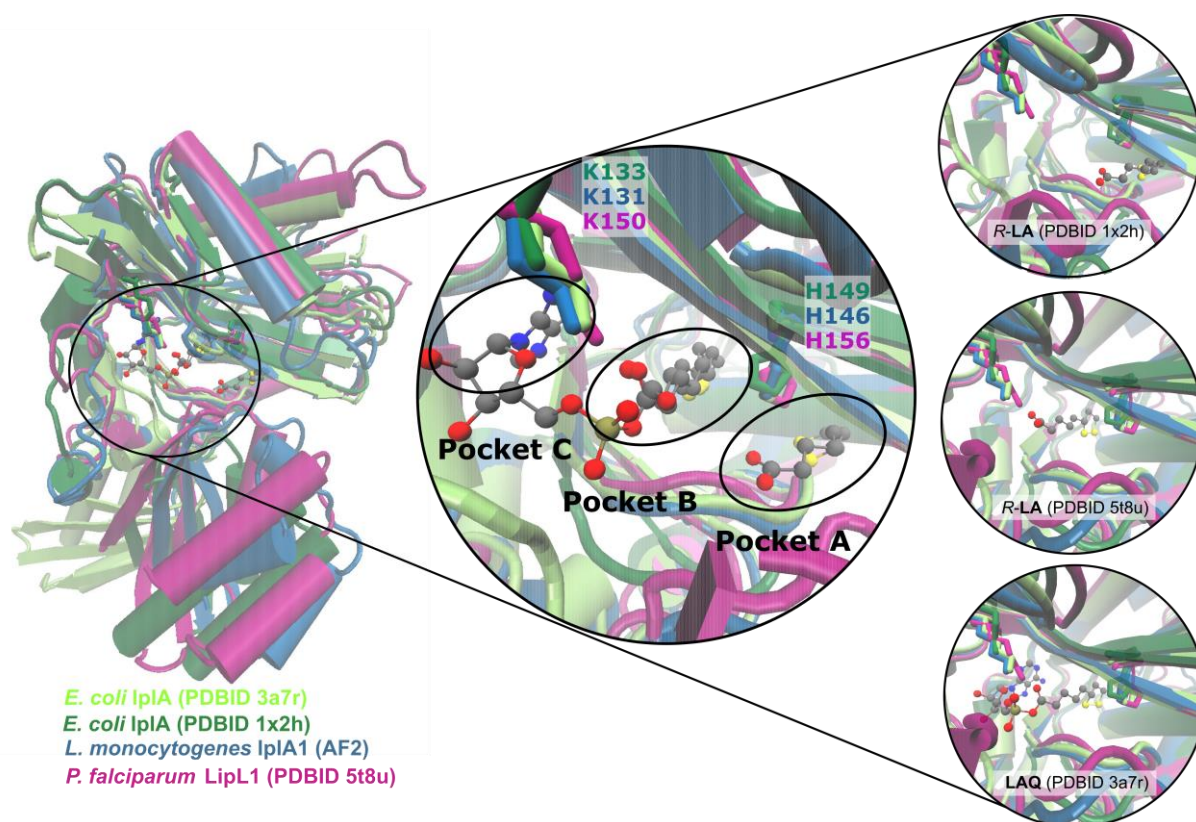
Supporting Figure S5. Alignment of LPL from *E. coli* (lplA, PDBID 1x2h, **LA**-bound crystal, dark green; PDBID 3a7r, **LAQ**-bound crystal, bright green), *L. monocytogenes* (lplA1, AF2 prediction, apo-form, blue) and *P. falciparum* (LipL1, PDBID 5t8u, **LA**-bound crystal, magenta) shows high structural similarity of the active site pocket (represented by lysine and histidine residues) with differences in the C-terminal protein domain (south) that was previously shown to be flexible depending on the protein-ligand interaction state.[3-4] During catalysis, the *E. coli* lplA undergoes structural changes. The structure PDBID 1x2h (dark green)[3] represents the **LA** loading state (**LA** in pocket A) and the PDBID 3a7r structure (bright green)[4a] depicts the intermediate state with **LAQ** as native intermediate with the **LA** domain being shifted to pocket B and the adenine group placed in pocket C.
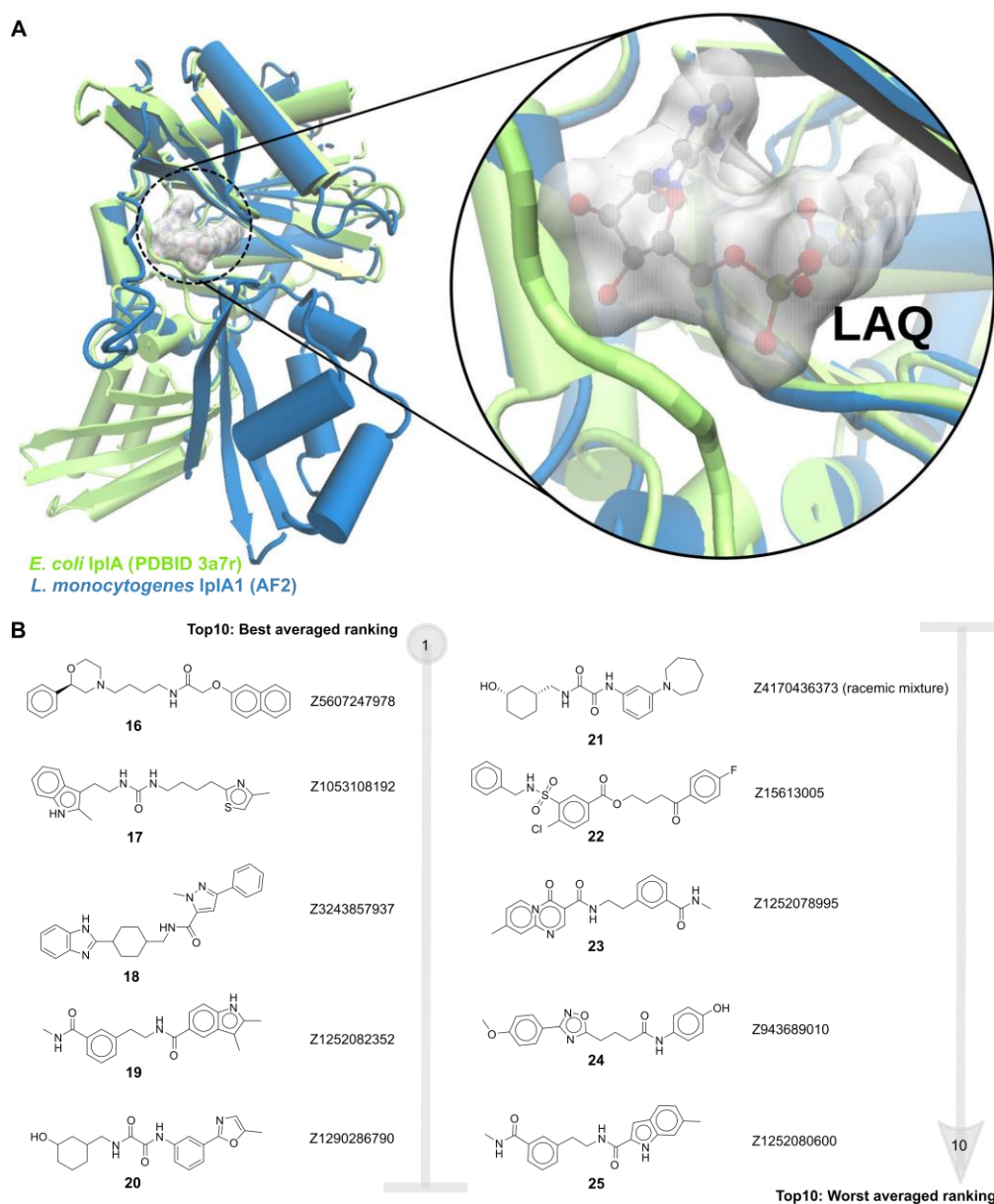
Supporting Figure S6. The pharmacophore search of the ZINC database was performed with *E. coli* lplA (PDBID 3a7r)[4a] based on the intermediate **LAQ** (A) to identify potential mimics which resulted in 126 hit compounds. These molecules were docked into *E. coli* lplA (PDBID 3a7r, green)[4a] as well as into the *L. monocytogenes* lplA1 structure (AF2, blue) as two representative LPL enzymes with different C-terminal orientation (south) to account for possible changes of the active pocket (online: Supporting_Excel_2_ZINC_Pharmacophore_Screen file, Supporting pyMOL file). (B) After filtering (see method section), the depicted ten compounds were purchased from Enamine for experimental validation. The number on the right to the molecule represents the Enamine ordering number.

Supporting Figure S7. Docking poses of potential inhibitors **C3** and **LAMe** (A, representative binding modes of *R*-enantiomers are shown) and their stability analysis (B) by molecular dynamics (MD) simulations in comparison to **LA** and **BrO** in *L. monocytogenes* lplA1 (AF2, blue) and *P. falciparum* LipL1 (PDBID 5t8u, magenta).[4b] RMSD_Lig and RMSF_Lig values are depicted as a measure of binding stability, demonstrating more stable binding of derivatives in lplA1. The calculations were run in *n* = 3 independent attempts and error bars represent SEM.
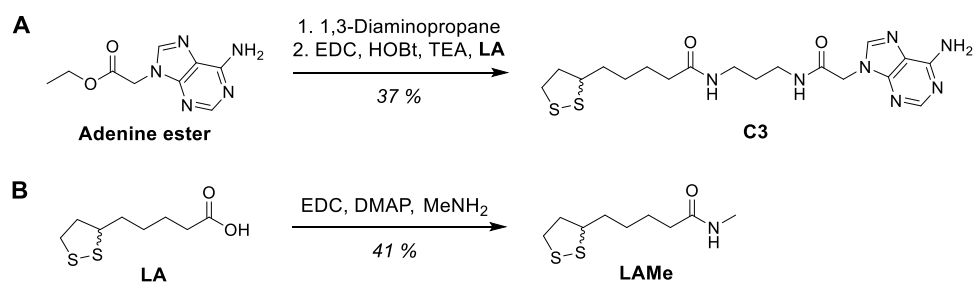
Supporting Scheme S2. Racemic synthesis of **C3** (A) and **LAMe** (B) by amide coupling as predicted LPL inhibitors.
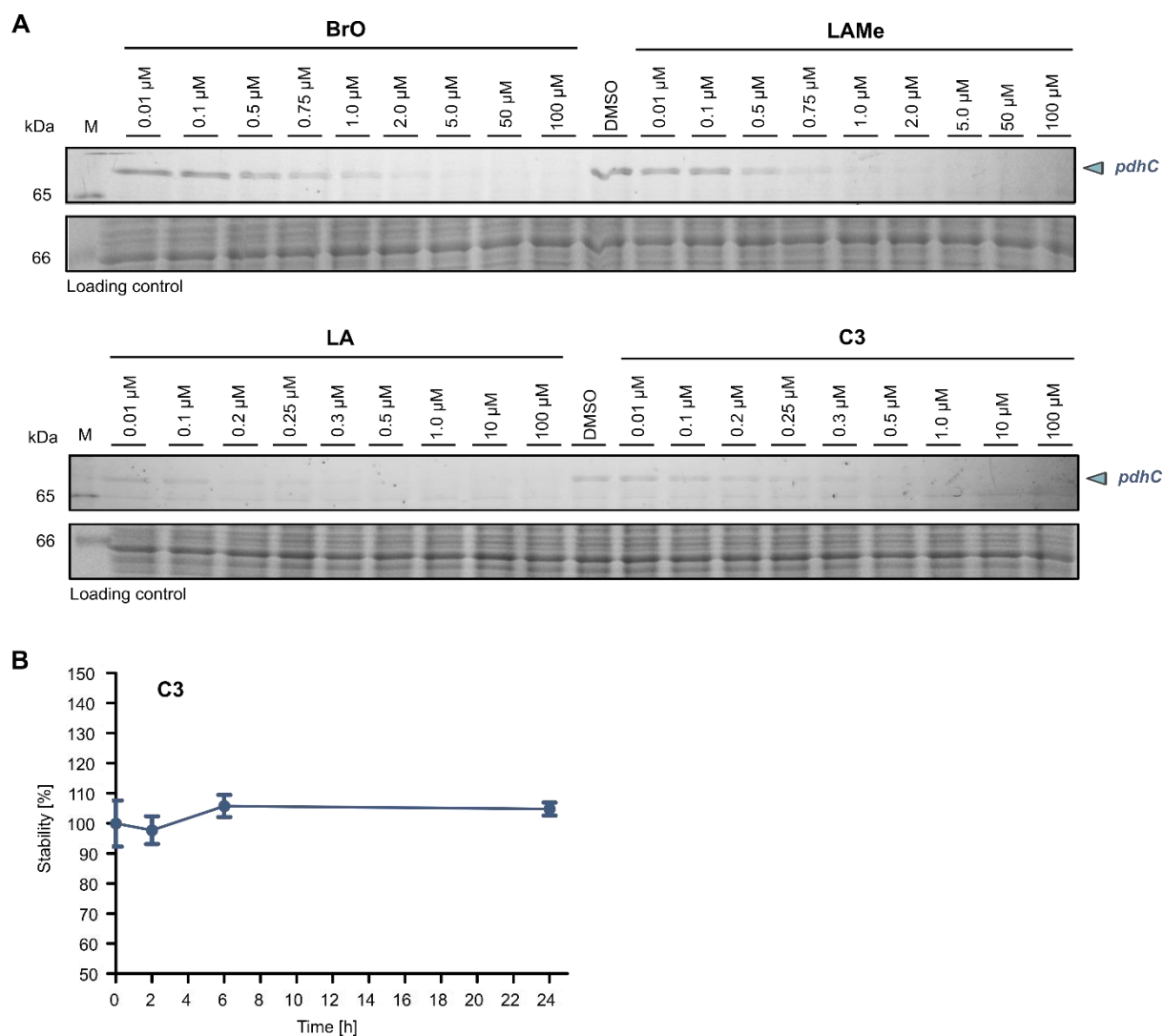
Supporting Figure S8. Investigation of intracellular binding affinity and stability of LPL substrates and inhibitors. (A) For intracellular EC_{50} determination, intact *L. monocytogenes* cells were treated concentration-dependently with compounds (**BrO**, **LAMe**, **LA**, **C3**) and probe **2** (100 µM). The residual fluorescent signals of the protein Q8Y863 (*pdhC*) indirectly reports compound binding affinities to LPL in competition to probe **2**. Coomassie staining proves equal protein amounts and 'M' represents a protein marker. The experiment was performed in three individual attempts (*n* = 3) and such a typical fluorescent analysis is represented. (B) The stability of compound **C3** was assessed by HPLC-MS in *L. monocytogenes* lysate after incubation for 0h, 2h, 6h, 24h. The measurement was carried out once with three technical replicates (*n* = 3). Error bars represent the SEM.
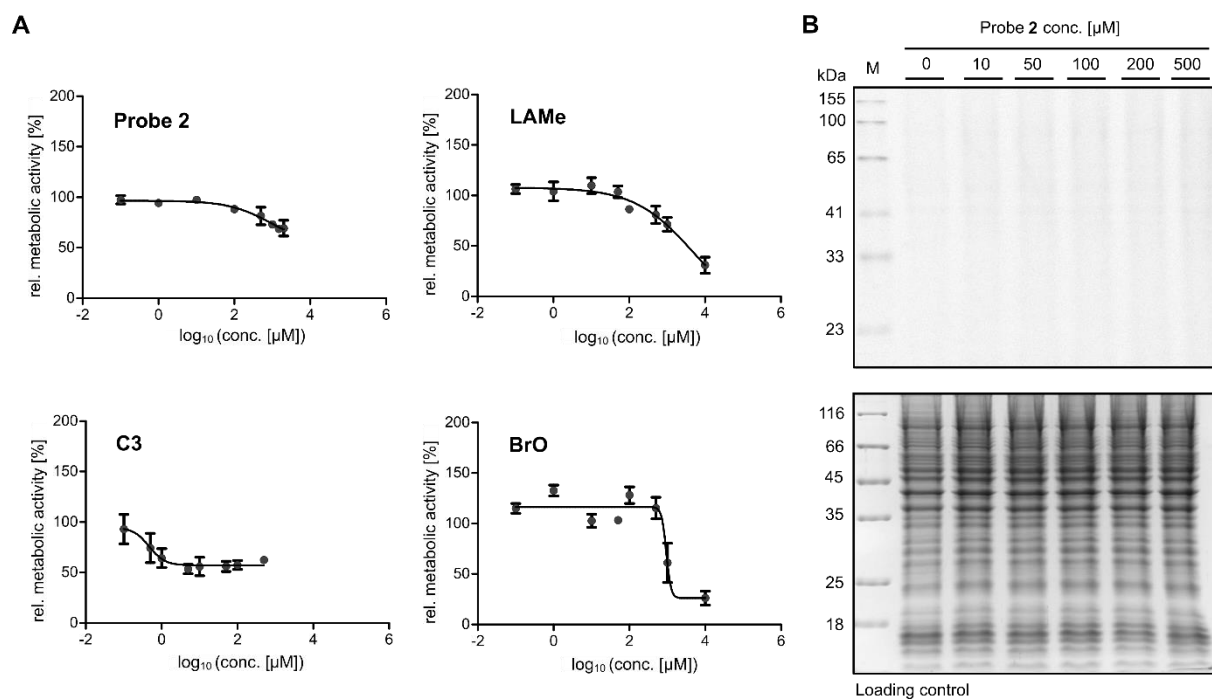
Supporting Figure S9. Application of LPL inhibitors and probe **2** in human cells. (A) HeLa cells were co-incubated with probe **2** (up to 2 mM), **C3** (up to 0.5 mM as solubility did not allow higher concentrations), **LAMe** and **BrO** (up to 10 mM) concentration-dependently for 24h and were analyzed for their remaining metabolic activity by 3-(4,5-Dimethylthiazol-2-yl)-2,5-diphenyltetrazoliumbromid (MTT) as a measure of compound toxicity. The experiments were performed in triplicates (n = 3) in at least two attempts. Mean values and a non-linear fit of such an experiment are shown exemplarily and error bars indicate SEM. (B) Intact HeLa cells were labeled concentration-dependently by probe **2** for 2h and analyzed by fluorescent SDS-PAGE analysis revealing no labeling as expected for the absence of LPL activity.[5] Coomassie staining served as loading control and 'M' indicates a protein marker.
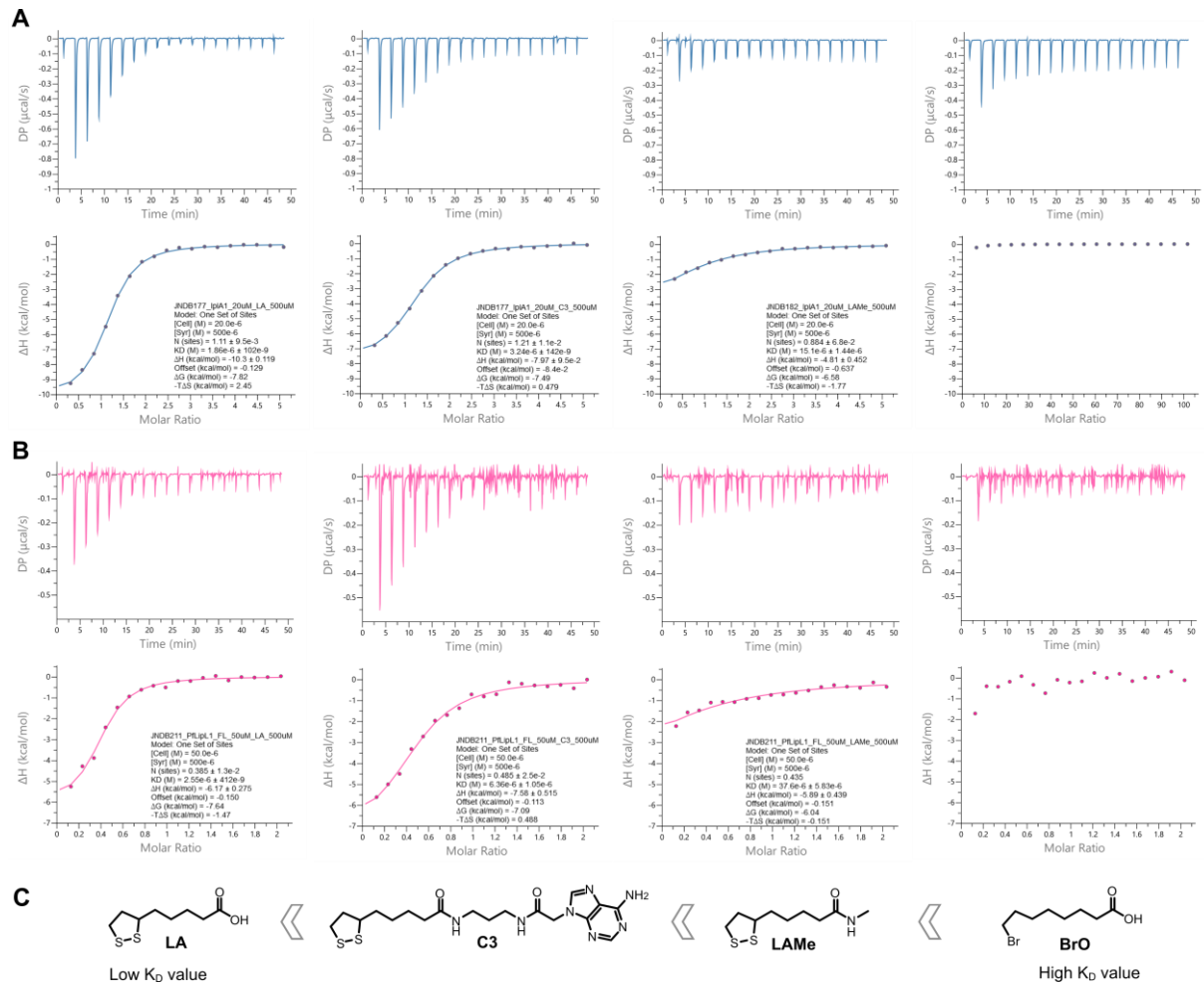
Supporting Figure S10. ITC measurements and analysis of recombinant *L. monocytogenes* lplA1 (A, blue, 20 μM) and *P. falciparum* LipL1 (B, magenta, 50 μM) proteins with compounds **LA** (500 μM), **C3** (500 μM), **LAMe** (500 μM) and **BrO** (10 mM, 500 μM, respectively) ordered from high to low LPL binding affinity (C). Experiments were performed at least twice (*n* ≥ 2) and representative examples are depicted. The same binding trend was observed for both proteins. Interestingly, lplA1 displayed lower K_D values for the same compounds compared to LipL1. For both ligases, the affinity to **BrO** is very low, and hence, binding could only be demonstrated qualitatively with 10 mM for lplA1 and 500 μM for LipL1 without further analysis. Of note, LipL1 precipitated during the experiments due to stirring which explains the observed low N-values and baseline instabilities (see method section).
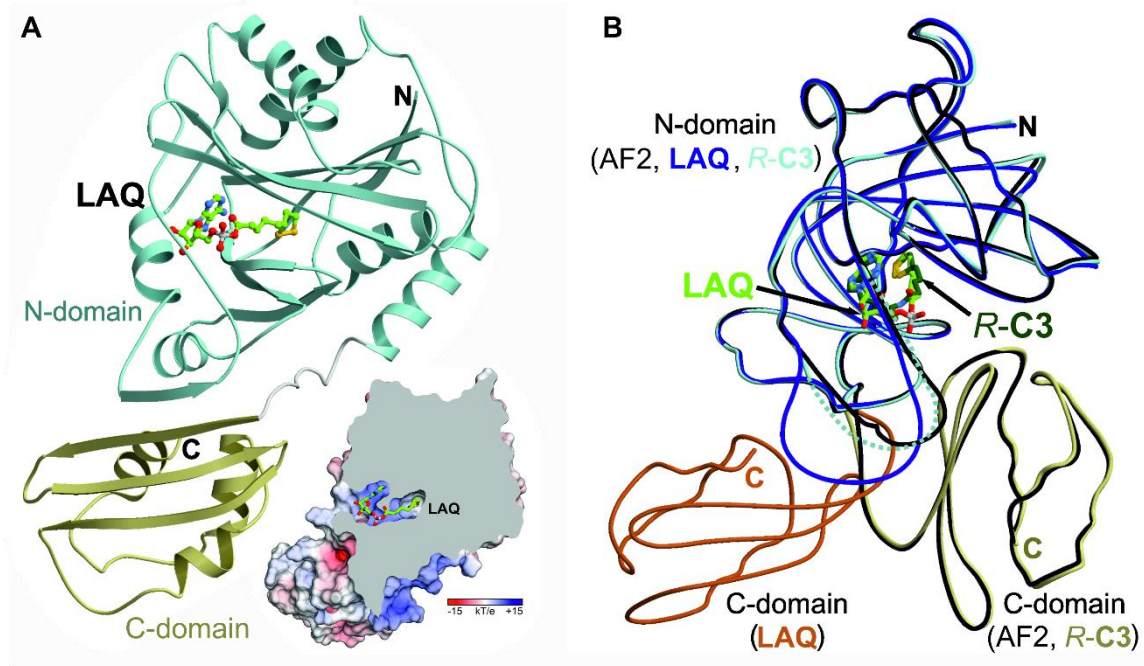
Supporting Figure S11. X-ray crystallography of *L. monocytogenes* lplA1. (A) The co-crystal of lplA1:**LAQ** (carbon atoms in green; PDBID 8crj) is depicted as a ribbon diagram consisting of a large N-terminal domain (1-241, cyan) and a small C-terminal domain (248-331, tan). Residues between the N- and C-domain are shown as grey coil. The surface cross section of the complex with colors indicates negative and positive electrostatic potentials and highlights the binding pocket. (B) The tube representation of the lplA1 prediction (AF2, black) perfectly aligns with the co-crystal of lplA1:*R*-**C3** (N-domain cyan, Pro165 – Ser180 unresolved due to flexibility; C-domain tan; PDBID 8crl) and lplA1:*R*-**LA** (PDBID 8cri, not shown), and hence, proves previous computational methods as valid (*R* indicates the absolute configuration of the stereocenter). The lplA1:**LAQ** complex (N-domain blue, C-domain orange) is stabilized after C-terminal rotation which holds the flexible loop in place. Despite different orientations of the C-domain, *R*-**C3** (dark green) still occupies the active pocket as intermediate mimic of **LAQ** (bright green).
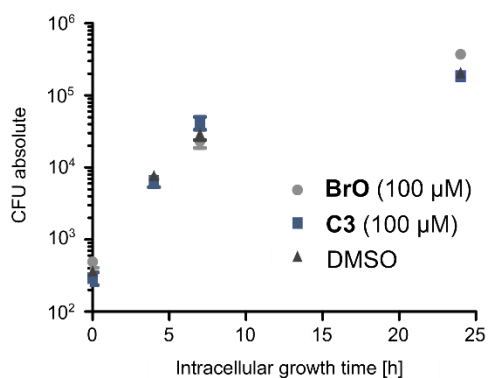
Supporting Figure S12. Intracellular growth assay of the Gram-positive bacterial strain *L. monocytogenes* inside mammalian cells in presence of LPL inhibitors. J774A.1 murine macrophage-like cells were infected in presence of 100 µM **C3** as the most potent LPL inhibitor, 100 µM **BrO** as weaker LPL inhibitor or DMSO with a naturally **LA** auxotrophic bacterial *L. monocytogenes* strain which relies on **LA** salvage. Cells were grown up to 24h to monitor intracellular bacterial growth. The experiment was performed in triplicates (*n* = 3) in two individual attempts, and mean values and error bars in SEM are shown. A previously reported lplA1 knockout mutant of *L. monocytogenes* showed a reduction of intracellular growth in these macrophages[6] and, hence, reduced growth of *L. monocytogenes* was also expected upon inhibition of LPL activity with a strong (**C3**) and weak inhibitor (**BrO**) in high concentrations in comparison to DMSO treatment.

3.2 References

[1]   a) M. Allary, J. Z. Lu, L. Zhu, S. T. Prigge, *Molecular Microbiology* **2007**, *63*, 1331-1344; b) G. A. Afanador, K. A. Matthews, D. Bartee, J. E. Gisselberg, M. S. Walters, C. L. Freel Meyers, S. T. Prigge, *Molecular Microbiology* **2014**, *94*, 156-171; c) C. Deschermeier, L.-S. Hecht, F. Bach, K. Rützel, R. R. Stanway, A. Nagel, F. Seeber, V. T. Heussler, *Cellular Microbiology* **2012**, *14*, 416-430; d) B. Falkard, T. R. S. Kumar, L.-S. Hecht, K. A. Matthews, P. P. Henrich, S. Gulati, R. E. Lewis, M. J. Manary, E. A. Winzeler, P. Sinnis, S. T. Prigge, V. Heussler, C. Deschermeier, D. Fidock, *Cellular Microbiology* **2013**, *15*, 1585-1604; e) M. J. Crawford, N. Thomsen-Zieger, M. Ray, J. Schachtner, D. S. Roos, F. Seeber, *The EMBO Journal* **2006**, *25*, 3214-3222.

[2]   N. Lakshminarayana, Y. Rajendra Prasad, L. Gharat, A. Thomas, P. Ravikumar, S. Narayanan, C. V. Srinivasan, B. Gopalan, *European Journal of Medicinal Chemistry* **2009**, *44*, 3147-3157.

[3]   K. Fujiwara, S. Toma, K. Okamura-Ikeda, Y. Motokawa, A. Nakagawa, H. Taniguchi, *Journal of Biological Chemistry* **2005**, *280*, 33645-33651.

[4]   a) K. Fujiwara, N. Maita, H. Hosaka, K. Okamura-Ikeda, A. Nakagawa, H. Taniguchi, *Journal of Biological Chemistry* **2010**, *285*, 9971-9980; b) A. J. Guerra, G. A. Afanador, S. T. Prigge, *Proteins: Structure, Function, and Bioinformatics* **2017**, *85*, 1777-1783.

[5]   J. E. Cronan, *Frontiers in Genetics* **2020**, *11*, 510.

[6]   a) M. O'Riordan, M. A. Moors, D. A. Portnoy, *Science* **2003**, *302*, 462-464; b) K. M. Keeney, J. A. Stuckey, M. X. D. O'Riordan, *Molecular Microbiology* **2007**, *66*, 758-770.

4|

Tailored cofactor traps for the in situ detection of hemithioacetal forming pyridoxal kinases

*These authors contributed equally.

Synopsis

A subclass of bacterial pyridoxal kinases (PLK)[1] utilizes a conserved lid-cysteine to transiently bind pyridoxal (**PL**) for catalyzing its phosphorylation into the active cofactor **PLP**. In order to block the enzymatic function by occupying the active pocket, the reversible binding aldehyde moiety of **PL** needs to be replaced through chemical synthesis to create an irreversible binder. Previously reported covalent cysteine-reactive warheads, an acrylamide (**A**) and a more reactive chloroacetamide (**Cl**),[2] were attached to pyridoxamin (**PM**) by chemical synthesis. As a proof of principle, covalent binding of the mildly reactive acrylamide inhibitor (**A-PM-I**) was demonstrated for recombinant *S. aureus* PLK by detecting adducts in intact mass spectrometry experiments which were absent for the human homologous protein PdxK (*h*PLK) lacking this signature residue.[3] Further, both compounds, **A-PM-I** and **Cl-PM-I**, reduced the enzymatic turnover from **PL** to **PLP** for recombinant *S. aureus* and *E. faecalis* PLK, albeit high compound excess was needed, hinting towards binding inside the active pocket. To prove covalent binding to the desired lid-cysteine, mutant proteins were expressed and purified which contain alanine in place of the lid-cysteine. After synthesis of probe molecules, that carry an additional alkyne tag at various positions for detection by activity-based protein profiling (ABPP), wild-type and mutant PLKs of both Gram-positive species were labeled and analyzed by fluorescent SDS-PAGE. In both cases, labeling intensity of the mutant decreased, verifying binding to the lid-cysteine. Interestingly, only the 3'-alcohol probe derivative (**A-PM-P1**) displayed labeling, which finding could be explained with clashes for the 2'-methyl-modified probe (**A-PM-P2**) and the protein backbone by means of computational modeling. Application of these probes in intact cells allowed for assessment of PLK selectivity over the complete bacterial proteome: While the mildly reactive **A-PM-P1** probe could rather selectively enrich Gram-positive PLK with few off-targets, the chloroacetamide probe (**Cl-PM-P1**) was identified as promiscuous binder. Instead, when the two acrylamide probes were applied in Gram-negative bacteria, such as *E. coli* and *P. aeruginosa*, **A-PM-P2** was identified as the only PLK binder, which again could be explained by steric hindrance with computational modeling, as the Gram-negative PLK scaffold differs from its homologous Gram-positive enzymes. Furthermore, the importance of the lid-cysteine for **PL** phosphorylation activity in Gram-negative bacteria was demonstrated and extended, as previously reported only for Gram-positive PLK.[1a] Hence, the probe compounds were verified as tool to discover bacterial PLK with catalytic relevant lid-cysteines inside whole proteomes. Finally, both inhibitor species were assessed for their antibiotic potential in *Enterococci* (*E. faecium* and *E. faecalis*) as **PLP** auxotrophic bacteria which are classified as critical pathogens by WHO.[4] Unfortunately, no effect on growth was identified up to 100 μM for neither the mildly reactive acrylamide (**A-PM-I**) nor the more reactive chloroacetamide (**Cl-PM-I**) inhibitor as vitamin B6 mimics.

In conclusion, the lid-cysteines in the active pocket of both Gram-positive and Gram-negative subclass PLKs were successfully addressed covalently by mimics of vitamin B6, carrying an irreversibly binding acrylamide or a chloroacetamide warhead. Although the mildly reactive acrylamide probe derivatives showed a rather selective enrichment of PLK over the whole proteome compared to the more reactive chloroacetamide probe, the efficacy of recombinant PLK inhibition of both moieties remained insufficient in activity assays, which might explain the absence of antibiotic activity in **PLP** auxotrophic *Enterococci* spp. However, the probes can be used in future studies to identify more potent PLK active site inhibitors by competitive profiling.

Author contributions

Ines Hübner and Stephan A. Sieber have designed the project, and Julia Friederich, Jan-Niklas Dienemann and Ines Hübner synthesized respective compounds in joint efforts. Jan-Niklas Dienemann cloned plasmid constructs with help of Ines Hübner, and recombinant wild-type and mutant pyridoxal kinases were expressed and purified by Jan-Niklas Dienemann and Julia Friederich. Ines Hübner and Jan-Niklas Dienemann examined covalent compound binding to recombinant proteins by intact mass spectrometry. Jan-Niklas Dienemann conducted activity and inhibition assays and assessed antibacterial activity. Jan-Niklas Dienemann, Ines Hübner and Julia Friederich carried out *in vitro* gel-based labeling of recombinant proteins, whereas gel-based and LC-MS/MS-based *in situ* labeling was performed by Jan-Niklas Dienemann. Sabine Schneider modelled protein and ligand interactions computationally. Stephan A. Sieber, Ines Hübner and Jan-Niklas Dienemann compiled the manuscript.

chemical biology

Articles

Tailored Cofactor Traps for the *in Situ* Detection of Hemithioacetal-Forming Pyridoxal Kinases

Ines Hübner,[†] Jan-Niklas Dienemann,[†] Julia Friederich, Sabine Schneider, and Stephan A. Sieber*

Cite This: *ACS Chem. Biol.* 2020, 15, 3227−3234

Read Online

ACCESS | Metrics & More | Article Recommendations | Supporting Information

ABSTRACT: Pyridoxal kinases (PLK) are crucial enzymes for the biosynthesis of pyridoxal phosphate, an important cofactor in a plethora of enzymatic reactions. The evolution of these enzymes resulted in different catalytic designs. In addition to the active site, the importance of a cysteine, embedded within a distant flexible lid region, was recently demonstrated. This cysteine forms a hemithioacetal with the pyridoxal aldehyde and is essential for catalysis. Despite the prevalence of these enzymes in various organisms, no tools were yet available to study the relevance of this lid residue. Here, we introduce pyridoxal probes, each equipped with an electrophilic trapping group in place of the aldehyde to target PLK reactive lid cysteines as a mimic of hemithioacetal formation. The addition of alkyne handles placed at two different positions within the pyridoxal structure facilitates enrichment of PLKs from living cells. Interestingly, depending on the position, the probes displayed a preference for either Gram-positive or Gram-negative PLK enrichment. By applying the cofactor traps, we were able to validate not only previously investigated *Staphylococcus aureus* and *Enterococcus faecalis* PLKs but also *Escherichia coli* and *Pseudomonas aeruginosa* PLKs, unravelling a crucial role of the lid cysteine for catalysis. Overall, our tailored probes facilitated a reliable readout of lid cysteine containing PLKs, qualifying them as chemical tools for mining further diverse proteomes for this important enzyme class.
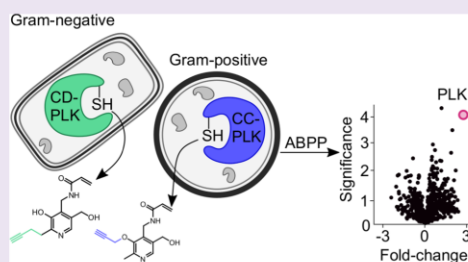
INTRODUCTION

Pyridoxal phosphate (PLP) is an essential enzyme cofactor which is highly conserved throughout all domains of life. PLP-dependent enzymes account for 4% of all known catalytic activities and are involved in various chemical transformations including racemization, transamination, decarboxylation, and carbon−carbon bond cleavage and formation. Due to the importance of PLP in, *e.g.*, glucose, lipid, and amino acid metabolism,[1−4] numerous PLP-dependent enzymes have been identified as drug targets[4−6] including alanine racemase[7,8] for the treatment of bacterial infections. Pyridoxal (PL), the precursor of PLP, is either synthesized *de novo* or taken up from the extracellular milieu via specialized transport systems. While many microorganisms are capable of both biosynthesis and uptake, eukaryotic cells rely solely on the uptake of PL and subsequent phosphorylation to PLP. This phosphorylation step of ingested PL as well as of the corresponding B6 vitamers pyridoxine (PN) and pyridoxamine (PM) is catalyzed by pyridoxal kinase (PLK).[9,10] This enzyme plays a crucial role in cellular PLP metabolism as corresponding cofactor deficiency results in human neurological disorders[6] as well as impairs virulence and survival of pathogenic bacteria.[11]

While a single PLK was believed for a long time to be the sole source of PL phosphorylation, discoveries in, *e.g.*, *Escherichia coli* as well as *Staphylococcus aureus* challenged

this assumption. An *E. coli* strain with a mutation in the corresponding PLK gene (*pdxK*) and an inactivated *de novo* biosynthesis pathway could still grow on PL,[12−14] which led to the discovery of a second kinase encoded by the *pdxY* gene, which was able to catalyze this transformation.[14] In fact, *pdxY* was also found in several other bacteria, indicating a more general role in prokaryotic PLP biosynthesis. Coincidentally, target identification studies with the natural product rugulactone led to the identification of an additional PLK encoded by *thiD* (ThiD1, UniProt ID: A0A0H2XGZ0).[15] ThiD1 was predicted to be involved in thiamine biosynthesis; however, this enzyme did not cluster with any of the thiamine biosynthesis genes, and a closer inspection of the *S. aureus* genome revealed an additional protein encoded by *thiD* (ThiD2, UniProt ID: A0A0H2XGE7), which is located in the thiamine biosynthesis operon. The uncharacterized ThiD1 enzyme was expressed recombinantly and revealed significant

3227
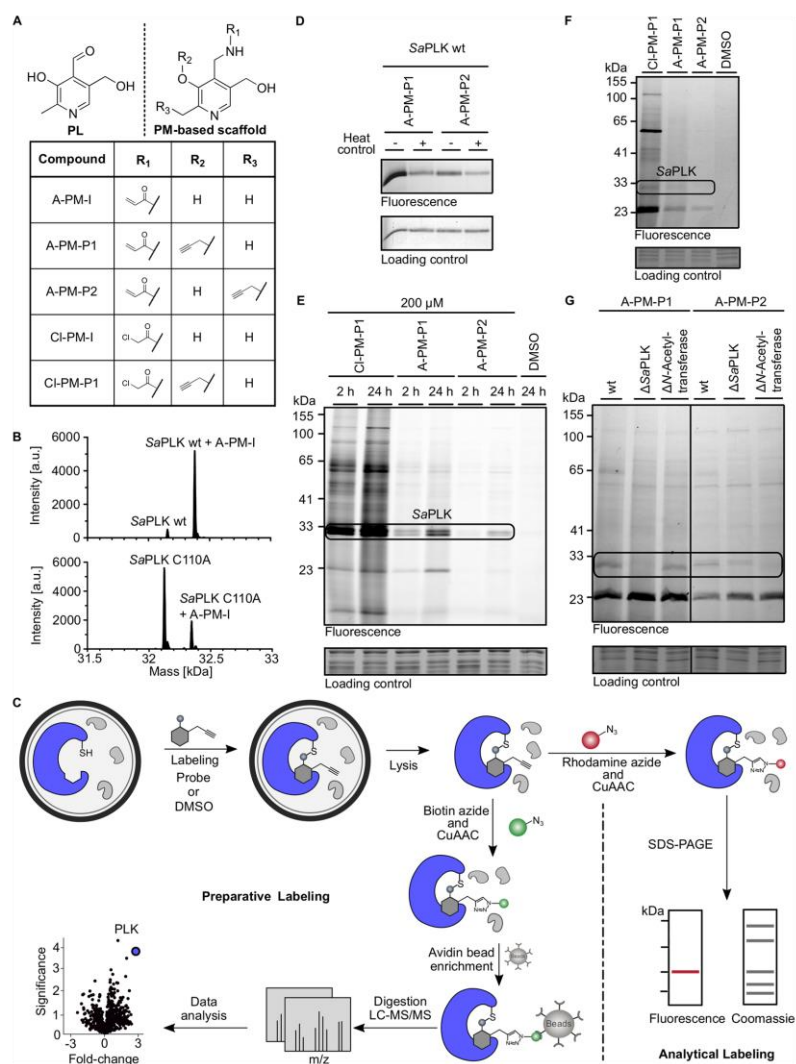
Figure 1. Design and validation of PL cofactor traps to target *Sa*PLK. (A) Molecular structures of inhibitors (A-PM-I and Cl-PM-I) and corresponding probes (A-PM-P1, A-PM-P2, Cl-PM-P1). (B) Mass spectra of intact *Sa*PLK wt and mutant after incubation with A-PM-I (100 equiv) for 24 h. (C) Schematic experimental workflow for target identification by activity-based protein profiling (ABPP). After incubation of intact cells with a probe or DMSO, cells were lysed and samples subjected to copper-catalyzed azide−alkyne cycloaddition (CuAAC) to attach rhodamine (analytical labeling) or biotin (preparative labeling) for downstream analysis. For analytical labeling, samples were analyzed via SDS-PAGE. For preparative studies, labeled proteins were enriched on avidin beads, enzymatically digested and analyzed by LC-MS/MS. (D) Gel-based labeling of recombinant *Sa*PLK. Wild type enzyme was incubated with probes (10 equiv) for 24 h and analyzed via SDS-PAGE. (E) Comparison of probes in spike-in studies with recombinant *Sa*PLK (1 μM) in *S. aureus* lysate after 2 and 24 h incubation time. Samples were analyzed via SDS-PAGE. (F) Comparison of *in situ* labeling of intact *S. aureus* cells using all probes (200 μM, 24 h) visualized by SDS-PAGE and fluorescence detection. (G) Intact *S. aureus* wt and *S. aureus* transposon mutants, ΔSAUSA300_0562 (*Sa*PLK) and ΔSAUSA300_2631 (putative *N*-acetyltransferase), were treated with A-PM-P1 and A-PM-P2 (200 μM, 24 h) and lysed and the samples analyzed via SDS-PAGE.

activity not only in the phosphorylation of 4-amino-5-hydroxymethyl-2-methyl-pyrimidine (HMP, the substrate of ThiD2 in the thiamine pathway) but also of PL and PN.[21] Indeed, metabolomic studies with a ThiD1 transposon mutant

Scheme 1. Synthesis of Inhibitors A-PM-I and Cl-PM-I As Well As the Corresponding Probes A-PM-P1, Cl-PM-P1, and A-PM-P2[a]
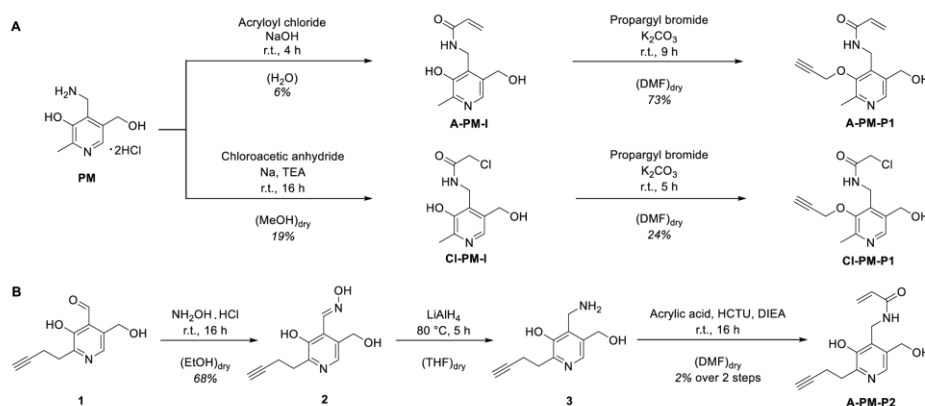
[a](A) A-PM-I and Cl-PM-I were synthesized by acylation of PM as has already been described by Ueda et al.[16] and Cravatt,[17] respectively. Probes A-PM-P1 and Cl-PM-P1 were synthesized by propargylation of inhibitors A-PM-I and Cl-PM-I, respectively. (B) Synthesis of A-PM-P2. Compound **1** was synthesized as described by Hoegl et al.[18] Compound **1** was converted to oxime **2**,[19] which was subsequently reduced by LiAlH₄ and acylated using acrylic acid to yield A-PM-P2.[20]

showed increased extracellular PL levels, suggesting that the designation as a thiamine biosynthesis enzyme could be expanded to include PL phosphorylation. We therefore reassigned the protein ThiD1 as *Sa*PLK and investigated the mechanism of PL phosphorylation by *Sa*PLK in more detail.[15,21] This enzyme contains a nucleophilic cysteine residue (Cys110) in its flexible lid region forming a covalent hemithioacetal with the PL 4′-aldehyde group. Cocrystal structures demonstrated that the lid shields the substrate pocket, and the corresponding hemithioacetal intermediate precisely positions the cofactor for deprotonation of the 5′-alcohol. This is facilitated via an active site cysteine (Cys214) which enables the deprotonated alcohol to perform an in-line attack onto the γ-phosphate of ATP. Mutation of the lid cysteine (C110A) completely abolished activity emphasizing the importance of covalent catalysis for this enzyme. A BLAST search revealed that Cys110 is conserved in a large number of homologous enzymes including *Enterococcus faecalis*, where the same C110A mutation resulted in a loss of PL turnover. These data imply that PLKs operating with two cysteine residues are common within Gram-positive bacteria and have been reclassified as a new class of dual cysteine (one in the lid, one in the active site) PLKs (CC-PLKs).[21] As Gram-negative lid cysteine containing PLKs, *e.g.*, *pdxY* in *Escherichia coli* (*Ec*PLK) or *Pseudomonas aeruginosa* (*Pa*PLK), bear an aspartate in the active site instead of a cysteine, the class of lid cysteine containing PLKs was expanded to CD-PLK (cysteine in the lid, aspartate in the active site; Supporting Information Figure S1). So far, the function and distribution of these enzymes in bacteria are unknown. Studies with *Ec*PLK indicated that the cysteine residue located five residues upstream compared to *Sa*PLK also forms a hemithioacetal, which suggests that this intermediate could be more common in PL catalysis.[12] Surprisingly, investigations on the catalytic mechanism of *Pa*PLK revealed the lid cysteine residue as not being directly involved in PL phosphorylation.[22] Thus,

sequence alignments of putative PLKs seem insufficient to predict the catalytic mechanism of these enzymes without in-depth biochemical studies.[22,23]

We here introduce a complementary tool for unbiased mining of the inventory of PLKs using hemithioacetal as an intermediate in catalysis. These tools employ the pyridoxal core structure equipped with an electrophilic trapping group in place of the aldehyde. PLKs with a reactive lid cysteine attack the warhead and become irreversibly trapped. Further functionalization of the cofactor trap with an alkyne group allowed whole proteome mining for lid cysteine containing PLKs in Gram-positive and Gram-negative bacteria.

■ RESULTS AND DISCUSSION

Design and Synthesis of PLK Traps. Given the presence of a mechanistically important cysteine in the lid loop of CC- and CD-PLKs, we considered the design of tailored electrophilic PL traps to irreversibly engage with this signature residue. Although *Sa*PLK tolerates PL derivatives,[18] we chose a stepwise approach for the synthesis and corresponding biological evaluation.

First, we selected the PL core scaffold and replaced the 4′-aldehyde with an electrophilic Michael acceptor moiety (Figure 1A). The synthesis started with the acylation of PM using acryloyl chloride to yield A-PM-I (Scheme 1A).[16] The ability of A-PM-I to covalently modify recombinant *Sa*PLK was confirmed via intact protein mass spectrometry (IPMS; Figure 1B), which reached completion overnight (Supporting Information Figure S2A), while treatment of the lid C110A mutant under the same conditions (100 equiv A-PM-I) led to only 25% labeling, validating Cys110 as the primary binding site. As expected, human PLK (*h*PLK) was not modified by A-PM-I confirming the lack of a cysteine in the lid (Supporting Information Figure 2B).

Tailored Probes for PLK Labeling. Encouraged by the IPMS data, we designed corresponding probe molecules by
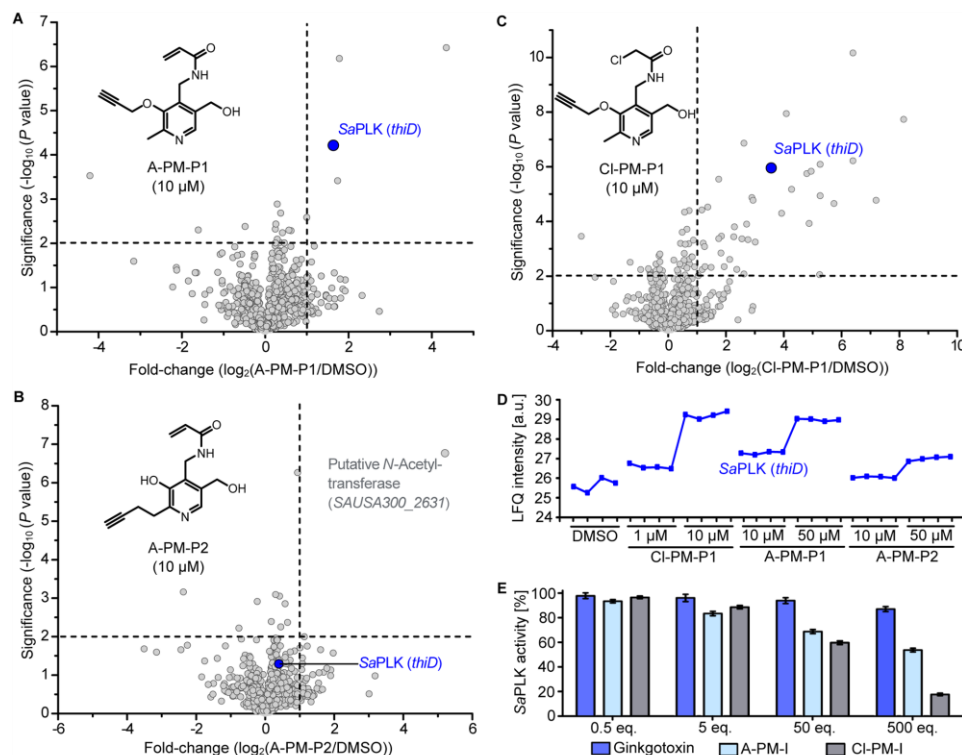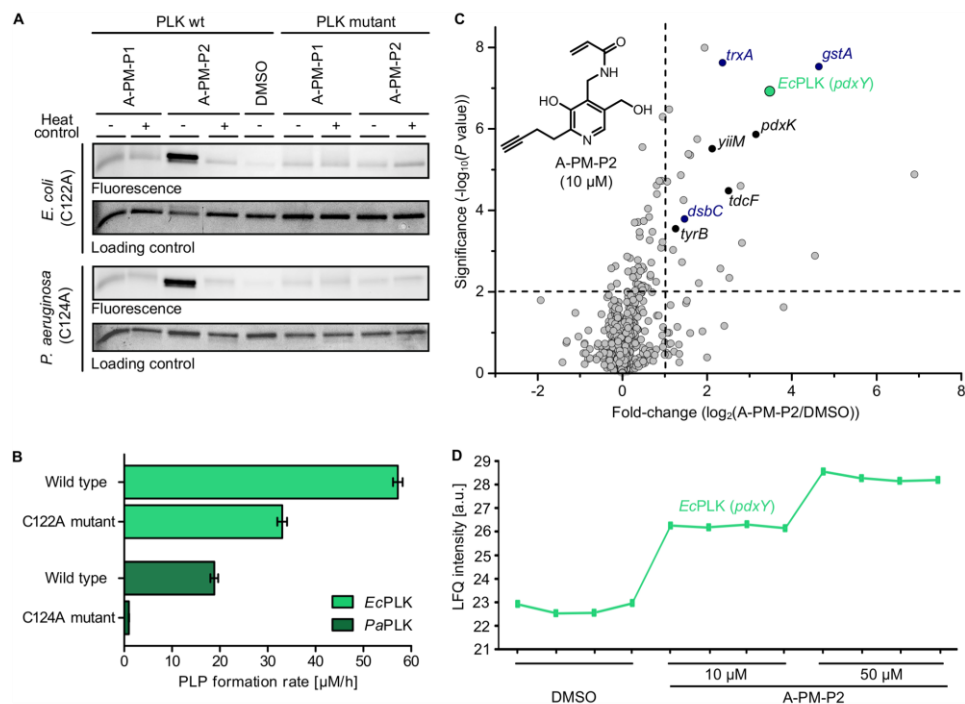
Figure 2. Target identification by chemical proteomic profiling and target validation. The volcano plots show enrichment of proteins after treatment (24 h) of *S. aureus* cells with (A) A-PM-P1 (10 μM), (B) A-PM-P2 (10 μM), and (C) Cl-PM-P1 (10 μM) on a log$_2$ scale. The vertical and horizontal threshold lines represent a log$_2$ enrichment ratio of 1 and a $-\log_{10}$ P value of 2 (two-sided two-sample *t*-test, n = 4 independent experiments per group), respectively. (D) Profile plot representation of proteomic data showing LFQ intensities of *Sa*PLK after treatment of intact *S. aureus* with Cl-PM-P1 (1 μM and 10 μM), A-PM-P1 (10 μM and 50 μM), and A-PM-P2 (10 μM and 50 μM; n = 4 independent experiments per group). (E) Influence of compounds A-PM-I, Cl-PM-I, and ginkgotoxin on *Sa*PLK phosphorylation activity. Activity was measured after incubation for 2 h at 25 °C (n = 3 independent experiments per group; data represent the mean ± SEM).

appending a small alkyne linker either via the 3′-alcohol (A-PM-P1) or the 2′-methyl group (A-PM-P2; Figure 1A). Upon protein binding, these probes can be functionalized with either rhodamine or biotin azide via click chemistry to facilitate visualization and identification of targeted proteins (Figure 1C). For A-PM-P1, the 3′-alcohol of A-PM-I was alkylated using propargyl bromide (Scheme 1A). For A-PM-P2, we used the alkylation strategy implemented by Hoegl *et al.* to synthesize compound **1**,[18] which was subsequently treated with an excess of hydroxylamine to yield the respective oxime **2**.[19] Reduction using LiAlH$_4$ followed by coupling to acrylic acid afforded A-PM-P2 (Scheme 1B).[20]

When recombinant wt and C110A mutant *Sa*PLKs were subjected to probe labeling and click to rhodamine azide, SDS-PAGE revealed more efficient labeling of *Sa*PLK wt by A-PM-P1 than A-PM-P2 (Figure 1D, Supporting Information Figure S3). This observation can be rationalized utilizing the cocrystal structure of *Sa*PLK in complex with the native PL cofactor (PDB: 4C5L)[21] as a basis for computational modeling. Fitting the probes into the structure revealed an open space at the 3′-

hydroxyl group to accommodate the alkyne handle of A-PM-P1 next to the β-hairpin and Val142. In contrast, steric clashes with the first β-strand and the propargylated 2′-substituent of A-PM-P2 were predicted (Supporting Information Figure S4A). In line with the IPMS data, the C110A mutant showed significantly weaker labeling for A-PM-P1, which was independent of protein heat inactivation, suggesting a nonspecific probe binding (Supporting Information Figure S3). On the basis of these results, we decided to expand our set of probes by replacing the acrylamide warhead of A-PM-P1 to the more reactive chloroacetamide. Inhibitor Cl-PM-I was synthesized by acylation of PM using chloroacetic anhydride, which was subsequently alkylated by propargyl bromide yielding probe Cl-PM-P1 (Scheme 1A). Next, we evaluated the selectivity of all probes by labeling lysates of *S. aureus* with spiked-in *Sa*PLK wt (Figure 1E). A comparison between all probes revealed a strongly elevated number of protein bands labeled by the chloroacetamide probe Cl-PM-P1 as compared to the Michael acceptor-based probes (A-PM-P1/P2) which almost exclusively labeled the spiked-in *Sa*PLK. In addition,

Figure 3. Labeling Gram-negative PLKs and target identification by chemical proteomic profiling. (A) Gel-based labeling experiments using recombinant *Ec*PLK and *Pa*PLK. Wild type and mutant enzymes were incubated with probes (10 equiv) for 24 h and analyzed via SDS-PAGE. (B) PL phosphorylation activity assay of Gram-negative PLKs was performed in cell lysate of an *E. coli* expression strain after overexpression of proteins ($n = 3$; data represent the mean ± SEM). (C) The volcano plot shows enrichment of proteins after treatment (24 h) of *E. coli* cells with A-PM-P2 ($10 \mu M$) on a $\log_2$ scale. The vertical and horizontal threshold lines represent a $\log_2$ enrichment ratio of 1 and a $-\log_{10} P$ value of 2 (two-sided two-sample *t*-test, $n = 4$ independent experiments per group), respectively. The green dot represents the target protein, *Ec*PLK. Black dots represent PLP associated enzymes, and blue dots represent proteins of the thioredoxin-like superfamily (assignment according to UniProtKB).[25] (D) Profile plot representation of proteomic data showing LFQ intensities of *Ec*PLK after treatment of intact *E. coli* cells with A-PM-P2 ($10 \mu M$ and $50 \mu M$; $n = 4$ independent experiments per group).

both Michael acceptor probes revealed very few protein bands upon incubation of intact *S. aureus* wt cells (Figure 1F). Interestingly, labeling in an intact *Sa*PLK transposon mutant strain showed that the 29 kDa band for *Sa*PLK only vanished with A-PM-P1 but remained with A-PM-P2, which supports our previous findings that only A-PM-P1 is able to bind to *Sa*PLK but not A-PM-P2 (Figure 1G). In contrast, Cl-PM-P1 incubation with intact *S. aureus* cells resulted in high background labeling (Figure 1F), suggesting an enhanced but nonspecific reactivity. Similar results were obtained via gel-based labeling experiments for recombinant *E. faecalis* PLK (*Ef*PLK), another confirmed CC-PLK (Supporting Information Figure S5A).[21]

***In Situ* Profiling in Gram-Positive Bacteria Reveals CC-PLKs.** To decipher the *in situ* selectivity of A-PM-P1, A-PM-P2, and Cl-PM-P1 for CC-PLKs in Gram-positive bacteria, intact *S. aureus* and *E. faecalis* cells were incubated with individual probes for 24 h, lysed, clicked to biotin azide, and enriched on avidin beads. Subsequent protein digest, LC-MS/MS analysis, and label-free quantification (LFQ) of

peptide spectra resulted in volcano plots with the most significant hits (fold-change > $\log_2 = 1$, significance > $-\log_{10} = 2$) depicted in the upper right corner (Figure 2A−C, Supporting Information Figure S5B,C). Strikingly, A-PM-P1 strongly labeled *Sa*PLK (Figure 2A) and *Ef*PLK (Supporting Information Figure S5B) with only few other off-targets. Profile plots of the LFQ data reveal concentration-dependent enrichment of both proteins *Sa*PLK (Figure 2D) and *Ef*PLK (Supporting Information Figure S5D). These proteomic data show that A-PM-P1 is able to enrich *Sa*PLK as well as *Ef*PLK *in situ* by covalent attachment to the lid cysteine Cys110, which has previously been proven as the primary binding site by gel-based labeling experiments of recombinant wt and mutant proteins. These findings confirm this probe as a reliable *in situ* tool for the detection of Gram-positive PLKs containing a lid cysteine relevant for PL catalysis.

As expected from the crystal structure and *in vitro* labeling studies, A-PM-P2 did not enrich the respective CC-PLKs (Supporting Information Figure S4A, Figure 2B, Supporting Information Figure S5C). Instead, a putative *N*-acetyltransfer-

ase was enriched, and this target was validated with an *in situ* gel-based labeling study using the corresponding transposon mutant (Figure 1G). The elevated reactivity of Cl-PM-P1 resulted in high background labeling (Figure 2C), confirming results from gel-based spike-in studies with recombinant SaPLK. A closer analysis of the corresponding off-targets revealed a large fraction (>58%) of proteins with medium or high reactive cysteine residues, explaining their binding to the chloroacetamide probe.[24] In agreement with the proteomic results, concentration-dependent inhibition of recombinant SaPLK and EfPLK with A-PM-I and Cl-PM-I was observed (Figure 2E, Supporting Information Figure S5E). In contrast, ginkgotoxin (4′-O-methylpyridoxine), an hPLK inhibitor, did not inhibit either SaPLK or EfPLK, highlighting a different binding mode in bacterial enzymes.

The Importance of the Lid Cysteine in Gram-Negative CD-PLKs. With a validated method for monitoring CC-PLKs using A-PM-P1 in Gram-positive bacteria, we next investigated Gram-negative *E. coli* and *P. aeruginosa*. Both bacteria encode PLKs with a cysteine in the lid region and an aspartate in the active site (Supporting Information Figure S1). However, contradictory data exist regarding the function of these cysteines. A cocrystal structure of the *E. coli* enzyme showed covalent engagement of the lid cysteine by PL.[12]

Notably, the structure revealed the hemithioacetal bound PL in only one monomer of the EcPLK homodimer, raising the question of whether it plays an essential role in enzyme turnover similar to CC-PLKs. Contrarily, a *P. aeruginosa* lid cysteine mutant remained active in phosphorylation assays, suggesting that it is dispensable for catalysis.[22]

To experimentally consolidate these diverging reports about CD-PLKs, we investigated the reactivity and accessibility of the lid cysteines with our probes. Starting with EcPLK, we incubated the recombinant wt as well as cysteine to alanine mutant proteins with the two probes A-PM-P1 and A-PM-P2 and analyzed labeling via fluorescent SDS-PAGE. Surprisingly, while A-PM-P1, the probe tailored for CC-PLK, failed to label either protein, A-PM-P2 revealed a clear signal solely for the wt (Figure 3A). A closer inspection of the *E. coli* cocrystal structure with bound PL (PDB: 1TD2)[12] revealed different preferences for the probes compared to SaPLK after computational modeling with A-PM-P1 and A-PM-P2: While collision of the 3′-alkyne handle of A-PM-P1 with Thr45 located at the small-helix-loop secondary structural element was predicted, A-PM-P2 can be accommodated into the binding pocket and subsequently react with Cys122 (Supporting Information Figure S4B). Next, enzymatic activity was assessed; however, in line with previous literature reports, the turnover of the purified protein in buffer was slow, indicating a requirement for cellular components for enhanced activity.[26] We thus utilized the lysate of *E. coli* expressing the recombinant protein and obtained a significantly higher phosphorylation activity with a catalytic turnover of 57 μM PLP/h (Figure 3B). *E. coli* cells lacking recombinant PLK expression were used as a control to subtract the basal PLK activity level. While the lid cysteine to alanine mutant still displayed activity, it was reduced by approximately 50%. A previous cocrystal structure of PL bound EcPLK showed the cysteine hemithioacetal formation only in every other subunit, which could provide a rationale for the observed activity data.[12]

Similarly, we assessed probe binding to recombinant CD-PLK of *P. aeruginosa*, PaPLK, and again obtained strong labeling solely by the A-PM-P2 probe, highlighting its better performance in engaging Gram-negative CD-PLKs (Figure 3A). As anticipated, the corresponding lid mutant lacked labeling. As with previous literature reports, assays with recombinant wt enzyme showed very limited activity.[22] Thus, we tested the PaPLK wt expression lysate which again revealed improved activity, albeit with a 3-fold reduced turnover compared to the *E. coli* wt enzyme. Importantly, the corresponding PaPLK lid mutant lacked enzymatic activity, indicating the importance of this residue for catalysis (Figure 3B).

For assessing *E. coli* labeling, intact cells were treated with A-PM-P2 followed by proteome enrichment. LC-MS/MS data analysis revealed several proteins rich in reactive cysteines such as thioredoxin-like superfamily proteins (Figure 3C, blue). Furthermore, several enzymes known for PL or PLP binding (Figure 3C, black) were among these hits, *e.g.*, aromatic-amino-acid aminotransferase (tyrB) and *E. coli* PLK (pdxK), the kinase lacking a reactive lid residue.[13] Importantly, EcPLK (pdxY), bearing the lid cysteine, exhibited strong enrichment in the A-PM-P2 treated samples (Figure 3C). A LFQ intensity profile plot further demonstrated the selectivity of EcPLK labeling by a concentration-dependent enrichment of the protein (Figure 3D). These results show that our pyridoxal inspired cofactor traps, combined with sequence alignments, are reliable tools in the correct assignment of catalytically relevant lid cysteines in the large and diverse class of PLKs.

■ CONCLUSION

Pyridoxal kinases are crucial enzymes for maintaining sufficient levels of the essential PLP cofactor in eukaryotic and prokaryotic cells. During evolution, several different enzyme classes evolved which all bear a similar structural fold but differ in the active site base as well as lid composition. While sequence alignments predict the existence of lid cysteines in Gram-positive and Gram-negative bacteria, their reactivity for hemithioacetal formation and relevance for catalytic turnover was largely unknown. Chemical cofactor probes with tailored electrophiles are able to solve this issue by monitoring the reactive lid cysteine. We rationalize that cysteines with relevance in catalysis attack the pyridoxal aldehyde forming a hemithioacetal. This is trapped by the probe and thus enabling a reliable readout for CC- and CD-PLKs *in vitro* as well as *in situ*. We were able to further customize this strategy with two complementary probes, A-PM-P1 fitting into Gram-positive CC-PLKs and A-PM-P2 binding into Gram-negative CD-PLKs. The lid cysteines of all wt enzymes in this study were modified by our tailored probes, highlighting their important role in catalysis. The probes thus represent suitable tools to further decipher these PLK subclasses in other bacterial cells with yet unknown function.

■ ASSOCIATED CONTENT

ⓢ Supporting Information

The Supporting Information is available free of charge at https://pubs.acs.org/doi/10.1021/acschembio.0c00787.

> Full experimental details, materials, procedures, characterization for all compounds, supplementary figures, and tables (PDF)

> Supplementary tables for proteomic data (XLSX)

■ AUTHOR INFORMATION

Corresponding Author

   Stephan A. Sieber − *Department of Chemistry, Chair of Organic Chemistry II, Center for Functional Protein Assemblies (CPA), Technische Universität München, 85748 Garching, Germany;* ● orcid.org/0000-0002-9400-906X; Email: stephan.sieber@tum.de

Authors

   Ines Hübner − *Department of Chemistry, Chair of Organic Chemistry II, Center for Functional Protein Assemblies (CPA), Technische Universität München, 85748 Garching, Germany*

   Jan-Niklas Dienemann − *Department of Chemistry, Chair of Organic Chemistry II, Center for Functional Protein Assemblies (CPA), Technische Universität München, 85748 Garching, Germany;* ● orcid.org/0000-0002-8346-3953

   Julia Friederich − *Department of Chemistry, Chair of Organic Chemistry II, Center for Functional Protein Assemblies (CPA), Technische Universität München, 85748 Garching, Germany; Department of Chemical Biology, Helmholtz Centre for Infection Research and German Centre for Infection Research (DZIF), 38124 Braunschweig, Germany*

   Sabine Schneider − *Department of Chemistry, Ludwig-Maximilians University Munich, 81377 Munich, Germany;* ● orcid.org/0000-0003-1054-8689

Complete contact information is available at:
https://pubs.acs.org/10.1021/acschembio.0c00787

Author Contributions

[†]I.H. and J.-N.D. contributed equally to this work. I.H. and S.A.S. conceived and designed the project. I.H., J.F., and J.-N.D. synthesized compounds. I.H. and J.-N.D. performed cloning. I.H., J.-N.D., and J.F. performed *in vitro* gel-based labeling experiments. I.H. and J.-N.D. performed *in situ* labeling (gel- and MS-based) and IPMS experiments. J.-N.D. and J.F. purified recombinant proteins. J.-N.D. performed activity assays. S.S. performed modeling. I.H., J.-N.D., and S.A.S. wrote the manuscript.

Notes

The authors declare no competing financial interest.

■ REFERENCES

(1) Di Salvo, M. L., Budisa, N., and Contestabile, R. (2013) PLP-dependent Enzymes: a Powerful Tool for Metabolic Synthesis of Non-canonical Amino Acids. *Beilstein Bozen Symp. Mol. Eng. Control*, 27−66.

(2) Percudani, R., and Peracchi, A. (2003) A genomic overview of pyridoxal-phosphate-dependent enzymes. *EMBO Rep. 4*, 850−854.

(3) Schneider, G., Käck, H., and Lindqvist, Y. (2000) The manifold of vitamin B6 dependent enzymes. *Structure 8*, R1−R6.

(4) Eliot, A. C., and Kirsch, J. F. (2004) Pyridoxal Phosphate Enzymes: Mechanistic, Structural, and Evolutionary Considerations. *Annu. Rev. Biochem. 73*, 383−415.

(5) Kappes, B., Tews, I., Binter, A., and MacHeroux, P. (2011) PLP-dependent enzymes as potential drug targets for protozoan diseases. *Biochim. Biophys. Acta, Proteins Proteomics 1814*, 1567−1576.

(6) Amadasi, A., Bertoldi, M., Contestabile, R., Bettati, S., Cellini, B., di Salvo, M. L., Borri-Voltattorni, C., Bossa, F., and Mozzarelli, A. (2007) Pyridoxal 5-Phosphate Enzymes as Targets for Therapeutic Agents. *Curr. Med. Chem. 14*, 1291−1324.

(7) Strominger, J. L., Ito, E., and Threnn, R. H. (1960) Competitive inhibition of enzymatic reactions by oxamycin. *J. Am. Chem. Soc. 82*, 998−999.

(8) Sassetti, C. M., Boyd, D. H., and Rubin, E. J. (2003) Genes required for mycobacterial growth defined by high density mutagenesis. *Mol. Microbiol. 48*, 77−84.

(9) Mukherjee, T., Hanes, J., Tews, I., Ealick, S. E., and Begley, T. P. (2011) Pyridoxal phosphate: Biosynthesis and catabolism. *Biochim. Biophys. Acta, Proteins Proteomics 1814*, 1585−1596.

(10) Di Salvo, M. L., Contestabile, R., and Safo, M. K. (2011) Vitamin B6 salvage enzymes: Mechanism, structure and regulation. *Biochim. Biophys. Acta, Proteins Proteomics 1814*, 1597−1608.

(11) El Qaidi, S., Yang, J., Zhang, J. R., Metzger, D. W., and Bai, G. (2013) The vitamin B6 biosynthesis pathway in streptococcus pneumoniae is controlled by pyridoxal 5′-phosphate and the transcription factor PdxR and has an impact on ear infection. *J. Bacteriol. 195*, 2187−2196.

(12) Safo, M. K., Musayev, F. N., Hunt, S., Di Salvo, M. L., Scarsdale, N., and Schirch, V. (2004) Crystal structure of the PdxY protein from Escherichia coli. *J. Bacteriol. 186*, 8074−8082.

(13) Safo, M. K., Musayev, F. N., Di Salvo, M. L., Hunt, S., Claude, J. B., and Schirch, V. (2006) Crystal structure of pyridoxal kinase from the Escherichia coli pdxK gene: Implications for the classification of pyridoxal kinases. *J. Bacteriol. 188*, 4542−4552.

(14) Yang, Y., Tsui, H. C. T., Man, T. K., and Winkler, M. E. (1998) Identification and function of the pdxY gene, which encodes a novel pyridoxal kinase involved in the salvage pathway of pyridoxal 5′-phosphate biosynthesis in Escherichia coli K-12. *J. Bacteriol. 180*, 1814−1821.

(15) Nodwell, M. B., Menz, H., Kirsch, S. F., and Sieber, S. A. (2012) Rugulactone and its Analogues Exert Antibacterial Effects through Multiple Mechanisms Including Inhibition of Thiamine Biosynthesis. *ChemBioChem 13*, 1439−1446.

(16) Ueda, T., Nakaya, K., Nagai, S., Sakakibara, J., and Murata, M. (1990) Syntheses of dihydrodioxepinopyridines, dihydrodioxocinopyridines, and a dihydrooxazepinopyridine. *Chem. Pharm. Bull. 38*, 19−22.

(17) Cravatt, B. F. Compositions and methods of modulating immune response, WO/2017/210600, 2017.

(18) Hoegl, A., Nodwell, M. B., Kirsch, V. C., Bach, N. C., Pfanzelt, M., Stahl, M., Schneider, S., and Sieber, S. A. (2018) Mining the cellular inventory of pyridoxal phosphate-dependent enzymes with functionalized cofactor mimics. *Nat. Chem. 10*, 1234−1245.

(19) Dale, T. J., Sather, A. C., and Rebek, J. (2009) Synthesis of novel aryl-1,2-oxazoles from ortho-hydroxyaryloximes. *Tetrahedron Lett. 50*, 6173−6175.

(20) E. Müller, T., and Pleier, A.-K. (1999) Intramolecular hydroamination of alkynes catalysed by late transition metals. *J. Chem. Soc., Dalton Trans.*, 583−588.

(21) Nodwell, M. B., Koch, M. F., Alte, F., Schneider, S., and Sieber, S. A. (2014) A subfamily of bacterial ribokinases utilizes a hemithioacetal for pyridoxal phosphate salvage. *J. Am. Chem. Soc. 136*, 4992−4999.

(22) Kim, M. I., and Hong, M. (2016) Crystal structure and catalytic mechanism of pyridoxal kinase from Pseudomonas aeruginosa. *Biochem. Biophys. Res. Commun. 478*, 300−306.

(23) Park, J., Burns, K., Kinsland, C., and Begley, T. P. (2004) Characterization of Two Kinases Involved in Thiamine Pyrophosphate and Pyridoxal Phosphate Biosynthesis in Bacillus subtilis: 4-

Amino-5-Hydroxymethyl-2-Methylpyrimidine Kinase and Pyridoxal Kinase. *J. Bacteriol.* *186*, 1571−1573.

(24) Zanon, P. R. A., Lewald, L., and Hacker, S. M. (2020) Isotopically Labeled Desthiobiotin Azide (isoDTB) Tags Enable Global Profiling of the Bacterial Cysteinome. *Angew. Chem., Int. Ed.* *59*, 2829−2836.

(25) Consortium, T. U. (2019) UniProt: a worldwide hub of protein knowledge. *Nucleic Acids Res.* *47*, D506−D515.

(26) Di Salvo, M. L., Hunt, S., and Schirch, V. (2004) Expression, purification, and kinetic constants for human and Escherichia coli pyridoxal kinases. *Protein Expression Purif.* *36*, 300−306.

CCC
RightsLink

ACS Publications
Most Trusted. Most Cited. Most Read.

Tailored Cofactor Traps for the in Situ Detection of Hemithioacetal-Forming Pyridoxal Kinases

Author: Ines Hübner, Jan-Niklas Dienemann, Julia Friederich, et al

Publication: ACS Chemical Biology

Publisher: American Chemical Society

Date: Dec 1, 2020

Copyright © 2020, American Chemical Society

**BACK**   **CLOSE WINDOW**

4.1 Supplementary figures and schemes

```
Staphylococcus aureus|A0A0H2XGZ0   -MALKKVLTIAGSDTSAGAGMQADLKTFQELDT-------YGMVALTAIVTMDK-DTWSH 51
Enterococcus faecalis|Q839G7       ---MEKVLTIAGSDSTGGAGIQADLKTFEEYGV-------FGFSSLTSIVTMDPTTGWSH 50
Bacillus subtilis|P39610           -MSMHKALTIAGSDSSGGAGIQADLKTFQEKNV-------YGMTALTVIVAMDPNNSWNH 52
Listeria monocytogenes|Q8Y971      -MTIKKTLTIAGSDSSGGAGLQADLKTFEEYGT-------YGFSAITTIVTMDPDNNWAH 52
Escherichia coli|P77150            --MMKNILAIQSHVVYGHAGNSAAEFPMRRLGANVWPLNTVQFSNHT-----QYG-KWTG 52
Pseudomonas aeruginosa|Q9HT57      MPRTPHLLAIQSHVVFGHAGNAAAVFPMQRIGINVWPLNTVQFSNHT-----QYG-RWTG 54
Vibrio vulnificus|Q8D4Q2           ---MQGILSIQSHVAYGHAGNSSAVFPMQRMGFEVWPIHTVQFSNHT-----QYQEGWTG 52
Salmonella typhimurium|Q8ZPM8      ---MKNILAIQSHVVFGHAGNSAAEFPMRRLGANVWPLNTVQFSNHT-----QYG-KWTG 51
Homo sapiens|O00764|               MEEECRVLSIQSHVIRGYVGNRAATFPLQVLGFEIDAVNSVQFSNHT-----GYA-HWKG 54
                                       *:*.    . .*  :   ::. .         :   *        *

Staphylococcus aureus|A0A0H2XGZ0   DVTPLPMD-VFEKQLETALS-IGPDAIKTGMLGTEEIIKRAGEVYEASN----AQYFVVD 105
Enterococcus faecalis|Q839G7       EVTELPET-LLEKQLISVFAGGPVAALKTGMMGNEQNIKMASKYIKQEK----IQKVVID 105
Bacillus subtilis|P39610           QVFPIDTD-TIRAQLATITDGIGVDAMKTGMLPTVDIIELAAKTIKEKQ----LKNVVID 107
Listeria monocytogenes|Q8Y971      GVTPIDAQ-LVREQLKTILSGGPVDAMKTGMLGSIEIIKATREAIDKYD----LKNVVID 107
Escherichia coli|P77150            CVMPPSHLTEIVQGIAAIDKLHTCDAVLSGYLGSAEQGEHILGIVRQVKAANPQAKYFCD 112
Pseudomonas aeruginosa|Q9HT57      QVLPPEQIPALVDGIAGIGELGNCDAVLSGYLGSAAQGRAILDVVARIKQANPRALYLCD 114
Vibrio vulnificus|Q8D4Q2           RAFSADDISELVRGLNNIGALEKCQAVLTGYQGSAEQCLAVEETVTKVKQANPDALYVCD 112
Salmonella typhimurium|Q8ZPM8      CVMPPSHLTEIVQGIADIGQLAHCDAVLSGYLGSAEQGEHILGIVRQVKAANPQAKYFCD 111
Homo sapiens|O00764|               QVLNSDELQELYEGLR-LNNMNKYDYVLTGYTRDKSFLAMVVDIVQELKQQNPRLVYVCD 113
                                     .        .    :           : :*         .       . *
```

Lid-Cys

```
Staphylococcus aureus|A0A0H2XGZ0   PVMVCKGEDE---VLNPGNTEAMIKYLLPKATVVTPNLFEAGQLSGLGKLNSIEDMKKAA 162
Enterococcus faecalis|Q839G7       PVIACKGTAQ---ILQPKSVEGLKNDLLPLALVATPNLIEAGILSGLGEISSVAEMEEAA 162
Bacillus subtilis|P39610           PVMVCKGANE---VLYPEHAQALREQLAPLATVITPNLFEASQLSGMDELKTVDDMIEAA 164
Listeria monocytogenes|Q8Y971      PVMVCKGEDE---LIQPENAEAIRDLLLPKATITTPNLFEAGQLSGLGKLTTLDDMKAAA 164
Escherichia coli|P77150            PVMGHPEKGC---IVAPGVAEFHVRHGLPASDIIAPNLVELEILCEH-AVNNVEEAVLAA 168
Pseudomonas aeruginosa|Q9HT57      PVMGHPEKGC---IVAPEVSDFLLEEAAAVADYLCPNQLELDSFCDR-QPNSLADCVEMA 170
Vibrio vulnificus|Q8D4Q2           PVMGAPDKGC---IVAPGIAENLLNRLMPMADVIVPNQFELSQFAEM-EIHTLDDAIIAC 168
Salmonella typhimurium|Q8ZPM8      PVMGHPEKGC---IVAPGVAEFHVRYALPASDIIAPNLIELEILSKH-SVNNVDDAVQAA 167
Homo sapiens|O00764                PVLGDKWDGEGSMYVPEDLLPVYKEKVVPLADIITPNQFEAELLSGR-KIHSQEEALRVM 172
                                   **:.        :                 :     **  .*   :.       .  :
```

```
Staphylococcus aureus|A0A0H2XGZ0   TIIFDKGAQHVIIKGGKAL--DQDKSYDLYYDGQTFYQ-----LTTDMFQ----QSYNHG 211
Enterococcus faecalis|Q839G7       KRIVQMGAKHVVVKGGHRL--AGEKALDLFYDGHTAHL-----LENELYP----TDYNHG 211
Bacillus subtilis|P39610           KKIHALGAQYVVITGGGKL--KHEKAVDVLYDGETAEV-----LESEMID----TPYTHG 213
Listeria monocytogenes|Q8Y971      KKIIELGAKYVVKGGKAL--ESDKAIDLLYDGKEFTI-----YEVEKIS----PSHNHG 213
Escherichia coli|P77150            RELIAQGPQIVLVKHLARAGYSRDRFEMLLVTADEAWH-----ISRPLVDFG--MRQPVG 221
Pseudomonas aeruginosa|Q9HT57      RSLLARGPRAILVKHLNYPGKAGDTFEMLLVAADQAWH-----LQRPLLAFP---RQPVG 222
Vibrio vulnificus|Q8D4Q2           QRALAKGPKVVLVKHLYC--LSDESFNMLLATQEGTYL-----AKRPHFEFA---KAPVG 218
Salmonella typhimurium|Q8ZPM8      RELIAQGPEIVLVKHLARAGYSSERFEMLLVTAQEAWH-----ISRPLVDFG--SRQPVG 220
Homo sapiens|O00764                DMLHSMGPDTVVITSSDLPSPQGSNYLIVLGSQRRRNPAGSVVMERIRMDIRKVDAVFVG 232
                                    *   :::.       .    :                             *
```

Base

```
Staphylococcus aureus|A0A0H2XGZ0   AGCTFAAATTAYLANGKSPKEAVIS--AKAFVASAIKNGWKMNDFVGPVDHGAYNR---- 265
Enterococcus faecalis|Q839G7       AGCTFSAAITAGLAKGYSVLEAVTL--AKKFVAAAIKHGIQVNPYVGHVWHGAYTH---- 265
Bacillus subtilis|P39610           AGCTFSAAVTAELAKGAEVKEAIYA--AKEFITAAIKESFPLNQYVGPTKHSALRL---- 267
Listeria monocytogenes|Q8Y971      AGCTFAAAITAGLAKGLTVEEAVAK--AKDFVTAAIKGGFALNEFIGPVWHGAYNK---- 267
Escherichia coli|P77150            VGDVTSGLLLVKLLQGATLQE------ALEHVTAAVYEIMVTTKAMQE------------ 263
Pseudomonas aeruginosa|Q9HT57      VGDLASGLFLSRLLLGDDLRN------AFEFTGAAVHEVLLETQACGS------------ 264
Vibrio vulnificus|Q8D4Q2           AGDLISAIFTAGLLKGWTPKQ------AFQHCHDACYGVLNATYQAGE------------ 260
Salmonella typhimurium|Q8ZPM8      VGDVTSGLLLVKLLQGATLQQ------ALEHVTAAVYEIMIATKTMQE------------ 262
Homo sapiens|O00764                TGDLFAA-----MLLAWTHKHPNNLKVACEKTVSTLHHVLQRTIQCAKAQAGEGVRPSPM 287
                                    .*  ::.    :  .             :              .
```

```
Staphylococcus aureus|A0A0H2XGZ0   -------IEHIDVEVTEV------------- 276
Enterococcus faecalis|Q839G7       -------AEQRMRKKA--------------- 274
Bacillus subtilis|P39610           -------NQQS-------------------- 271
Listeria monocytogenes|Q8Y971      -------AENR-------------------- 271
Escherichia coli|P77150            -YELQVVAAQDRIAKPEHYFSATKL------ 287
Pseudomonas aeruginosa|Q9HT57      -YELELVRAQDRIAHPRVRFDAVRL------ 288
Vibrio vulnificus|Q8D4Q2           -WELQTIAAQQEFVEPSKHFPLEEVTLKTVE 290
Salmonella typhimurium|Q8ZPM8      -YELQVVAAQDRIANPEHYFSATRL------ 286
Homo sapiens|O00764                QLELRMVQSKRDIEDPEIVVQATVL------ 312
                                      :
```

Supplementary Figure S1. Multiple sequence alignment of putative PL kinases highlighting lid cysteines (Cys) (green) and catalytic bases Cys (C) and Asp (D) (blue) using Clustal O (1.2.4).[5] Sequences of *S. aureus* USA300 (UniProt ID: A0A0H2XGZ0, *Sa*PLK), *E. faecalis* V583 (UniProt ID: Q839G7, *Ef*PLK), *B. subtilis* 168 (UniProt ID: P39610), *L. monocytogenes* EGD-e (UniProt ID: Q8Y971), *E. coli* K12 (UniProt ID: P77150, *Ec*PLK), *P. aeruginosa* PAO1 (UniProt ID: Q9HT57, *Pa*PLK), *V. vulnificus* CMCP6 (UniProt ID: Q8D4Q2), *S. typhimurium* LT2 (UniProt ID: Q8ZPM8) and *Homo sapiens* (UniProt ID: O00764, *h*PLK) were aligned.
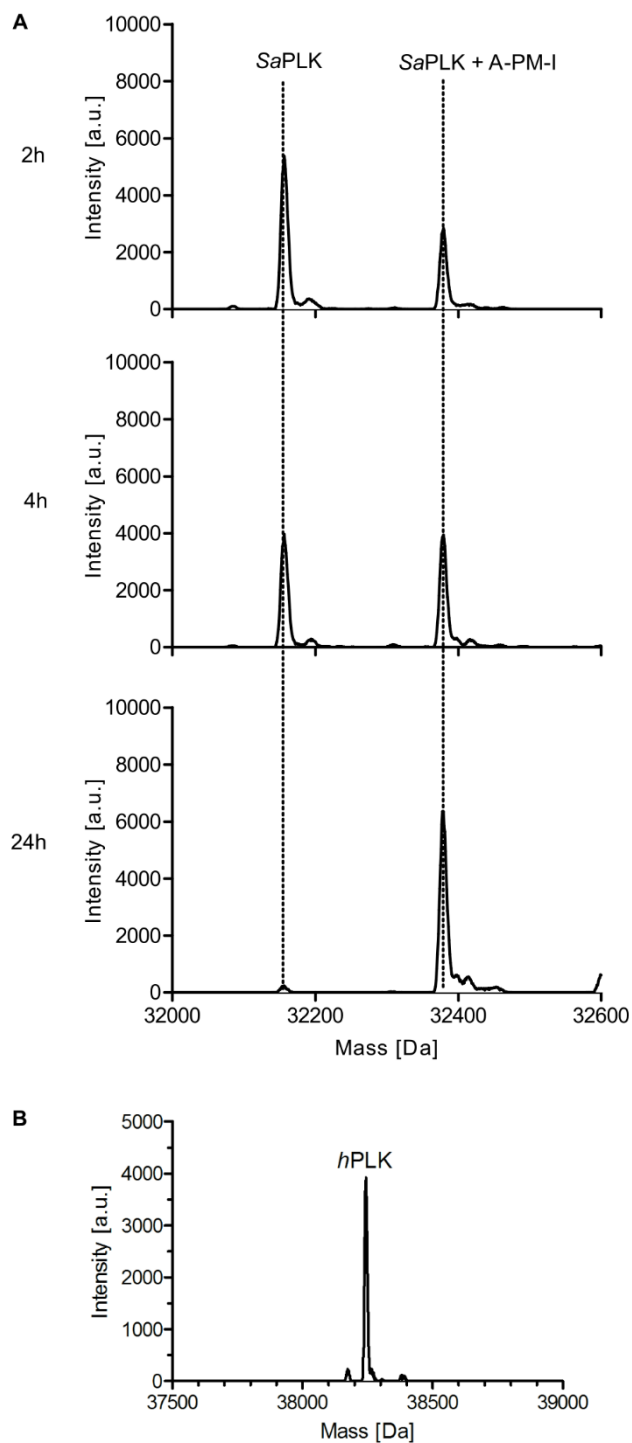
Supplementary Figure S2. IPMS studies of PLKs. (A) Time-dependent modification of *Sa*PLK wt with **A-PM-I** (100 eq.). (B) IPMS analysis of *h*PLK after treatment with **A-PM-I** for 24 h (100 eq).
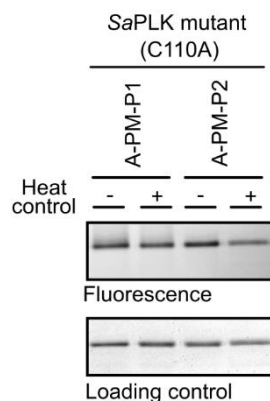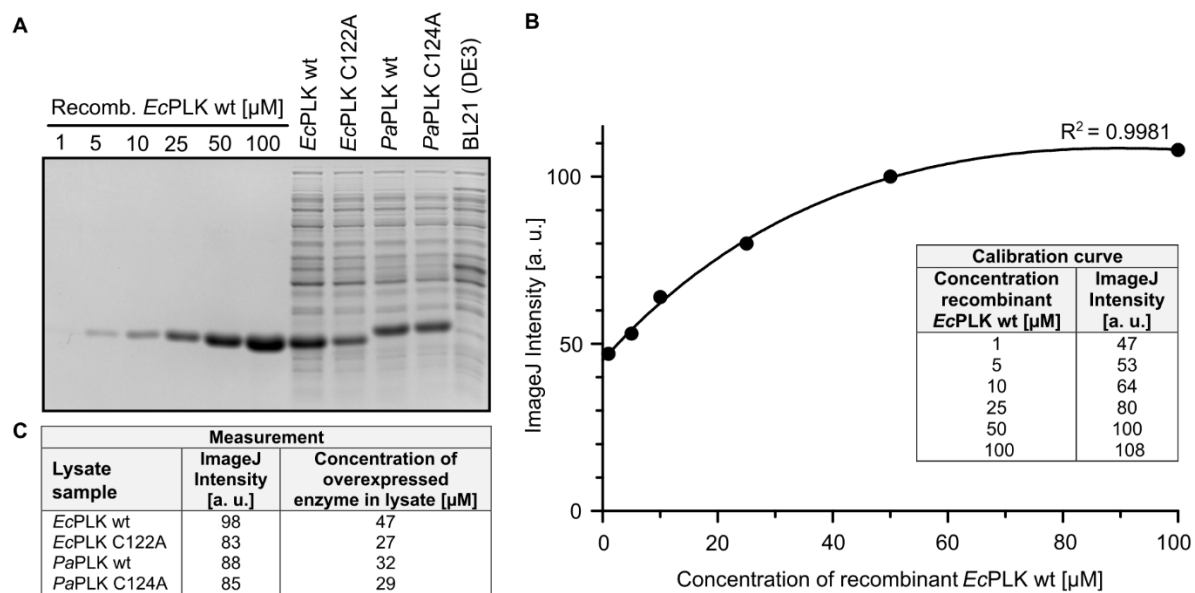
Supplementary Figure S3. Gel-based labeling of recombinant *Sa*PLK mutant (C110A). The enzyme was incubated with probes (10 eq.) for 24 h and visualized via SDS-PAGE.
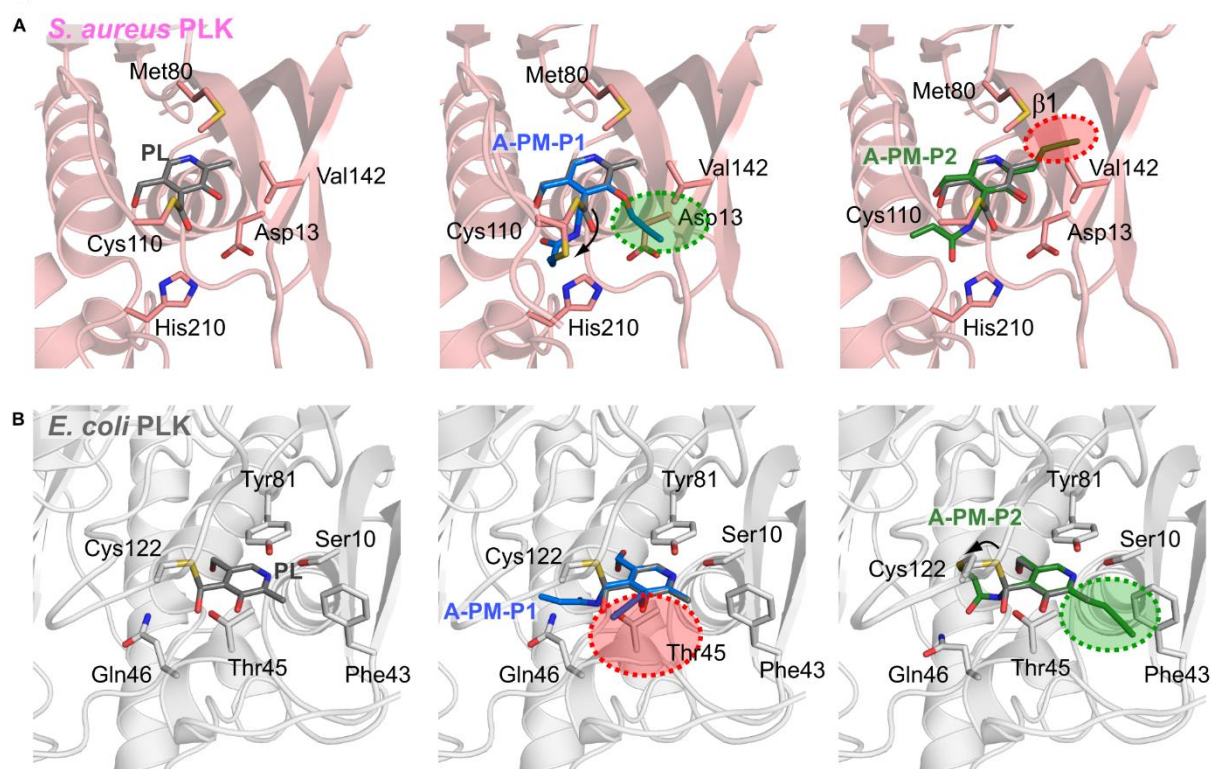
Supplementary Figure S4. Close-up view of the **PL**-binding site of (A) the Gram-positive *Sa*PLK (*thiD*, PDB code: 4C5L, pink)[1a] and (B) Gram-negative *Ec*PLK (*pdxY*, PDB code: 1TD2, gray).[1c] The left panels present the respect binding sites with **PL** (gray stick model) as previously obtained by co-crystallization.[1a, 1c] The structures of **A-PM-P1** (blue stick model, middle panel) and **A-PM-P2** (green stick model, right panel) have been modeled into the available X-ray crystal structures using atoms of the covalently bound **PL** as reference points. For *Sa*PLK, the alkyne handle positioned at the 3'-OH group in **A-PM-P1** can slot next to the β-hairpin and Val142 (A, middle panel), as indicated by the green circle. Consequently, the arrow indicates the conformational change of the lid loop and its lid Cys110 to react with the warhead of the accommodated probe. In contrast, the alkyne moiety positioned at the 2'-methyl group in **A-PM-P2** clashes with the first β-strand in *Sa*PLK (A, right panel), highlighted by the red circle. Vice versa, in *Ec*PLK, **A-PM-P1** clashes with Thr45 located at the small-helix-loop secondary structural element (B, middle panel, red circle) while **A-PM-P2** fits well into the binding pocket and conformational change as well as covalent engagement with the lid Cys122 is indicated by the arrow (B, right panel).

72
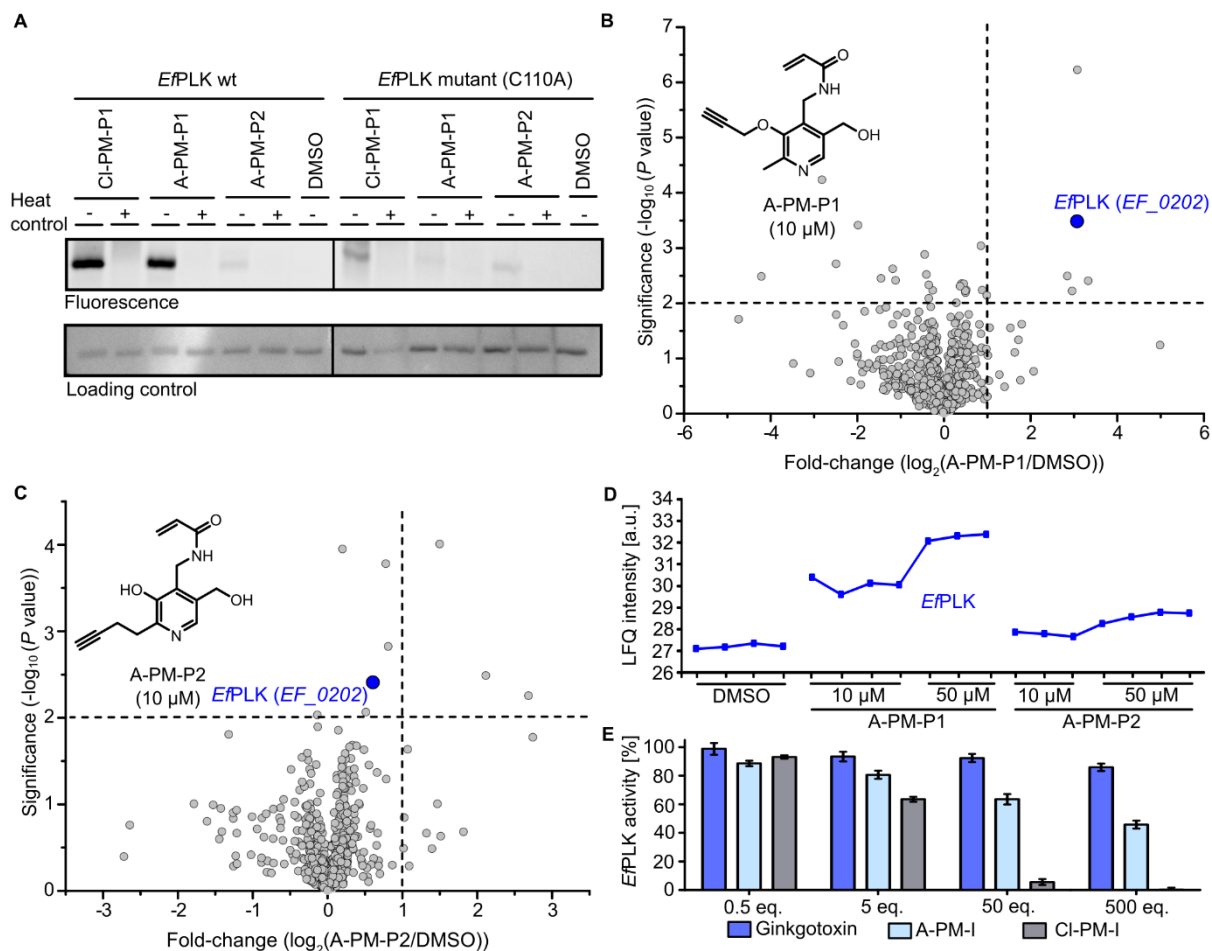
Supplementary Figure S5. Target identification by chemical proteome profiling and target validation in *E. faecalis*. (A) Gel-based labeling of recombinant *Ef*PLK. Wild type and mutant (C110A) enzymes were incubated with probes (10 eq.) for 24 h and visualized via SDS-PAGE. The volcano plots show enrichment of proteins after treatment (24 h) of *E. faecalis* (B) **A-PM-P1** (10 μM) and (C) **A-PM-P2** (10 μM) on a $\log_2$ scale. The vertical and horizontal threshold lines represent a $\log_2$ enrichment ratio of 1 and a $-\log_{10}$ P value of 2 (two-sided two-sample t-test, at least n = 3 independent experiments per group), respectively. (D) Profile plot representation of proteomic data showing LFQ intensities of *Ef*PLK after treatment of intact *E. faecalis* cells with **A-PM-P1** (10 μM and 50 μM) and **A-PM-P2** (10 μM and 50 μM) (at least n = 3 independent experiments per group). (E) Influence of the compounds **A-PM-I**, **Cl-PM-I** and ginkgotoxin on *Ef*PLK phosphorylation activity. Activity was measured after incubation for 2 h at 25 °C (n = 3 independent experiments per group; data represent the mean ± SEM).

A

Recomb. *Ec*PLK wt [µM]

1 5 10 25 50 100

B

Calibration curve	
Concentration recombinant *Ec*PLK wt [µM]	ImageJ Intensity [a. u.]
1	47
5	53
10	64
25	80
50	100
100	108

$R^2 = 0.9981$

C

Measurement		
Lysate sample	ImageJ Intensity [a. u.]	Concentration of overexpressed enzyme in lysate [µM]
*Ec*PLK wt	98	47
*Ec*PLK C122A	83	27
*Pa*PLK wt	88	32
*Pa*PLK C124A	85	29

Supplementary Figure S6. Determining the concentration of overexpressed PLKs in lysate using ImageJ. (A) Gel containing varying concentrations of recombinant *Ec*PLK wt as well as overexpressed PLK lysates. (B) Gray values for recombinant enzyme bands were analyzed using ImageJ and a calibration curve was calculated. (C) Calibration curve was used to determine the protein concentration of PLKs in lysates.

4.2 References

[1]   a) M. B. Nodwell, M. F. Koch, F. Alte, S. Schneider, S. A. Sieber, *Journal of the American Chemical Society* **2014**, *136*, 4992-4999; b) M. I. Kim, M. Hong, *Biochemical and Biophysical Research Communications* **2016**, *478*, 300-306; c) M. K. Safo, F. N. Musayev, S. Hunt, M. L. di Salvo, N. Scarsdale, V. Schirch, *Journal of Bacteriology* **2004**, *186*, 8074-8082.

[2]   F. Huang, X. Han, X. Xiao, J. Zhou, *Molecules* **2022**, *27*, 7728.

[3]   A. K. Gandhi, J. V. Desai, M. S. Ghatge, M. L. di Salvo, S. Di Biase, R. Danso-Danquah, F. N. Musayev, R. Contestabile, V. Schirch, M. K. Safo, *PLOS ONE* **2012**, *7*, e40954.

[4]   G. Mancuso, A. Midiri, E. Gerace, C. Biondo, *Pathogens* **2021**, *10*, 1310.

[5]   F. Sievers, A. Wilm, D. Dineen, T. J. Gibson, K. Karplus, W. Li, R. Lopez, H. McWilliam, M. Remmert, J. Söding, J. D. Thompson, D. G. Higgins, *Molecular Systems Biology* **2011**, *7*, 539.

5|
Addressing mycobacterial ThiD with B-vitamin-based cofactor traps

5.1 Objective

The previous chapter 4 dealt with the successful identification of bacterial lid-cysteine containing PLKs using vitamin B6-based cofactor probes. ThiD and PLK proteins share certain homologies based on their typical ribokinase fold and catalyze similar reactions, *e.g. Sa*PLK cannot only phosphorylate **PL** but also **HMP**, which is the actual substrate-scaffold of ThiD proteins.[1] Here, sequence identity comparison of mycobacterial ThiD proteins (Fig. 5.1, A) reveals around 30% identity with *Sa*PLK[2] (Gram-positive) while only around 20% homology was identified for *E. coli* PdxY[3] (Gram-negative PLK).[4]

A

Sequence Identity [%]	E. coli_PdxY (PLK)	S. aureus _PLK	M. tuberculosis _ThiD	M. smegmatis _ThiD	UniProt ID
E. coli_PdxY (PLK)	100	20	20	17	P77150
S. aureus _PLK	20	100	34	33	A0A0H2XGZ0
M. tuberculosis _ThiD	20	34	100	71	P9WG77
M. smegmatis _ThiD	17	33	71	100	I7G2G7

B

```
sp|P77150|PDXY_ECOLI            -----------MMKNILAIQSHVVYGHAGNSAAEFPMRRLGANVWPLNTVQFSNHTQYGK      49
tr|A0A0H2XGZ0|A0A0H2XGZ0_STAA3  ----------MALKKVLTIAGSDTSAGAGMQADLKTFQELDTYGMV--ALTAIVTMDKDT      48
sp|P9WG77|THID_MYCTU            MNYLPLAPPGMTPPRVLSIAGSDSGGGAGIQADMRTMALLGVHACV--AVTAVTV-QNTL      57
tr|I7G2G7|I7G2G7_MYCS2          MKLLPLTPPGQTPTRVMTIAGTDSGGGAGIQADLRTFAMLGVHGCV--AVAAVTV-QNSV      57
                                          .:::*  .  .  ** .*   :  *..    ::       :

sp|P77150|PDXY_ECOLI            WTGCVMPPSHLTEIVQGIAAIDKLHTCDAVLSGYLGSAEQGEHILGIVRQVKAANPQAKY     109
tr|A0A0H2XGZ0|A0A0H2XGZ0_STAA3  WSHDVTPL-PMDVFEKQLET-ALSIGPDAIKTGMLGTEEIIKR---AGEVYEASN-AQYF     102
sp|P9WG77|THID_MYCTU            GVKDIHEV-PNDVVAGQIEAVVTDIGVQAAKTGMLASSRIVAT---VAATWRRLELSVPL     113
tr|I7G2G7|I7G2G7_MYCS2          GVKGFHEV-PVDIIAGQIQVVAEDIGIQAAKTGMLASAEIIGA---VAETWRGLGTEAPL     113
                                  .        .   :.       :* :* *.:  .

sp|P77150|PDXY_ECOLI            FCDPVMGHPEKGCIVAPGVAEFHVRHGLPASDIIAPNLVELEILCEHAVNNVE-EAVLAA     168
tr|A0A0H2XGZ0|A0A0H2XGZ0_STAA3  VVDPVMVCKGEDEVLNPGNTEAMIKYLLPKATVVTPNLFEAGQLSGLGKLNSIEDMKKAA     162
sp|P9WG77|THID_MYCTU            VVDPVCASMHGDPLLAPSALDSLRGQLFPLATLLTPNLDEARLLVDIEVVDAE-SQRAAA     172
tr|I7G2G7|I7G2G7_MYCS2          VVDPVCASMHGDPLLHPSALDSVRNELFPIASLVTPNLDEVRLITGIEVVDEA-TQRDAA     172
                                 . ***   . :: *.  :      :*: :::*** *   :    :       **

sp|P77150|PDXY_ECOLI            RELIAQGPQIVLVKHLARAGYSRDRFEMLLVTADEAWHISRPLVDFGMRQPVGVGDVTSG     228
tr|A0A0H2XGZ0|A0A0H2XGZ0_STAA3  TIIFDKGAQHVIIKGGKALD--QDKSYDLYYDGQTFYQLTTDMFQQS--YNHGAGCTFAA     218
sp|P9WG77|THID_MYCTU            KALHALGPQWVLVKGGHLRS--SDGSCDLLYDGVSCYQFDAQRLPTG--DDHGGGDTLAT     228
tr|I7G2G7|I7G2G7_MYCS2          KALHALGPKWALVKGGHLRT--SAQSPDLLYNGTDFYEFGAERIDTG--HDHGAGDTLAA     228
                                 :    *  : .::*          *    .   .:    .     .  * * .:

sp|P77150|PDXY_ECOLI            LLLVKLLQGATLQEALEHVTAAVYEIMVTTKAMQEYELQVVAAQDRIAKPEHYFSATKL-     287
tr|A0A0H2XGZ0|A0A0H2XGZ0_STAA3  ATTAYLANGKSPKEAVISAKAFVASAIKNGWKMNDFVGP--------VDHGAYNRIEHID     270
sp|P9WG77|THID_MYCTU            AIAAALAHGFTVPDAVDFGKRWVTECLRAAYPLGRGHGP--------VSPL--FRLS---     275
tr|I7G2G7|I7G2G7_MYCS2          AAACALAHGMDMPDAVAFAKGWVTECLRAAYPLGHGHGP--------VSAL--FRLHHGS     278
                                 * :*       :*:    . *  .:        :           ..

sp|P77150|PDXY_ECOLI            ------      287
tr|A0A0H2XGZ0|A0A0H2XGZ0_STAA3  VEVTEV     276
sp|P9WG77|THID_MYCTU            ------     275
tr|I7G2G7|I7G2G7_MYCS2          ------     278
```

Fig. 5.1: Comparison of mycobacterial ThiD proteins and pyridoxal kinases. Presented are from top to bottom: *Ec*PLK (UniProt ID: P77150), *Sa*PLK (UniProt ID: A0A0H2XGZ0), *Mt*ThiD (UniProt ID: P9WG77) and *Ms*ThiD (UniProt ID: I7G2G7). (A) The identity matrix represents sequence homologies which clusters mycobacterial ThiD proteins with high similarity (71%) compared to bacterial pyridoxal kinases (17-34%). Dark blue indicates high similarity and fading to white color visualizes decreasing homology. (B) The sequence alignment shows that the lid-region (blue) is partially conserved in all proteins while the lid-cysteines (yellow) are slightly shifted. Alignment was performed with Clustal Omega (1.2.4).[4-5]

Further, alignment of AlphaFold2-predicted mycobacterial ThiD proteins[4] suggests conserved flexible lid regions that carry lid-cysteines (C119) similarly to *Sa*PLK (C110) and *Ec*PLK (C122), shifted by only a few amino acids (Fig. 2.5, 5.1 B). Of note, the presence of the lid-cysteines is exclusive to mycobacterial ThiD proteins compared to other bacterial ThiD proteins.[4, 6] Moreover, *Mt*ThiD (*Rv0422c*) was

proposed as an essential enzyme in literature[7] being centrally placed within the vitamin B1 (**TPP**) biosynthesis pathways,[1b, 1c] so it is intriguing to see whether previously reported vitamin B6 (**PLP**) cofactor traps could covalently address the conserved lid-cysteine even in mycobacterial ThiD due to protein homology.

Within this chapter, the application of previously introduced vitamin B6-based traps is shown and discussed in *M. smegmatis* prior to the development and application of analogous **HMP**-based probes. Addressing the lid-cysteine of mycobacterial ThiD inside the active pocket might block enzymatic activity to interfere with biosynthesis of vitamin B1, possibly resulting in antimycobacterial effects as previously observed with ThiD transposon mutants.[7a, 7b]

5.2 Attempt to profile ThiD in *M. smegmatis* using vitamin B6-based probes

As previous PLK-studies showed that chloroacetamide warheads have a high reactivity, leading to broad labeling of diverse cysteines,[8] the following gel-based labeling in *M. smegmatis* was carried out with vitamin B6-based probes equipped with the milder-reactive acrylamide warhead that previously enriched Gram-positive and Gram-negative PLK selectively, depending on the alkyne attachment site.[8]

Intact *M. smegmatis* cells were labeled with **A-PM-P1** and **A-PM-P2** from 200 µM down to 12.5 µM concentration-dependently at rt for 24h. Interestingly, both compounds showed a similar labeling pattern which is more intense for **A-PM-P1** (3'-OH modified). Of note, a band around 30 kDa could also be labeled by **A-PM-P1**, hinting towards the expected mass for *Ms*ThiD (Fig. 5.2, A).
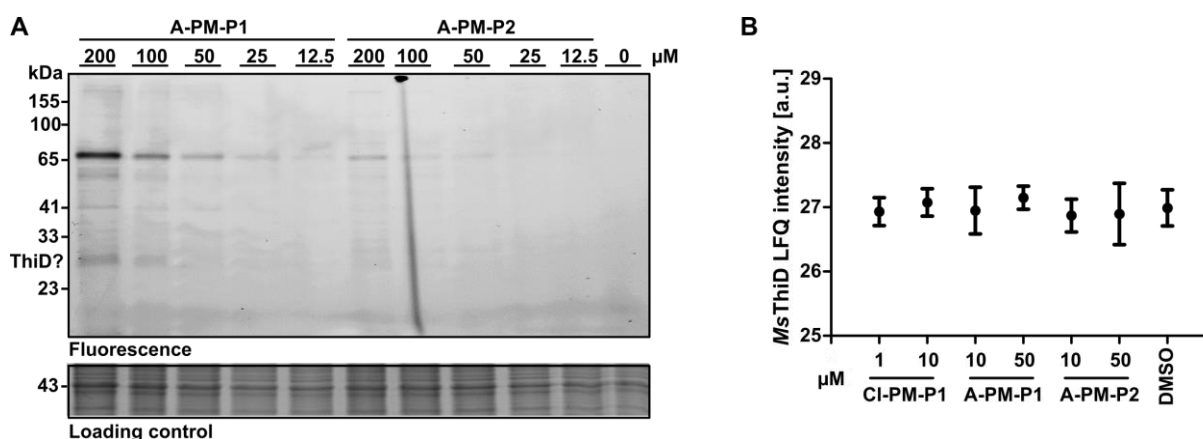
Fig. 5.2: Application of vitamin B6-based probes[8] for ABPP in intact *M. smegmatis* cells. (A) Concentration-dependent analytical labeling (200 µM – 12.5 µM, 24h, rt) revealed fluorescent bands around 30 kDa (ThiD?) for **A-PM-P1** while a similar but less intense labeling is observed for **A-PM-P2**. Coomassie staining served as loading control. (B) *Ms*ThiD peptides, detected by LC-MS/MS, were not enriched in probe-treated samples (**Cl-PM-P1**, **A-PM-P1**, **A-PM-P2**) compared to DMSO treatment (n ≥ 3, error bars represent 95% confidence interval), indicating that the vitamin B6-based probes are not suitable to profile *Ms*ThiD.

Encouraged by this result, LC-MS/MS-based detection was performed with high and low labeling concentrations for both compounds (10 µM and 50 µM each) for detection a concentration-dependent labeling behavior of *Ms*ThiD compared to DMSO. Additionally, **Cl-PM-P1** (10 µM and 1 µM) was also included as a more reactive derivative of P1 as analytical labeling around 30 kDa was weak. Unfortunately, as depicted in Fig. 5.2 B, *Ms*ThiD could not be enriched for any of the vitamin B6-based probe candidates. It seems plausible that *Ms*ThiD does not accept probes based on the vitamin B6 scaffold. Secondly, the tag positions could hinder binding to ThiD proteins.

Therefore, the traps were re-designed by changing the core structure from vitamin B6 to **HMP** as vitamin B1 precursor for fine-tuning of ThiD profiling. Moreover, the enrichment tag was introduced at the 5'-position pointing to the ATP-binding pocket to preclude backbone clashes.

5.3 HMP-based probe synthesis and validation

HMP-Azide was synthesized from thiamine as starting material. The thiazolidine motif served as leaving group and allowed for substitution at the 5'-position by an azide as biorthogonal handle.[9] Subsequent amidation by acryloyl chloride and chloroacetic anhydride yielded **A-HMP-Azide** and **Cl-HMP-Azide**, respectively, as depicted in scheme 5.1. These **HMP**-based azide probes represent homologues of the vitamin B6-based probes with a different core structure and a modified tag position.
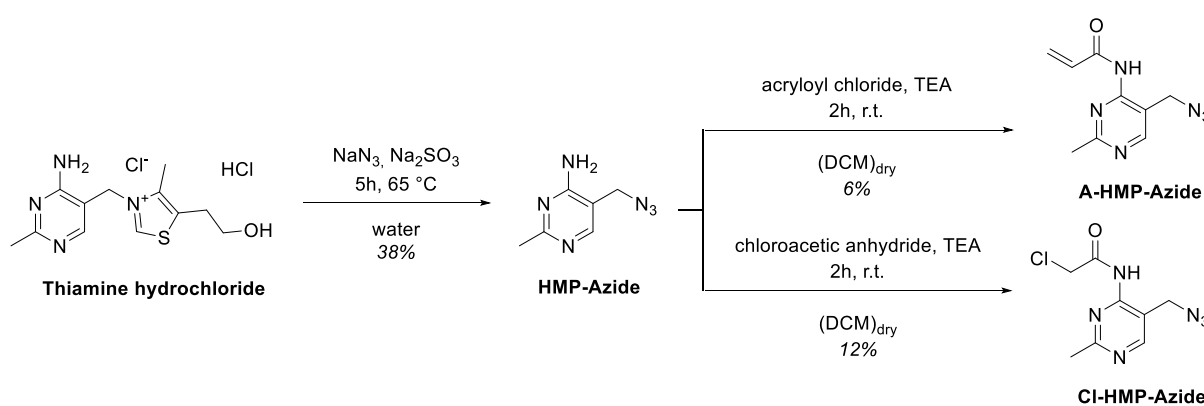
Scheme 5.1. Synthesis scheme of **HMP**-based probes as vitamin B1 biosynthesis precursor mimics for targeting mycobacterial ThiD. Thiamine hydrochloride was substituted by sodium azide to obtain **HMP-Azide** as intermediate.[9] Subsequently, **A-HMP-Azide** and **Cl-HMP-Azide** as probes were obtained by amidation with acryloyl chloride and chloroacetic anhydride with overall yields of 2% and 5%, respectively.

After successful synthesis, the labeling suitability of both probes was compared to the vitamin B6-based probes. As **HMP** is also accepted by *Sa*PLK as a substrate,[1a] labeling of the recombinant *Sa*PLK protein served as a benchmark to compare labeling of the **HMP**-based probes with the previous established vitamin B6-based probes (Fig. 5.3).[8]
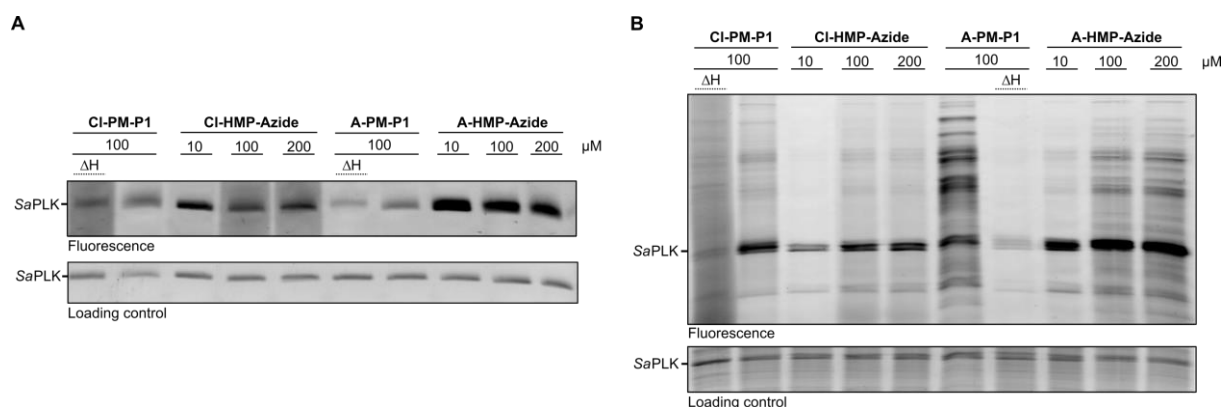
Fig. 5.3. Benchmarking of **HMP**-based probes' labeling properties in comparison to vitamin B6-based probes using recombinant *Sa*PLK (30 kDa). ΔH indicates heat-denatured proteins (0.4% (w/v) SDS, 95 °C, 30 min) prior to labeling, and Coomassie staining served as loading control. (A) Recombinant *Sa*PLK (1 µM) was labeled (24h, rt) in different concentrations of **Cl/A-HMP-Azides** in comparison to **Cl/A-PM-P1** probes (100 µM). Fluorescence analysis revealed superior labeling behavior of the new probes even at 10-fold lower concentrations. (B) Additionally, recombinant *Sa*PLK (1 µM) was added into *S. aureus* background lysate (1 mg mL^{-1}) for assessment of labeling specificity. Although all probes showed a similar labeling pattern, **HMP**-based probes were more selective for *Sa*PLK at low concentrations (10 µM) compared to vitamin B6-based probes. Of note, **A-HMP-Azide** could be identified as the best probe candidate in terms of reactivity and selectivity during both procedures.

Of note, both **HMP**-based showed superior labeling properties of *Sa*PLK compared to the vitamin B6-based probes, although **PL** is its preferred substrate. This finding might hint towards a well-accepted attachment site for the azide-tag at the 5'-position pointing towards the ATP binding pocket (Fig. 5.3, A). Further, during labeling of spiked-in *Sa*PLK in *S. aureus* lysate background for selectivity assessment, a preference for *Sa*PLK is detectable over other labeled proteins even at low **HMP**-based probe concentrations of 10 µM (Fig. 5.3, B). Throughout these experiments, **A-HMP-Azide** was identified as the best probe candidate for *Sa*PLK labeling.

5.4 Application of HMP-based probes to address mycobacterial ThiD

After validation of the new **HMP**-based probes for their labeling properties, they were applied concentration-dependently in intact *M. smegmatis* cells. Despite being demonstrated as cell permeable within this experiment, neither **Cl-HMP-Azide** nor **A-HMP-Azide** could label proteins around 30 kDa that would hint towards labeling of *Ms*ThiD (Fig. 5.4). Lysis was performed with addition of 0.4% SDS so that insoluble proteins were solubilized prior to SDS-PAGE. Interestingly, in contrast to expectations, **A-HMP-Azide** seemed to possess a higher reactivity compared to **Cl-HMP-Azide**. Of note, only **A-HMP-Azide** was identified as temperature sensitive during synthesis, which, unexpectedly, might be a clue for intrinsic higher reactivity compared to the chloroacetamide derivative.
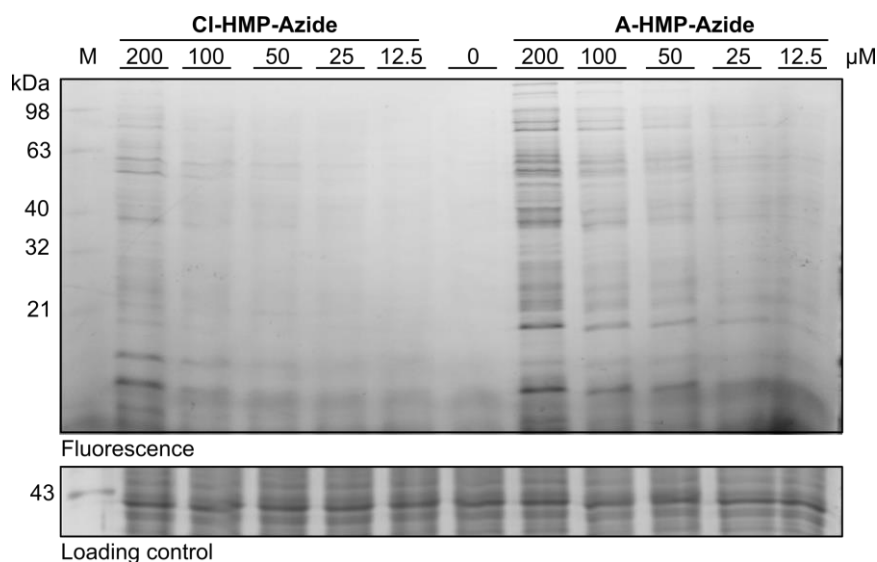
Fig. 5.4. Application of **HMP**-based probes for analytical ABPP in intact *M. smegmatis* cells. M represents a marker with reference protein sizes, and Coomassie staining served as loading control. Mycobacteria were incubated with **Cl-HMP-Azide** and **A-HMP-Azide** (200 – 12.5 µM, 24h, rt) and labeled proteins were analyzed by fluorescent SDS-PAGE. No specific bands could be identified around 30 kDa that would hint towards labeling of *Ms*ThiD.

As the initial *in-situ* analytical labeling experiment with **HMP**-based probes looked even less promising than with previous vitamin B6-probes, MS-based detection was omitted and direct cloning and expression attempts were undertaken to obtain the recombinant ThiD proteins of both *M. smegmatis* (*Ms*ThiD) and *M. tuberculosis* (*Mt*ThiD) for recombinant, covalent target engagement studies. This also allowed comparing mycobacterial ThiD protein labeling behavior as *M. tuberculosis* wild-type cells can only exclusively be handled with S3 clearance, which would not be possible in-house.

Previous unpublished in-house studies could demonstrate that expression of N-terminal His$_6$-tagged ThiD proteins of *M. smegmatis* as well as *M. tuberculosis* resulted in unsoluble protein constructs. Therefore, the gateway cloning technology was successfully used to introduce mycobacterial ThiD sequences into a plasmid containing an additional solubility tag (maltose binding protein, MBP). This strategy finally resulted in the expression of soluble ThiD fusion proteins. Attempts to cleave off the MBP-tag by TEV protease in case of recombinant *Mt*ThiD fusion protein resulted in unsoluble protein precipitate (not shown) so that further studies had to be carried out with the bigger fusion proteins containing masses around 70 kDa instead of 30 kDa.

As the probes were found to be cell-permeable, an *in-situ* labeling experiment inside the *E. coli* expression strain was performed after ThiD fusion protein expression to validate intracellular ThiD binding and to determine selectivity over other proteins. Intact *E. coli* cells were treated for 3h with both **HMP**-based probes concentration-dependently, resulting in concentration-dependent labeling of overexpressed *Ms*ThiD and *Mt*ThiD fusion proteins (around 70 kDa, Fig. 5.5). As observed before, **A-HMP-Azide** showed enhanced labeling for both proteins; however, particularly for **Cl-HMP-Azide**, labeling was weak at lower concentrations despite very high abundance of expressed ThiD. This finding

indicates that labeling efficiency is low. Of note, the MBP-tag does not contain any cysteine so that labeling could only occur on the ThiD domain.[4]
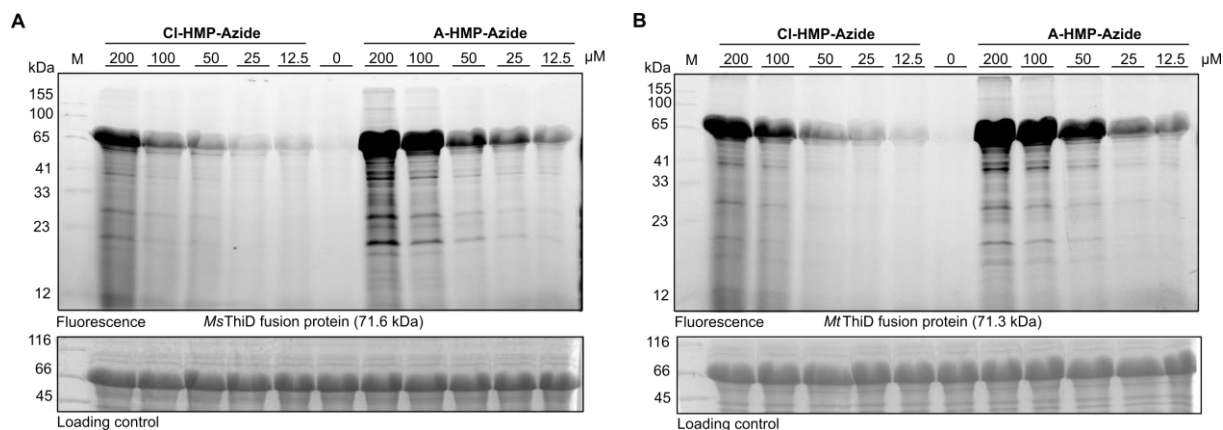
Fig. 5.5. Fluorescent SDS-PAGE analysis of overexpressed *Ms*ThiD (A) and *Mt*ThiD (B) fusion proteins (around 70 kDa) in *E. coli* after intracellular labeling with **HMP**-based probes (3h, rt). M represents a marker as a protein size reference, and Coomassie staining served as loading control. Again, **A-HMP-Azide** showed better performance compared to **Cl-HMP-Azide** for both protein constructs. Of note, the MBP solubility tag does not contain any cysteine,[4] and hence, labeling is attributable to the ThiD domains which contain four and five cysteine residues, respectively.[4]

Closer examination of the amount of cysteines within the ThiD domains revealed that four and five residues are present in *Ms*ThiD and *Mt*ThiD, respectively.[4] This finding raises doubts about the validity of assuming that the lid-cysteine C119 is the sole cysteine residue involved in covalent interaction. The poor ionization behavior of the large fusion proteins during intact protein mass spectrometry (IPMS) limited the approach of identifying the amount of probe modifications per fusion protein. Hence, the subsequent work focused on the construction of ThiD fusion protein mutants with alanine residues in place of the lid-cysteines, which should completely eradicate the labeling upon probe incubation if binding solely occurs on the signature residue. All four mycobacterial ThiD-MBP fusion proteins were successfully expressed and purified by affinity purification.

Recombinant protein labeling experiments using both probes with 10-fold or 100-fold excess in wild-types and mutants of mycobacterial ThiD fusion proteins (1 µM) revealed reduced labeling of the mutant proteins compared to wild-type constructs (Fig. 5.6, upper panel). This finding underlines that the designed **HMP**-based probes partially target the desired lid-cysteine albeit at high compound concentrations of 100 µM. As previously observed, treatment with **A-HMP-Azide** resulted in more intense labeling.
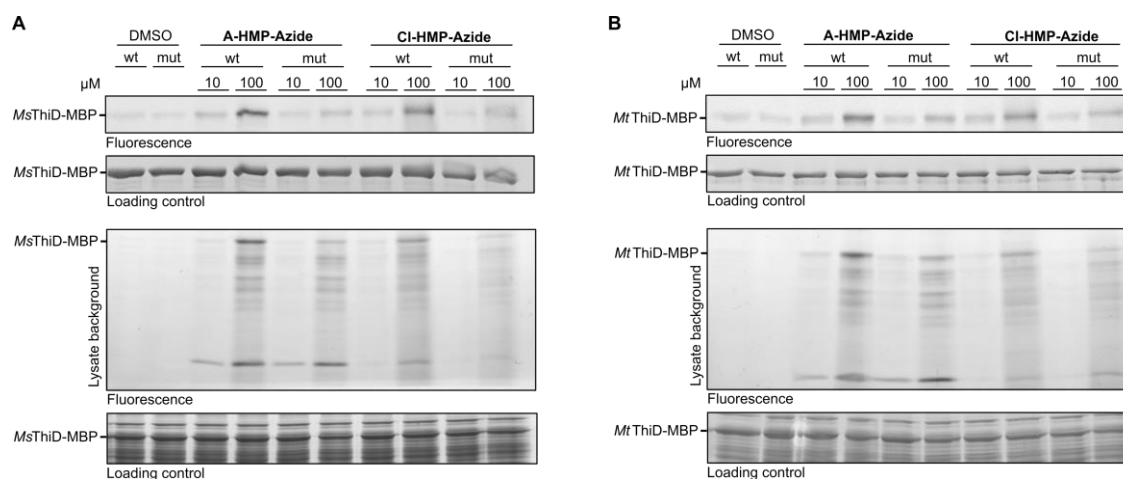
Fig. 5.6. Fluorescent SDS-PAGE analysis after labeling with **A-HMP-Azide** and **Cl-HMP-Azide** of recombinant *Ms*ThiD (A) and *Mt*ThiD (B) wild-type and mutant fusion proteins that contain an alanine in place of a cysteine in the lid region (C119A). The upper panels present labeling results of purified proteins (1 µM, around 70 kDa), while the lower panels depict respective labeling with additional lysate background (1 mg mL^{-1}). Coomassie staining served as loading control. In both ThiD proteins, labeling by **A-HMP-Azide** and **Cl-HMP-Azide** was decreased in the C119A constructs, indicating partial binding to the desired lid-cysteine within the **HMP**-binding pockets.

The same binding trends were observed when lysate backgrounds with spiked-in ThiD fusion proteins were analyzed (Fig. 5.6, lower panel). It is crucial to take into account that both probes also exhibit considerable off-reactivity with other cysteines present in the ThiD protein structure itself, as well as with cysteines in other background proteins. This observation highlights a lack of specifity for the active pocket of ThiD proteins, despite the use of the adapted **HMP** scaffold. Exemplarily, heat-denatured *Ms*ThiD-MBP constructs were also strongly labeled by **A-HMP-Azide** and **Cl-HMP-Azide**, further indicating that protein labeling is unrelated to the fold but rather dependent on intrinsic compound reactivity (Fig. 5.7).
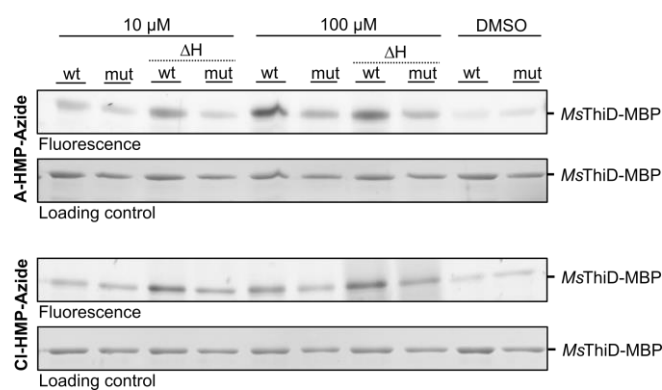
Fig. 5.7. Heat control experiments with *Ms*ThiD wild-type and C119A mutant fusion proteins (1 µM). Protein labeling by **A-HMP-Azide** and **Cl-HMP-Azide** was compared to native and heat-denatured constructs (ΔH; 0.4% SDS, 95 °C, 30 min). Unexpectedly, the experimental results suggest that probe reactivity rather than the three-dimensional protein fold drives labeling properties. Coomassie staining served as loading control.

After having demonstrated partial binding of the covalent traps to the desired lid-cysteine, which should result in irreversible occupation of the active pocket and therefore decrease enzymatic activity, effects of the compounds on the growth of *M. smegmatis* (in-house) and the *M. tuberculosis* (Forschungszentrum Borstel) strains were investigated. Unfortunately, none of the **HMP**-Azide

compounds could reduce the growth of mycobacteria up to 100 µM (data not shown). However, as the **HMP**-azide probes were demonstrated for binding in the active pocket, they could be used for competitive profiling of active site ThiD inhibitors in future studies.

5.5 Conclusion

*Mt*ThiD was previously discussed in literature regarding its essentiality.[7] This protein is involved in the biosynthesis of thiamine pyrophosphate (vitamin B1, **TPP**)[1b, 1c, 10] that supports crucial enzymatic steps, such as oxidative decarboxylation in the pyruvate dehydrogenase complex in synergy with **LA**, and therefore contributes to central metabolism pathways for energy production and metabolic flux.[11] Targeting this ThiD enzyme would be a new strategy to affect growth of *M. tuberculosis* as one of the deadliest bacteria today.[12] As presented in chapter 4, ThiD-homologous PLK enzymes could be covalently addressed by vitamin B6-based cysteine reactive traps.[8] Interestingly, mycobacterial ThiD proteins also contain a conserved cysteine in the lid, although being catalytically irrelevant for **HMP-P** phosphorylation during **TPP** biosynthesis. Addressing this cysteine in the active pocket covalently with a small molecule would block substrate binding in the catalytic center, which demonstrates a potential to inhibit the enzymatic activity.

Within this chapter, the covalent engagement of the certain lid-cysteine in mycobacterial ThiD proteins was studied. The use of previously established vitamin B6 based-cofactor traps[8] did not address this enzyme in intact *M. smegmatis* cells as a representative mycobacterial strain. This finding guided the design and synthesis of a new core structure based on the ThiD substrate motif (**HMP**) together with a differently positioned azide-handle for downstream analysis with rhodamine-alkyne by means of click-chemistry and fluorescent SDS-PAGE analysis. Both modifications were shown to be superior in labeling *Sa*PLK compared to previous vitamin B6-based probes. Still, despite cell permeability, their *in-situ* application did not hint towards the desired targeting of *Ms*ThiD in the whole proteome of *M. smegmatis*, and hence, direct target interaction studies were performed with the recombinant *Ms*ThiD enzyme and its respective lid-cysteine to alanine mutant (C119A). This approach also allowed for the direct study of the respective *Mt*ThiD enzymes without the need of culturing *M. tuberculosis*. Although both **HMP**-probe molecules could address recombinant *Ms*ThiD and *Mt*ThiD covalently, albeit at high concentrations of 100 µM, other background proteins were also labeled.

Secondly, the desired lid-cysteine residue could not be exclusively addressed over other cysteines present in the protein domain itself, or in background proteins. Both findings hint towards side effects for an application due to missing selectivity for the active ThiD pocket despite the adopted core structure. Heat-denatured protein labeling experiments support this drawback.

Thirdly, although partial engagement with the lid-cysteine residue could be demonstrated with a high excess of compound compared to target protein, no antimycobacterial effect could be identified neither in *M. smegmatis* nor in *M. tuberculosis* strains up to 100 µM of **HMP**-based compounds. These findings suggest the use of the herein developed probes for competitive profiling to identify more potent ThiD inhibitors in the future.

Overall, both probes were demonstrated as promiscuous binders with partial affinity for the active pocket of recombinant mycobacterial ThiD during our studies. Moreover, a facile mutation of this catalytically irrelevant lid-cysteine to a non-nucleophilic residue would render this antibiotic strategy obsolete and poses this strategy at high risk for resistance development. Instead, the herein developed probes bear potential for the discovery of more potent ThiD inhibitors by competitive screenings. To conclude, the covalent engagement of the lid-cysteine of mycobacterial ThiD could not be classified as a promising strategy during our studies to reduce growth of *M. tuberculosis* as an alternative antimicrobial strategy, despite that *Mt*ThiD is discussed as essential in literature reports.[7] However, the developed **HMP**-based probes could serve as discovery tool for non-covalent active site ThiD inhibitors.

5.6 References

[1]   a) M. B. Nodwell, M. F. Koch, F. Alte, S. Schneider, S. A. Sieber, *Journal of the American Chemical Society* **2014**, *136*, 4992-4999; b) C. T. Jurgenson, T. P. Begley, S. E. Ealick, *Annual Review of Biochemistry* **2009**, *78*, 569-603; c) C. T. Jurgenson, S. E. Ealick, T. P. Begley, *EcoSal Plus* **2009**, *3*, 3.6.3.7.

[2]   a) C. L. Tung, H. Y. Lam, J. Xu, X. Li, *Chemical Communications* **2014**, *50*, 5298-5300; b) M. L. di Salvo, I. Nogués, A. Parroni, A. Tramonti, T. Milano, S. Pascarella, R. Contestabile, *Biochimica et Biophysica Acta* **2015**, *1854*, 1160-1166.

[3]   M. K. Safo, F. N. Musayev, S. Hunt, M. L. di Salvo, N. Scarsdale, V. Schirch, *Journal of Bacteriology* **2004**, *186*, 8074-8082.

[4]   UniProtConsortium, *Nucleic Acids Research* **2023**, *51*, D523-D531.

[5]   F. Sievers, A. Wilm, D. Dineen, T. J. Gibson, K. Karplus, W. Li, R. Lopez, H. McWilliam, M. Remmert, J. Söding, J. D. Thompson, D. G. Higgins, *Molecular Systems Biology* **2011**, *7*, 539.

[6]   S. F. Altschul, W. Gish, W. Miller, E. W. Myers, D. J. Lipman, *Journal of Molecular Biology* **1990**, *215*, 403-410.

[7]   a) C. M. Sassetti, D. H. Boyd, E. J. Rubin, *Molecular Microbiology* **2003**, *48*, 77-84; b) M. A. DeJesus, E. R. Gerrick, W. Xu, S. W. Park, J. E. Long, C. C. Boutte, E. J. Rubin, D. Schnappinger, S. Ehrt, S. M. Fortune, C. M. Sassetti, T. R. Ioerger, *mBio* **2017**, *8*, e02133-02116; c) K. Raman, K. Yeturu, N. Chandra, *BMC Systems Biology* **2008**, *2*, 109.

[8]   I. Hübner, J.-N. Dienemann, J. Friederich, S. Schneider, S. A. Sieber, *ACS Chemical Biology* **2020**, *15*, 3227-3234.

[9]   J.-B. He, Y.-L. Ren, Q.-S. Sun, G.-Y. You, L. Zhang, P. Zou, L.-L. Feng, J. Wan, H.-W. He, *Bioorganic & Medicinal Chemistry* **2014**, *22*, 3180-3186.

[10]   M. Kanehisa, S. Goto, *Nucleic Acids Research* **2000**, *28*, 27-30.

[11]   M. S. Patel, N. S. Nemeria, W. Furey, F. Jordan, *Journal of Biological Chemistry* **2014**, *289*, 16615-16623.

[12]   E. L.-H. MacLean, P. Miotto, L. González Angulo, M. Chiacchiaretta, T. M. Walker, M. Casenghi, C. Rodrigues, T. C. Rodwell, P. Supply, E. André, M. Kohli, M. Ruhwald, D. M. Cirillo, N. Ismail, M. Zignol, *PLOS Global Public Health* **2023**, *3*, e0001754.

6|

Research conclusion and outlook

In summary, this thesis highlights the urgent need for new strategies to address antimicrobial resistance, which is about to become a global health crisis.[1] Current estimates suggest that if immediate action is not taken, drug-resistant microbes could cause 10 Mio deaths annually by 2050, surpassing the number of deaths attributed to cancer.[1b] Therefore, new strategies need to be offered to tackle this current 'silent pandemic'.[1e]

Societal, regulatory, and economic factors currently hinder the development of novel antimicrobial compounds.[1b, 2] Briefly, awareness campaigns could help to administer antimicrobials more responsibly and joint forces of political, private, industrial and non-governmental organizations could contribute to new business structures in the environment of antimicrobial drug development, making investments more attractive. Several strategies, such as improvement of sanitation and surveillance of resistance spread, as well as vector control, but also vaccine development, and innovative small molecule concepts can aid in tackling the antimicrobial resistance crisis (chapter 1).

The thesis focuses on investigating novel antimicrobial concepts based on cofactor-dependent metabolism using activity-based protein profiling (ABPP). Pathogenic and human metabolism differ, enabling the development of safe drugs. Pathogens, such as the parasite *P. falciparum* (Lipoic acid salvage, chapter 2.1), as well as *M. tuberculosis* (vitamin B1 biosynthesis, chapter 2.3) and *Enterococci* (vitamin B6 metabolism, chapter 2.2), which were previously listed as pathogens of critical concern, were analyzed with priority.[3]

In the context of lipoic acid-dependent metabolism, the attractiveness of developing LPL inhibitors is explored. Lipoic acid auxotroph strains, including pathogens like *L. monocytogenes* and *P. falciparum*, rely on lipoate salvage for the function of their essential energy metabolism and metabolic flux.[4] A probe molecule was successfully developed and incorporated by LPL in place of lipoate onto lipoate-dependent enzymes, enabling the monitoring of LPL activity by fluorescent SDS-PAGE. This ABPP-technique allowed for screens of a compiled library by computational methods containing potential LPL inhibitors, and could identify two hits (**C3** and **LAMe**), which were further verified as LPL inhibitors by ITC and co-crystallography. While none of the compounds inhibited the growth of *L. monocytogenes,* they demonstrated promising antimalarial activity by killing the parasite *P. falciparum* in erythrocytes in the low micromolar range with low to moderate toxicity in human cells (chapter 3). Further optimization of these compounds is required for pre-clinical development.

Furthermore, the thesis investigates PLK (chapter 4) and ThiD (chapter 5) proteins of bacterial pathogens involved in vitamin B6 salvage[5] and vitamin B1 biosynthesis,[6] respectively. These proteins share homologous structural folds and some relevant subclasses contain a conserved lid-cysteine in the active pocket, conserved across bacterial species. While some Gram-positive and Gram-negative bacteria contain a catalytically relevant lid-cysteine for transient **PL** binding in PLK,[7] such a cysteine

residue is absent in most ThiD proteins with exception to mycobacteria. *M. tuberculosis* and *M. smegmatis* contain a conserved but non-catalytic lid-cysteine inside the active pocket of ThiD.[8]

For both of these homologous enzyme classes, binding of respective tailored cofactor mimics, containing an acrylamide or a chloroacetamide warhead,[9] was demonstrated to the lid-cysteines, as evidenced by decreased labeling of alanine-mutant proteins. Despite assays with recombinant Gram-positive PLK could additionally demonstrate a reduction of activity, albeit at high compound excess, no antibiotic activity against **PLP** auxotrophic *Enterococci* spp. by addressing PLK nor antimycobacterial activity by addressing the **TPP**-biosynthesis enzyme ThiD was observed. The selectivity of the cysteine-reactive compounds needs to be improved to diminish off-target binding, as assessed by ABPP. These findings suggest that both binding affinity and target selectivity should be increased. It is uncertain whether these proteins could serve as suitable new antibacterial drug-targets based on the presented experimental data, although ThiD of *M. tuberculosis* has been previously discussed as a potential drug target based on transposon mutant studies.[10] However, targeting non-catalytic cysteines, as in the case of mycobacterial ThiD, may easily lead to mutations that are not addressable by acrylamide or chloroacetamide warheads anymore, raising questions about the applicability of the presented concept beyond research. Therefore, the developed B-vitamin probes should rather be considered as a tool for active site inhibitor discovery for PLK and ThiD proteins in future studies.

In conclusion, no antibacterial effects were observed with the cofactor mimics of vitamin B6 and vitamin B1 that covalently target lid-cysteines of PLK and ThiD, respectively. Still, they bear potential as tool throughout inhibitor discovery by competitive profiling as they bound into the active pockets of PLK and ThiD. Promising results were obtained in the discovery of LPL inhibitors by lipoate-probes, suggesting lipoate salvage as a potential strategy for antimalarial drug development based on killing of the parasite *P. falciparum* in erythrocytes. Future studies should focus on enhancing the potency of lead molecules to inhibit lipoate salvage in bacteria more effectively, potentially leading also to antibiotic effects, as suggested by LPL knockout growth experiments in *L. monocytogenes* (Δ*lplA1*).[4b, 4c]

6.1 References

[1]   a) C. J. L. Murray, K. S. Ikuta, F. Sharara, L. Swetschinski, G. Robles Aguilar, A. Gray, C. Han, C. Bisignano, P. Rao, E. Wool, S. C. Johnson, A. J. Browne, M. G. Chipeta, F. Fell, S. Hackett, G. Haines-Woodhouse, B. H. Kashef Hamadani, E. A. P. Kumaran, B. McManigal, S. Achalapong, R. Agarwal, S. Akech, S. Albertson, J. Amuasi, J. Andrews, A. Aravkin, E. Ashley, F.-X. Babin, F. Bailey, S. Baker, B. Basnyat, A. Bekker, R. Bender, J. A. Berkley, A. Bethou, J. Bielicki, S. Boonkasidecha, J. Bukosia, C. Carvalheiro, C. Castañeda-Orjuela, V. Chansamouth, S. Chaurasia, S. Chiurchiù, F. Chowdhury, R. Clotaire Donatien, A. J. Cook, B. Cooper, T. R. Cressey, E. Criollo-Mora, M. Cunningham, S. Darboe, N. P. J. Day, M. De Luca, K. Dokova, A. Dramowski, S. J. Dunachie, T. Duong Bich, T. Eckmanns, D. Eibach, A. Emami, N. Feasey, N. Fisher-Pearson, K. Forrest, C. Garcia, D. Garrett, P. Gastmeier, A. Z. Giref, R. C. Greer, V. Gupta, S. Haller, A. Haselbeck, S. I. Hay, M. Holm, S. Hopkins, Y. Hsia, K. C. Iregbu, J. Jacobs, D. Jarovsky, F. Javanmardi, A. W. J. Jenney, M. Khorana, S. Khusuwan, N. Kissoon, E. Kobeissi, T. Kostyanev, F. Krapp, R. Krumkamp, A. Kumar, H. H. Kyu, C. Lim, K. Lim, D. Limmathurotsakul, M. J. Loftus, M. Lunn, J. Ma, A. Manoharan, F. Marks, J. May, M. Mayxay, N. Mturi, et al., *The Lancet* **2022**, *399*, 629-655; b) J. O'Neill, **2016**, The Review on Antimicrobial Resistance, Tackling drug-resistant infections globally: final report and recommendations; c) WHO, **2014**, Antimicrobial resistance – global report on surveillance; d) M. Davis, *Journal of Pharmacy Practice and Research* **2020**, *50*, 463-464; e) R. A. Rayan, *World Journal of Clinical Cases* **2023**, *11*, 1267-1274; f) Editorial, *EClinicalMedicine* **2021**, *41*, 101221.

[2]   a) C. Årdal, M. Balasegaram, R. Laxminarayan, D. McAdams, K. Outterson, J. H. Rex, N. Sumpradit, *Nature Reviews Microbiology* **2020**, *18*, 267-274; b) T. Minssen, K. Outterson, S. Rogers Van Katwyk, P. H. D. Batista, C. I. R. Chandler, F. Ciabuschi, S. Harbarth, A. S. Kesselheim, R. Laxminarayan, K. Liddell, M. T. Osterholm, L. Price, S. J. Hoffman, *Bulletin of the World Health Organization* **2020**, *98*, 823-823a; c) J. F. Hayes, *Antibiotics* **2022**, *11*, 644.

[3]   a) G. Mancuso, A. Midiri, E. Gerace, C. Biondo, *Pathogens* **2021**, *10*, 1310; b) E. L.-H. MacLean, P. Miotto, L. González Angulo, M. Chiacchiaretta, T. M. Walker, M. Casenghi, C. Rodrigues, T. C. Rodwell, P. Supply, E. André, M. Kohli, M. Ruhwald, D. M. Cirillo, N. Ismail, M. Zignol, *PLOS Global Public Health* **2023**, *3*, e0001754.

[4]   a) J. E. Cronan, *Frontiers in Genetics* **2020**, *11*, 510; b) M. O'Riordan, M. A. Moors, D. A. Portnoy, *Science* **2003**, *302*, 462-464; c) K. M. Keeney, J. A. Stuckey, M. X. D. O'Riordan, *Molecular Microbiology* **2007**, *66*, 758-770; d) G. A. Afanador, K. A. Matthews, D. Bartee, J. E. Gisselberg, M. S. Walters, C. L. Freel Meyers, S. T. Prigge, *Molecular Microbiology* **2014**, *94*, 156-171; e) S. C. Nair, J. T. Munro, A. Mann, M. Llinás, S. T. Prigge, *Proceedings of the National Academy of Sciences of the United States of America* **2023**, *120*, e2210929120; f) M. D. Spalding, S. T. Prigge, *Microbiology and Molecular Biology Reviews* **2010**, *74*, 200-228.

[5]   a) M. L. di Salvo, R. Contestabile, M. K. Safo, *Biochimica et Biophysica Acta* **2011**, *1814*, 1597-1608; b) T. Mukherjee, J. Hanes, I. Tews, S. E. Ealick, T. P. Begley, *Biochimica et Biophysica Acta* **2011**, *1814*, 1585-1596.

[6]   a) C. T. Jurgenson, T. P. Begley, S. E. Ealick, *Annual Review of Biochemistry* **2009**, *78*, 569-603; b) C. T. Jurgenson, S. E. Ealick, T. P. Begley, *EcoSal Plus* **2009**, *3*, 3.6.3.7.

[7]   a) M. K. Safo, F. N. Musayev, S. Hunt, M. L. di Salvo, N. Scarsdale, V. Schirch, *Journal of Bacteriology* **2004**, *186*, 8074-8082; b) M. I. Kim, M. Hong, *Biochemical and Biophysical Research Communications* **2016**, *478*, 300-306; c) M. B. Nodwell, M. F. Koch, F. Alte, S. Schneider, S. A. Sieber, *Journal of the American Chemical Society* **2014**, *136*, 4992-4999.

[8]   a) UniProtConsortium, *Nucleic Acids Research* **2023**, *51*, D523-D531; b) S. F. Altschul, W. Gish, W. Miller, E. W. Myers, D. J. Lipman, *Journal of Molecular Biology* **1990**, *215*, 403-410.

[9]   F. Huang, X. Han, X. Xiao, J. Zhou, *Molecules* **2022**, *27*, 7728.

[10]   a) C. M. Sassetti, D. H. Boyd, E. J. Rubin, *Molecular Microbiology* **2003**, *48*, 77-84; b) M. A. DeJesus, E. R. Gerrick, W. Xu, S. W. Park, J. E. Long, C. C. Boutte, E. J. Rubin, D. Schnappinger,

S. Ehrt, S. M. Fortune, C. M. Sassetti, T. R. Ioerger, *mBio* **2017**, *8*, e02133-02116; cK. Raman, K. Yeturu, N. Chandra, *BMC Systems Biology* **2008**, *2*, 109.

Part III

APPENDIX

7|

Experimental section (chapter 3)

by **Jan-Niklas Dienemann**, Shu-Yu Chen, Manuel Hitzenberger, Montana L. Sievert, Stephan M. Hacker,

Sean T. Prigge, Martin Zacharias, Michael Groll & Stephan A. Sieber.

7.1 Computational methods

7.1.1 Structural prediciton of *L. monocytogenes* EGD-e lplA1 with AlphaFold2

In order to obtain a lplA1 structural model prediction by AlphaFold2 (AF2) of *L. monocytogenes* EGD-e, we followed the protocol as previously described using the amino acid sequence as obtained from UniProtKB (lplA1, UniProt ID: Q8Y8H3, gene name: *lmo0931*).[1]

7.1.2 Docking and simulation

All compounds were generated, protonated at pH = 7.4, and optimized with MMFF94 forcefield[2] using openbabel.[3] The optimized ligand structures were docked using autodock vina.[4] Docking poses with the highest docking score and an orientation similar to the crystal structure were manually selected. Docking poses of 9 crosslinkable probe candidates (**1b** – **4**) on *E. coli* lplA (PDBID 1x2h)[5] are depicted in Fig. S4A. Similarly, docking poses of **LA**, **BrO**, **LAMe**, **C3** on lplA1 (AF2) of *L. monocytogenes* and LipL1 (PDBID 5t8u)[6] of *P. falciparum* are depicted in Fig. 3B and Fig. S7A. The docked ligands together with the corresponding enzymes are solvated in water box 8 Å from the solute and neutralized with 0.15 M potassium chloride using tleap from AmberTools22.[7] Atomic interactions are described by ff14SB[8] for protein, tip3p[9] for water, and GAFF2[10] for the ligands. The charges of ligands were assigned using AM1-BCC model.[11] Each simulation box first underwent a maximum 1500 cycles energy minimization with 10 kcal/mol positional restraint on the solutes and equilibrated consecutively with positional restraints at 10 kcal/mol, 5 kcal/mol, and 2.5 kcal/mol for 25 picoseconds each under isothermal-isovolume (NVT) ensemble and 2 kcal/mol, 1 kcal/mol, and 0.1 kcal/mol for 100 picoseconds each under isothermal-isobaric (NPT) ensemble. The equilibrated systems were simulated in three individual attempts under NPT ensemble for 400 ns in which the later 200 ns was submitted for root-mean square deviation (RMSD), root-mean square fluctuation (RMSF), and molecular mechanics generalized Born surface area (MMGB/SA) calculations. Temperature is maintained at 310.15 K with Langevin dynamics and Verlet algorithm.[12] The pressure is maintained at 1 bar using Monte Carlo barostat.[13] Binding free energy calculation with MMGB/SA is implemented with MMPBSA.py[14] using the modified GBn model[15] with the atomic radii assigned with modified Bondi radii set.[15]

7.1.3 Identification of putative inhibitors from ZINC Database

In order to obtain putative small molecule inhibitors of lipoate protein ligase (LPL), a search of the ZINC database[16] of purchasable compounds was conducted. To this end, we used the ZINCPharmer[17] web server (http://zincpharmer.csb.pitt.edu) which is a pharmacophore-based search engine. The pharmacophoric features used for the search were derived from the PDBID 3a7r structure (a complex of *E. coli* lplA and lipoyl-AMP [**LAQ**]).[5] The search returned 126 compounds which are able to form similar interactions with the protein as **LAQ**. As the conducted pharmacophore search was agnostic to the steric features of the binding site, the obtained compounds where docked to the **LAQ** binding site of PDBID 3a7r as well as to the **LAQ** binding site of the *L. monocytogenes* lplA1 (AF2) model (see online Supporting_Excel_2_ZINC_Pharmacophore_Screen file, Supporting pyMOL file). The applied docking procedure was identical to the approach described above. The list of compounds selected for purchase was subsequently assembled by manual curation: The top 50 compounds of each ligase, selected by their docking score, were screened for overlapping compounds. These identified 29 molecules were assorted by their averaged ranking position in order to determine the commercially available best

performing ten compounds for experimental validation (see Fig. S6, online Supporting_Excel_2_ZINC_ Pharmacophore_Screen file).

7.2 Biochemistry

7.2.1 Media and buffers

Table 7.1. Media and buffers.

	LB-medium (1 L)	BHI-medium (1 L)	Improved minimal medium (IMM, 1 L)
Media	5 g Peptone 2.5 g Yeast extract 2.5 g NaCl pH 7.5 in 1 L ddH$_2$O	7.5 g Pig brain infusion 10 g Pig heart infusion 10 g Peptone 2 g Glucose 5 g NaCl 2.5 g Na$_2$HPO$_4$ pH 7.4 in 1 L ddH$_2$O	The improved minimal medium for *Listeria* spp. was prepared as reported by Phan-Thanh & Gormon and contained 24 nM DL-α-lipoic acid (LA).[18] Omitting LA addition resulted in no growth of *L. monocytogenes* EGD-e.

	PBS	TEN			Wash buffer 3
General Buffers	10.0 mM Na$_2$HPO$_4$ 1.80 mM KH$_2$PO$_4$ 140 mM NaCl 2.70 mM KCl pH 7.4 in ddH$_2$O	40 mM TRIS-HCl 150 mM NaCl 1 mM EDTA pH 7.4 in ddH$_2$O		**Tag-free Protein Purification**	20 mM Imidazole pH 7.4 in PBS

	Lysis buffer 1	Wash buffer 1	Wash buffer 2	Elution buffer 1	SEC buffer 1
Protein Purification (*Lm* IplA1)	50 mM TRIS-HCl 10 mM Imidazole 300 mM NaCl pH 7.4 in ddH$_2$O	50 mM TRIS-HCl 10 mM Imidazole 1 M NaCl pH 7.4 in ddH$_2$O	50 mM TRIS-HCl 40 mM Imidazole 300 mM NaCl pH 7.4 in ddH$_2$O	50 mM TRIS-HCl 500 mM Imidazole 300 mM NaCl pH 7.4 in ddH$_2$O	20 mM TRIS-HCl 100 mM NaCl 5 mM MgCl$_2$ pH 7.5 in ddH$_2$O

	Lysis buffer 2	Wash buffer 4	Wash buffer 5	Elution buffer 2	SEC buffer 2
Protein Purification (*Pf* LipL1)	20 mM HEPES 10 mM Imidazole 200 mM NaCl pH 7.5 in ddH$_2$O	20 mM HEPES 10 mM Imidazole 1 M NaCl pH 7.5 in ddH$_2$O	20 mM HEPES 40 mM Imidazole 200 mM NaCl pH 7.5 in ddH$_2$O	20 mM HEPES 500 mM Imidazole 200 mM NaCl pH 7.5 in ddH$_2$O	20 mM HEPES 100 mM NaCl pH 7.5 in ddH$_2$O

	Loading buffer (2×)	Coomassie solution	Destaining solution
SDS-PAGE buffers	63 mM TRIS-HCl 10% glycerol 0.25‰ (w/v) Bromphenol blue 2% (w/v) SDS 5% (w/v) β-ME in ddH$_2$O	0.25% (w/v) Coomassie brilliant blue R250 10% (v/v) Acetic acid 50% (v/v) Ethanol abs. in ddH$_2$O	10% (v/v) Acetic acid 20% (v/v) Ethanol abs. in ddH$_2$O

7.2.2 Cultivation of bacterial strains, mammalian cells and parasites

E. coli K12, which is classified biosafety level 1, was handled on an open bench under sterile conditions. *L. monocytogenes* (biosafety level 2) was handled in biosafety cabinets. For pre-cultures grown in culture tubes at 200 rpm, 37°C, 5 mL media (Table 7.1) were inoculated with 5 µL bacterial solution from glycerol-cryostocks [50% (v/v), –80 °C]. Medium was inoculated freshly with pre-cultures (1:100) and agitated at 200 rpm, 37 °C to obtain stationary phase bacterial cultures as indicated in the Table 7.2 below.

Table 7.2. Bacterial growth information.

Bacteria	Strain	Medium	Flask	Growth time to stationary phase	OD_{600}
E. coli	K12 wt	100 mL LB	500 mL, unbaffled	6h	3.5 - 4.0
	K12 Δ*lipB* (*E. coli* Keio Knockout Collection)	100 mL LB + Kanamycin (25 µg mL^{-1})	500 mL, unbaffled	16h	2.0 - 2.5
L. monocytogenes	EGD-e wt	100 mL BHI	500 mL, unbaffled	6h	2.2 - 3.0

Chemicals and media for cell culture maintenance were purchased from Sigma Aldrich and solutions were warmed to 37 °C in a water bath before use. Cells were handled in sterile work benches.

HeLa cells were cultivated in T175 culture flasks (Sarstedt) in high glucose Dulbecco's modified Eagle's (DMEM) medium supplemented with 2 mM L-glutamine and 10% (v/v) heat-deactivated fetal bovine serum (FBS) in a humidified 5% CO_2 atmosphere at 37 °C. HeLa cells were split every 2 – 3 days to *ca.* 1.3×10^4 cells per cm^2. Accutase solution was used for cell detachment during standard passaging.

Adherent J774A.1 murine macrophage-like cells were grown in tissue culture flasks with hydrophobic surface for suspension cells (Sarstedt) in high glucose DMEM medium supplemented with 2 mM L-glutamine and 10% (v/v) heat-deactivated FBS in a humidified 5% CO_2 atmosphere at 37 °C. The macrophages were split into new flasks every 2 – 3 days to *ca.* 2×10^4 cells per cm^2. For detachment, cells were washed twice with TEN buffer followed by incubation with Accutase solution at 37 °C for 30 min.

Asexual stage *P. falciparum* NF54^{attB} parasites were cultured in red blood cells (RBCs) at 2% hematocrit in CMA (Complete Medium with Albumax) containing RPMI1640 medium with L-glutamine (USBiological Life Sciences), supplemented with 20 mM HEPES, 0.2% sodium bicarbonate, 12.5 µg/mL hypoxanthine, 5 g/L Albumax II (Life Technologies), and 25 µg/mL gentamicin. Cultures were maintained at 37 °C in flasks containing a gas mixture of 94% N_2, 3% O_2, and 3% CO_2.

7.2.3 Analytical labeling – fluorescence detection

SDS-PAGE

Stacking gels contained 4% (w/v) acrylamide (in 50 mM TRIS, pH 6.8) and resolving gels consisted of 12.5 or 15% (w/v) acrylamide (in 300 mM TRIS, pH 8.8). The gels were run in a TRIS-glycine buffer (25 mM TRIS, 192 mM glycine, 0.1% (w/v) SDS, pH 8.3). Samples were applied with 30 or 40 µL volume, depending on the gel size. Protein marker Roti®-Mark Standard (Carl Roth) and fluorescent marker BenchMark™ Fluorescent Protein Standard (Thermo Fisher) served as protein size reference. The gels

were run at 60 mA for 2.5–5h in an EV265 Consort (Hoefer). Fluorescence bands were visualized on a LAS-4000 (Fujifilm) equipped with a Fujinon VRF43LMD3 lens and a 575DF20 filter (Fujifilm) using 520 nm EPI excitation wavelength. Finally, proteins were stained by Coomassie-solution overnight at rt under gentle mixing followed by destaining in destaining solution.

Gel-based fluorescent labeling in bacteria

After growing the desired amount of bacterial strain to stationary phase, cultures were harvested (6,000 g, 10 min, 4 °C) and washed with PBS (15 mL; 5,000 g, 10 min, 4 °C). After resuspension of the pellet to a final OD_{600} = 40 in PBS, 200 µL of bacterial suspension were incubated with 2 µL probe (100× DMSO-stock) or 2 µL DMSO as control for 2h at 37°C, 800 rpm in Eppendorf tubes. In case of a competition experiment, the bacterial culture was co-treated additionally with 2 µL compound (100× DMSO stock) while being labeled with the probe. After centrifugation (6,000 g, 10 min, 4 °C) and removal of the supernatant, the bacterial pellet was washed with PBS (2×0.5 mL) and resuspended in 200 µL 0.4% (w/v) SDS in PBS for lysis by sonification (3×10 sec pulses, 70% intensity) at rt. The lysate was cleared by centrifugation (21,000 g, 30 min, rt) and 50 µL of the supernatant were subjected to click-chemistry as follows by incubation of reactants for 1h at rt: 1 µL rhodamine azide or alkyne (5 mM in DMSO), 1 µL tris(2-carboxyethyl)phosphine (TCEP, 52 mM in ddH$_2$O), 3 µL 1× tris(benzyltriazoyl-methyl)amine (TBTA, 1.67 mM in 80% *t*BuOH and 20% DMSO) and 1 µL CuSO$_4$ (50 mM in ddH$_2$O). The reaction was stopped by adding 50 µL loading buffer (2×) and the samples were analyzed by SDS-PAGE as described above.

Gel-based fluorescent labeling in HeLa cells

HeLa cells in 2 mL medium were seeded into a 6-well plate and grown overnight. When the cells reached ca. 90% confluency, the medium was aspirated, and the cells were washed with 1 mL PBS. 1 mL FCS-free medium and 10 µL DMSO as control or 10 µL probe **2** (100× DMSO stock) were added concentration- dependently to label proteins *in-situ* for 2h at 37 °C. After aspiration of the medium, the cells were washed with 1 mL PBS and lysed with 100 µL lysis buffer (1% (w/v) NP-40, 1% (w/v) sodiumdeoxycholate, 0.1% (w/v) SDS in PBS) during an incubation time of 5 min on ice. The cells were scraped off the wells and transferred quantitatively to an Eppendorf tube to perform sonification (1×10 sec pulse, 10% intensity) on ice. The cell debris was pelletized by centrifugation (13,000 rpm, 20 min, 4 °C) and 50 µL of the supernatant were clicked to rhodamine azide and analyzed by SDS-PAGE as described above.

7.2.4 Preparative labeling – mass spectrometry

Labeling and lysis. The procedure was performed similarly as previously described.[19] After growing the desired amount of bacterial strain to stationary phase, cultures were harvested (6,000 g, 10 min, 4 °C) and washed with PBS (15 mL; 5,000 g, 10 min, 4 °C). After resuspension of the pellet to a final OD_{600} = 40 in PBS, 1 mL of bacterial suspension was incubated for 2h at 37 °C, 800 rpm with 10 µL probe (5 mM or 10 mM (100× DMSO-stock); 50 µM or 100 µM final concentration) or 10 µL DMSO as control or 10 µL DL-α-Lipoic acid (**LA**) or 8-Bromo octanoic acid (**BrO**) (50 mM DMSO stock, 500 µM final concentration) in case of a competition experiment. For competition experiments, samples that were pre-treated with **LA** or **BrO** (final concentration: 500 µM, 10-fold excess) were additionally incubated with 10 µL probe (5 mM DMSO-stock, 50 µM final concentration) for 2h at 37 °C, 800 rpm. All samples

were prepared in four replicates. The labeled cultures were harvested by centrifugation (6,000 g, 10 min, 4 °C) and the bacterial pellets were washed with PBS (2×1 mL) and resuspended in 1 mL 0.4% (w/v) SDS in PBS for lysis by sonication (3×10 sec pulses, 70% intensity) at rt. The lysates were cleared by centrifugation (21,000 g, 30 min, rt) and the protein concentrations of the supernatants were measured using the Pierce BCA Protein assay kit (Thermo Fisher Scientific, Pierce Biotechnology) to adjust their concentration to 1 mg mL^{-1} in 500 µL 0.4% (w/v) SDS-PBS in 15 mL falcon tubes. Residual lysate was flash frozen in liquid nitrogen and stored at –80°C.

Click, enrichment and digestion. The concentration adjusted samples were subjected to click-reaction for 1h at rt using 3 µL azide-PEG3-biotin (Jena Bioscience, CLK-AZ104P4-100, 10 mM in DMSO), 10 µL TCEP (52 mM in ddH$_2$O), 30 µL 1× TBTA ligand (1.67 mM in 80% tBuOH and 20% DMSO) and 10 µL CuSO$_4$ per 500 µL sample. Next, proteins were precipitated with ice-cold acetone (2 mL, MS grade) at –20 °C for 1h, centrifuged (16,900 g, 4 °C, 30 min) and washed twice with ice-cold methanol (1 mL, MS grade). Resuspension between the washing steps was achieved by sonication (10 sec, 10% intensity), and the protein pellets were frozen overnight at –20°C before they were solubilized by sonication (10 sec, 10% intensity) in 500 µL 0.4% (w/v) SDS in PBS to perform enrichment on avidin agarose beads (A9207, Sigma-Aldrich, pre-washed three times with 0.4% (w/v) SDS in PBS (1 mL); centrifugation: 400 g, 2 min, rt). The solubilized protein samples were centrifuged (18,000 g, 5 min, rt), and the supernatants were added quantitatively to 50 µL bead slurry per sample. After incubation with agitation for 1h at rt, the slurry was transferred to columns (BioEcho Spin columns, 050-003-250) to rinse the beads as follows: 0.4% (w/v) SDS in PBS (4×0.6 mL), 6 M urea (3×0.6 mL), PBS (4×0.6 mL). Using 200 µL denaturation-buffer (7 M urea, 2 M thiourea in 20 mM HEPES, pH 7.5), the beads (carrying the enriched proteins) were resuspended prior to reduction with 2 µL TCEP (500 mM, Sigma Aldrich; 1h, 37 °C, 450 rpm). Subsequent alkylation was performed with 4 µL 2-iodoacetamide (IAA, 500 mM in 50 mM aqueous triethylammonium bicarbonate (TEAB), Sigma Aldrich; 30 min, rt, 450 rpm). The reaction was stopped by adding 4 µL dithiothreitol (DTT, 500 mM, Sigma Aldrich; 30 min, rt, 450 rpm). Next, the samples were digested by Lys-C (1 µL, 0.5 µg µL^{-1}, Fujifilm Wako; 1–2h, rt, 450 rpm), diluted with 600 µL TEAB (50 mM) and further digested by trypsin (1.5 µL, 0.5 µg µL^{-1} in 50 mM acetic acid, Promega; 16h, 37 °C, 450 rpm) before the reaction was stopped by acidification using 10 µL formic acid (FA). The samples were centrifuged (16,000 g, 3 min, rt) and the supernatant was loaded onto equilibrated (0.1% (v/v) trifluoroacetic acid, TFA) SepPak C18 columns (50 mg, Waters). After washing the trapped peptides (3×1 mL 0.1% (v/v) TFA, 1×0.5 µL 0.5% (v/v) FA), they were eluted (3×250 µL elution buffer; 80% (v/v) acetonitrile (ACN), 0.5% (v/v) FA) into 2 mL LoBind Eppendorf tubes, lyophilized and dissolved in 25 µL 1% (v/v) FA by sonication. Next, the samples were filtered through 0.22 µm filter units (VWR) by centrifugation (13,000 g, 2 min, rt) which were equilibrated with 300 µL 1% (v/v) FA. Finally, the filtrate was transferred into MS-vials and stored at –20 °C until the MS-measurements were performed.

MS-measurement and data analysis. MS-measurement of peptide samples was performed on a Q-Exactive Plus instrument equipped with a Nanospray Flex ion source (ES071, Thermo Fisher) coupled to an Ultimate 3000 Nano-HPLC (Thermo Fisher). 1 µL of samples were loaded on an Acclaim C18 PepMap100 trap column (75 µm inner diameter × 2 cm, Acclaim, PN164535) with 0.1% (v/v) TFA and separation of peptides was performed on an Aurora series AUR2-25075C18A column (75 µm inner diameter × 25 cm, Serial No. IO257504282) constantly heated to 40 °C. The gradient was run from 5–32% (v/v) acetonitrile with 0.1% (v/v) FA during a 152 min method (7 min 5%, in 105 min to 22%, in 10 min to 32%, in 10 min to 90%, 10 min wash at 90%, then to 5% in 0.1 min and hold for 9.9 min) at a flow rate of 400 nL min^{-1}. MS data on the Q-Exactive Plus instrument was acquired with the following parameters: survey scans (300–1,500 m/z) were acquired at a resolution of 140,000 and the maximum injection time was set to 80 ms (AGC target value 3e^6). Data-dependent HCD fragmentation scans of the 12 most intense ions of the survey scans were acquired in a scan range of 200–2,000 m/z at a

resolution of 17,500, maximum injection time was set to 100 ms (AGC target value 1e[5]). The isolation window was set to 1.6 m/z. Unassigned and singly charged ions were excluded for measurement and the dynamic exclusion of peptides was enabled for 60 s. The lock-mass ion 445,12002 from ambient air was used for real-time mass calibration on the Q-Exactive Plus. MaxQuant (version 1.6.5.0) was used to analyze the obtained raw files of the label-free quantification with Andromeda[20] using the following settings: variable modifications: oxidation (methionine), acetylation (N-terminus); fixed modifications: carbamidomethylation (cysteine); proteolytic enzyme: trypsin/P; missed cleavages: 2; 'No fractions', 'LFQ', 'Requantify', 'Match between runs' and 'Second Peptide' were enabled. Other default settings were not changed. Searches were performed against the following FASTA files from UniProtKB which were deposited at the PRIDE database together with the raw files: *E. coli* K12 (taxon identifier: 83333, downloaded: 20 July 2021), *L. monocytogenes* EGD-e (taxon identifier: 169963, downloaded: 19 October 2021).[21]

Perseus (version 1.6.2.3) was used for statistical analysis.[22] The following protocol was used to filter data: (1) $\log_2$ transformation of LFQ intensities. (2) Annotation of rows into groups - DMSO (control), probe treatments with respective concentrations and competition samples (**LA**, **BrO**). (3) Removal of potential contaminants. (4) Removal of peptides 'only identified by site'. (5) Removal of reverse peptides. (6) Filtration of rows for at least 3 valid values in each group. (7) Imputation of missing values from normal distribution over the total matrix. (8) Addition of annotations derived from data banks. (9) A two-sided two-sample Student's *t*-test with FDR = 0.05 (95%) was performed to apply cut-off criteria for hits with *P* values ≥ 0.05 ($-\log_{10}$ (*P* value) = 1.3) and an enrichment factor of 4 ($\log_2(x)$ = 2) as indicated in the volcano plots. Detailed information about hits can be found online in the Supporting_Excel_1_ Mass_Spectrometry file.

Binding site identification

Binding site identification was performed with lysates obtained from the previous section using the condition of 50 µM probe treatment, with modifications to a previously published procedure where the digestion and enrichment steps were swapped.[23]

IsoDTB click. Two distinct replicate samples were prepared as light or heavy tagged version. After adjusting the protein concentration to 1 mg mL^{-1} in 0.4 % (w/v) SDS in PBS (absolute protein amount per sample: *E. coli* Δ*lipB* – 1 mg, *L. monocytogenes* – 0.5 mg), one technical replicate was clicked to the heavy and the other technical replicate to the light isoDTB tag[24] by adding 120 µL of a click solution per mL protein sample, containing 60 µL 1× TBTA ligand (0.9 mg mL^{-1} in 80% *t*BuOH and 20% DMSO), 20 µL CuSO₄·5H₂O (12.5 mg mL^{-1} in ddH₂O), 20 µL TCEP (13 mg mL^{-1} in ddH₂O) and 20 µL of the respective isoDTB tag (5 mM in DMSO). The technical replicates were incubated 1h at rt, before light- and heavy-labeled samples were pooled and added into the 4-fold total sample volume of cold acetone to precipitate all proteins at –20 °C overnight. The protein pellets were centrifuged (21,000 g, 30 min, 4°C) before the supernatant was aspirated. The precipitate was resuspended in ice-cold methanol (1 mL, MS-grade) by sonication (10 sec, 10% intensity) and centrifuged (13,000 g, 10 min, 4°C) to repeat the washing step a second time after supernatant removal.

Digestion. The air-dried pellets were solubilized in 300 µL urea-solution (8 M in 0.1 M aqueous TEAB) by sonication (10 sec, 10% intensity) and centrifuged (13,000 g, 3 min, rt). The supernatant was transferred into a LoBind Eppendorf tube and proteins were reduced by 15 µL DTT (31 mg mL^{-1} in ddH₂O; 45 min, 37 °C, 850 rpm) and alkylated by 15 µL IAA (74 mg mL^{-1} in ddH₂O; 30 min, rt, 850 rpm). The reaction was stopped with 15 µL DTT (31 mg mL^{-1} in ddH₂O; 30 min, rt, 850 rpm). Next, 900 µL

TEAB (0.1 M in ddH$_2$O) was added prior to proteolytic cleavage by 40 µL trypsin (0.5 mg mL^{-1} in 50 mM acetic acid, Promega; 16h, 37 °C, 200 rpm) per 1 mg initial absolute protein amount.

Enrichment. Subsequently, the peptide solution was diluted 1:1 using 0.2% (v/v) NP-40 in PBS, and isoDTB-conjugated peptides were enriched on high capacity streptavidin agarose beads (50 µL slurry, Fisher Scientific, 10733315) in 0.1% (v/v) NP-40 in PBS for 1h at rt with agitation. The suspension was centrifuged (1,000 g, 2 min, rt) and the supernatant was removed. The beads were resuspended in 600 µL 0.1% (v/v) NP-40 in PBS and transferred quantitatively to a centrifuge column (Fisher Scientific, 11894131) to perform washing of the beads by gravity flow: 2×600 µL 0.1% (v/v) NP-40 in PBS, 3×600 µL PBS and 3×600 µL ddH$_2$O. After the rinsing process, the remaining peptides were eluted once with 200 µL and two times with 100 µL elution buffer (0.1% FA in 50% aqueous ACN) into 2 mL LoBind Eppendorf tubes by centrifugation (5,000 g, 3 min, rt) prior to lyophilization. The peptides were dissolved in 30 µL 1% FA (in ddH$_2$O) by sonication and the solution was filtered through hydrophilic filters (0.22 µM, Merck, UVC30GVNB) that were equilibrated with the same solution by centrifugation (17,000 g, 3 min, rt). The samples were transferred into MS-vials and stored at −20°C until the MS-measurement was performed.

MS-measurement and data analysis. The MS-measurement was performed with the same hardware as described in the previous section. 5 µL sample were injected and run with the following settings: The gradient was run from 5–40% (v/v) ACN with 0.1% (v/v) FA during a 152 min method (7 min 5%, in 105 min to 40%, in 10 min to 60%, in 10 min to 90%, 10 min wash at 90%, then to 5% in 0.1 min and held for 9.9 min) at a flow rate of 400 nL min^{-1}. The measurement was run in a Top10 data-dependent mode, and full MS scans were collected in a scan range of 300–1500 m/z with a resolution of 70,000 and an AGC target of 3e^6 with 80 ms maximum injection time. The most intense peaks were selected for MS2 measurement with isotope exclusion and dynamic exclusion (exclusion duration: 60 sec) and a minimum AGC target of 1e^3. Unassigned and singly charged ions were excluded for measurement. Peptide match was 'preferred'. MS2 spectra were acquired at a resolution of 17,500 and maximum injection time was set to 100 ms (AGC target value 1e^5). With a window of 1.6 m/z, isolation was performed in the quadrupole. The fragments were created using higher-energy collisional dissociation (HCD, normalized collision energy: 27%) and detected in the orbitrap. The raw data was analyzed as previously described following the 'General setup of analysis software' and 'Quantification with FragPipe' protocol with a lysine-specific 'closed search' for 707 Da and 713 Da as expected variable modifications for the light- and heavy-tagged peptides, respectively.[23] FASTA files for *E. coli* (UP000000625) and *L. monocytogenes* (UP000000817) were downloaded from UniProtKB on 3rd January 2022 and decoys were added.[21] The deposited files can be downloaded from the PRIDE database. Detailed information about the analysis can be found online in the Supporting_Excel_1_ Mass_Spectrometry file.

7.2.5 Overexpression and purification of Lipoate Protein Ligases (LPL)

A pET-28a(+) plasmid encoding the *L. monocytogenes* lplA1 (UniProtID: Q8Y8H3; gene name: *lmo0931*) wild-type sequence was purchased from TwistBioscience and verified by DNA sequencing (Genewiz). The plasmid was transformed into chemically competent *E. coli* BL21 (DE3) cells for protein expression and purification to obtain a recombinant lplA1 protein that carries an N-terminal His$_6$-tag followed by a thrombin cleavage site. For protein overexpression, 2 L LB medium containing 25 µg mL^{-1} kanamycin were inoculated (1:100) with an overnight culture of the lplA1 expression strain (grown in 25 µg mL^{-1} kanamycin) to grow bacteria to an OD$_{600}$ of 0.6-0.9 (2.5h, 37 °C, 200 rpm). The overexpression was induced with 1 mM isopropyl-1-thio-β-D-galactopyranoside (IPTG) and the cultures were incubated for 19h at 18 °C, 200 rpm. The bacteria were harvested (6,000 g, 10 min, 4 °C) and washed with PBS

(50 mL). After centrifugation (6,000 g, 10 min, 4 °C) and removal of supernatant, the pellet was resuspended in 30 mL lysis buffer 1 and lysed by sonication on ice (6×15 sec, 70% intensity). To perform affinity purification on an ÄKTA pure 25 FPLC protein purification system (GE Healthcare, software: unicorn 7.5) coupled to a fraction collector (F9-C, GE Healthcare), the cell debris was removed by centrifugation (18,000 g, 30 min, 4 °C) and the supernatant was filtered through a 0.45 µm PVDF filter (Whatman GD/X25, Cytiva) before it was transferred *via* sample pump (S9, Cytiva) onto an equilibrated 5 mL HisTrap HP column (Cytiva). The column was washed with lysis buffer 1 (25 mL), followed by wash buffer 1 (35 mL) and wash buffer 2 (35 mL). The protein was eluted with elution buffer 1 (35 mL) and fractions containing proteins based on UV-detection were pooled and concentrated in centrifugal filters (Amicon, 10 kDa cut-off, 4,000 g, 4°C) while the buffer was changed to PBS. Starting with 2 L culture volume, roughly 1.5 mL of pure lplA1 (700–800 µM, m = 40,252.62 Da, ε = 34,380 M^{-1} cm^{-1}, measured by NanoDrop, Thermo) in PBS could be obtained that were flash frozen in 50 µL working stocks in liquid nitrogen and stored at –80 °C. The purity of *L. monocytogenes* lplA1 was verified by SDS-PAGE which is why the protein was used for ITC experiments without further purification.

For crystallography, a tag-free lplA1 protein was desired. Therefore, freshly purified lplA1 from 2 L LB *via* affinity chromatography was concentrated and dialyzed in PBS (1 L) at 4 °C overnight in presence of thrombin (200 units, Serva). For removal of the tag or uncleaved protein, the protein solution was diluted 10-fold in wash buffer 3 and run through an equilibrated 5 mL HisTrap HP column in wash buffer 3. The protein-containing flow-through was concentrated in centrifugal filters (Amicon, 30 kDa cut-off, 4,000 g, 4 °C) to 1 mL and transferred to an Eppendorf tube for centrifugation (16,000 rpm, 5 min, 4°C). Next, preparative size-exclusion chromatography was performed over 1.25 column volumes with the supernatant using a 120 mL equilibrated Superdex column (HiLoad 16/600 Superdex 75 pg, Cytiva) in SEC buffer 1 (150 mL) on the same purification system. Monomeric protein fractions were pooled, concentrated and the protein concentration was measured on a NanoDrop instrument (Thermo) using the following extinction coefficient of the tag-free lplA1 protein: ε = 34,380 M^{-1} cm^{-1}, m = 38,370.57 Da. The tag-free lplA1 protein was diluted roughly 3-fold in SEC buffer 1 to obtain 2 mL of 20 mg mL^{-1} protein solution which was directly subjected to the crystallographic analysis.

N-terminally His$_6$-tagged *P. falciparum* LipL1 protein (UniProtID: Q8IEG9; gene name: *lipL1*) was produced similarly to a previously reported workflow with the exact same expression strain.[25] In brief, 2 L LB media (100 µg mL^{-1} ampicillin, 25 µg mL^{-1} kanamycin, 34 µg mL^{-1} chloramphenicol) were inoculated (1:100) with an overnight culture of the expression strain (grown in ampicillin, kanamycin and chloramphenicol) in order to grow the bacterial culture to an OD_{600} of 0.6 (3h, 37 °C, 200 rpm). The overexpression was induced with 0.5 mM isopropyl-1-thio-β-D-galactopyranoside (IPTG) and the cultures were incubated for 21h at 18 °C, 200 rpm. The bacteria were harvested (6,000 g, 10 min, 4 °C) and washed with PBS (50 mL). After centrifugation (6,000 g, 10 min, 4 °C) and removal of supernatant, the pellet was resuspended in 30 mL lysis buffer 2 and lysed as described above. The protein was purified by affinity purification as describe above using lysis buffer 2, wash buffer 4 and 5 and elution buffer 2. After concentration in centrifugal filters (Amicon, 10 kDa cut-off, 4,000 g, 4 °C) and centrifugation (16,000 rpm, 5 min, 4 °C), the protein was subjected to a size-exclusion chromatography as described above using SEC buffer 2. Monomeric protein fractions were pooled, concentrated and the protein concentration was measured using the following extinction coefficient of the *P. falciparum* LipL1 protein: ε = 52,370 M^{-1} cm^{-1}, m = 46,601.77 Da. Starting with 2 L culture volume, roughly 1.2 mL of pure protein LipL1 (120 µM) in SEC buffer 2 were obtained and flash frozen in liquid nitrogen as 125 µL working aliquots before storage at –80°C. The purity of *P. falciparum L*ipL1 was verified by SDS-PAGE.

7.2.6 Crystallography

Protein crystallization

Crystallization experiments of tag-free lplA1 from *Listeria monocytogenes* (20 mg mL^{-1}) were performed using the sitting drop vapor diffusion method at 20 °C. For co-crystallization experiments, the ligand (100 mM stock solution in DMSO, 100 mM stock solution in ddH$_2$O for ATP) was added to lplA1 to a final concentration of 2 mM, respectively. Crystallization droplets had a maximum volume of 0.4 µL with a protein to reservoir ratio of either 1:1, 2:1 or 3:1. The distinct crystallization parameters for each of the recorded datasets (Supporting Table S3) are:

LplA1:LAQ (PDBID 8crj): 0.2 M NH$_4$Cl, 2.2 M (NH$_4$)$_2$SO$_4$; 2 mM **LA**, 2 mM ATP, 5 mM MgCl$_2$

LplA1:*R*-LA (PDBID 8cri): 0.1 M MES (pH 6.0), 1.0 M LiCl, 20% PEG 6K; 2 mM **LA**

LplA1:*R*-C3 (PDBID 8crl): 0.1 M TRIS (pH 8.5), 0.2 M CaCl$_2$, 25% PEG 4K; 2 mM **C3**

Protein structure determination

Crystals were cryoprotected by a 7:3 mixture of mother liquor and 100% (v/v) ethylene glycol and vitrified in liquid nitrogen. High resolution datasets of lplA1 variants were recorded with synchrotron radiation of λ = 1.0 Å at the beamline X06SA, Swiss Light Source (SLS), Paul Scherrer Institute, Villigen, Switzerland. Reflection intensities were evaluated with the program package XDS and data reductions were carried out with XSCALE[26] (Table 7.3). First, we solved the lplA1:**LAQ** structure by Patterson search calculations with PHASER[27] and coordinates of lipoate protein ligase from *Mycoplasma hyopneumoniae* (PDBID 6jom, sequence identity 33%).[28] Using COOT[29] in combination with REFMAC,[30] the lplA1 sequence was built in iterative rounds. The model was completed with the reaction product **LAQ**. Water molecules were automatically placed with ARP/wARP solvent.[31] Restrained and TLS (Translation/Libration/Screw) REFMAC refinements yielded excellent R$_{work}$ and R$_{free}$ values as well as root-mean-square deviation (rmsd) values of bond lengths and angles (Supporting Table S3). For all other datasets lplA1:**LAQ** served as starting model for initial phasing. Model building and structural refinement were performed as described above. Crystals obtained in space group P2$_1$ contain one liganded and one apo-enzyme in the asymmetric unit. In the apo-structure residues 89-105, 116-144, 165-182 and 188-193 are only partially defined in the electron density map, resulting in an increased R$_{free}$ value. All crystal structures have been deposited in the RCSB Protein Data Bank (Table 7.3).

Table 7.3. X-ray data collection and refinement statistics.

	LplA1:LAQ	*LplA1:R-LA*	*LplA1:R-C3*
Crystal parameters			
Space group	P4$_1$2$_1$2	P2$_1$	P2$_1$
Cell constants	a=b=79.3 Å	a=58.9 Å	a=59.3 Å
	c=225.1 Å	b=72.8 Å	b=74.3 Å
		c=93.1 Å	c=92.7 Å
		β=98.0	β=98.1
LplA1 / AU[a]	1	2	2
Data collection			
Beam line	X06SA, SLS	X06SA, SLS	X06SA, SLS
Wavelength (Å)	1.0	1.0	1.0
Resolution range (Å)[b]	30-2.6 (2.7-2.6)	30-2.1 (2.2-2.1)	30-2.6 (2.7-2.6)
No. observations	103068	129957	71037
No. unique reflections[c]	22722	44270	23850
Completeness (%)[b]	98.4 (99.0)	97.1 (98.9)	96.4 (98.8)
R$_{merge}$ (%)[b, d]	5.3 (69.1)	5.5 (66.0)	8.0 (67.3)
I/σ (I)[b]	15.4 (2.1)	10.7 (2.1)	9.1 (2.4)
Refinement (REFMAC5)			
Resolution range (Å)	30-2.6	30-2.1	30-2.6
No. refl. working set	21558	42047	22646
No. refl. test set	1135	2213	1192
No. non hydrogen	2879	4832	4662
No. of ligands	1	1	1
Solvent	70	110	29
R$_{work}$/R$_{free}$ (%)[e]	17.3 / 20.6	22.3 / 25.1	23.7 / 27.3
r.m.s.d. bond (Å) / (angle)[f]	0.002 / 1.2	0.002 /1.2	0.005 / 1.3
Average B-factor (Å^2)	73.9	47.4	57.5
Ramachandran Plot (%)[g]	97.6 / 2.4 / 0	97.3 / 2.7 / 0	96.8 / 3.2 / 0
PDB accession code	**8crj**	**8cri**	**8crl**

[a] Asymmetric unit

[b] Values in parentheses for resolution range, completeness, R$_{merge}$ and I/σ (I) correspond to highest resolution shell

[c] Data reduction was carried out with XDS and from a single crystal. Friedel pairs were treated as identical reflections

[d] R$_{merge}$(I) = Σ$_{hkl}$Σ$_j$ | I(hkl)$_j$ - <I(hkl)> | / Σ$_{hkl}$ Σ$_j$ I(hkl)$_j$, where I(hkl)$_j$ is the jth measurement of the intensity of reflection hkl and <I(hkl)> is the average intensity

[e] R = Σ$_{hkl}$ | |F$_{obs}$| - |F$_{calc}$| |/Σ$_{hkl}$ |Fobs|, where R$_{free}$ is calculated without a sigma cut off for a randomly chosen 5% of reflections, which were not used for structure refinement, and R$_{work}$ is calculated for the remaining reflections

[f] Deviations from ideal bond lengths/angles

[g] Percentage of residues in favored region / allowed region / outlier region

7.2.7 Biological assays

ITC measurements

ITC measurements were conducted on a MircoCal PEAQ-ITC instrument (Malvern) at 25 °C in PBS. Each experiment was composed of 19 injections with an interval of 150 seconds (initial injection with 0.4 µL followed by 18 injections with 2.1 µL) for 4.2 seconds which were performed with a constant stirring speed of 750 rpm. DMSO was added to 2% (v/v) in dialysis buffer for the cell solution and the syringe solution. The MicroCal PEAQ ITC analysis software was used for K_D value and error analysis which fitted the data points with a single binding site model and a subtraction of a fitted offset as obtained from the control experiment. Each experiment was repeated at least twice and a typical analysis for each compound is shown in Fig. S10 exemplarily. Of note, binding for **BrO** to LPL could only be demonstrated qualitatively as ITC was at its limit of fidelity for K_D value analysis.

Recombinant *L. monocytogenes* lplA1 protein was dialyzed in PBS (1 L) at 4 °C overnight and diluted to a protein concentration of 20 µM before injection into the cell. Compounds (**LA**: 500 µM, **C3**: 500 µM, **LAMe**: 500 µM, **BrO**: 10 mM) were loaded into the syringe after dilution to their indicated concentration. In order to determine the heat of dilution, a control titration of compound into buffer without protein was performed. Of note, high concentrations of **BrO** were necessary to show LPL binding qualitatively due to low heat development.

Recombinant *P. falciparum* LipL1 protein was dialyzed in PBS (1 L) at 4 °C overnight and diluted to a protein concentration of 50 µM prior to injection into the cell. Compounds (**LA**: 500 µM, **C3**: 500 µM, **LAMe**: 500 µM, **BrO**: 500 µM) were loaded into the syringe after dilution to their indicated concentration. In order to determine the heat of dilution, a control titration of compound into buffer without protein was performed. Of note, the LipL1 protein precipitated due to stirring during the runs which explains the observed N-values around 0.3 – 0.5 and baseline instabilities. Lower protein concentrations produced too little heat for detection and attempts to stabilize the protein in solution failed, such as slower stirring or addition of 5% (w/v) glycerol or 10% (v/v) DMSO.

Intracellular EC$_{50}$ determination in bacteria

In order to determine intracellular EC$_{50}$ values in *L. monocytogenes* EGD-e, compounds were added in a competition experiment concentration-dependently to read-out the residual labeling of Q8Y863 (*pdhC*) as reporter protein for residual lipoate protein ligase activity with probe **2** (10 mM,100× DMSO-stock, 100 µM final concentration). The procedure was followed as described above in 'Gel-based Fluorescent Labeling in Bacteria'. After SDS-PAGE and fluorescence visualization, the intensity values of the fluorescent bands of the reporter protein Q8Y863 (*pdhC*, ca. 70 kDa band, double modifications after click-chemistry with probe and rhodamine dye might contribute to reduced migration behavior) were determined by ImageJ as reported previously:[32] A rectangle was drawn around the bands of interest to plot their profile of intensity by using the 'gel analyzer tool'. The respective signal intensities were quantified as peak area and were normalized relative to DMSO treatment. The values were plotted in GraphPad Prism (version 5.03) against the log-transformed compound concentrations [nM]. Intracellular EC$_{50}$ values were calculated from three independent biological replicates (*n* = 3) by fitting the obtained mean values using the function 'log(inhibitor) vs. response - Variable slope (four parameters)'. Coomassie staining of the gels revealed equal protein amounts and served as loading control. Such a representative fluorescent analysis is presented in Fig. S8A.

Compound stability assay in lysate

The assay was performed with major modifications compared to a previously published protocol.[33] 50 mL BHI medium were inoculated 1:100 with an overnight culture of *L. monocytogenes* and were incubated overnight at 37 °C, 200 rpm. After centrifugation (6,000 g, 10 min, 4 °C), the bacterial pellet was washed with PBS (25 mL) and resuspended to $OD_{600} = 40$ in PBS prior to lysis on ice with sonication (3×10 sec, 70% intensity). The lysate was cleared by centrifugation (21,000 g, 1h, 4°C) and the protein concentration was measured using the Pierce BCA Protein assay kit (Thermo Fisher Scientific, Pierce Biotechnology) to adjust the concentration to 0.9 mg mL^{-1} in PBS. The lysate was flash frozen in aliquots in liquid nitrogen, stored at –80°C and thawed on ice to assess the compound stability in lysate. 198 µL of lysate were pre-incubated for 10 min at 37 °C, 400 rpm prior to the addition of 2 µL compound (100× DMSO-stock, 10 mM, final concentration 100 µM) followed by elongated incubation at 37 °C, 400 rpm. 25 µL of aliquots were taken after 0h, 2h, 6h and 24h incubation time and added to 100 µL ice-cold acetone to precipitate proteins. Samples were directly centrifuged (21,000 g, 30 min, 4 °C) and 100 µL of the supernatant were lyophilized and frozen at –20 °C. The pellet was dissolved in 50 µL 80% (v/v) aqueous ACN and filtered through modified nylon centrifugal filters (modified nylon, pore size 0.45 µm, VWR) before the MS-measurement with 2 µL sample volume was performed in three technical replicates in positive mode on an LTQ-Orbitrap XL instrument (Thermo Scientific) with ESI ion source (spray voltage: 4 kV, capillary temp.: 275 °C, capillary voltage: 24 V, tube lens: 110 V) coupled to an Dionex Ultimate 3000 HPLC system (Thermo Scientific; XBridge^{TM} BEH130 C18 column, 5 µm, 4.6×100 mm). Xcalibur 2.2 Qual Browser was used to determine the peak area for compound quantification. The mean peak area values of each time point were referenced to 0h as percent value and plotted in GraphPad Prism (version 5.03) against the sampling time (Fig. S8B).

MTT assay

In order to determine compound effects with regards to metabolic activity in mammalian cells, 4,000 HeLa cells in 200 µL medium were seeded into a sterile flat-bottom 96-well plate and grown for 24h. After the medium was aspirated, 100 µL of FBS-free medium supplemented with 1% (v/v) DMSO or a concentration range of compounds in 1% (v/v) DMSO were added. The cells were incubated for another 24h, before 20 µL MTT (5 mg mL^{-1} in sterile PBS, Sigma-Aldrich) was added for a co-incubation time of 2h in order to get metabolized. After the supernatant was removed by aspiration, the generated formazan crystals as a measure of metabolic activity were fully solubilized in 200 µL DMSO prior to analysis on a Tecan Infinite M200 microplate reader (Tecan, Austria). The wells were scanned at 570 nm and background that was obtained at 630 nm was subtracted. The DMSO-normalized absorbance values were plotted in GraphPad Prism (version 5.03) against the log-transformed concentration and were fitted using the function 'log(inhibitor) vs. response - Variable slope (four parameters)'.[33] The experiment was performed at least two times in triplicates and such a representative analysis is presented in Fig. S9A.

Bacterial growth assay

For cytotoxicity determination of the probe molecules (**1** – **4**) in comparison to **BrO**, overnight cultures of Gram-negative *E. coli* Δ*lipB* cells were grown. After dilution of 1:1,000 into fresh medium, 99 µL were added in triplicates into a sterile 96-well plate containing 1 µL DMSO or 1 µL of a 100× compound DMSO-stock (5 mM and 50 mM stocks for 50 µM and 500 µM final concentration, respectively). Outer wells that only contained media served as sterile controls. The plate was incubated at 37 °C in a Tecan Infinite M200 microplate reader (Tecan, Austria) and wells were analyzed for bacterial growth every

30 minutes by OD_{600} measurements after shaking 30 seconds at 350 rpm prior to measurement. Growth after 20h was referenced to DMSO treatment to detect toxic effects of compounds. The experiments were performed in triplicates in two independent experiments and results were plotted with GraphPad Prism (version 5.03, Fig. S1A, S2A).

For identification of antibacterial properties of the inhibitors **C3**, **LAMe** and **BrO**, bacterial overnight cultures of *L. monocytogenes* were diluted 1:10,000 into fresh BHI or 1:1,000 into fresh improved minimal medium (IMM). 99 µL of this solution were added in a sterile 96-well plate to 1 µL DMSO or to 1 µL of a 100× compound-stock in DMSO in triplicates. Sterile controls with 1 µL DMSO in 99 µL medium without inoculum were included. The plate was incubated for 20h in case of BHI or 40h in case of IMM at 37 °C, 350 rpm prior to optical inspection of turbidity inside the inoculated wells. No antibiotic effect was identified up to 100 µM (results not shown).

Macrophage infection assay

The assay was performed with major modifications compared to a previously published protocol.[34] In order to determine the bacterial growth behavior inside murine macrophage-like cells in presence of lipoate protein ligase inhibitors, 10^5 J774A.1 cells in 100 µL medium were seeded into a sterile flat-bottom 96-well plate and incubated overnight to roughly double their amount. In parallel, *L. monocytogenes* cultures (5 mL) were inoculated 1:1,000 from an overnight culture and were grown for 16h in BHI at 37 °C, 200 rpm in presence of 100 µM compound (**C3**, **LAMe** and **BrO** had no effect on bacterial growth neither in BHI nor in IMM) or DMSO (0.1% (v/v) DMSO in total). On the next day, FBS-free DMEM was inoculated with *L. monocytogenes* to 200 CFU per µL in presence of 100 µM compound or DMSO (0.1% (v/v) DMSO in total). The murine macrophage-like cells were washed with 150 µL sterile PBS and 100 µL of the prepared bacterial solution was added in triplicates to obtain a multiplicity of infection (MOI) of roughly 0.1. After the plate was kept on ice for 15 min and was incubated at 37 °C for 15 min, the wells were washed with sterile PBS (3×200 µL). 150 µL of FBS-free DMEM with 100 µM compound or DMSO and 10 µg mL^{-1} gentamycin were added (0.1% (v/v) DMSO in total) to kill extracellular bacteria. The plates were incubated for 24h at 37 °C and 5% CO_2 atmosphere and samples were taken time dependently after 0h, 4h, 7h, and 24h after optical inspection of the cells under the microscope to ensure their fitness. For intracellular CFU determination, the cells were washed with sterile PBS (3×200 µL) and lysed with 2×100 µL 0.05% (w/v) Triton X-100 in ddH$_2$O (1 min, rt). Lysates were transferred quantitatively with additional 300 µL sterile PBS into sterile Eppendorf tubes. 10 µL of up to 1,000-fold dilution series were plated on BHI agar plates which were incubated at 37 °C for one day until CFU values were enumerated. Triplicate measurements from two independent biological attempts were averaged and absolute CFU values were plotted against growth time with GraphPad Prism (version 5.03, Fig. S12).

***P. falciparum* growth inhibition assay**

NF54^{attB} parasites were seeded at 1% parasitemia, 2% hematocrit in a flat bottom 96-well plate. **LAMe** was added from 1,000× stock solutions in DMSO to generate a 2-fold concentration series (0.098 µM - 100 µM). **C3** was added from 1,000× stock solutions in DMSO to generate a 1.5-fold concentration series (1.7 µM - 100 µM). **BrO** from 1,000× stock solutions in DMSO was added in a 16-fold series at low concentrations (0.000012 µM - 3.125 µM) and a 4-fold series at high concentrations (3.125 µM - 3200 µM). The final concentration of DMSO was 0.1% (v/v) for all culture conditions, except for the 3200 µM **BrO** condition, which had a final concentration of 0.2% DMSO (v/v). After 72 hours of incubation at 37 °C in a gas mixture of 94% N_2, 3% O_2, and 3% CO_2, culture samples were collected and

diluted 1:5 in PBS and analyzed immediately or stored at 4 °C. Parasite growth was then determined using a SYBR Green I DNA quantitation assay, as described previously.[35] Briefly, 20 μL of the diluted culture samples were stained with 80 μL of 1× SYBR Green I (Invitrogen) for 30 minutes at room temperature while shaking. Post-incubation, 150 μL of PBS were added to each well to dilute unbound SYBR Green dye. Fluorescence was measured with an Attune Nxt Flow Cytometer (Thermo Fisher Scientific), with a 50 μL acquisition volume, and a running speed of 25 μL/minute with 10,000 total events collected. Parasitemias were calculated as the percentage of RBCs positive for SYBR Green fluorescence. Each assay was performed with four technical replicates, which were averaged to generate a single biological replicate. EC_{50} values were calculated from two independent biological replicates by fitting the obtained %-survival mean values using the function 'log(inhibitor) vs. response - Variable slope (four parameters)' from GraphPad Prism (version 5.03, Fig. 4E).

7.3 Chemical synthesis

General remarks. DL-α-Lipoic acid (**LA**, CAS: 1077-28-7, ≥ 98%) and 8-Bromo octanoic acid (**BrO**, CAS: 17696-11-6, 95%) were ordered from Acros Organics. 7-Octynoic acid (7OA, probe **1b**, CAS: 10297-09-3, 95%) and the ten compounds that originated from the ZINC database screen (Fig. S6B, purity ≥ 90%) were purchased from Enamine. Other chemicals with reagent or higher grade were ordered from Sigma Aldrich, VWR, TCI, Roth and Alfa Aesar. Reactions that were sensitive to air or moisture were performed under argon atmosphere in flame-dried reaction flasks. Aluminium-coated silica gel plates (silica gel 60, F_{254}, Merck KGaA) were used for TLC, and compound spots were visualized by UV light (λ = 254 nm) and/or chemical staining: $KMnO_4$-stain (3.0 g $KMnO_4$, 20.0 g K_2CO_3 and 5 mL 5% NaOH in 300 mL ddH_2O) or CAM-stain (5.00 g Cer-(IV)-sulfate, 25.0 g ammonium molybdate and 50.0 mL concentrated sulphuric acid in 450 mL water) followed by heat treatment (ca. 250 °C). Column chromatography was performed with silica gel Geduran® Si 60 (40-63 µm, Merck KGaA).

High performance liquid chromatography (HPLC). Where indicated, compounds were purified by preparative, reversed-phase HPLC with a Waters 2545 quaternary gradient module which was equipped with a Waters 2998 photodiode array detector and a fraction collector connected to a YMC Triart C18 column (250×10 mm, 5 µm). The gradient (15 min length) was run as follows using ddH_2O and acetonitrile (ACN, HPLC-grade) as mobile phase: The fraction of ACN was increased from 2% to 30% during 1 min, and then from 30% to 60% during 8 min, followed by a raise to 98% ACN during 1 min. The mobile phase composition was kept for 1 min to wash the column before the system was flushed back to 2% ACN during 2 min with subsequent rinsing for 2 min.

Mass spectrometry. Low-resolution mass spectra (LRMS) were recorded on an MSQ Plus instrument (Thermo Fisher) equipped with a Dionex Ultimate 3000 separation module (Thermo Fisher). Data was visualized and processed using Chromeleon 7.2.7 (Thermo Fisher). High-resolution mass spectra (**HRMS**) were recorded on two different instruments as indicated. **Method A (ESI-FT)**: An LTQ-FT Ultra (Thermo Fisher) was equipped with an ESI ion source and data was visualized and processed using Xcalibur 2.2 (Thermo Fisher). **Method B (ESI-ToF):** A SynaptXS mass spectrometer (Waters) was coupled to an ACQUITY Premier HPLC system (Waters) which was connected to a Waters XBridge C18 column (3.5 µm, 4.6×100 mm). Compounds were ionized by an ESI ion source and subsequently detected with a time of flight (ToF) detector. Data was evaluated with Waters Masslynx V4.2.

Nuclear magnetic resonance (NMR) spectroscopy. ^{1}H-NMR (300, 400 or 500 MHz) and ^{13}C-NMR (75, 101 or 126 MHz) experiments for purity and structural analysis were conducted on Avance-I/III HD NMR systems (Bruker Co.) with Topspin software (V2.1/3, Bruker Co.) at room temperature. Chemical shifts of deuterated solvents are given in parts per million (ppm) and their residual proton signals ($CDCl_3$ δ = 7.26 ppm, DMSO-d_6 δ = 2.50 ppm) or residual carbon signals ($CDCl_3$ δ = 77.16 ppm, DMSO-d_6 δ = 39.52 ppm) were used as internal reference. Coupling constants (J) are given in hertz (Hz) and signal multiplicities are indicated as follows: *br* s – broad singlet, s – singlet, d – doublet, ddd – doublet of doublet of doublets, t – triplet, td – triplet of doublets, p – quintet and m – multiplet. The spectra were evaluated with MestReNova (Mestrelab Research).

7.3.1 Synthetic procedures

5-(1,2-dithiolan-3-yl)-*N*-methylpentanamide (LAMe)

LAMe

$C_9H_{17}NOS_2$
M = 219.36 g/mol
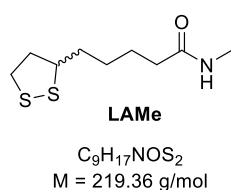
LAMe was synthesized similarly to a previously reported procedure.[36] To a stirred solution of DL-α-Lipoic acid (500 mg, 2.4 mmol, 1.0 equiv.) in acetonitrile (8 mL) was added EDC·HCl (464.6 mg, 2.4 mmol, 1.0 equiv.) and DMAP (296.1 mg, 2.4 mmol, 1.0 equiv.). After 10 minutes, methylamine solution (2M in THF, 1.4 mL, 2.7 mmol, 1.12 equiv.) was added dropwise and the yellow suspension was stirred for 5h at rt in darkness. Water (10 mL) and EtOAc (10 mL) were added to the reaction mixture and the aqueous phase was extracted with EtOAc (2 × 10 mL). The combined organic layers were washed with 5% aqueous citric acid solution (3 × 10 mL), saturated aqueous $NaHCO_3$ solution (3 × 10 mL) and brine (2 × 10 mL). Next, the organic phase was dried over Na_2SO_4, filtered and concentrated *in vacuo* to obtain a yellow solid. Purification by column chromatography (100% EtOAc), uptake in DMSO and 100-fold dilution with water, followed by lyophilization, yielded 216 mg (981 μmol, 41%) of a pale yellow solid as the title compound.

TLC: R_f = 0.34 (100% EtOAc, UV, CAM).

^{1}H-NMR (300 MHz, DMSO-d_6): δ [ppm] = 7.67 (*br* s, 1H), 3.66 – 3.54 (m, 1H), 3.25 – 3.05 (m, 2H), 2.55 (d, *J* = 4.6 Hz, 3H), 2.47 – 2.34 (m, 1H), 2.04 (t, *J* = 7.3 Hz, 2H), 1.94 – 1.79 (m, 1H), 1.72 – 1.59 (m, 1H), 1.59 – 1.41 (m, 3H), 1.41 – 1.23 (m, 2H).

^{13}C-NMR (75 MHz, DMSO-d_6): δ [ppm] = 172.3, 56.1, 39.9, 38.1, 35.1, 34.1, 28.4, 25.4, 25.0.

HRMS (Method A, ESI, *m/z*): ($C_9H_{18}NOS_2^+$ [M+H]$^+$) found: 220.0823; calc.: 220.0824.

The NMR characteristics are in agreement with literature.[36]

N-(3-(2-(6-amino-9H-purin-9-yl)acetamido)propyl)-5-(1,2-dithiolan-3-yl)pentanamide (C3)

C3

$C_{18}H_{27}N_7O_2S_2$
M = 437.58 g/mol
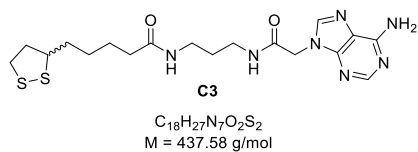
The intermediate 9-aminopropylaminoacetlyadenine was synthesized as previously described.[37] In brief, ethyl adenyl-9-acetate (100.0 mg, 452 μmol, 1.0 equiv.) was dissolved in 1,3-diaminopropane (811 μL, 9.7 mmol, 21.5 equiv.) and stirred for 1h at rt. The off-white precipitate was isolated by filtration, was washed with DCM (5 mL) and was dried under reduced pressure. 87.5 mg (78%, 351 μmol) of the intermediate were obtained as a pale brown solid that were subjected to the next step without further purification. The subsequent reaction was carried out in analogy to a previously reported procedure.[38] DL-α-Lipoic acid (79.7 mg, 386.1 μmol, 1.1 equiv.), triethylamine (269 μL, 1.93 mmol, 5.5 equiv.) and HOBt (52.2 mg, 386.1 μmol, 1.1 equiv.) were dissolved in dry DMF (4 mL) under argon atmosphere and stirred at 0 °C for 15 min before EDC·HCl (74.0 mg, 386.1 μmol, 1.1 equiv.) was added. After 15 min, 9-aminopropylaminoacetlyadenine (intermediate, 87.5 mg, 351.0 μmol, 1.0 equiv.) was added and the suspension was stirred overnight at rt in the dark. Saturated aqueous NaHCO₃ solution (20 mL) was added to give a brown suspension. The formed precipitate was isolated by filtration and washed with water (5 × 10 mL). The precipitate was suspended in water by sonication and frozen in liquid nitrogen to perform lyophilization, in order to obtain 72.3 mg (165.2 μmol, 47%) of the title compound as an off-white solid (overall yield 37%).

¹H-NMR (500 MHz, DMSO-d_6): δ [ppm] = 8.28 (t, J = 5.6 Hz, 1H), 8.10 (s, 1H), 8.05 (s, 1H), 7.78 (t, J = 5.7 Hz, 1H), 7.21 (s, 2H), 4.81 (s, 2H), 3.64 − 3.54 (m, 1H), 3.20 − 3.13 (m, 1H), 3.13 − 3.00 (m, 5H), 2.43 − 2.34 (m, 1H), 2.04 (t, J = 7.3 Hz, 2H), 1.90 − 1.79 (m, 1H), 1.69 − 1.60 (m, 1H), 1.58 − 1.45 (m, 5H), 1.38 − 1.28 (m, 2H).

¹³C-NMR (126 MHz, DMSO-d_6): δ [ppm] = 172.0, 166.3, 155.9, 152.5, 149.8, 141.8, 118.3, 56.2, 45.0, 40.1, 38.1, 36.8, 36.3, 35.3, 34.2, 29.2, 28.4, 25.1.

HRMS (Method A, ESI, m/z): ($C_{18}H_{28}N_7O_2S_2^+$ [M+H]⁺) found: 438.1734; calc.: 438.1740.

8-Azido octanoic acid (1a)

1a

$C_8H_{15}N_3O_2$
M = 185.23 g/mol
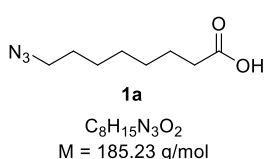
The compound **1a** was synthesized as previously described.[39] After reaction of 8-Bromo octanoic acid (223 mg, 1.0 mmol, 1.0 equiv.) with sodium azide (97.5 mg, 1.5 mmol, 1.5 equiv.) in DMF (2 mL) for 20h at rt, the solvent was removed under reduced pressure. Next, 1M HCl solution (5 mL) was added to perform extraction with ethyl acetate (3 × 5 mL). The organic phases were washed with aqueous 5% (w/v) LiCl solution (1 × 15 mL) and brine (1 × 15 mL), dried over Na₂SO₄, filtered, and concentrated *in vacuo*. Subsequent purification of the brown crude oil by column chromatography (10% EtOAc/hexane, 1% Formic acid) yielded the title compound as a pale yellow oil (139.6 mg, 754 μmol, 75%).

TLC: R_f = 0.13 (10% EtOAc/hexane, KMnO₄).

¹H-NMR (400 MHz, CDCl₃): δ [ppm] = 8.79 (*br* s, 1H), 3.26 (t, J = 6.9 Hz, 2H), 2.36 (t, J = 7.5 Hz, 2H), 1.93 − 1.48 (m, 4H), 1.44 − 1.27 (m, 6H).

¹³C-NMR (101 MHz, CDCl₃): δ [ppm] = 180.1, 51.6, 34.1, 29.0, 28.9, 26.6, 24.7.

HRMS (Method A, ESI, m/z): ($C_8H_{14}N_3O_2^-$ [M-H]⁻) found: 184.1091; calc.: 184.1092.

The characterization matches with previous literature reports.[40]

2-(prop-2-yn-1-yl)cyclohexan-1-one (6)

C$_9$H$_{12}$O
M = 136,19 g/mol
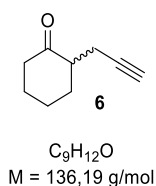
The compound **6** was synthesized similarly to a previously reported protocol.[41] In brief, cyclohexanone (**5**, 1.0 g, 10.2 mmol, 1.2 equiv.) was added dropwise at 0 °C to a solution of anhydrous THF (28 mL) containing LDA (2M in THF, 5.1 mL, 10.2 mmol, 1.2 equiv.). The pale yellow reaction mixture was stirred for 1h prior to the dropwise addition of propargyl bromide (80% in toluene, 944 µL, 8.49 mmol, 1.0 equiv.). The solution was stirred overnight while being allowed to reach rt. The dark orange reaction mixture was acidified with 2M HCl to pH = 1 and extracted with EtOAc (3 × 15 mL) and DCM (2 × 15 mL). The combined organic phases were washed with brine (1 × 15 mL), dried over Na$_2$SO$_4$, filtered, and concentrated *in vacuo* to obtain a red-brown oil as crude product (1.21 g). The crude oil was purified by column chromatography (2% EtOAc/hexane), yielding 547.8 mg (4.02 mmol, 47%) of the title compound **6** as a pale yellow oil.

TLC: R_f = 0.52 (10% EtOAc/hexane, CAM).

¹H-NMR (500 MHz, CDCl$_3$): δ [ppm] = 2.62 (ddd, *J* = 17.1, 4.6, 2.7 Hz, 1H), 2.52 − 2.37 (m, 3H), 2.36 − 2.26 (m, 1H), 2.19 (ddd, *J* = 17.1, 8.5, 2.7 Hz, 1H), 2.14 − 2.05 (m, 1H), 1.96 (t, *J* = 2.7 Hz, 1H), 1.95 − 1.89 (m, 1H), 1.82 − 1.62 (m, 2H), 1.48 − 1.37 (m, 1H).

¹³C-NMR (75 MHz, CDCl$_3$): δ [ppm] = 211.0, 82.7, 69.5, 49.7, 42.0, 33.4, 28.0, 25.3, 19.0.

HRMS (Method B, ESI-ToF, *m/z*): (C$_9$H$_{13}$O$^+$ [M+H]$^+$) found: 137.0970; calc.: 137.0961.

The NMR analysis is in agreement with literature.[41]

7-(prop-2-yn-1-yl)oxepan-2-one (7)

C$_9$H$_{12}$O$_2$
M = 152.19 g/mol
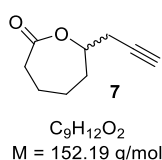
The compound **7** was synthesized similarly to a previously published protocol.[41] In brief, 2-(prop-2-yn-1-yl)cyclohexan-1-one (**6**, 547.8 mg, 4.02 mmol, 1.0 equiv.) was dissolved in anhydrous DCM (14 mL) and *m*-CPBA (77%, 1.35 g, 6.03 mmol, 1.5 equiv.) was slowly added at rt. The stirred solution turned to a white suspension after 1h and was stirred in total for 72h at rt. The solution was filtered, and the organic phase was washed with 5% (w/v) aqueous Na$_2$S$_2$O$_3$ solution (2 × 15 mL), aqueous saturated NaHCO$_3$ solution (2 × 10 mL) and brine (2 × 15 mL). The organic phase was dried over Na$_2$SO$_4$, filtered, and concentrated *in vacuo* to obtain 503 mg of a yellow viscous oil as crude product that was purified by column chromatography (10% EtOAc/hexane), yielding 273.0 mg (1.79 mmol, 45%) of the title compound **7** as a pale yellow viscous oil.

TLC: R_f = 0.23 (20% EtOAc/hexane, CAM).

¹H-NMR (300 MHz, CDCl$_3$): δ [ppm] = 4.37 (td, *J* = 8.4, 5.0 Hz, 1H), 2.82 − 2.57 (m, 3H), 2.48 (ddd, *J* = 16.7, 8.1, 2.7 Hz, 1H), 2.33 − 2.16 (m, 1H), 2.04 (t, *J* = 2.7 Hz, 1H), 2.02 − 1.83 (m, 2H), 1.71 − 1.47 (m, 3H).

¹³C-NMR (75 MHz, CDCl$_3$): δ [ppm] = 174.8, 79.7, 78.4, 71.0, 35.0, 33.6, 28.3, 26.4, 23.0.

HRMS (Method A, ESI, *m/z*): (C$_9$H$_{13}$O$_2^+$ [M+H]$^+$) found: 153.0910; calc.: 153.0910.

Methyl 6-hydroxynon-8-ynoate (8)

$C_{10}H_{16}O_3$
M = 184.24 g/mol
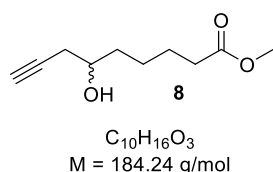
The compound **8** was synthesized in analogy to a previously reported procedure.[42] In brief, 7-(prop-2-yn-1-yl)oxepan-2-one (**7**, 261.3 mg, 1.8 mmol, 1.0 equiv.) was dissolved in anhydrous methanol (6 mL) before H_2SO_4 (10% solution in MeOH, 165 µL, 180 µmol, 0.1 equiv.) was added. The mixture was stirred for 2h at rt before water (3 mL) and saturated aqueous $NaHCO_3$ solution (3 mL) were added to stop the reaction. The mixture was extracted with EtOAc (3 × 10 mL). The merged organic phases were washed with brine (1 × 15 mL), dried over Na_2SO_4, filtered, and concentrated *in vacuo* to yield 289.1 mg (1.64 mmol, 91%) of the title compound **8** as a pale yellow oil.

TLC: R_f = 0.20 (20% EtOAc/hexane, CAM).

¹H-NMR (500 MHz, CDCl₃): δ [ppm] = 3.84 − 3.73 (m, 1H), 3.67 (s, 3H), 2.64 − 2.26 (m, 4H), 2.05 (t, J = 2.6 Hz, 1H), 1.88 (*br* s, 1H), 1.76 − 1.60 (m, 2H), 1.60 − 1.33 (m, 4H).

¹³C-NMR (75 MHz, CDCl₃): δ [ppm] = 174.2, 80.9, 71.1, 69.8, 51.7, 35.9, 34.1, 28.8, 25.3, 24.9.

HRMS (Method A, ESI, *m/z*): ($C_{10}H_{17}O_3^+$ [M+H]⁺) found: 185.1171; calc.: 185.1172.

Methyl 6-(tosyloxy)non-8-ynoate (9)

$C_{17}H_{22}O_5S$
M = 338.42 g/mol
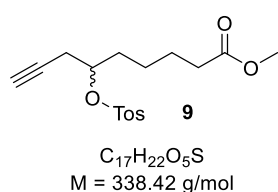
Methyl 6-hydroxynon-8-ynoate (**8**, 267 mg, 1.45 mmol, 1.0 equiv.) was diluted in anhydrous pyridine (4.8 mL), and tosyl chloride (414 mg, 2.17 mmol, 1.5 equiv.) was added while the reaction was cooled on ice. After 15 min, the pale yellow solution was allowed to reach rt and was stirred for 72h. The brownish solution was diluted with DCM (10 mL) and washed with brine (2 × 10 mL). The aqueous solution was extracted with DCM (3 × 10 mL), and the combined organic phases were dried over Na_2SO_4, filtered, and concentrated *in vacuo* to yield 402 mg (1.12 mmol, 82%) of the title compound **9** as an orange-brown oil.

TLC: R_f = 0.16 (10% EtOAc/hexane, CAM).

¹H-NMR (400 MHz, CDCl₃): δ [ppm] = 7.80 (d, J = 8.4 Hz, 2H), 7.34 (d, J = 8.3 Hz, 2H), 4.61 − 4.49 (m, 1H), 3.66 (s, 3H), 2.55 − 2.49 (m, 2H), 2.45 (s, 3H), 2.22 (t, J = 7.4 Hz, 2H), 1.96 (t, J = 2.7 Hz, 1H), 1.83 − 1.62 (m, 4H), 1.60 − 1.48 (m, 2H).

¹³C-NMR (101 MHz, CDCl₃): δ [ppm] = 173.9, 145.0, 134.1, 130.0, 128.0, 80.0, 78.5, 71.5, 51.7, 33.9, 33.1, 24.8, 24.5, 24.2, 21.8.

HRMS (Method A, ESI, *m/z*): ($C_{17}H_{23}O_5S^+$ [M+H]⁺) found: 339.1259; calc.: 339.1261.

Methyl 6-(acetylthio)non-8-ynoate (10)
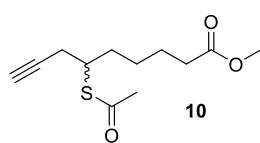
$C_{12}H_{18}O_3S$
M = 242.33 g/mol

Methyl 6-(tosyloxy)non-8-ynoate (**9**, 378 mg, 1.12 mmol, 1.0 equiv.) was dissolved in anhydrous DMF (3.7 mL) before potassium thioacetate (510 mg, 4.47 mmol, 4.0 equiv.) was added. The solution was stirred for 2h at 70 °C before the solution was concentrated to dryness. The residue was dissolved in water (5 mL) and DCM (5 mL). The layers were separated, and the aqueous phase was extracted with DCM (3 × 10 mL). The combined organic phases were washed with aqueous 5% (w/v) LiCl solution (1 × 10 mL) and brine (1 × 10 mL), dried over Na_2SO_4, filtered, and concentrated *in vacuo* to yield 280 mg of a brown oil as crude product. After purification by column chromatography (5% EtOAc/hexane), the title compound **10** was obtained with 125 mg (517 µmol, 46%) as a golden colored oil.

TLC: R_f = 0.28 (10% EtOAc/hexane, UV, CAM).

^{1}H-NMR (400 MHz, $CDCl_3$): δ [ppm] = 3.67 (s, 3H), 3.66 – 3.51 (m, 1H), 2.65 – 2.45 (m, 2H), 2.38 – 2.24 (m, 5H), 2.02 (t, *J* = 2.6 Hz, 1H), 1.87 – 1.74 (m, 1H), 1.71 – 1.59 (m, 3H), 1.51 – 1.32 (m, 2H).

^{13}C-NMR (101 MHz, $CDCl_3$): δ [ppm] = 195.6, 174.1, 80.9, 70.7, 51.7, 42.6, 34.0, 32.7, 30.9, 26.5, 25.1, 24.7.

HRMS (Method A, ESI, *m/z*): ($C_{12}H_{19}O_3S^+$ [M+H]$^+$) found: 243.1050; calc.: 243.1049.

6-Mercaptonon-8-ynoic acid (2)
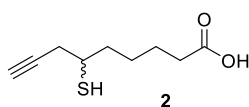
$C_9H_{14}O_2S$
M = 186.07 g/mol

Methyl 6-(acetylthio)non-8-ynoate (**10**, 94.8 mg, 391 µmol, 1.0 equiv.) was dissolved in methanol (1.3 mL). Next, 2M aqueous LiOH solution (978 µL, 1.96 mmol, 5.0 equiv.) was added. The mixture was stirred at rt for 2h. The solution was acidified with 1M HCl to pH = 1 and extracted with EtOAc (3 × 5 mL). The combined organic phases were washed with brine (1 × 10 mL), dried over Na_2SO_4, filtered, and concentrated *in vacuo* to yield 53.3 mg of a golden colored oil as crude product. The oil was purified by preparative HPLC yielding 51.8 mg (278 µmol, 71%) of probe **2** as a transparent viscous oil.

HPLC: t_R = 8.1 min.

TLC: R_f = 0.15 – 0.48 (50% EtOAc/hexane, CAM).

^{1}H-NMR (400 MHz, $CDCl_3$): δ [ppm] = 2.98 – 2.88 (m, 1H), 2.61 – 2.46 (m, 2H), 2.38 (t, *J* = 7.4 Hz, 2H), 2.09 (t, *J* = 2.6 Hz, 1H), 1.85 – 1.74 (m, 2H), 1.72 – 1.42 (m, 5H).

^{13}C-NMR (101 MHz, $CDCl_3$): δ [ppm] = 179.2, 81.2, 71.1, 39.0, 37.1, 33.9, 29.4, 26.8, 24.4.

HRMS (Method A, ESI, *m/z*): ($C_9H_{13}O_2S^-$ [M-H]$^-$) found: 185.0643; calc.: 185.0642.

Methyl 5-(1,2-dithiolan-3-yl)pentanoate (11)

C$_9$H$_{16}$O$_2$S$_2$
M = 220.35 g/mol
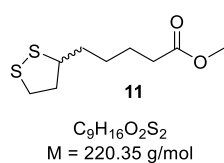
The compound **11** was synthesized with variation to a previously published protocol.[43] In brief, to a stirred solution of DL-α-Lipoic acid (1.0 g, 4.9 mmol, 1.0 equiv.) in acetonitrile (10 mL) in darkness was added EDC·HCl (939.3 mg, 4.9 mmol, 1.0 equiv.) and DMAP (598.6 mg, 4.9 mmol, 1.0 equiv.). After 10 minutes, anhydrous methanol (222.5 µL, 5.5 mmol, 1.12 equiv.) was added dropwise and the solution was stirred for 4h at rt. Water (10 mL) and EtOAc (10 mL) were added to the reaction mixture and the aqueous phase was extracted with EtOAc (2 × 10 mL). The combined organic layers were washed with 5% (w/v) aqueous citric acid solution (3 × 10 mL), saturated aqueous NaHCO$_3$ solution (3 × 10 mL) and brine (2 × 10 mL). Next, the organic phase was dried over Na$_2$SO$_4$, filtered, and concentrated *in vacuo* without further purification to yield 773 mg (3.5 mmol, 72%) of a yellow viscous oil as title compound **11**.

TLC: R_f = 0.78 (25% EtOAc/hexane, UV, KMnO$_4$).

^{1}H-NMR (400 MHz, CDCl$_3$): δ [ppm] = 3.66 (s, 3H), 3.60 - 3.53 (m, 1H), 3.22 - 3.07 (m, 2H), 2.50 - 2.41 (m, 1H), 2.32 (t, *J* = 7.4 Hz, 2H), 1.95 - 1.85 (m, 1H), 1.74 - 1.57 (m, 4H), 1.53 - 1.39 (m, 2H).

^{13}C-NMR (101 MHz, CDCl$_3$): δ [ppm] = 174.1, 56.5, 51.7, 40.4, 38.6, 34.7, 34.0, 28.9, 24.8.

HRMS (Method A, ESI, *m/z*): (C$_9$H$_{17}$O$_2$S$_2$$^+$ [M+H]$^+$) found: 221.0666; calc.: 221.0665.

The NMR characteristics are in agreement with previous reports.[44]

Methyl 6,8-dimercaptooctanoate (12)

C$_9$H$_{18}$O$_2$S$_2$
M = 222.36 g/mol

To a stirred solution of Methyl 5-(1,2-dithiolan-3-yl)pentanoate (**11**, 611.0 mg, 2.8 mmol, 1.0 equiv.) in anhydrous methanol (25 mL) in darkness was slowly added NaBH$_4$ (839.2 mg, 22.2 mmol, 8.0 equiv.) at 0 °C. After the evolution of H$_2$ has stopped, the solution was stirred for 1h at rt. To stop the reaction, 2M HCl was added dropwise to pH = 1 at 0 °C. After the addition of brine (10 mL) and diethylether (10 mL), the aqueous phase was extracted with diethylether (2 × 10 mL). The combined organic phases were washed with water (10 mL), brine (10 mL), dried over Na$_2$SO$_4$, filtered, and concentrated *in vacuo* at rt without further purification to yield 569 mg (2.6 mmol, 93%) of an oxidation sensitive pale yellow oil as title compound **12**.

TLC: R_f = 0.30 (10% EtOAc/hexane, KMnO$_4$).

^{1}H-NMR (300 MHz, CDCl$_3$): δ [ppm] = 3.67 (s, 3H), 2.99 – 2.85 (m, 1H), 2.80 – 2.59 (m, 2H), 2.32 (t, *J* = 7.2 Hz, 2H), 1.97 – 1.83 (m, 1H), 1.79 – 1.44 (m, 7H), 1.38 – 1.27(m, 2H).

^{13}C-NMR (75 MHz, CDCl$_3$): δ [ppm] = 174.1, 51.7, 42.9, 39.4, 38.9, 34.0, 26.7, 24.7, 22.4.

HRMS (Method A, ESI, *m/z*): (C$_9$H$_{17}$O$_2$S$_2$$^-$ [M-H]$^-$) found: 221.0677; calc.: 221.0675.
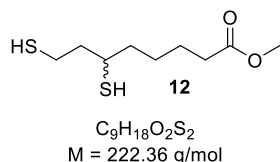
The NMR characteristics match with previous reports.[45]

Methyl 6-mercapto-8-(prop-2-yn-1-ylthio)octanoate (13)

$C_{12}H_{20}O_2S_2$
M = 260.41 g/mol
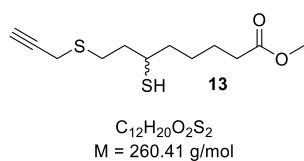
To a stirred solution of Methyl 6,8-dimercaptooctanoate (**12**, 569 mg, 2.6 mmol, 1.0 equiv.) in anhydrous DMF (12 mL) was added TEA (709 µL, 5.1 mmol, 2.0 equiv.) at rt. After 15 minutes, propargyl bromide (80% in toluene, 331 µL, 3.1 mmol, 1.2 equiv.) was added dropwise within 10 minutes, and the solution was stirred overnight at rt. The reaction mixture was acidified with 1M HCl to pH = 1 and extracted with diethylether (3 × 15 mL). The combined organic phases were washed with 5% (w/v) aqueous LiCl solution (5 × 10 mL), brine (1 × 15 mL), dried over Na_2SO_4, filtered, and concentrated *in vacuo* to yield 623 mg of a yellow liquid as crude product that was purified by column chromatography (2% EtOAc/hexane → 5% EtOAc/hexane → 10% EtOAc/hexane) yielding 306 mg (1.2 mmol, 46%) of the title compound **13** as a bright yellow oil with minor traces of **11** as oxidized side product. Of note, the propargylation was detected on the sulfur atom at position 8 as the free thiol proton at position 6 creates a doublet signal (1.37 ppm) based on the interaction with the single proton bound to carbon at position 6.

TLC: R_f = 0.44 (10% EtOAc/hexane, CAM).

^{1}H-NMR (400 MHz, CDCl$_3$): δ [ppm] = 3.67 (s, 3H), 3.25 (d, *J* = 2.6 Hz, 2H), 2.96 – 2.76 (m, 3H), 2.33 (t, *J* = 7.3 Hz, 2H), 2.25 (t, *J* = 2.6 Hz, 1H), 2.01 – 1.86 (m, 1H), 1.78 – 1.43 (m, 7H), 1.37 (d, *J* = 7.5 Hz, 1H).

^{13}C-NMR (101 MHz, CDCl$_3$): δ [ppm] = 174.1, 80.1, 71.3, 51.7, 39.9, 38.7, 38.1, 34.0, 29.4, 26.7, 24.7, 19.4.

HRMS (Method A, ESI, *m/z*): ($C_{12}H_{19}O_2S_2^-$ [M-H]$^-$) found: 259.0833; calc.: 259.0832.

6-Mercapto-8-(prop-2-yn-1-ylthio)octanoic acid (3)

$C_{11}H_{18}O_2S_2$
M = 246.07 g/mol
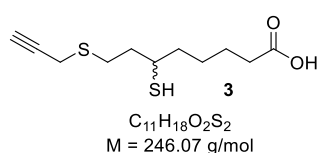
Methyl 6-mercapto-8-(prop-2-yn-1-ylthio)octanoate (**13**, 20.0 mg, 76.8 µmol, 1.0 equiv.) was dissolved in methanol (260 µL). Next, 2M aqueous LiOH solution (115 µL, 230.4 µmol, 3.0 equiv.) was added causing a cloudy precipitate that disappeared after 10 minutes. The mixture was stirred for 1h at rt in darkness. The solution was acidified with 1M HCl to pH = 1 and extracted with EtOAc (3 × 5 mL). The combined organic phases were washed with brine (2 × 10 mL), dried over Na_2SO_4, filtered, and concentrated *in vacuo* at rt to yield 18.5 mg of a colorless oil as crude product. The oil was purified by column chromatography (50% EtOAc/hexane) yielding 12.9 mg (52.4 µmol, 68%) of the probe **3** as a transparent oil.

TLC: R_f = 0.16 (50% EtOAc/hexane, CAM).

^{1}H-NMR (300 MHz, CDCl$_3$): δ [ppm] = 3.25 (d, *J* = 2.6 Hz, 2H), 2.99 – 2.76 (m, 3H), 2.38 (t, *J* = 7.2 Hz, 2H), 2.25 (t, *J* = 2.6 Hz, 1H), 2.06 – 1.89 (m, 1H), 1.80 – 1.49 (m, 7H), 1.37 (d, *J* = 7.5 Hz, 1H).

^{13}C-NMR (101 MHz, CDCl$_3$): δ [ppm] = 179.0, 80.1, 71.3, 39.8, 38.7, 38.1, 33.9, 29.4, 26.6, 24.5, 19.4.

HRMS (Method A, ESI, *m/z*): ($C_{11}H_{17}O_2S_2^-$ [M-H]$^-$) found: 245.0676; calc.: 245.0675.

Methyl 6,8-bis(tritylthio)octanoate (14)

C_{47}H_{46}O_2S_2
M = 707.00 g/mol
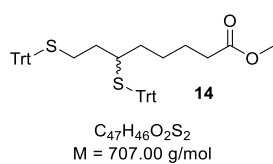
To a stirred solution of Methyl 6,8-dimercaptooctanoate (**12**, 345 mg, 1.55 mmol, 1.0 equiv.) in anhydrous DCM (2 mL) was added TEA (430 µL, 3.10 mmol, 2.0 equiv.) at rt. After 15 minutes, in anhydrous DCM (3 mL) pre-dissolved trityl chloride (865 mg, 3.10 mmol, 2.0 equiv.) was added dropwise within 15 minutes, and the solution was stirred overnight at rt. The yellow suspension was acidified with 1M HCl to pH = 1 and washed with water (2 × 15 mL) and brine (2 × 15 mL). After drying over Na_2SO_4, filtration, and concentration *in vacuo*, 1.06 g of a yellow viscous oil as crude product was yielded that was purified by column chromatography (5% EtOAc/hexane) to obtain 630 mg (891 µmol, 57%) of the title compound **14** as a pale yellow viscous oil. Attempts to measure HRMS failed.

TLC: R_f = 0.13 (5% EtOAc/hexane; UV, CAM).

1H-NMR (400 MHz, CDCl_3): δ [ppm] = 8.49 – 6.74 (m, 30H), 3.66 (s, 3H), 2.13 (t, *J* = 7.2 Hz, 2H), 2.09 – 1.91 (m, 2H), 1.38 – 1.20 (m, 5H), 1.15 – 1.01 (m, 1H), 0.99 – 0.84 (m, 3H).

13C-NMR (101 MHz, CDCl_3): δ [ppm] = 174.1, 145.3, 145.1, 129.7, 129.7, 127.9, 127.7, 126.7, 126.6, 67.5, 66.8, 51.6, 44.7, 34.0, 33.5, 33.2, 29.1, 25.6, 24.9.

Methyl 2-(prop-2-yn-1-yl)-6,8-bis(tritylthio)octanoate (15)

C_{50}H_{48}O_2S_2
M = 745.05 g/mol
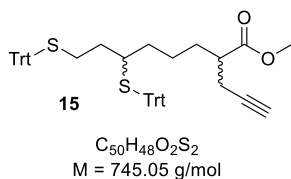
Methyl 6,8-bis(tritylthio)octanoate (**14**, 190 mg, 269 µmol, 1.2 equiv.) was dissolved in anhydrous THF (1 mL) and added at −78 °C dropwise to a solution of LDA (2M in THF, 134 µL, 269 µmol, 1.2 equiv.) in THF (300 µL). The pale orange reaction mixture was stirred for 1h at −78 °C prior to the dropwise addition of propargyl bromide (80% in toluene, 24 µL, 224 µmol, 1.0 equiv.). The solution was stirred for 2h at −78 °C. The brown reaction mixture was acidified with 1M HCl to pH = 1 while kept on ice and was then extracted with DCM (3 × 10 mL). The combined organic phases were washed with brine (1 × 15 mL), dried over Na_2SO_4, filtered, and concentrated *in vacuo* to yield 179.5 mg of a bright brown viscous oil as crude product that was purified by column chromatography (10% EtOAc/hexane) yielding 101 mg (136 µmol, 60%) of the title compound **15** as a highly viscous pale yellow opaque oil. Attempts to measure HRMS failed.

TLC: R_f = 0.66 (10% EtOAc/hexane, UV, CAM [yellow]).

1H-NMR (400 MHz, CDCl_3): δ [ppm] = 7.45 – 7.18 (m, 30H), 3.78 – 3.57 (m, 3H), 2.47 – 2.34 (m, 2H), 2.34 – 2.22 (m, 1H), 2.15 – 2.01 (m, 2H), 2.01 – 1.89 (m, 1H), 1.40 – 1.13 (m, 5H), 1.11 – 0.99 (m, 1H), 0.97 – 0.78 (m, 3H).

13C-NMR (101 MHz, CDCl_3): δ [ppm] = 174.9, 145.2, 145.1, 129.8, 129.7, 128.0, 127.9, 126.7, 126.6, 81.5, 70.0, 67.5, 66.8, 51.9, 44.7, 44.3, 42.5, 33.3, 31.2, 29.1, 23.5.

2-(3-(1,2-dithiolan-3-yl)propyl)pen-4-ynoic acid (4)

4

$C_{11}H_{16}O_2S_2$

M = 244.37 g/mol
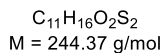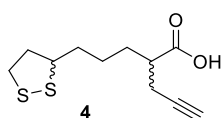
Methyl 2-(prop-2-yn-1-yl)-6,8-bis(tritylthio)octanoate (**15**, 115.3 mg, 155 µmol, 1.0 equiv.) was dissolved in DMSO (2 mL) to obtain a clear yellow solution. Next, 2M aqueous LiOH solution (232 µL, 464 µmol, 3.0 equiv.) was added causing a color change to deep yellow. The mixture was stirred for 72h at rt. The orange solution was acidified with 1M HCl to pH = 1 and extracted with DCM (3 × 15 mL). The combined organic phases were washed with brine (1 × 50 mL), dried over Na_2SO_4, filtered, and concentrated *in vacuo* to yield 96.2 mg of the thiol-protected carboxylic acid as a yellow viscous crude oil. **TLC**: R_f = 0.31 (20% EtOAc/hexane, CAM).

A previous reported strategy with iodine for removal of trityl groups and simultaneous oxidation was carried out.[46] Without further purification, the oil (96.2 mg, 132 µmol, 1.0 equiv.) was dissolved in a solution of 1% I_2 in anhydrous methanol (16.7 mg, 65.8 µmol, 0.5 equiv., 1.7 mL methanol) and stirred at rt for 16h open to air in darkness. The reaction was stopped with an aqueous solution of 5% (w/v) $Na_2S_2O_3$ (2 mL) before it was extracted with EtOAc (3 × 5 mL). The combined organic phases were washed with brine (1 × 10 mL), dried over Na_2SO_4, filtered, and concentrated *in vacuo* to yield a bright yellow viscous oil as crude product (98.0 mg) that was purified by column chromatography (20% EtOAc/hexane → 100% EtOAc) yielding 3.8 mg (15.5 µmol, 10% over 2 steps) of probe **4** diastereoisomers as a pale yellow oil.

TLC: R_f = 0.06 (20% EtOAc/hexane, CAM).

^{1}H-NMR (400 MHz, $CDCl_3$): δ [ppm] = 3.58 (p, J = 6.7 Hz, 1H), 3.26 – 3.06 (m, 2H), 2.66 – 2.43 (m, 4H), 2.03 (t, J = 2.6 Hz, 1H), 1.96 – 1.85 (m, 1H), 1.81 – 1.42 (m, 6H).

^{13}C-NMR (101 MHz, $CDCl_3$): δ [ppm] = 179.4, 81.0, 70.4, 56.3, 56.3, 44.0, 43.9, 40.4, 40.3, 38.7, 34.9, 34.8, 30.7, 30.6, 26.7, 26.6, 21.0, 20.9.

HRMS (Method A, ESI, *m/z*): ($C_{11}H_{15}O_2S_2^-$ [M-H]$^-$) found: 243.0519; calc.: 243.0519.

7.3.2 NMR spectra

¹H-NMR (300 MHz, DMSO-d_6) of **LAMe**:
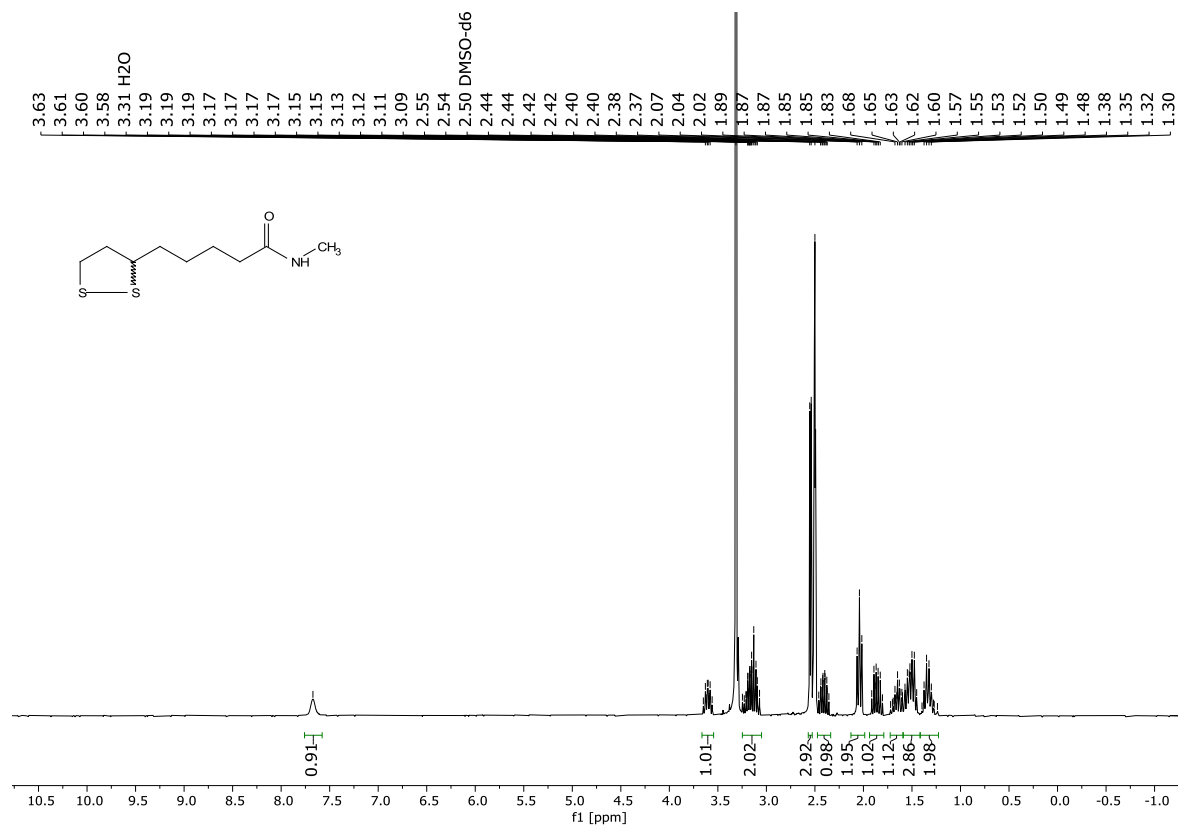
¹³C-NMR (75 MHz, DMSO-d_6) of **LAMe**:
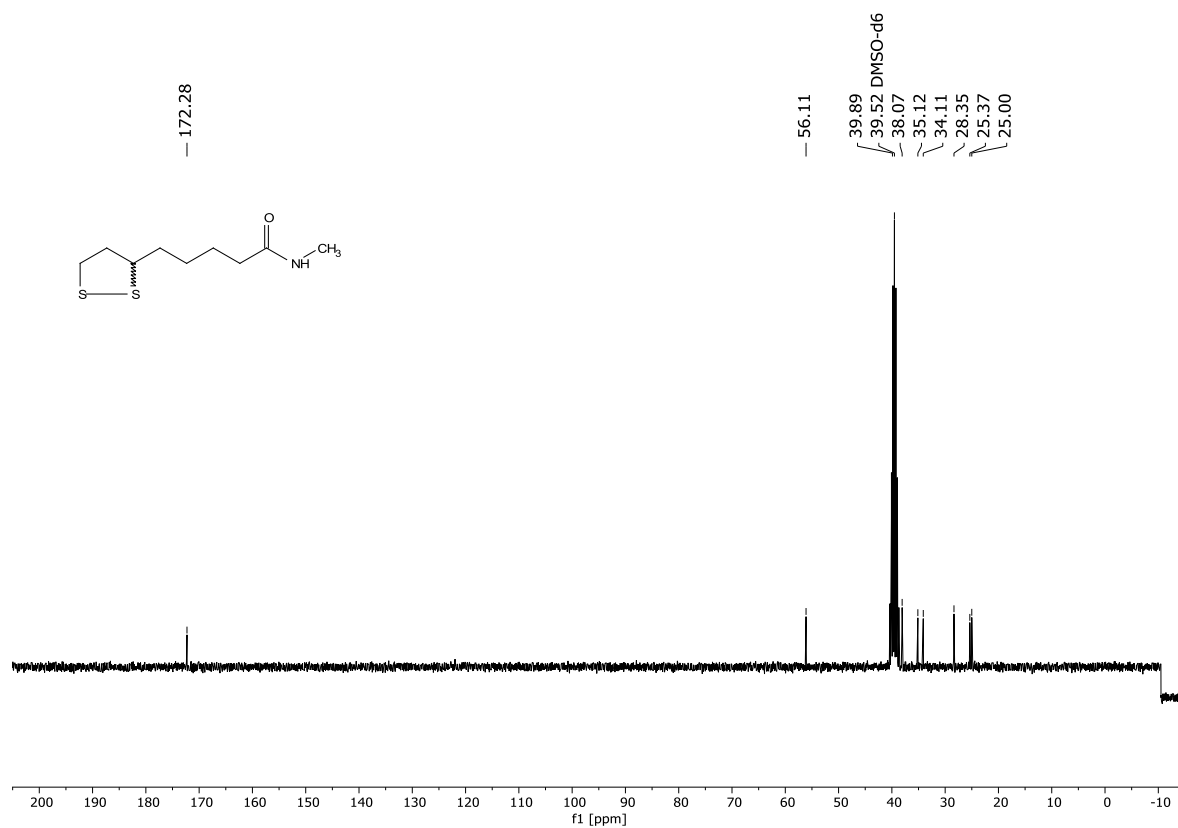
¹H-NMR (500 MHz, DMSO-*d*₆) of **C3**:
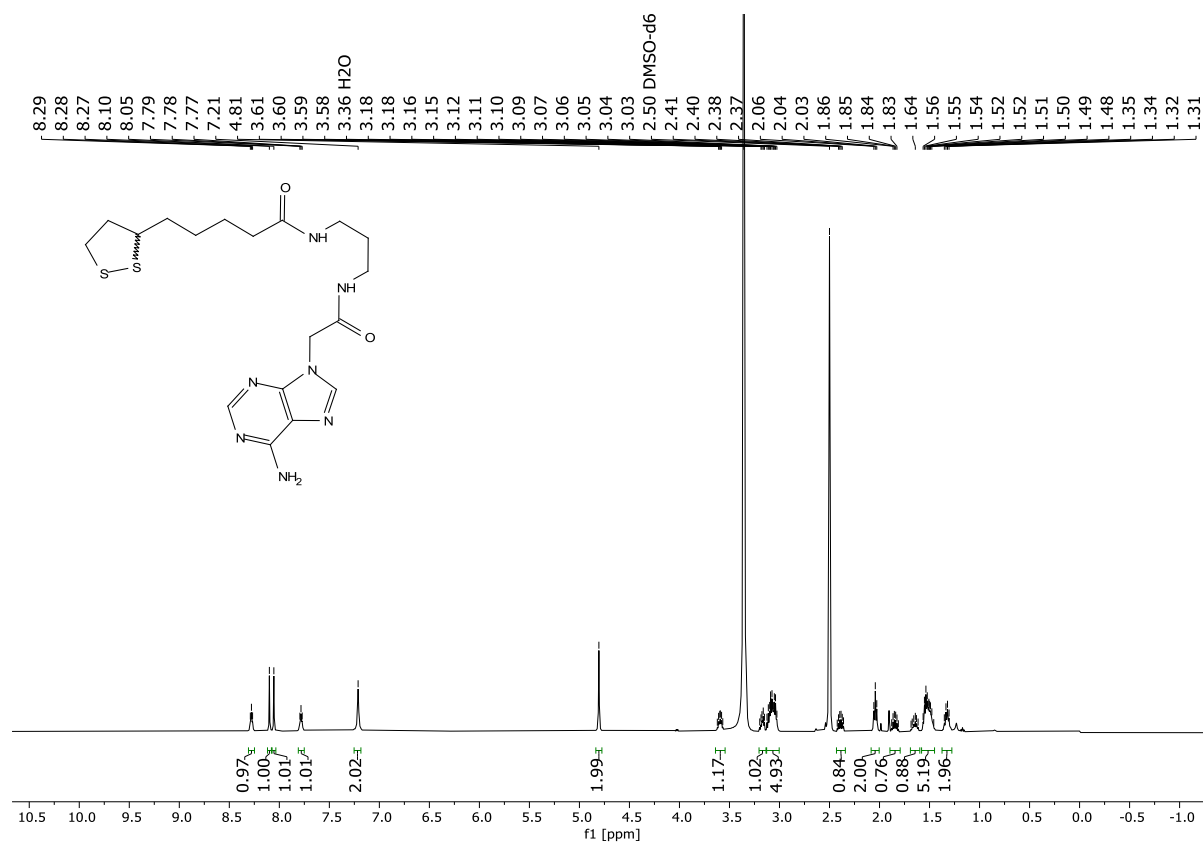
¹³C-NMR (126 MHz, DMSO-*d*₆) of **C3**:
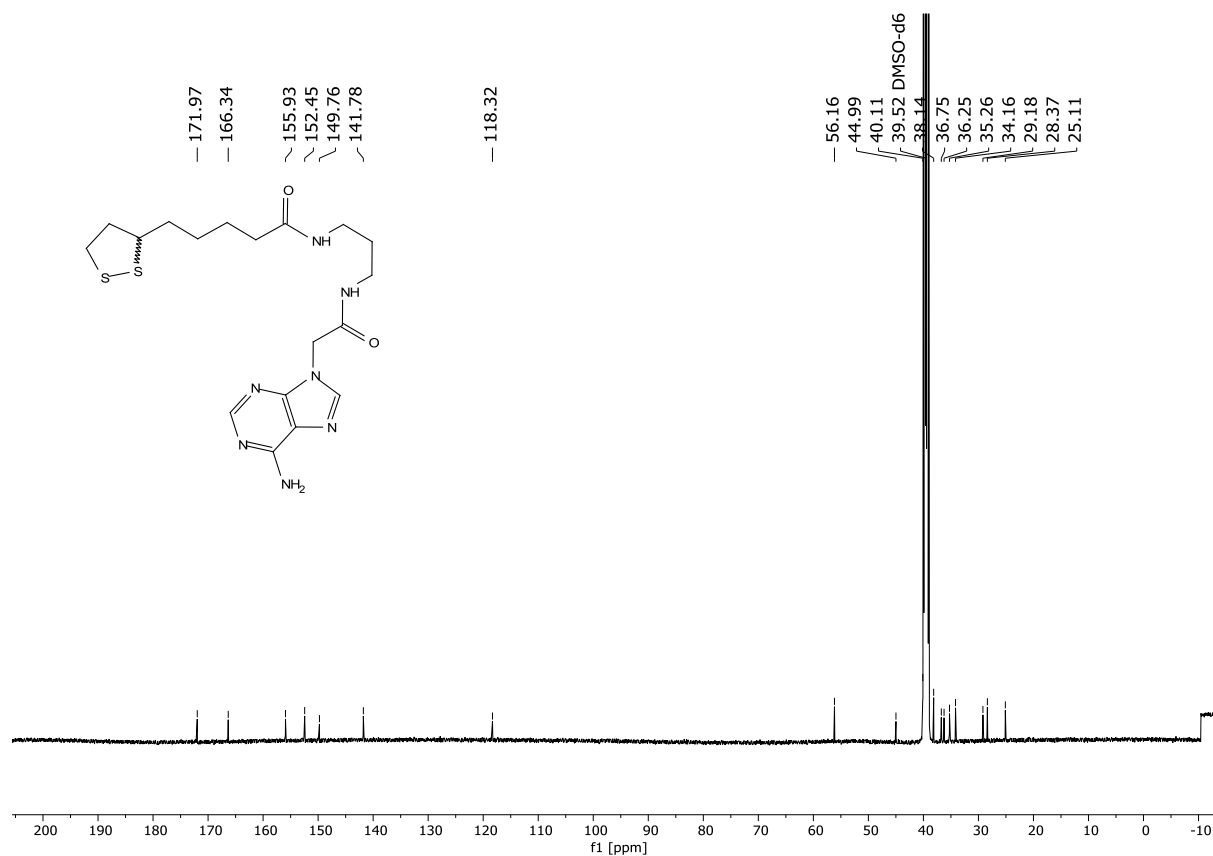
¹H-NMR (400 MHz, CDCl₃) of probe **1a**:
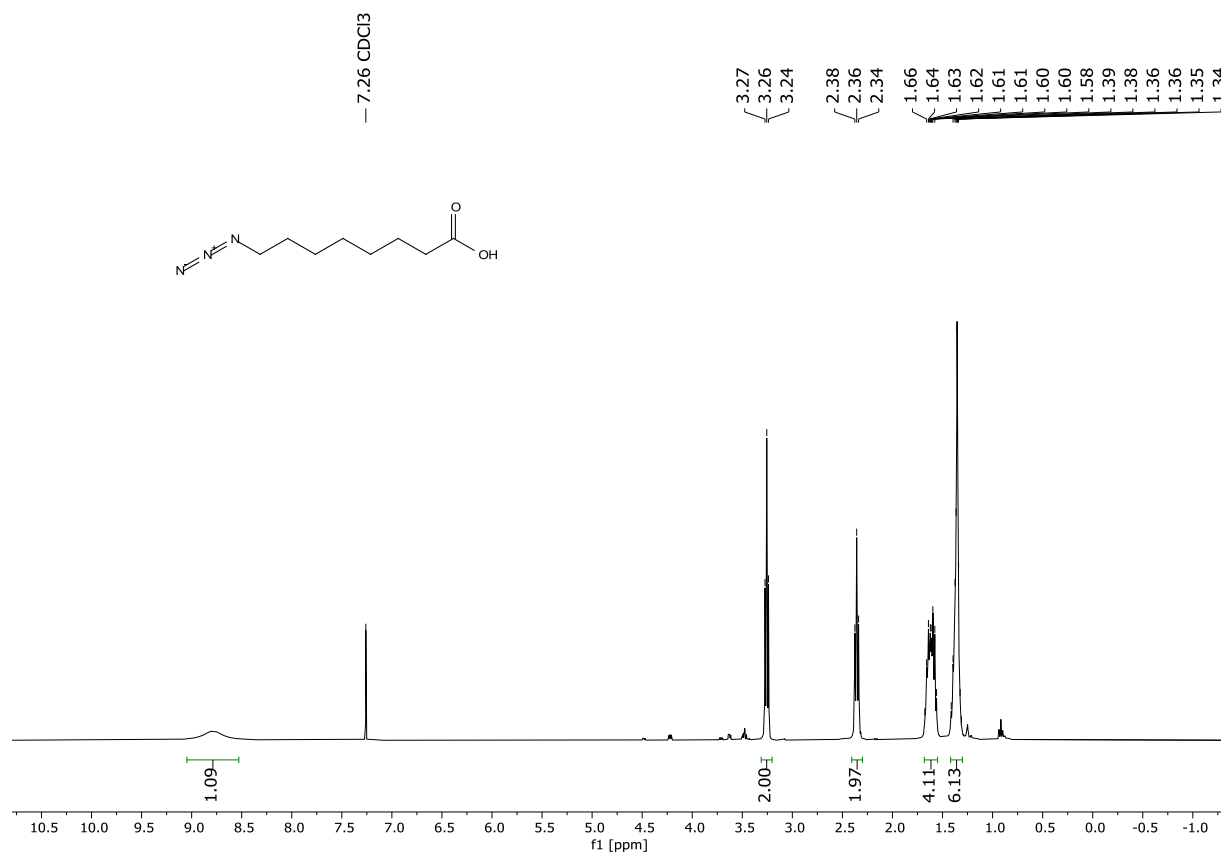
¹³C-NMR (101 MHz, CDCl₃) of probe **1a**:
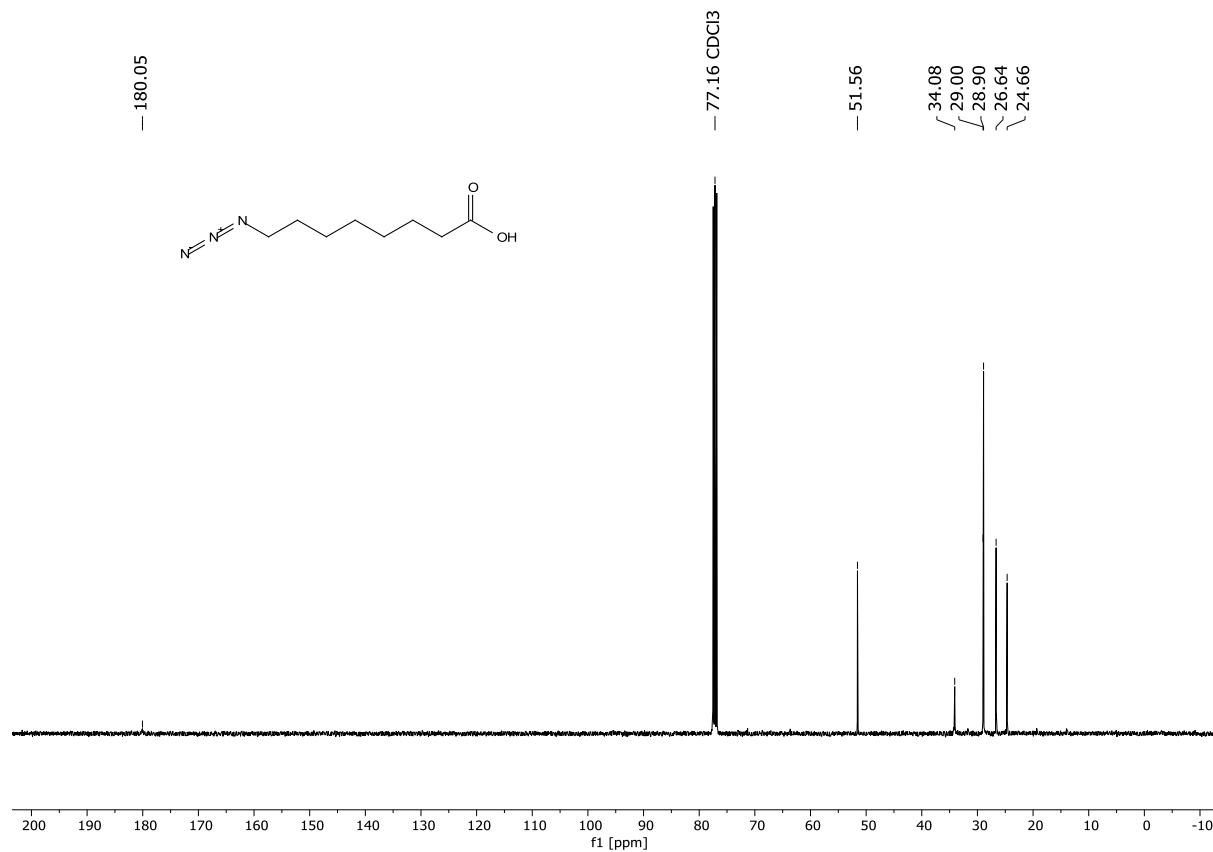
¹H-NMR (400 MHz, CDCl₃) of probe **1b**:
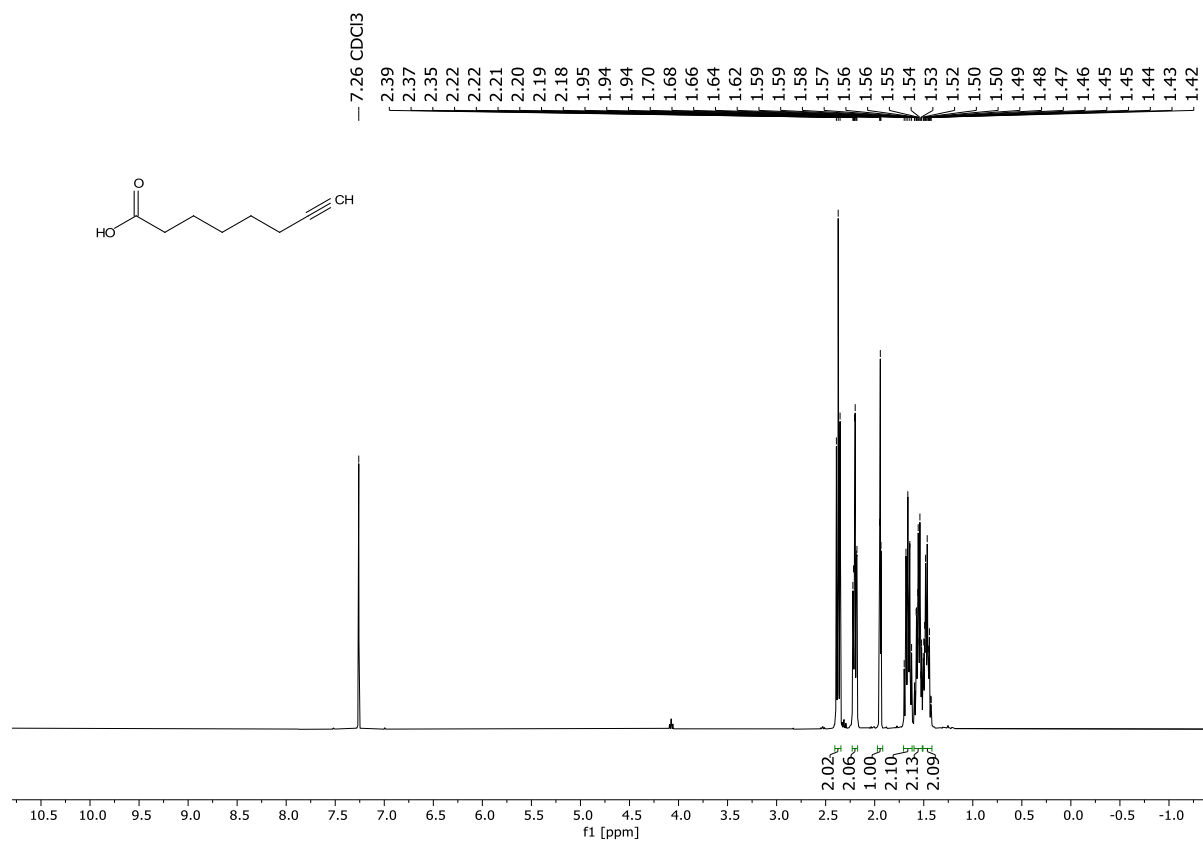
¹³C-NMR (101 MHz, CDCl₃) of probe **1b**:
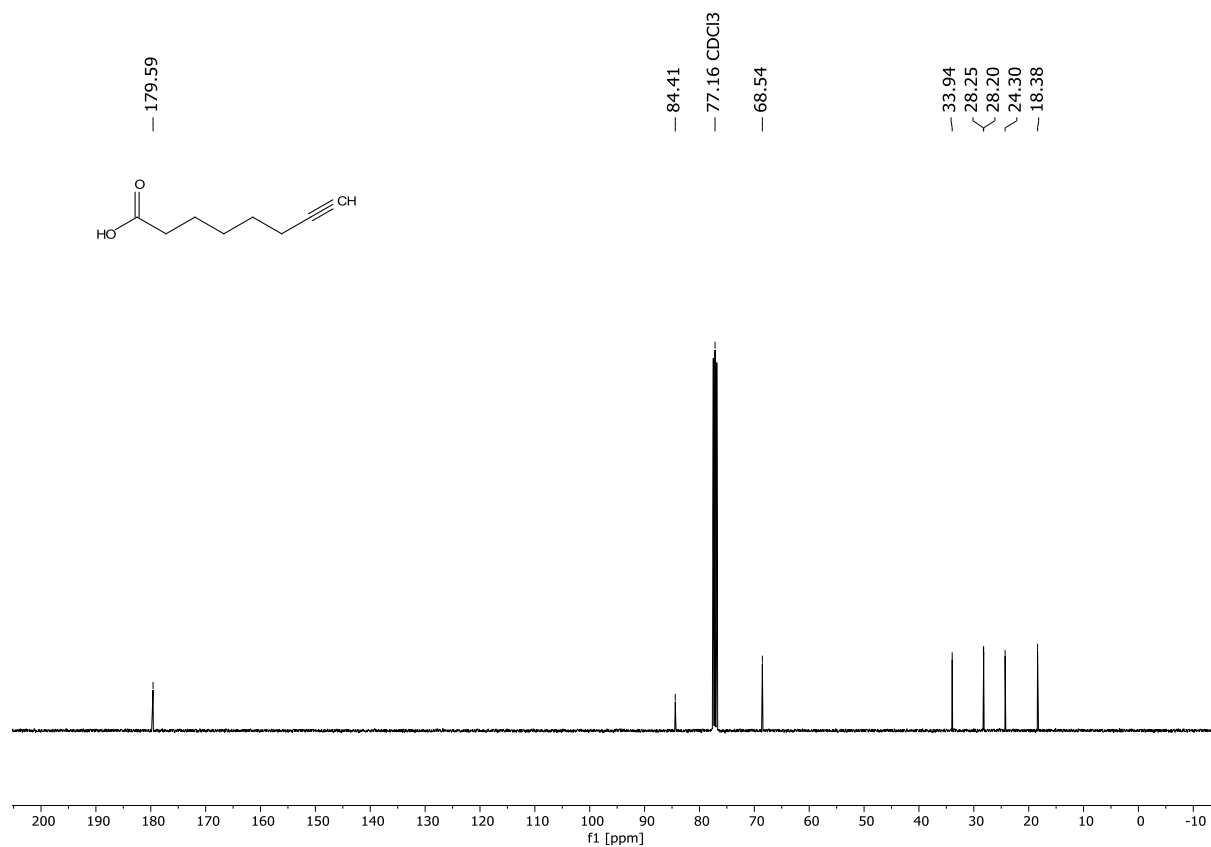
¹H-NMR (400 MHz, CDCl₃) of probe **2**:
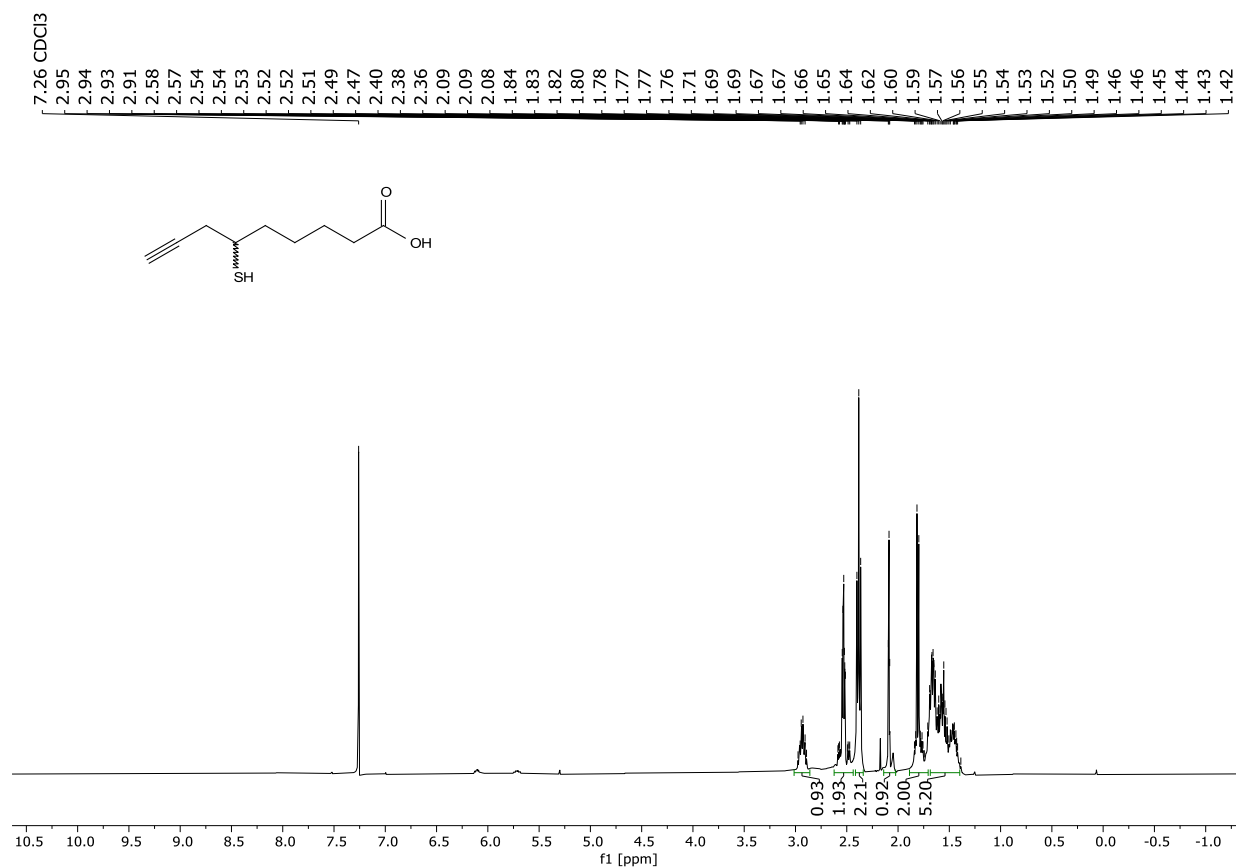
¹³C-NMR (101 MHz, CDCl₃) of probe **2**:
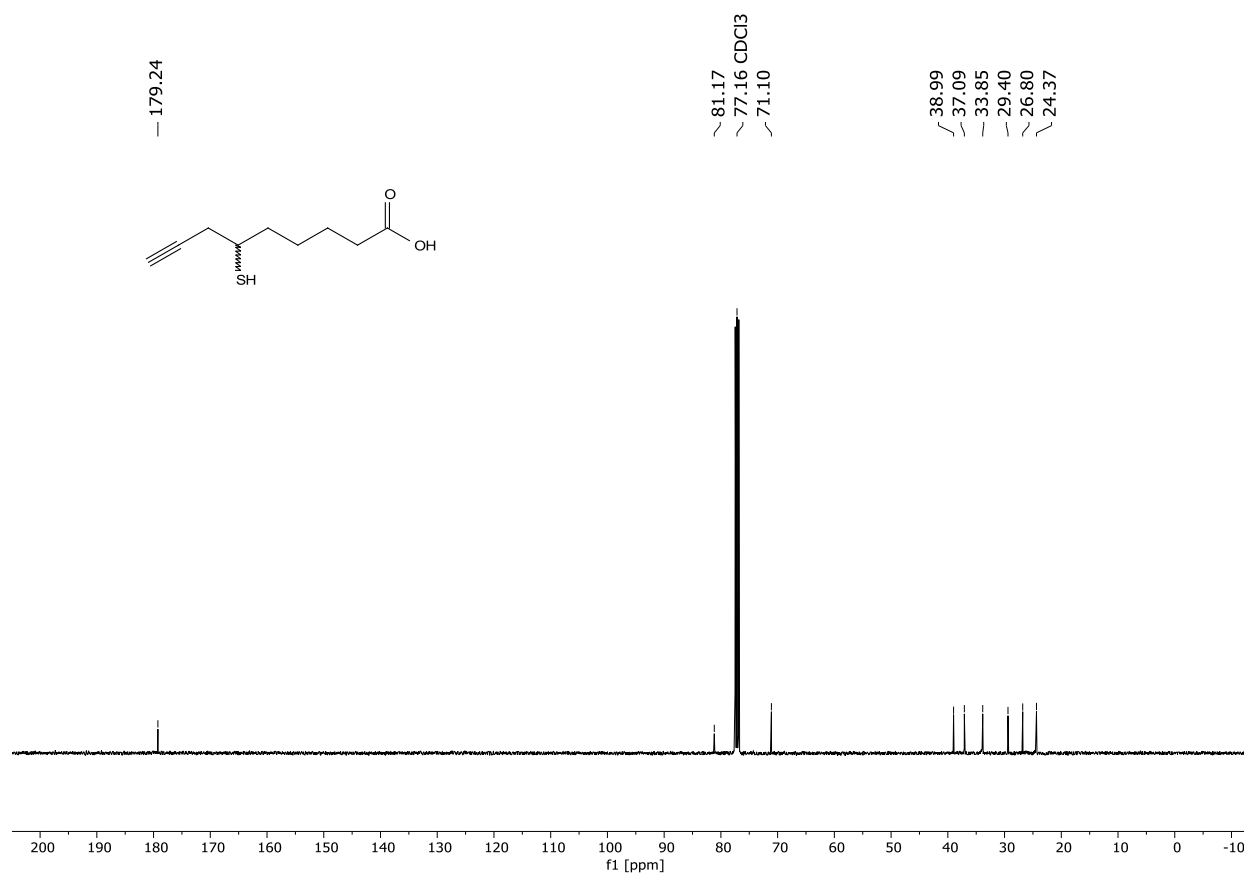
^{1}H-NMR (300 MHz, CDCl$_3$) of probe **3**:
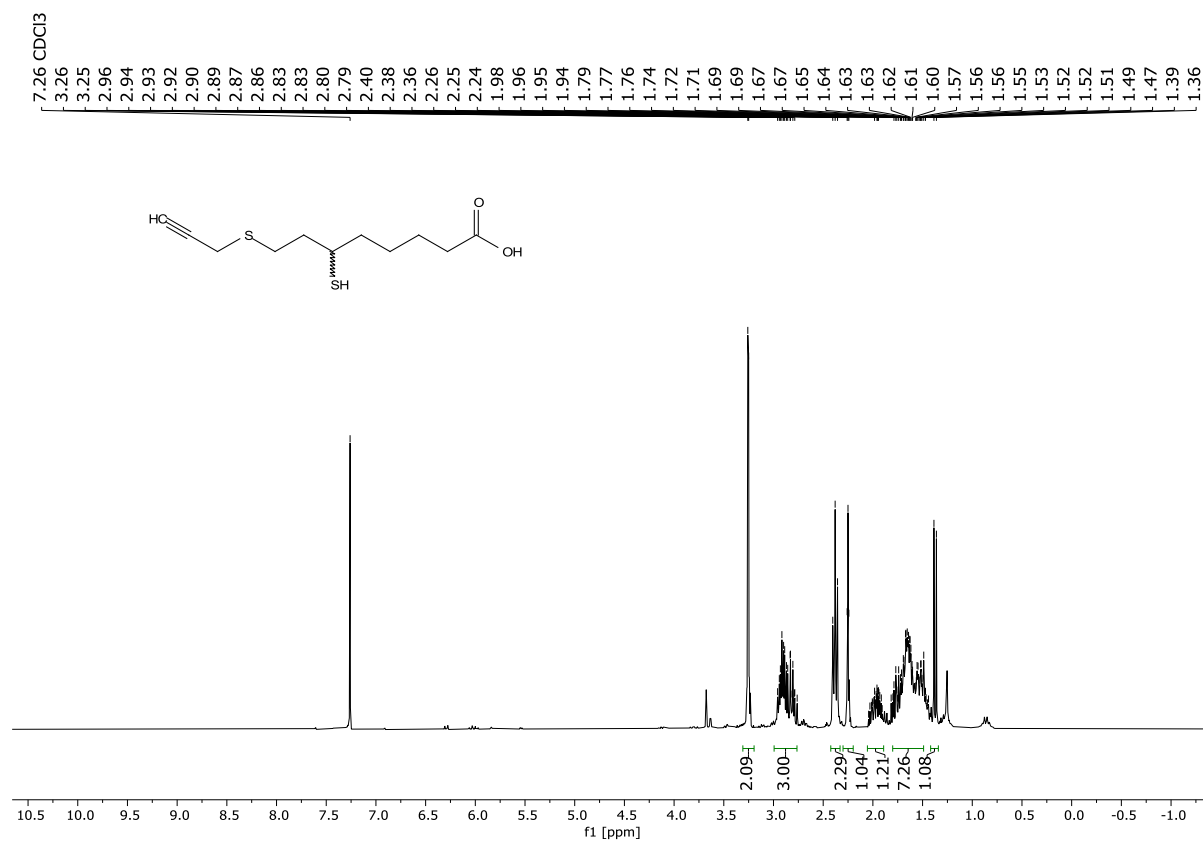
^{13}C-NMR (101 MHz, CDCl$_3$) of probe **3**:
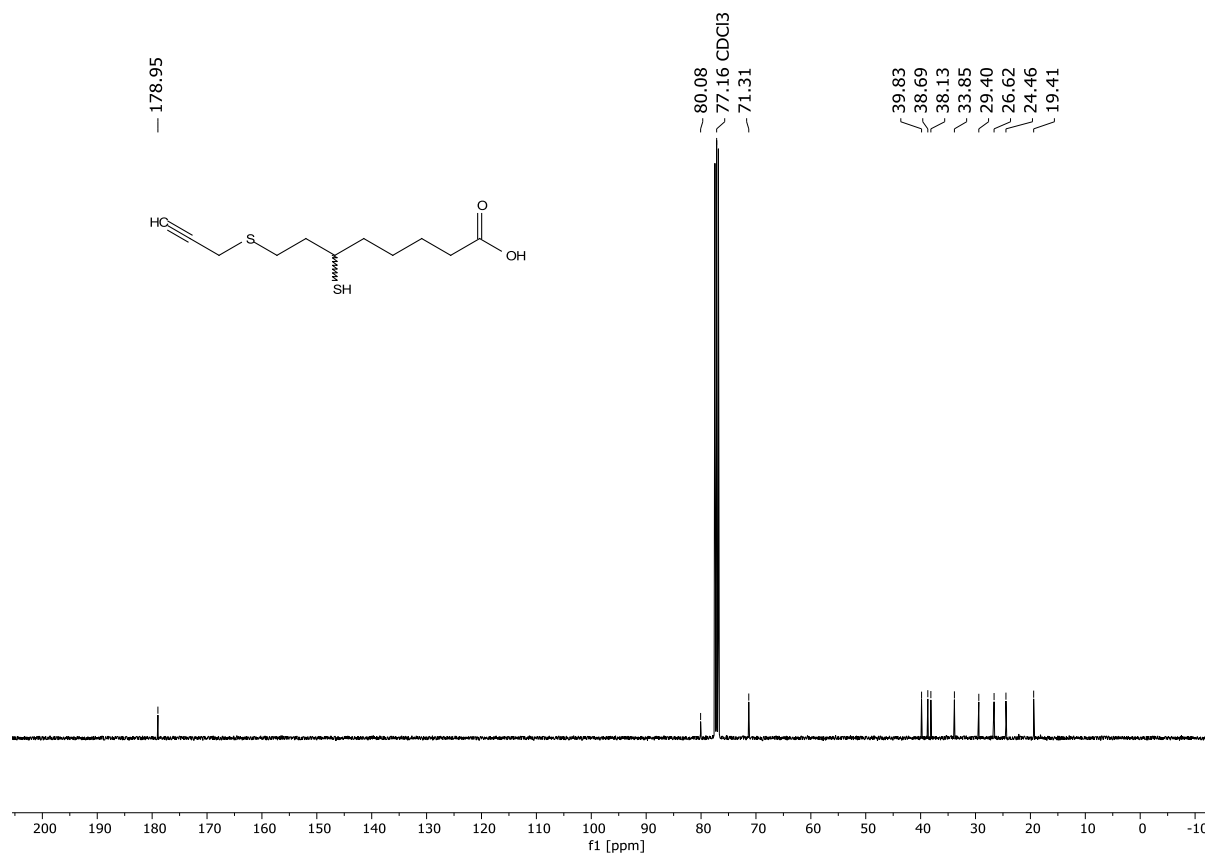
¹H-NMR (400 MHz, CDCl₃) of probe **4**:
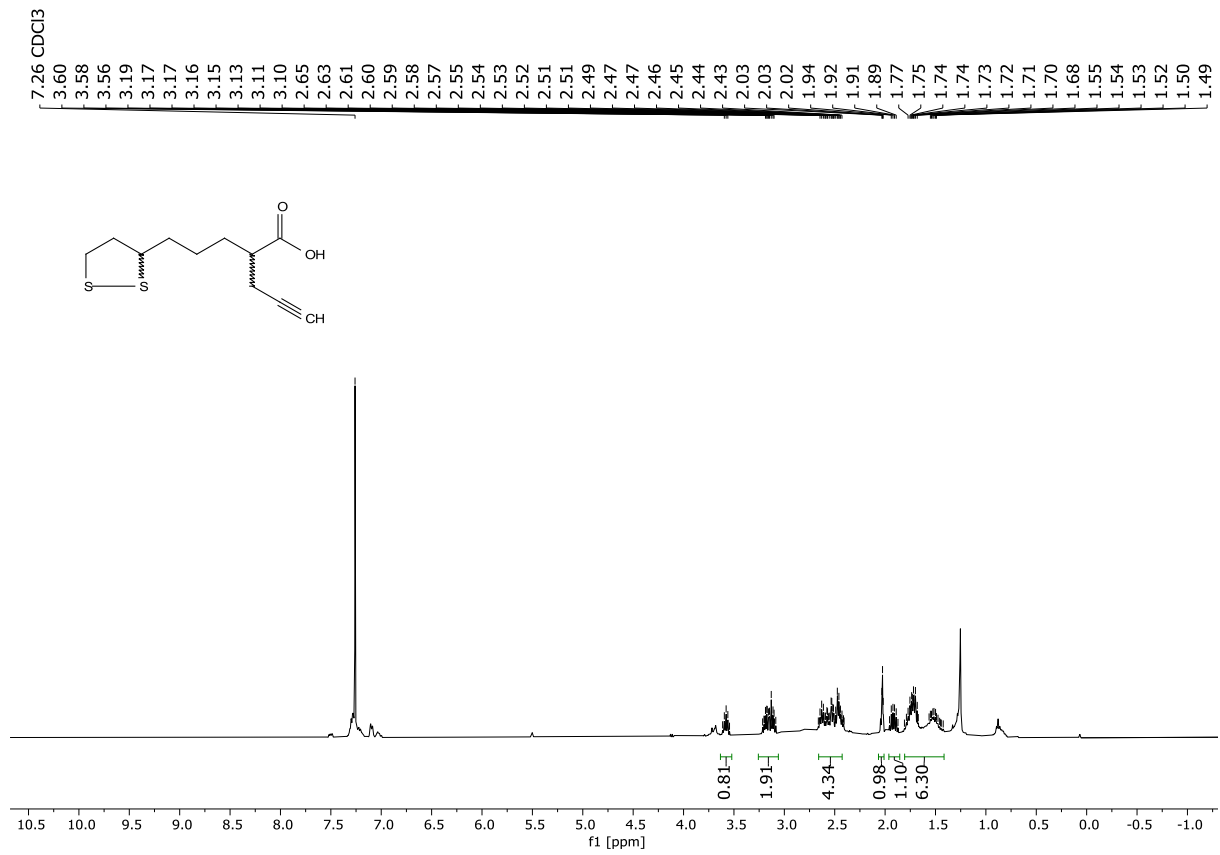
¹³C-NMR (101 MHz, CDCl₃) of probe **4**:

¹H-NMR (500 MHz, CDCl₃) of compound **6**:
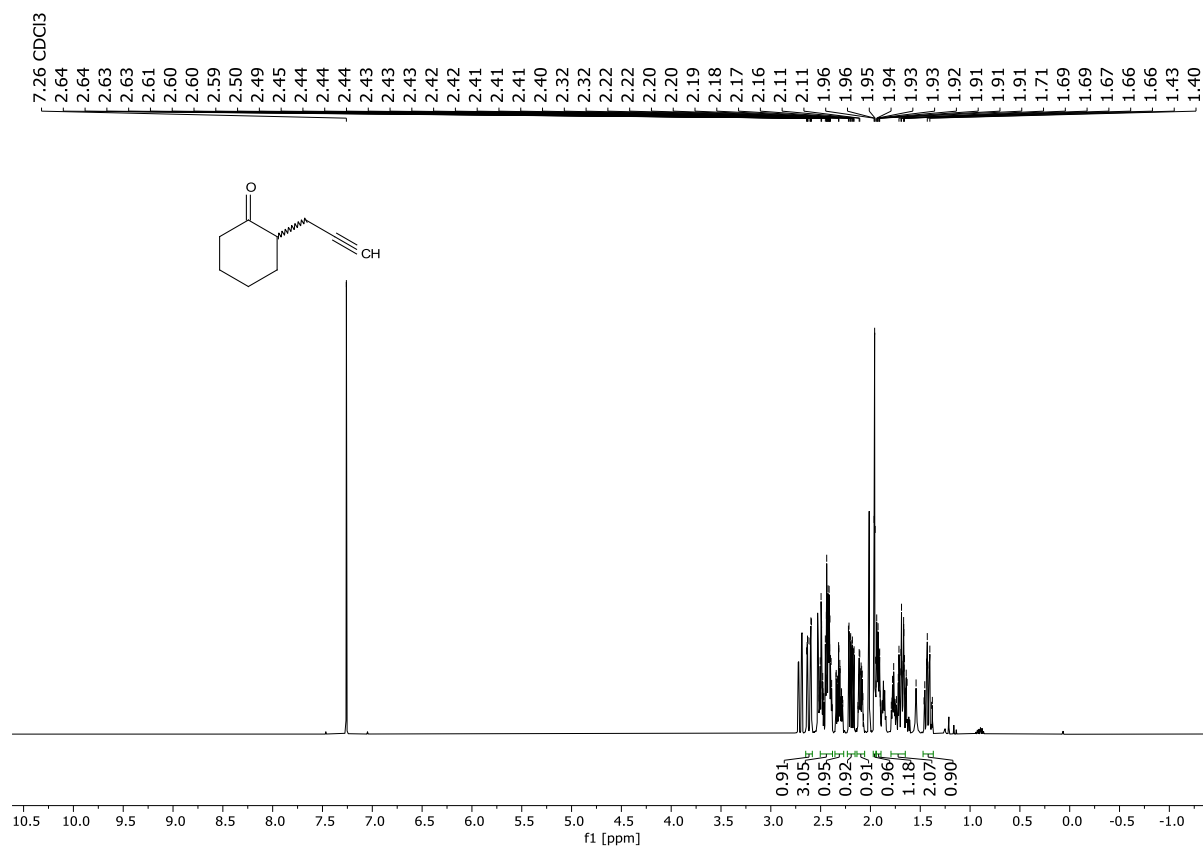
¹³C-NMR (75 MHz, CDCl₃) of compound **6**:
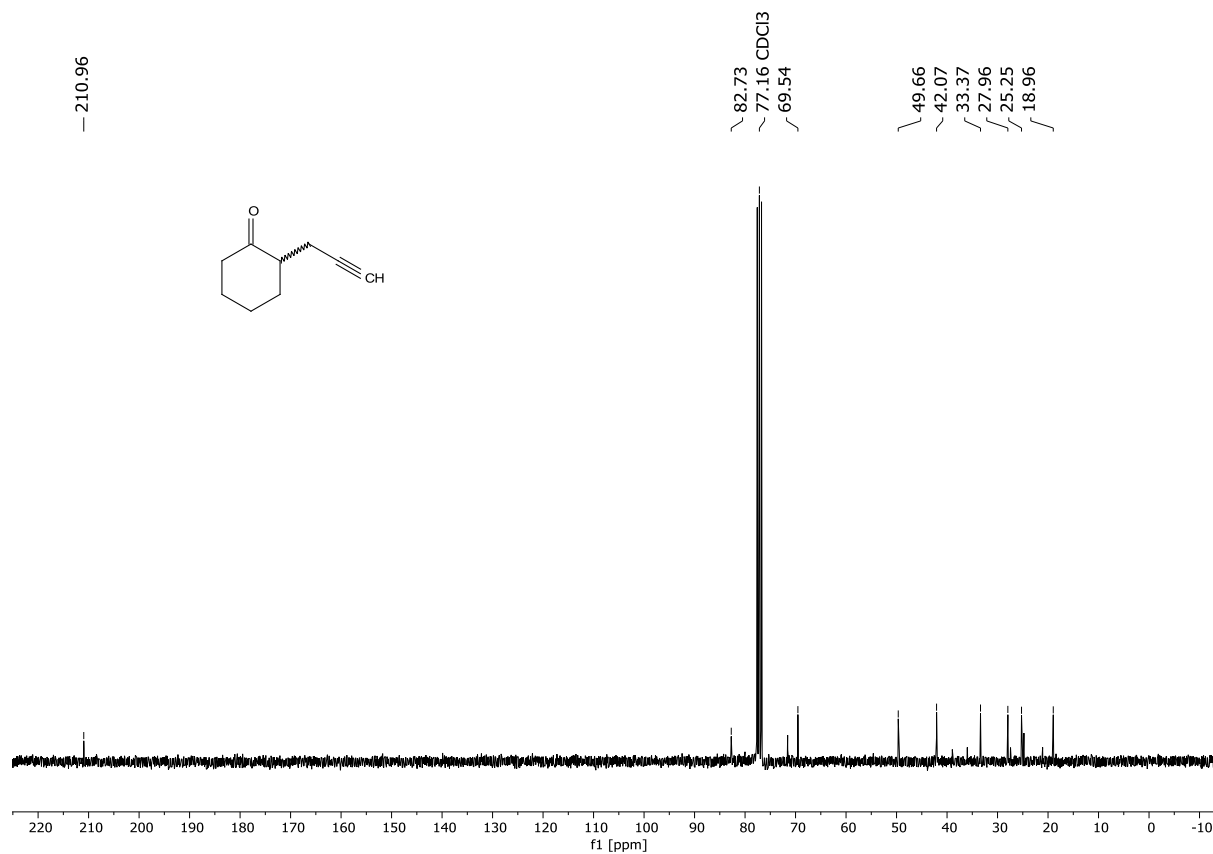
¹H-NMR (300 MHz, CDCl₃) of compound **7**:
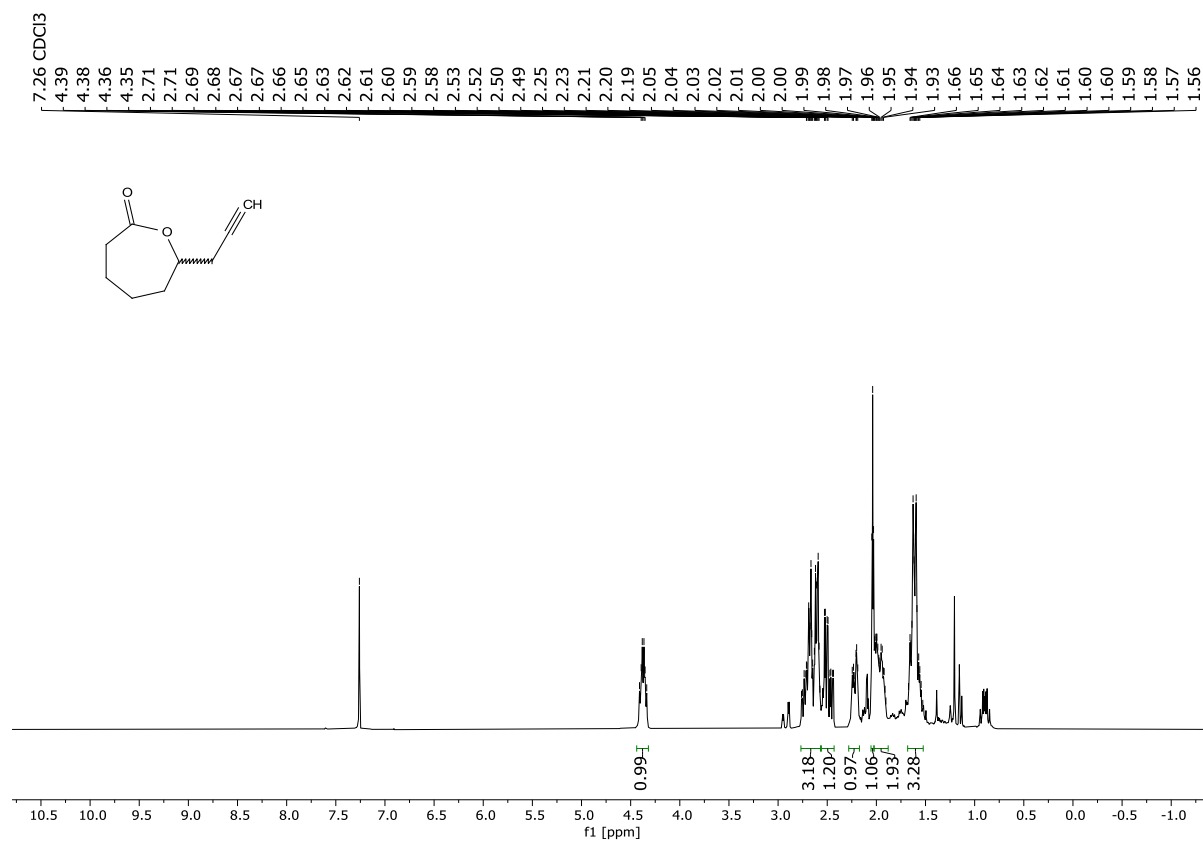
¹³C-NMR (75 MHz, CDCl₃) of compound **7**:
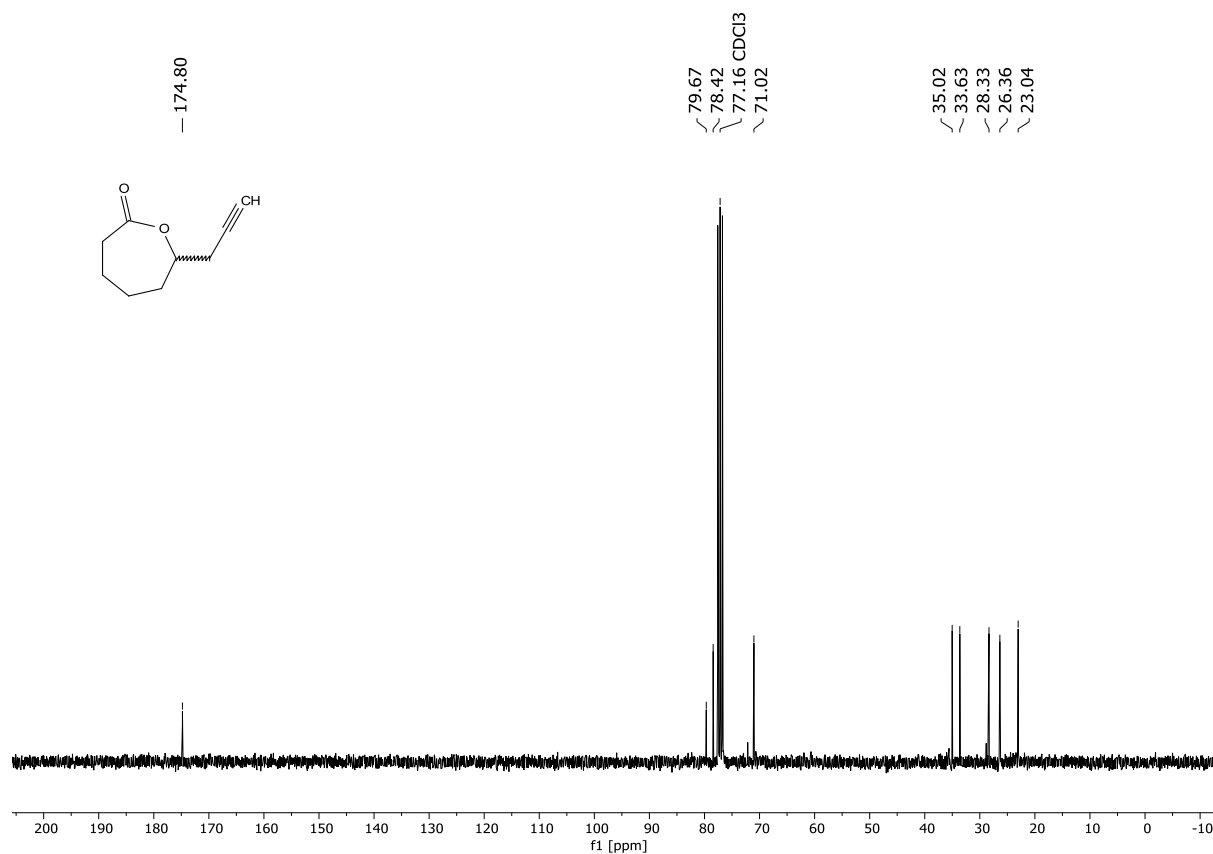
¹H-NMR (500 MHz, CDCl₃) of compound **8**:
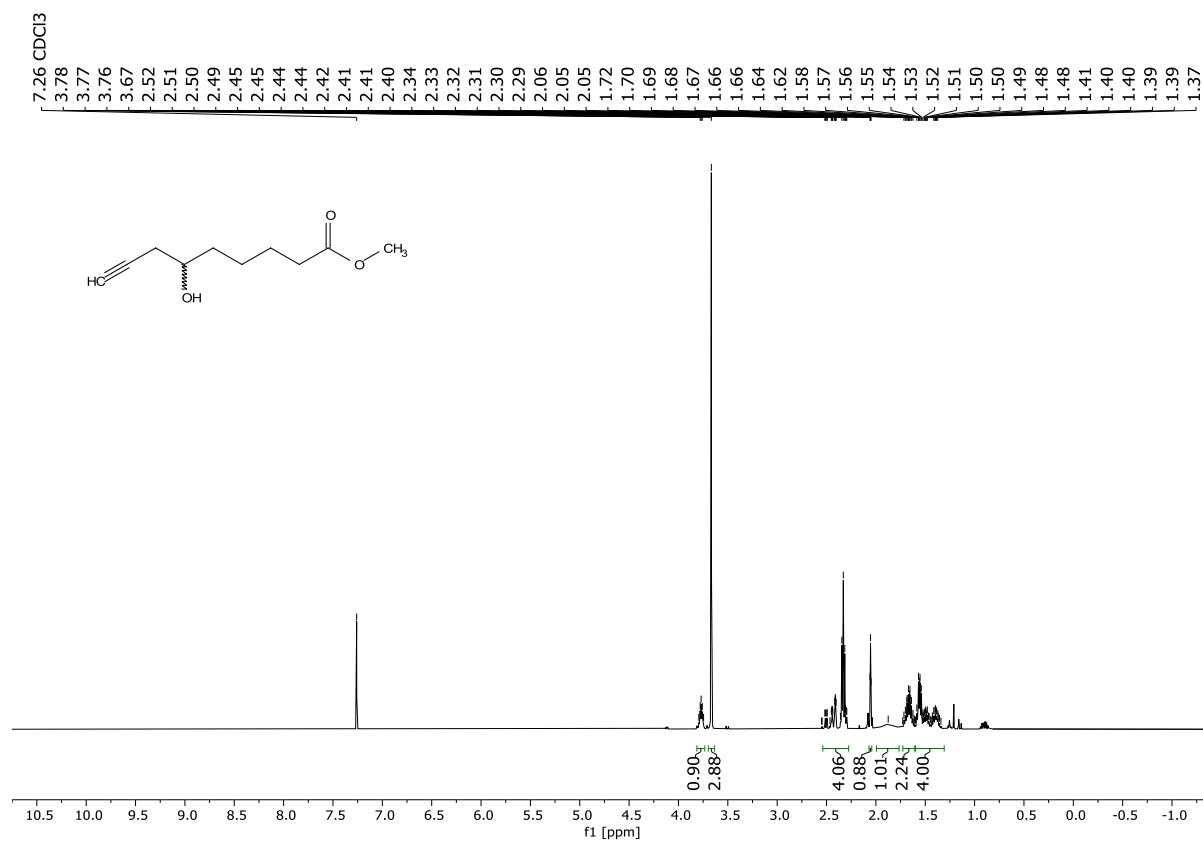
¹³C-NMR (75 MHz, CDCl₃) of compound **8**:
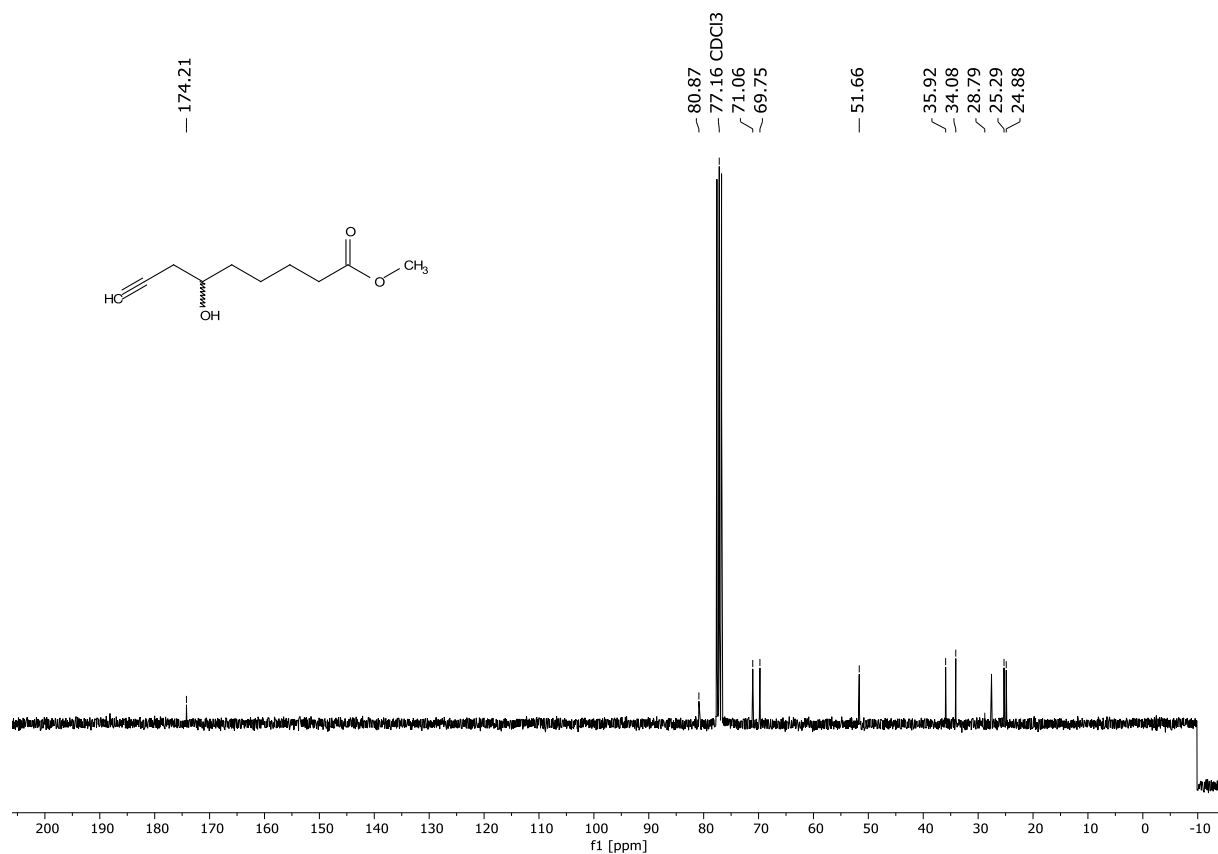
^{1}H-NMR (400 MHz, CDCl$_3$) of compound **9**:
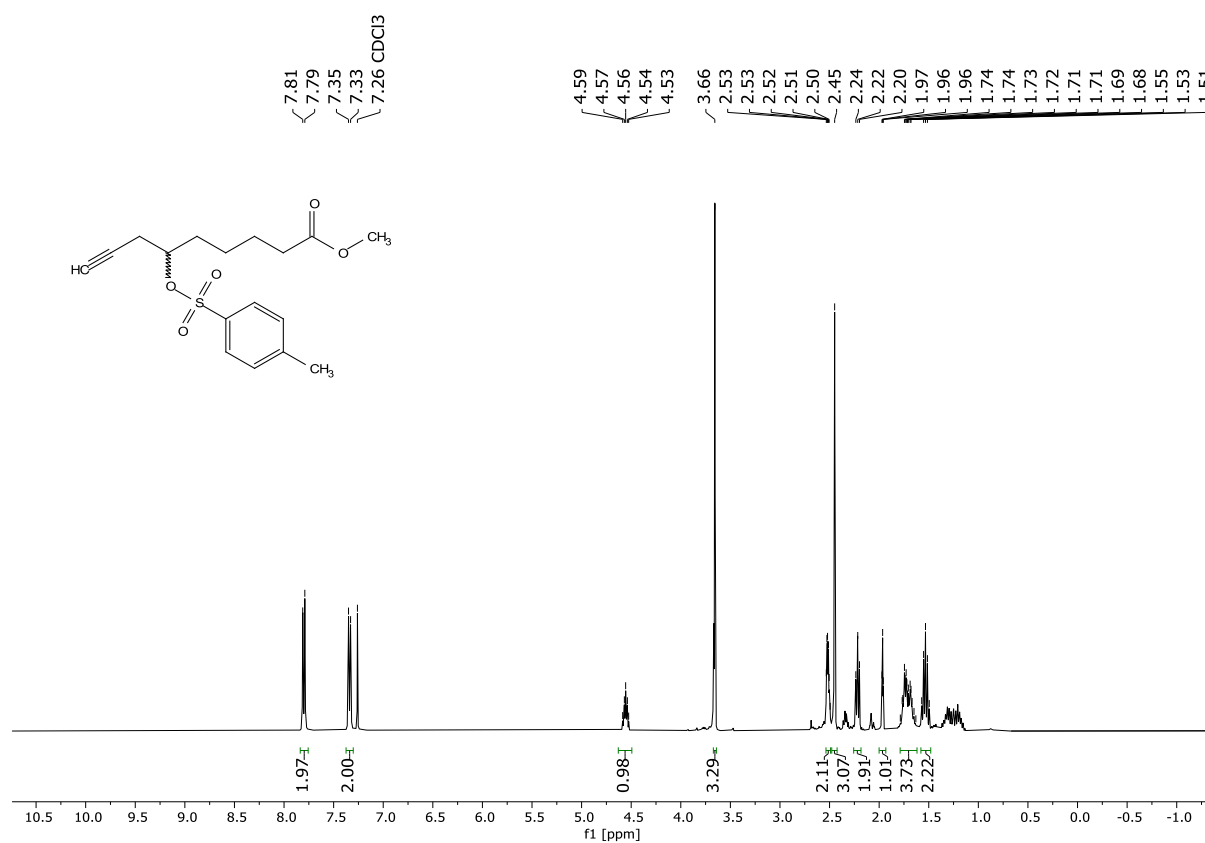
^{13}C-NMR (101 MHz, CDCl$_3$) of compound **9**:
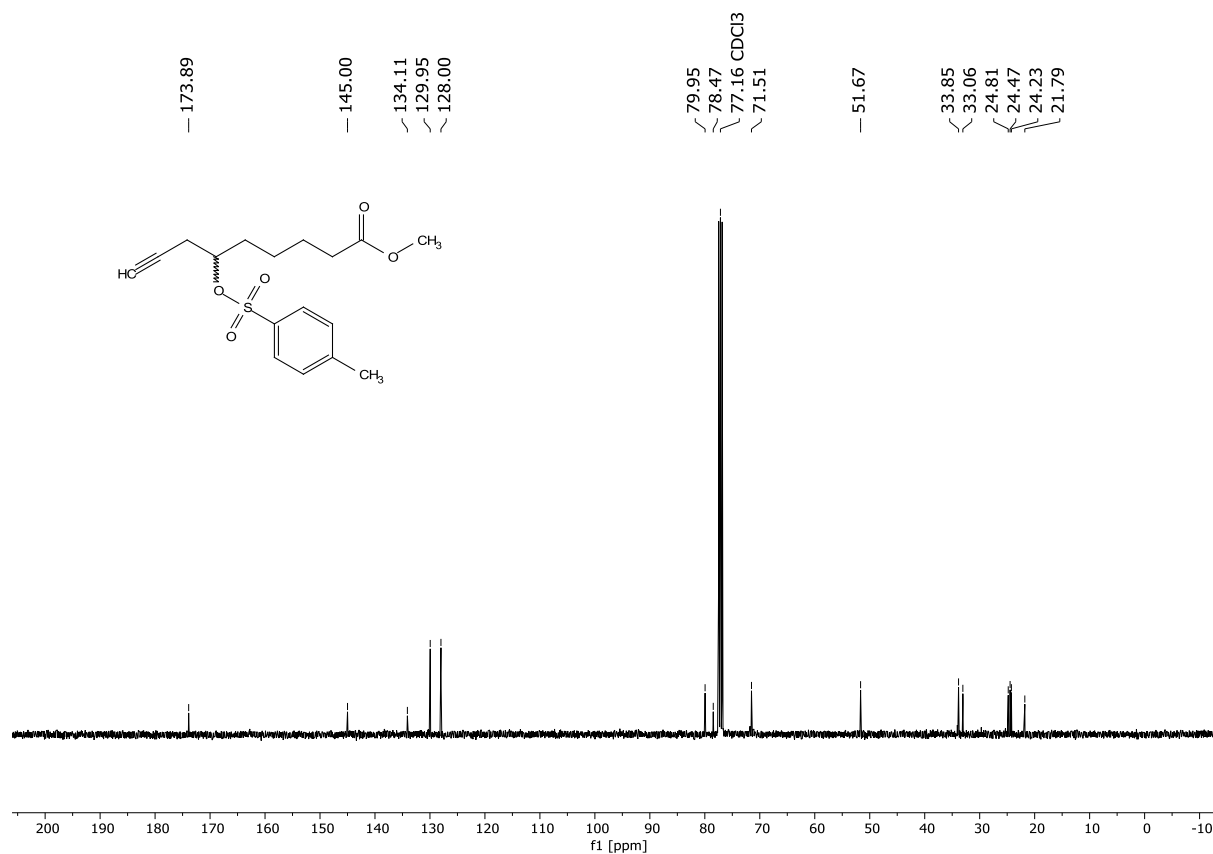
¹H-NMR (400 MHz, CDCl₃) of compound **10**:
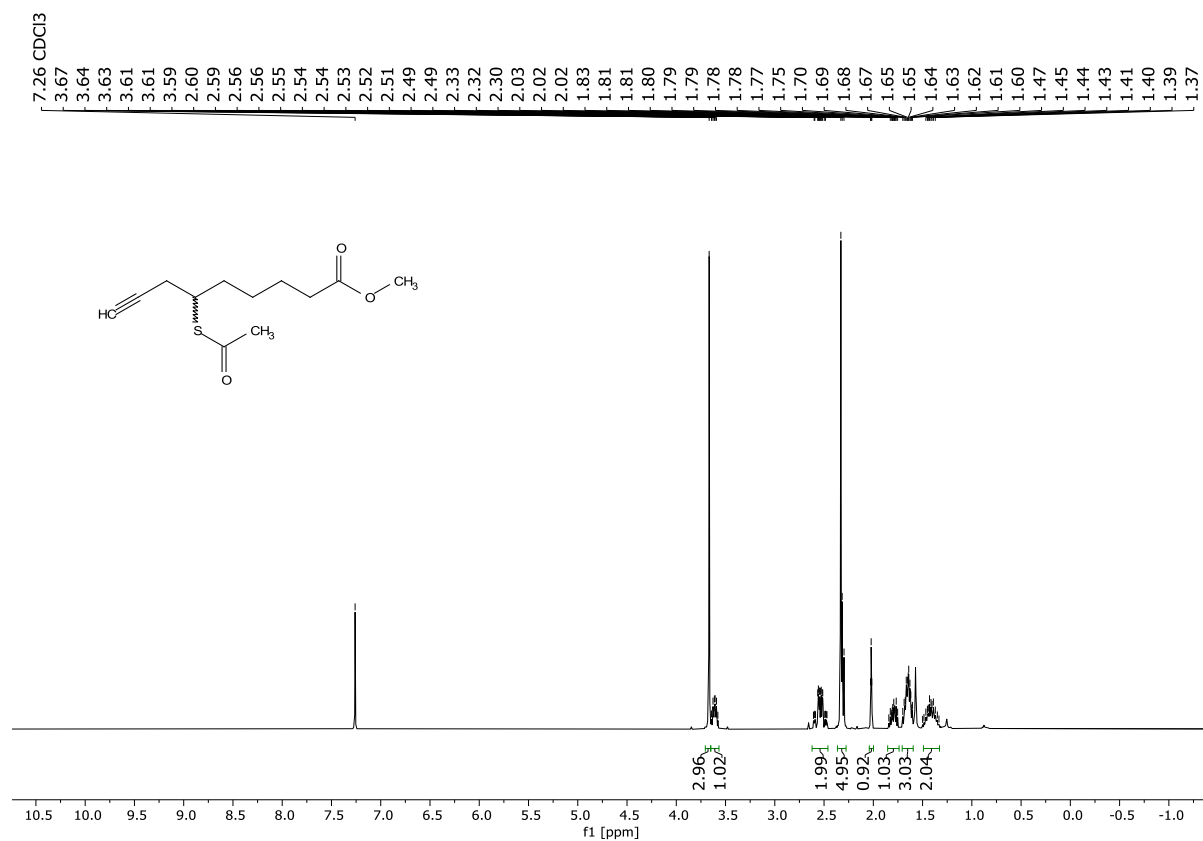
¹³C-NMR (101 MHz, CDCl₃) of compound **10**:
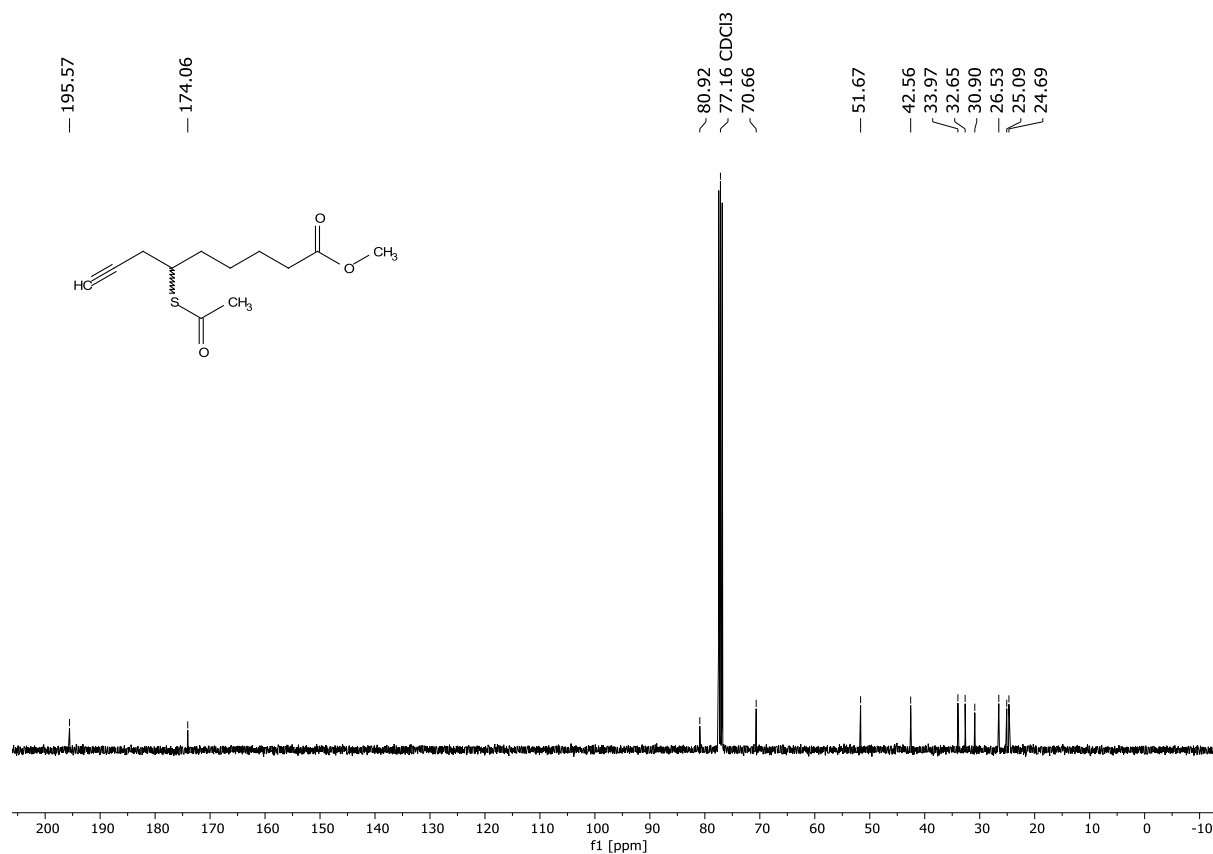
¹H-NMR (400 MHz, CDCl₃) of compound **11**:
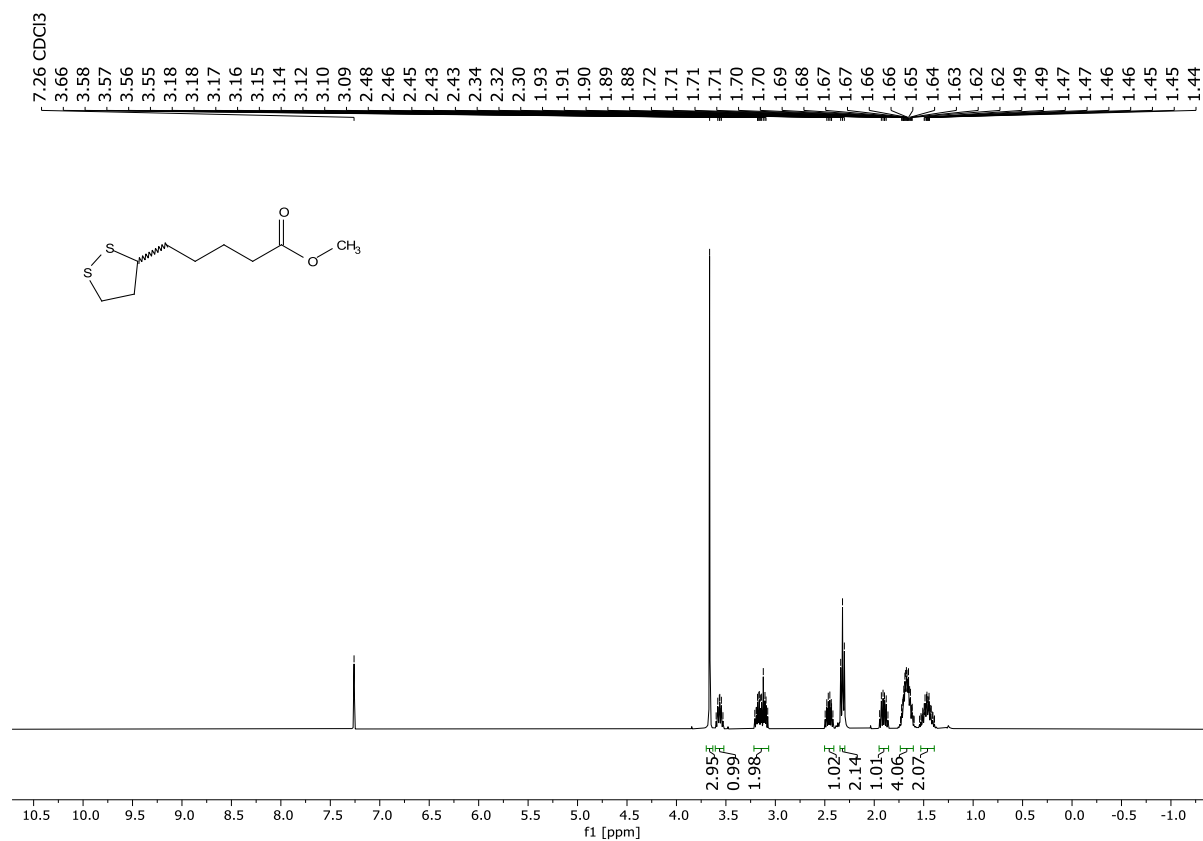
¹³C-NMR (101 MHz, CDCl₃) of compound **11**:
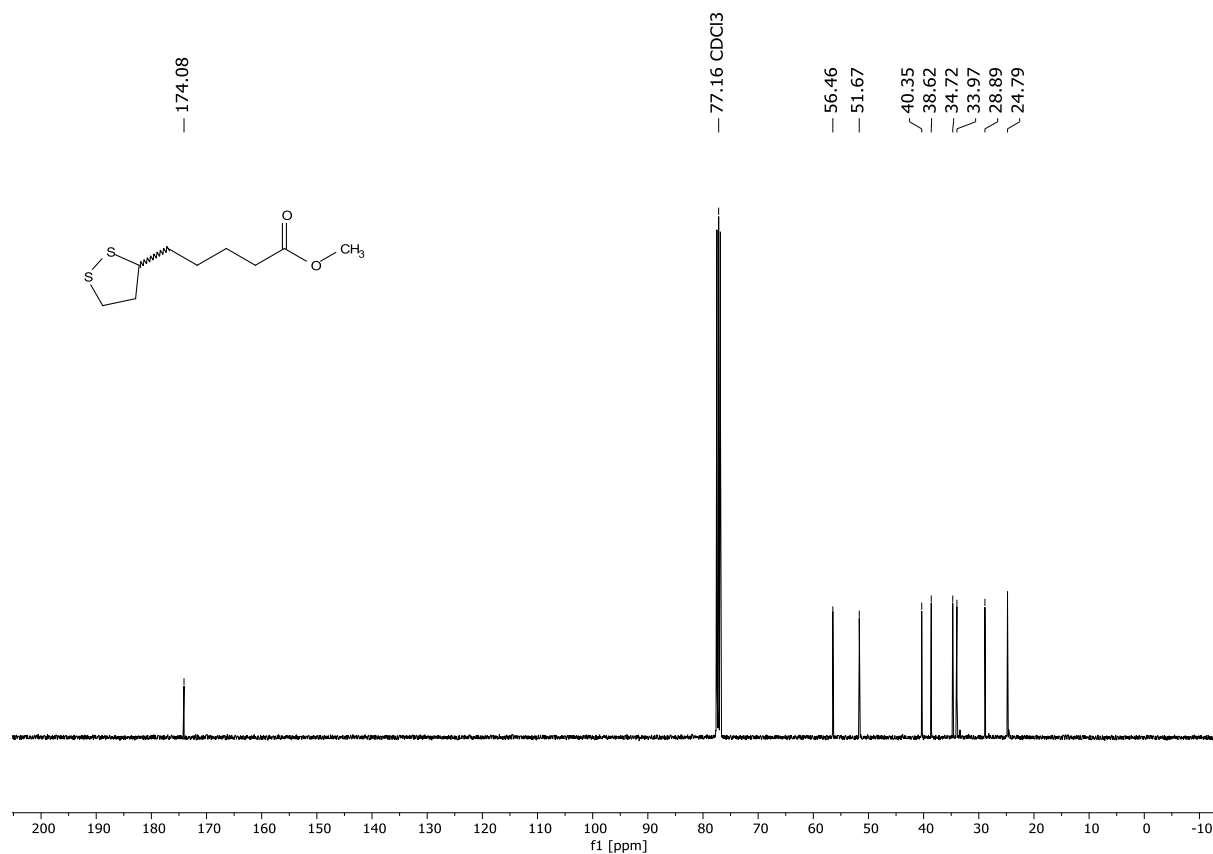
¹H-NMR (300 MHz, CDCl₃) of compound **12**:
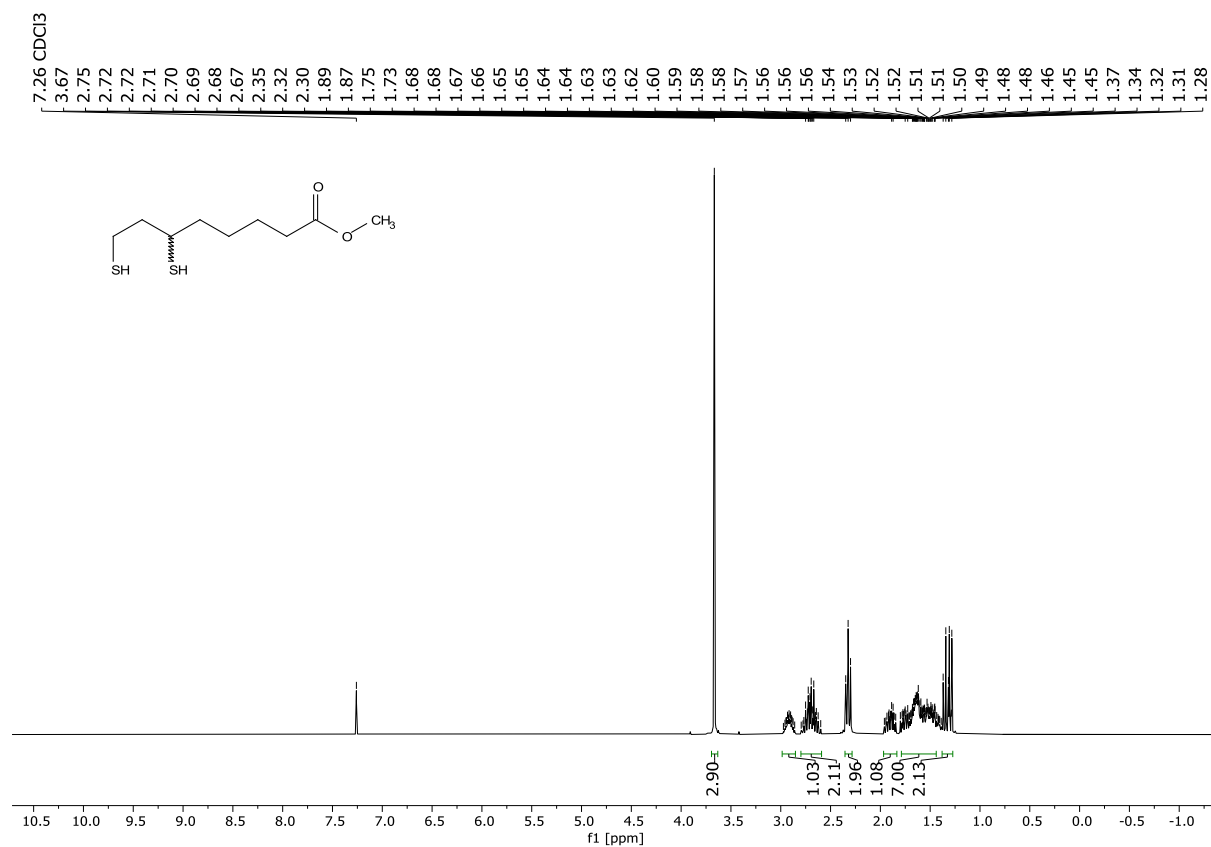
¹³C-NMR (75 MHz, CDCl₃) of compound **12**:
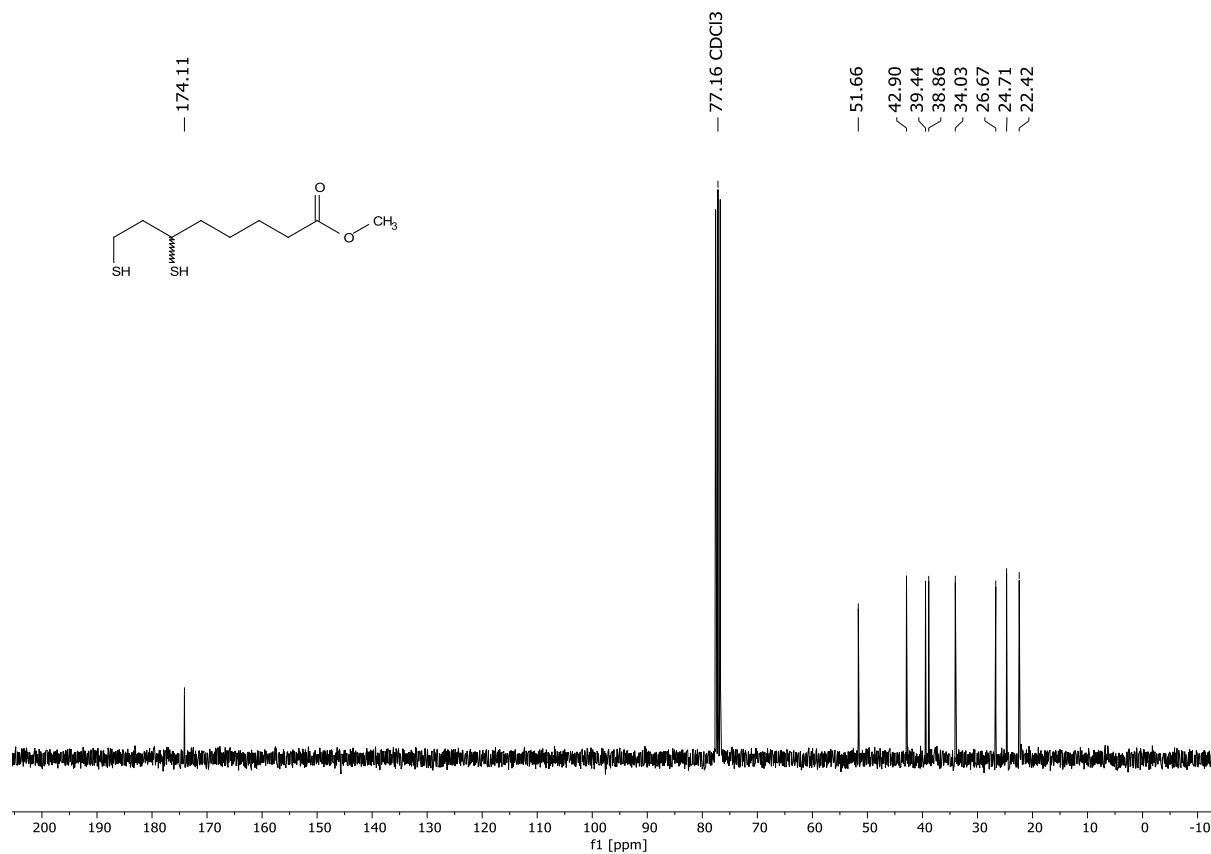
1H-NMR (400 MHz, CDCl$_3$) of compound **13**:
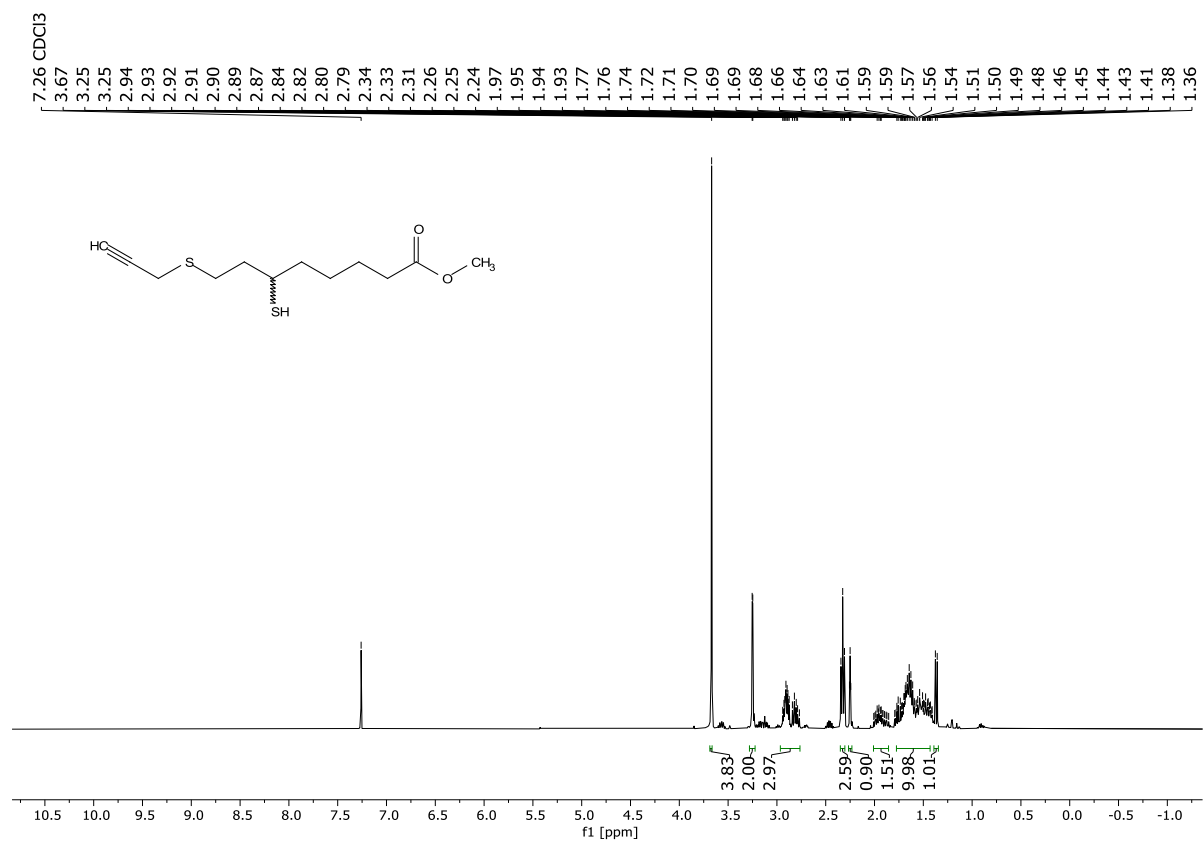
13C-NMR (101 MHz, CDCl$_3$) of compound **13**:
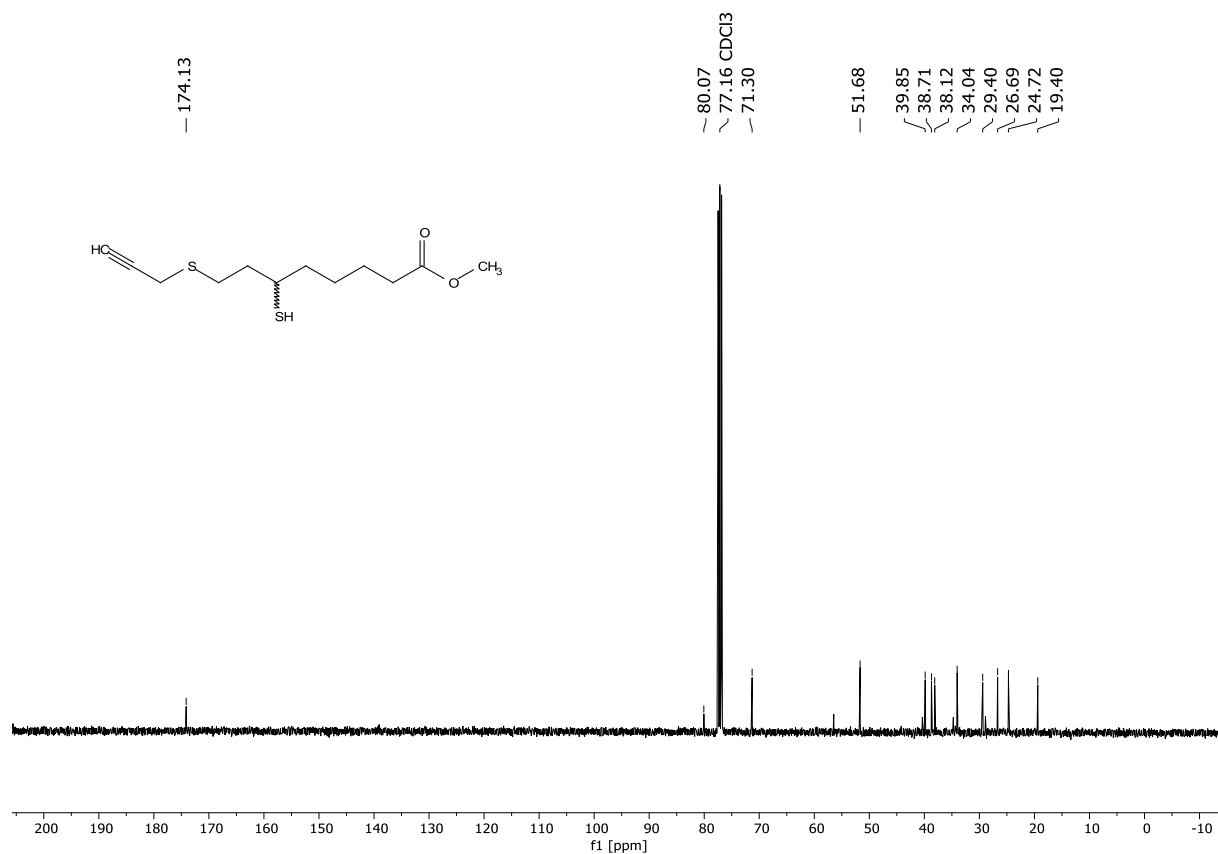
¹H-NMR (400 MHz, CDCl₃) of compound **14**:
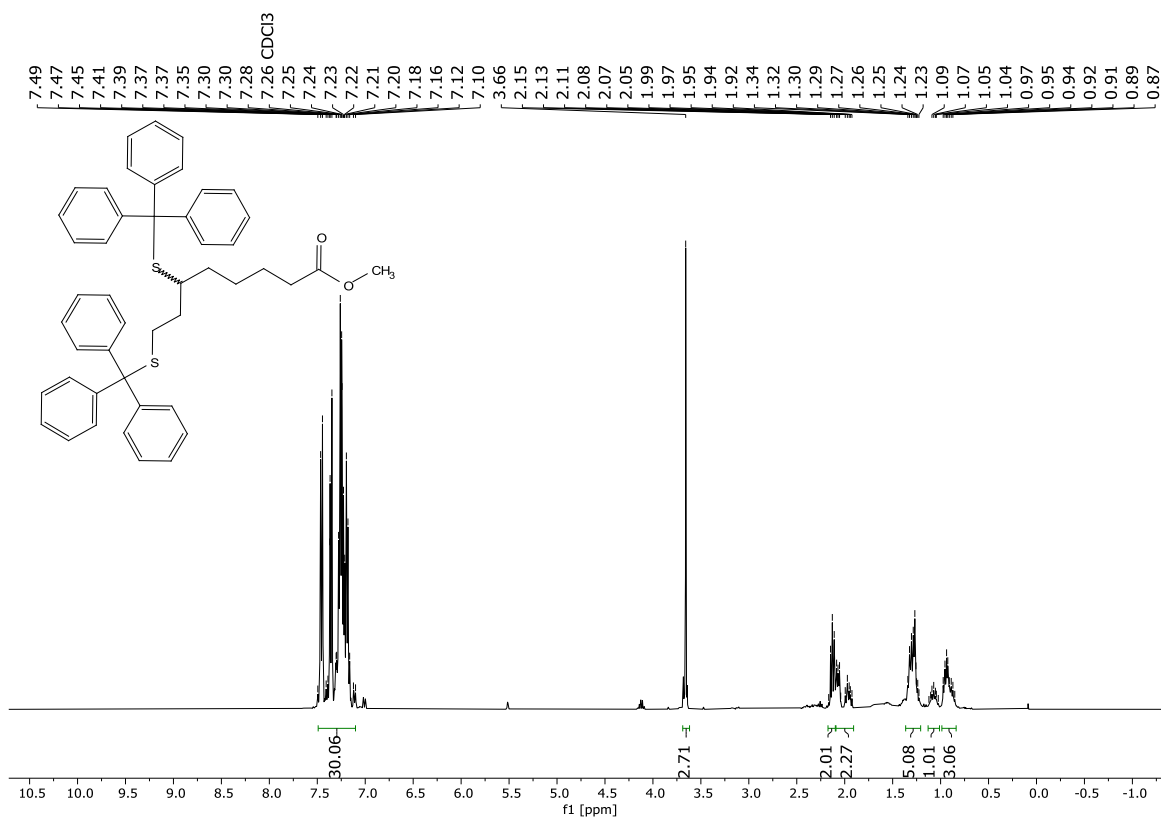
¹³C-NMR (101 MHz, CDCl₃) of compound **14**:
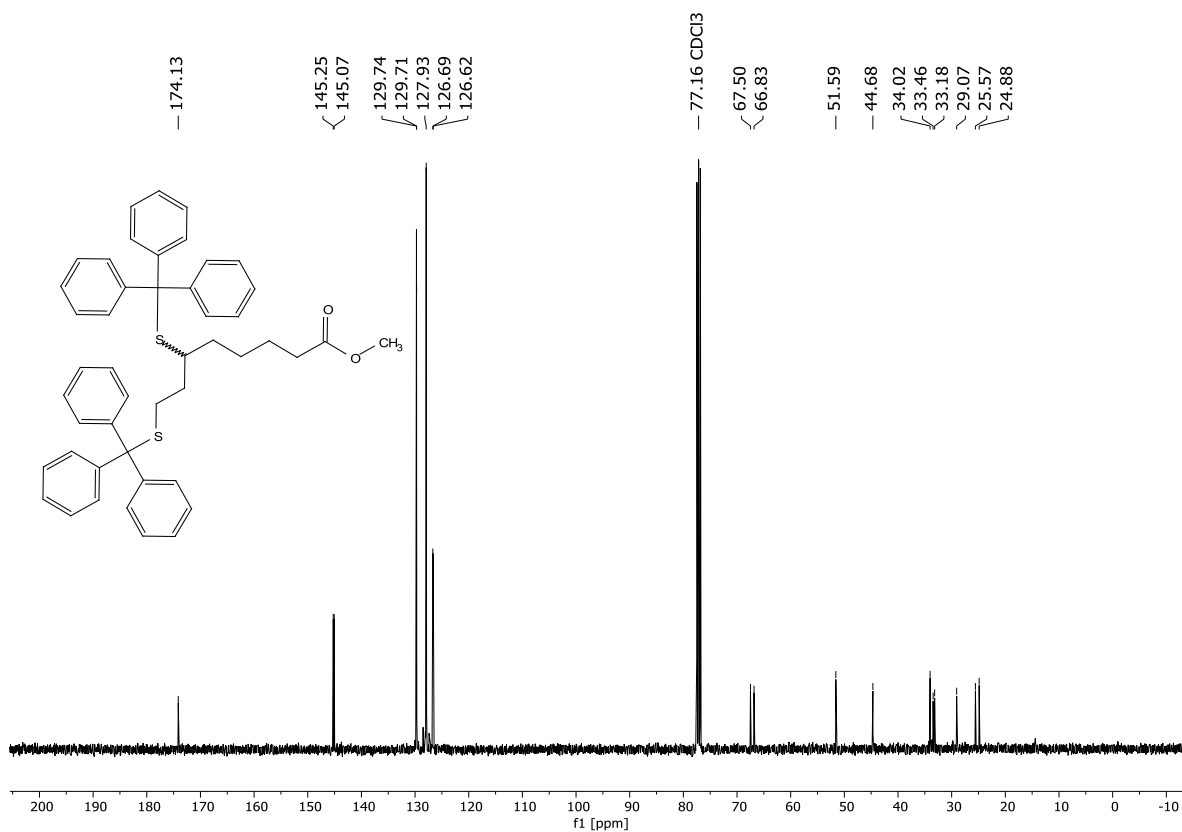
¹H-NMR (400 MHz, CDCl₃) of compound **15**:
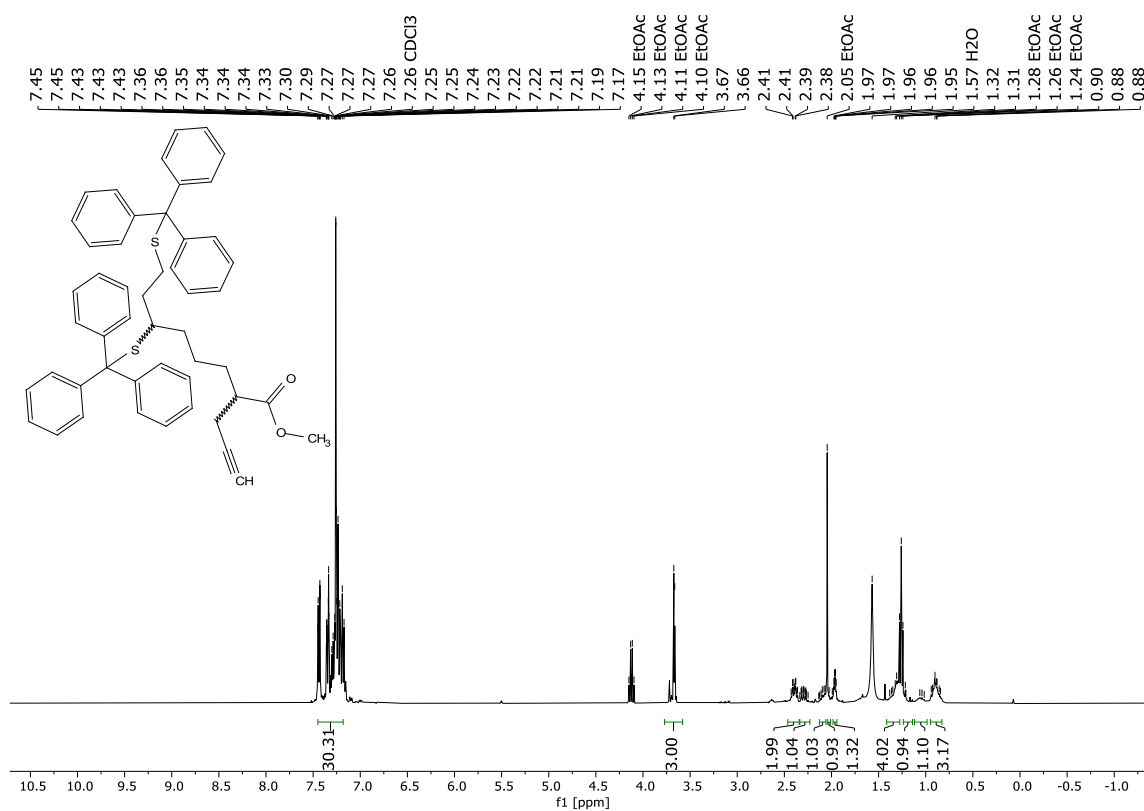
¹³C-NMR (101 MHz, CDCl₃) of compound **15**:
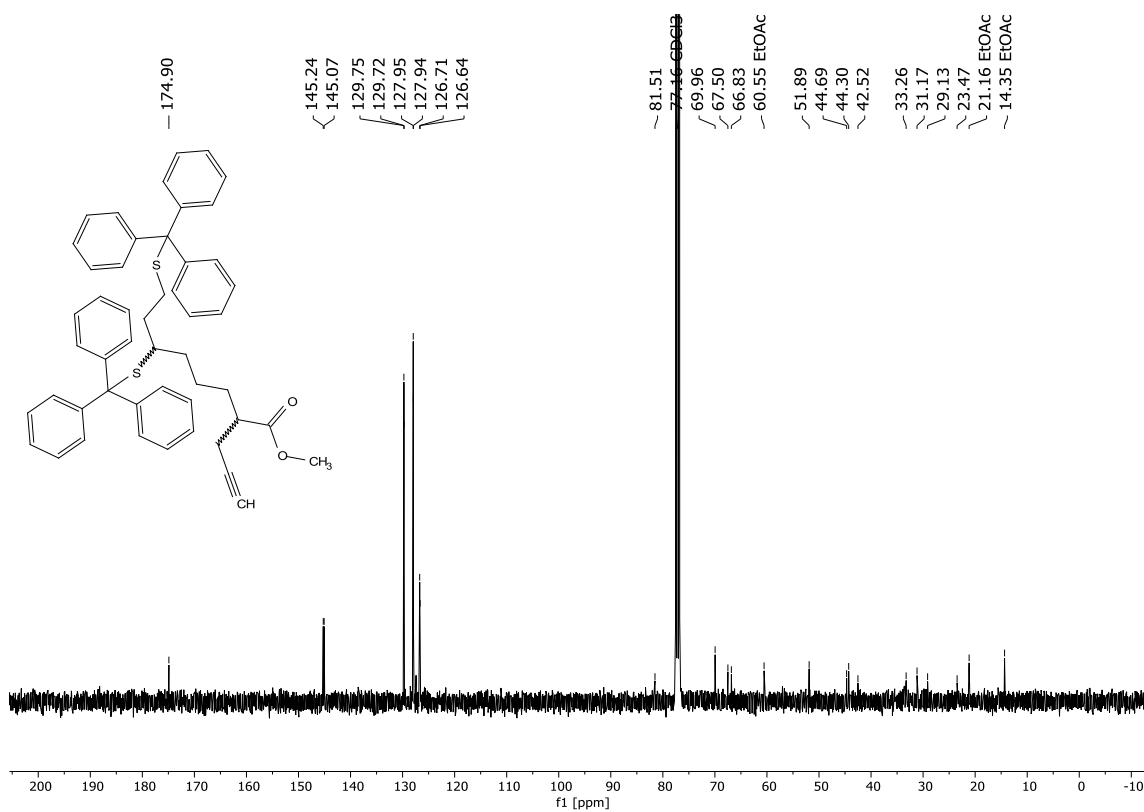
7.4 References

[1]   a) M. Mirdita, K. Schütze, Y. Moriwaki, L. Heo, S. Ovchinnikov, M. Steinegger, *Nature Methods* **2022**, *19*, 679-682; b) UniProtConsortium, *Nucleic Acids Research* **2023**, *51*, D523-D531.

[2]   T. A. Halgren, *Journal of Computational Chemistry* **1996**, *17*, 616-641.

[3]   N. M. O'Boyle, M. Banck, C. A. James, C. Morley, T. Vandermeersch, G. R. Hutchison, *Journal of Cheminformatics* **2011**, *3*, 33.

[4]   O. Trott, A. J. Olson, *Journal of Computational Chemistry* **2010**, *31*, 455-461.

[5]   K. Fujiwara, S. Toma, K. Okamura-Ikeda, Y. Motokawa, A. Nakagawa, H. Taniguchi, *Journal of Biological Chemistry* **2005**, *280*, 33645-33651.

[6]   A. J. Guerra, G. A. Afanador, S. T. Prigge, *Proteins: Structure, Function, and Bioinformatics* **2017**, *85*, 1777-1783.

[7]   D. A. Case, H. M. Aktulga, K. Belfon et al., **2022**, Amber 2022, University of California, San Francisco (US).

[8]   J. A. Maier, C. Martinez, K. Kasavajhala, L. Wickstrom, K. E. Hauser, C. Simmerling, *Journal of Chemical Theory and Computation* **2015**, *11*, 3696-3713.

[9]   W. L. Jorgensen, J. Chandrasekhar, J. D. Madura, R. W. Impey, M. L. Klein, *Journal of Chemical Physics* **1983**, *79*, 926-935.

[10]   J. Wang, R. M. Wolf, J. W. Caldwell, P. A. Kollman, D. A. Case, *Journal of Computational Chemistry* **2004**, *25*, 1157-1174.

[11]   A. Jakalian, D. B. Jack, C. I. Bayly, *Journal of Computational Chemistry* **2002**, *23*, 1623-1641.

[12]   N. Grønbech-Jensen, O. Farago, *Molecular Physics* **2013**, *111*, 983-991.

[13]   J. Åqvist, P. Wennerström, M. Nervall, S. Bjelic, B. O. Brandsdal, *Chemical Physics Letters* **2004**, *384*, 288-294.

[14]   B. R. Miller, III, T. D. McGee, Jr., J. M. Swails, N. Homeyer, H. Gohlke, A. E. Roitberg, *Journal of Chemical Theory and Computation* **2012**, *8*, 3314-3321.

[15]   H. Nguyen, D. R. Roe, C. Simmerling, *Journal of Chemical Theory and Computation* **2013**, *9*, 2020-2034.

[16]   J. J. Irwin, T. Sterling, M. M. Mysinger, E. S. Bolstad, R. G. Coleman, *Journal of Chemical Information and Modeling* **2012**, *52*, 1757-1768.

[17]   D. R. Koes, C. J. Camacho, *Nucleic Acids Research* **2012**, *40*, W409-W414.

[18]   R. J. Premaratne, W. J. Lin, E. A. Johnson, *Applied and Environmental Microbiology* **1991**, *57*, 3046-3048.

[19]   I. Hübner, J.-N. Dienemann, J. Friederich, S. Schneider, S. A. Sieber, *ACS Chemical Biology* **2020**, *15*, 3227-3234.

[20]   J. Cox, M. Mann, *Nat Biotechnol* **2008**, *26*, 1367-1372.

[21]   UniProtConsortium, *Nucleic Acids Research* **2023**, *51*, D523-D531.

[22]   S. Tyanova, T. Temu, P. Sinitcyn, A. Carlson, M. Y. Hein, T. Geiger, M. Mann, J. Cox, *Nature Methods* **2016**, *13*, 731-740.

[23]   P. R. A. Zanon, F. Yu, P. Musacchio, L. Lewald, M. Zollo, K. Krauskopf, D. Mrdović, P. Raunft, T. E. Maher, M. Cigler, C. Chang, K. Lang, F. D. Toste, A. Nesvizhskii, S. M. Hacker, *ChemRxiv preprint* **2021**, DOI: 10.26434/chemrxiv-22021-w26437rss-v26432.

[24]   P. R. A. Zanon, L. Lewald, S. M. Hacker, *Angewandte Chemie International Edition* **2020**, *59*, 2829-2836.

[25]   G. A. Afanador, K. A. Matthews, D. Bartee, J. E. Gisselberg, M. S. Walters, C. L. Freel Meyers, S. T. Prigge, *Molecular Microbiology* **2014**, *94*, 156-171.

[26]   W. Kabsch, *Acta Crystallographica Section D* **2010**, *66*, 125-132.

[27]   A. J. McCoy, R. W. Grosse-Kunstleve, P. D. Adams, M. D. Winn, L. C. Storoni, R. J. Read, *Journal of Applied Crystallography* **2007**, *40*, 658-674.

[28]   K. Zhu, H. Chen, J. Jin, N. Wang, G. Ma, J. Huang, Y. Feng, J. Xin, H. Zhang, H. Liu, *Frontiers in Cellular and Infection Microbiology* **2020**, *10*, 156.

[29]   P. Emsley, K. Cowtan, *Acta Crystallographica Section D* **2004**, *60*, 2126-2132.

[30]   G. N. Murshudov, P. Skubak, A. A. Lebedev, N. S. Pannu, R. A. Steiner, R. A. Nicholls, M. D. Winn, F. Long, A. A. Vagin, *Acta Crystallographica Section D* **2011**, *67*, 355-367.

[31]   G. Langer, S. X. Cohen, V. S. Lamzin, A. Perrakis, *Nature Protocols* **2008**, *3*, 1171-1179.

[32]   M. H. Wright, B. Clough, M. D. Rackham, K. Rangachari, J. A. Brannigan, M. Grainger, D. K. Moss, A. R. Bottrill, W. P. Heal, M. Broncel, R. A. Serwa, D. Brady, D. J. Mann, R. J. Leatherbarrow, R. Tewari, A. J. Wilkinson, A. A. Holder, E. W. Tate, *Nature Chemistry* **2014**, *6*, 112-121.

[33]   M. Schwarz, I. Hübner, S. A. Sieber, *ChemBioChem* **2022**, *23*, e202200253.

[34]   D. Balogh, K. Eckel, C. Fetzer, S. A. Sieber, *RSC Chemical Biology* **2022**, *3*, 955-971.

[35]   a) R. P. Swift, K. Rajaram, H. B. Liu, A. Dziedzic, A. E. Jedlicka, A. D. Roberts, K. A. Matthews, H. Jhun, N. N. Bumpus, S. G. Tewari, A. Wallqvist, S. T. Prigge, *PLOS Pathogens* **2020**, *16*, e1008316; b) S. G. Tewari, B. Kwan, R. Elahi, K. Rajaram, J. Reifman, S. T. Prigge, A. B. Vaidya, A. Wallqvist, *Scientific Reports* **2022**, *12*, 1167.

[36]   M. Brufani, L. Medici, R. M. Bettolo, L. M. Migneco, R. Marzella, R. Figliola, A. La Bella, *US20110212954A1,* **2009**.

[37]   E. Enkvist, D. Lavogina, G. Raidaru, A. Vaasa, I. Viil, M. Lust, K. Viht, A. Uri, *Journal of Medicinal Chemistry* **2006**, *49*, 7150-7159.

[38]   J. W. Trzciński, L. Morillas-Becerril, S. Scarpa, M. Tannorella, F. Muraca, F. Rastrelli, C. Castellani, M. Fedrigo, A. Angelini, R. Tavano, E. Papini, F. Mancin, *Biomacromolecules* **2021**, *22*, 467-480.

[39]   M. Fernández-Suárez, H. Baruah, L. Martínez-Hernández, K. T. Xie, J. M. Baskin, C. R. Bertozzi, A. Y. Ting, *Nature Biotechnology* **2007**, *25*, 1483-1487.

[40]   K. Shen, B. Bai, Y.-H. Liu, T. L. Lowary, *Angewandte Chemie International Edition* **2021**, *60*, 24859-24863.

[41]   L. Tan, S. Maji, C. Mattheis, Y. Chen, S. Agarwal, *Macromolecular Bioscience* **2012**, *12*, 1721-1730.

[42]   A. A. Burke, L. Barrows, M. J. Solares, A. D. Wall, C. E. Jakobsche, *Chemistry – A European Journal* **2018**, *24*, 17681-17685.

[43]   S. Kumar, S. Soni, W. Danowski, C. L. F. van Beek, B. L. Feringa, P. Rudolf, R. C. Chiechi, *Journal of the American Chemical Society* **2020**, *142*, 15075-15083.

[44]   M. J. Torres, A. Fierro, C. D. Pessoa-Mahana, J. Romero-Parra, G. Cabrera, M. Faúndez, *European Journal of Pharmacology* **2017**, *799*, 41-47.

[45]   N. Lakshminarayana, Y. Rajendra Prasad, L. Gharat, A. Thomas, P. Ravikumar, S. Narayanan, C. V. Srinivasan, B. Gopalan, *European Journal of Medicinal Chemistry* **2009**, *44*, 3147-3157.

[46]   J. L. Wahlstrom, R. C. Ronald, *Journal of Organic Chemistry* **1998**, *63*, 6021-6022.

8|

Experimental section (chapter 4)

8.1 Biochemistry

8.1.1 Media and buffers

Table 8.1. Media and buffers.

	LB-medium (1 L)	B-medium (1 L)	BHI-medium (1 L)
Media	5 g Peptone 2.5 g Yeast extract 2.5 g NaCl pH 7.5 in 1 L ddH$_2$O	10 g Peptone 5 g Yeast extract 5 g NaCl 1 g K$_2$HPO$_4$ pH 7.5 in 1 L ddH$_2$O	7.5 g Brain infusion 10 g Peptone 5 g NaCl 10 g Heart-infusion 2.5 g Na$_2$HPO$_4$ 2 g Glucose pH 7.4 in 1 L ddH$_2$O

	PBS	SEC-buffer	K-buffer
Buffers	10.0 mM Na$_2$HPO$_4$ 1.80 mM KH$_2$PO$_4$ 140 mM NaCl 2.70 mM KCl pH 7.4 in ddH$_2$O	50 mM HEPES 250 mM NaCl pH 8.0 in ddH$_2$O	50 mM HEPES 50 mM KCl 10 mM MgCl$_2$ pH 7.9 in ddH$_2$O

	Lysis buffer	Wash buffer 1	Wash buffer 2	Wash buffer 3	Elution buffer
His-tagged protein buffers	20 mM HEPES 10 mM Imidazol 150 mM NaCl 2 mM β-Mercapto-ethanol (β-ME) 0.2% (v/v) NP-40 pH 8.0 in ddH$_2$O	20 mM HEPES 10 mM Imidazol 150 mM NaCl 2 mM β-ME pH 8.0 in ddH$_2$O	20 mM HEPES 10 mM Imidazol 1 M NaCl 2 mM β-ME pH 8.0 in ddH$_2$O	20 mM HEPES 40 mM Imidazol 150 mM NaCl 2 mM β-ME pH 8.0 in ddH$_2$O	20 mM HEPES 500 mM Imidazol 150 mM NaCl 2 mM β-ME pH 8.0 in ddH$_2$O

	Running gel (10×)	Loading buffer (2×)	Staining solution	Destaining solution
SDS-PAGE buffers	24.8 mM Tris/HCl 192 mM Glycine 3.5 mM SDS pH 8.3 in ddH$_2$O	63 mM Tris/HCl 10% glycerol 0.25 ‰ (w/v) Bromphenol blue 2% (w/v) SDS 5% (w/v) β-ME in ddH$_2$O	0.25% (w/v) Coomassie brilliant blue R250 10% (v/v) Acetic acid 50% (v/v) Ethanol abs. in ddH$_2$O	10% (v/v) Acetic acid 20% (v/v) Ethanol abs. in ddH$_2$O

8.1.2 Bacterial strains

E. coli K12, which is classified for biosafety level 1, was handled on an open bench under sterile conditions. All other bacteria are categorized within biosafety level 2 and were handled in biosafety cabinets only (Table 8.1, 8.2).

For pre-cultures, 5 mL media were inoculated with bacteria and grown at 200 rpm at 37 °C.

Table 8.2. Bacterial strains and media. Transposon mutants were cultured in the presence of erythromycin (ERY).

Species	Strain	Medium
S. aureus wt	USA 300 LAC JE2	B
S. aureus ΔSAUSA300_0562 (Δ*thiD*, here Δ*Sa*PLK)	USA 300 Nebraska transposon mutant library	B (10 µg mL^{-1} ERY in EtOH)
S. aureus ΔSAUSA300_2631 (Δputative *N*-Acetyltransferase)	USA 300 Nebraska transposon mutant library	B (10 µg mL^{-1} ERY in EtOH)
E. faecalis	V583	BHI
E. faecium	DMS 20477	BHI
E. coli	K12	LB
P. aeruginosa	PAO1	LB

8.1.3 ABPP – analytical *in situ* labeling

Day cultures of *S. aureus* were used to inoculate 50 mL B-media and bacteria were grown to stationary phase (OD$_{600}$ of 7.6, 12 h). The cells were harvested (5,000 g, 10 min, 4 °C) and washed with PBS (15 mL; 5,000 g, 10 min, 4 °C). The pellet was resuspended in PBS to obtain a calculated OD$_{600}$ of 40. To 200 µL of OD$_{600}$ of 40 culture, 2 µL 20 mM probe (final concentration: 200 µM, 1% (v/v) DMSO) or DMSO was added. The cultures were incubated (24 h, 25 °C, 800 rpm) and harvested by centrifugation (5,000 g, 10 min, 4 °C). The pellet was washed with PBS (2×0.5 mL) and resuspended in 200 µL 0.4% (w/v) SDS in PBS. The cells were lysed by bead disruption (Precellys 24 Homogenizer, *Bertin Technologies*) using the following cycle three times: 30 sec at 6,500 rpm, with 20 sec cooling break using liquid nitrogen air flow. The lysed cells were transferred to Eppendorf tubes and centrifuged (16,000 g, 30 min, r. t.). 50 µL supernatant were subjected to click-reaction as described in section "Labeling of Recombinant PLK". The click reaction was stopped by the addition of 50 µL loading buffer (2×). Samples were subsequently analyzed *via* SDS-PAGE and fluorescence visualization.

8.1.4 ABPP – preparative *in situ* labeling

Labeling and lysis. Day cultures of *S. aureus*, *E. faecalis* and *E. coli* were used to inoculate fresh media and bacteria were grown to stationary phase (*S. aureus*: OD$_{600}$ of 8.3, 12 h; *E. faecalis*: OD$_{600}$ of 2.0, 6 h; *E. coli*: OD$_{600}$ of 3.1, 6 h). The cells were harvested (5,000 g, 10 min, 4 °C) and washed with PBS (15 mL; 5,000 g, 10 min, 4 °C). Pellets were resuspended in PBS to obtain a calculated OD$_{600}$ of 40. To 1 mL of OD$_{600}$ of 40 culture, 10 µL probe (final concentrations indicated in corresponding figures, 1% (v/v) DMSO) or DMSO was added. The cultures were incubated (24 h, 25 °C, 800 rpm) and harvested by centrifugation (5,000 g, 10 min, 4 °C). The pellets were washed with PBS (2×1 mL) and resuspended in 1 mL 0.4% (w/v) SDS in PBS for lysis. *E. coli* samples were lysed by sonication (3×20 s, 80%, Sonopuls HD 2070 ultrasonic rod, *Bandelin electronic GmbH*) with cooling breaks on ice. *E. faecalis* and *S. aureus* samples were transferred into 2 mL lysis tubes for bead disruption (Precellys 24 Homogenizer, *Bertin Technologies*) using the following cycle three times: 30 sec at 6,500 rpm, with 20 sec cooling break using liquid nitrogen air flow. The lysed cells were transferred to Eppendorf tubes and lysate was cleared (16,000 g, 30 min, r. t.). Protein concentration was measured using the Pierce BCA Protein assay kit (*Thermo Fisher Scientific, Pierce Biotechnology*) and sample concentrations were adjusted to equal protein amounts (1-2 mg mL^{-1}) in a total volume of 500 µL.

Click reaction and protein precipitation. The samples were subjected to click-reaction for 1 h at r. t. using 3 μL biotin-azide (10 mM in DMSO), 10 μL TCEP (52 mM in ddH$_2$O), 30 μL 1 × TBTA ligand (1.67 mM stock) and 10 μL CuSO$_4$ per 500 μL sample. Subsequently, proteins were precipitated with ice-cold acetone (4 volumes) at −20 °C overnight, centrifuged (16,900 × g, 4 °C, 15 min) and washed twice with ice-cold methanol (1 mL). Pellets were resuspended in 500 μL 0.4% (w/v) SDS in PBS by sonication (10 sec, 10% intensity, Sonopuls HD 2070 ultrasonic rod, *Bandelin electronic GmbH*).

Protein enrichment. All aqueous solutions were prepared using MS-grade water. Affinity enrichment was performed with avidin agarose resin (A9207 Sigma-Aldrich, pre-washed three times with 0.4% (w/v) SDS in PBS (1 mL); 400 × g for 2 min was used to pellet beads; 50 μL of bead slurry was used for enrichment). The protein samples were centrifuged (18,000 × g, 5 min, r. t.), added to the bead suspension and incubated with agitation for 1 h at r. t. The samples were transferred to washing columns and beads were washed as follows: 0.4% (w/v) SDS in PBS (4×0.6 mL), 6 M urea (3×0.6 mL), PBS (4×0.6 mL).

On bead digest. The beads with bound proteins were resuspended in 200 μL X-buffer (7 M urea, 2 M thiourea in 20 mM HEPES, pH 7.5) and reduced by adding 2 μL TCEP (5 mM) followed by incubation for 1 h (37 °C, 450 rpm). Alkylation was performed with 4 μL IAA (500 mM in 50 mM triethylammonium bicarbonate (TEAB)) followed by incubation for 30 min (r. t., 450 rpm). The reaction was stopped by adding 4 μL DTT (10 mM) and incubation of 30 min (r. t., 450 rpm). The samples were digested by Lys-C (1 μL, 0.5 μg μL^{-1}, *Wako*) for 2 h (r. t., 450 rpm) and diluted with TEAB (50 mM, 0.6 mL). Trypsin (1.5 μL, 0.5 μg μL^{-1} in 50 mM acetic acid, *Promega*) was added to digest the samples for 16 h (37 °C, 450 rpm). On the next day, the reaction was stopped by acidification using formic acid (FA, 10 μL, final pH below 3.0).

Desalting and filtration. The digested protein samples were centrifuged (16,000 g, 3 min, r. t.) and the supernatant was loaded on 50 mg SepPak C18 columns (*Waters*) equilibrated with 0.1% (v/v) trifluoroacetic acid (TFA). The peptides were washed three times with 1 mL 0.1% (v/v) TFA and 500 μL 0.5% (v/v) FA. Afterwards, the peptides were eluted three times with 250 μL elution buffer (80% (v/v) acetonitrile (ACN), 0.5% (v/v) FA), lyophilized and stored at −80 °C until further usage. The lyophilized peptides were dissolved in 25 μL 1% (v/v) FA, and filtered through 0.22 μm PVDF filters (*Millipore*), which were equilibrated with 300 μL 1% (v/v) FA. The filtrate was transferred into MS-vials and stored at −20 °C until the measurements were performed.

MS-measurement and data analysis. MS-measurement of *S. aureus* and *E. faecalis* samples was performed on a Q Exactive Plus instrument equipped with an electronspray easy source (*Thermo Fisher*) coupled to an Ultimate 3000 Nano-HPLC (*Thermo Fisher*). Samples were loaded on a 2 cm Acclaim C18 PepMap100 trap column (particles 3 μm, 100 A, inner diameter 75 μm, *Thermo Fisher*) with 0.1% (v/v) TFA and separated on a 50 cm PepMap RSLC C18 column (particles 2 μm, 100 A, inner diameter 75 μm, *Thermo Fisher*) constantly heated to 50 °C. The gradient was run from 5–32% (v/v) acetonitrile, 0.1% (v/v) formic acid during a 152 min method (7 min 5%, 105 min to 22%, 10 min to 32%, 10 min to 90%, 10 min wash at 90%, 10 min equilibration at 5%) at a flow rate of 300 nL min^{-1}.

MS-measurement of *E. coli* samples was performed on a slightly different setup. The Q Exactive Plus instrument was equipped with a Nanospray Flex ion source (ES071, *Thermo Fisher*) and separation of peptides was performed at a flow rate of 400 nL min^{-1} on a 25 cm Aurora Series emitter C18 column (AUR2-25075C18A, particles 1.6 μm, inner diameter 75 μm, *Ionopticks*) constantly heated to 40 °C.

MS data on the Q Exactive Plus instrument was acquired with the following parameters: survey scans (m/z 300-1,500) were acquired at a resolution of 140,000 and the maximum injection time was set to 80 ms (AGC target value 3e^6). Data-dependent HCD fragmentation scans of the 10 most intense ions

of the survey scans were acquired at a resolution of 17,500, maximum injection time was set to 100 ms (AGC target value 1e^5). The isolation window was set to 1.6 m/z. Unassigned and singly charged ions were excluded for measurement and the dynamic exclusion of peptides enabled for 60 s. The lock-mass ion 445,12002 from ambient air was used for real-time mass calibration on the Q Exactive Plus. Data were acquired using Xcalibur software (version 4.1.31.9, *Thermo Fisher*) and MaxQuant (version 1.6.1.0) was used to analyze the obtained raw files of the label-free quantification with Andromeda.[1] The following settings were applied: variable modifications: oxidation (methionine), acetylation (N-terminus); fixed modifications: carbamidomethylation (cysteine); proteolytic enzyme: trypsin/P; missed cleavages: 2; "No fractions", "LFQ", "Requantify" and "Match between runs" were enabled; "Second Peptide" was disabled. Searches were performed against the following FASTA files from UniProtKB: *S. aureus* USA300 (taxon identifier: 367830, downloaded: 1 April 2019), *E. faecali*s V583 (taxon identifier: 226185, downloaded:1 April 2019), *E. coli* K12 (taxon identifier: 83333, downloaded: 7 April 2020).[2]

Perseus (version 1.6.2.3) was used for analysis.[3] The protocol for data-filtering was used as follows: (1) LFQ intensities were log$_2$ transformed. (2) Rows were annotated into groups - DMSO (control) and probe treatments with corresponding concentration. (3) Potential contaminants were removed. (4) Peptides only identified by site were removed. (5) Reverse peptides were removed. (6) Rows were filtered for at least 3 valid values in at least one group. (7) Imputation of missing values from normal distribution. (8) Annotations derived from data banks were added. (9) Volcano plots were created with cut-off lines FDR = 0.05 (95%) and s0 = 0.3 based on two-sided two sample Student's *t*-tests.

8.1.5 Cloning

Recombinant PLK (*pdxY*) proteins of *E. coli* K12 (UniProt ID: P77150) and *P. aeruginosa* PAO1 (UniProt ID: Q9HT57) were constructed to carry an N-terminal His$_6$-tag. The Invitrogen™ Gateway™ cloning system (*Thermo Scientific*) was used following the manufacturer's cloning protocol. Primers for wild type (wt) genes were designed to carry *att*B1 or *att*B2 sequences (Table 8.3) to shuffle the respective PCR products into donor vector pDONR201^{Kan} (pDONR201_*Ec*PLK_wt, pDONR201_*Pa*PLK_wt) and destination vector pET300^{Amp} (pET300_*Ec*PLK_wt, pET300_*Pa*PLK_wt).

Mutant plasmids (pET300_*Ec*PLK_C122A, pET300_*Pa*PLK_C124A) were obtained using the QuikChange II site-directed mutangenesis protocol (*Agilent*) with the respective pET300 wt plasmids as DNA templates. The primer sequences (Table 8.3) were designed using QuikChange Primer Design (*Agilent*). After amplification of the desired mutant plasmid using Phusion HF Polymerase, the wt plasmids were digested by *Dpn*I and the remaining mutant plasmids were transformed into chemically competent *E. coli* XL1-Blue, which were subsequently plated on LB agar supplemented with appropriate antibiotic (Table 8.4). Single colonies were picked and grown in 5 mL LB medium containing appropriate antibiotic. On the next day, plasmid DNA was isolated using E.Z.N.A. Plasmid mini Kit I (*OMEGA Bio-Tek*) according to the manufacturer's protocol. The plasmid concentration was measured using an Infinite$^®$ M200 Pro plate reader with a NanoQuant plate (*Tecan Group Ltd.*) and the sequences were verified by DNA sequencing (*Genewiz*). Plasmids (Table 8.4) were transformed into chemically competent *E. coli* BL21 (DE3) cells for protein expression.

Table 8.3. Primers used for Gateway cloning and QuikChange site-directed mutagenesis. *Att*B1- and *att*B2-sequences are indicated in lower case.

Primer name	DNA sequence (5' → 3')
E. coli pdxY wt fwd w/ *att*B1	ggggacaagtttgtacaaaaaagcaggctttATGATGAAAAATATTCTCGCTATCC
E. coli pdxY wt rev w/ *att*B2	ggggaccactttgtacaagaaagctgggtgTCAGAGCTTTGTTGCGCT
E. coli pdxY C122A fwd	GTCATCCGGAAAAAGGCGCTATCGTTGCACCGGGTG
E. coli pdxY C122A rev	CACCCGGTGCAACGATAGCGCCTTTTTCCGGATGAC
P. aeruginosa pdxY wt fwd w/ *att*B1	ggggacaagtttgtacaaaaaagcaggctttATGCCACGTACGCCCCAC
P. aeruginosa pdxY wt rev w/ *att*B2	ggggaccactttgtacaagaaagctgggtgCTAAAGGCGCACTGCGTCGAA
P. aeruginosa pdxY C124A fwd	CCCGGAAAAAGGCGCCATCGTGGCCCCG
P. aeruginosa pdxY C124A rev	CGGGGCCACGATGGCGCCTTTTTCCGGG

Table 8.4. Plasmids used or prepared in this study.

Plasmid	Gene – UniProt ID	Resistance (final concentration)	Source
pDONR201	empty	Kanamycin (25 µg mL^{-1})	*Invitrogen*
pET300	empty	Ampicillin (100 µg mL^{-1})	*Invitrogen*
pDONR201_*Ec*PLK_wt	*pdxY* – P77150	Kanamycin (25 µg mL^{-1})	This study
pET300_*Ec*PLK_wt	*pdxY* – P77150	Ampicillin (100 µg mL^{-1})	This study
pET300_*Ec*PLK_C122A	*pdxY* – P77150	Ampicillin (100 µg mL^{-1})	This study
pDONR201_*Pa*PLK_wt	*pdxY* – Q9HT57	Kanamycin (25 µg mL^{-1})	This study
pET300_*Pa*PLK_wt	*pdxY* – Q9HT57	Ampicillin (100 µg mL^{-1})	This study
pET300_*Pa*PLK_C124A	*pdxY* – Q9HT57	Ampicillin (100 µg mL^{-1})	This study

8.1.6 Protein overexpression and purification

For protein overexpression, 1 L LB medium containing 100 µg mL^{-1} ampicillin was inoculated (1:100) with overnight cultures of the corresponding expression strains and grown to an OD$_{600}$ of 0.6 (37 °C, 200 rpm). To induce protein overexpression, isopropyl-1-thio-β-D-galactopyranoside (IPTG) was added (*Ec*PLK wt: 1mM, *Ec*PLK C122A: 1mM, *Pa*PLK wt: 10 µM, *Pa*PLK C124A: 10 µM) and bacteria were incubated under the following conditions: *Ec*PLK wt: 22h, 25 °C; *Ec*PLK C122A: 22h, 18 °C; *Pa*PLK wt: 22h, 18 °C, *Pa*PLK C124A: 22h, 18 °C. Bacteria were harvested (6,000 g, 10 min, 4 °C), washed with PBS and resuspended in 30 mL lysis buffer. Lysis was performed by sonication using the following protocol twice: 7 min at 30% intensity, 3 min at 80% intensity (Sonopuls HD 2070 ultrasonic rod, *Bandelin electronic GmbH*). The supernatant was cleared (18,000 g, 30 min, 4 °C) and transferred into a Superloop (*GE Healthcare*) for loading onto a 5 mL pre-equilibrated HisTrap HP column (*GE Healthcare*) installed at an ÄKTA Purifier 10 FPLC system equipped with a UV-detector (UPC900, P900, Box 900,

Frac950, *Thermo Fisher*). The column was washed using the following buffers: Wash buffer 1 (40 mL), wash 2 buffer (40 mL), wash 3 buffer (40 mL), and the protein was eluted with elution buffer (25 mL). Fractions containing proteins were pooled and concentrated using ultra-centrifugal filters (Amicon, 10 kDa cut-off). Next, preparative size-exclusion chromatography was performed using a 120 mL pre-equilibrated Superdex column (HiLoad 16/60 Superdex 75 or 200 prep grade, *GE Healthcare*) and SEC buffer (1.5 column volumes). Homodimeric protein fractions were pooled, concentrated and protein concentration was measured on an Infinite® M200 Pro plate reader with a NanoQuant plate (*Tecan Group Ltd.*) using the following extinction coefficients: *Ec*PLK wt: ε = 29,910 M^{-1} cm^{-1}; *Ec*PLK C122A: ε = 29,910 M^{-1} cm^{-1}; *Pa*PLK wt: ε = 26,930 M^{-1} cm^{-1}; *Pa*PLK C124A: ε = 26,930 M^{-1} cm^{-1}). The proteins (*Ec*PLK wt: 1.6 mM, *Ec*PLK C122A: 586 µM, *Pa*PLK wt: 332 µM, *Pa*PLK C124A: 496 µM) were stored at – 80 °C in SEC buffer.

N-terminally STREPII-tagged *Sa*PLK wt (*sav0580*, *S. aureus* Mu50, with TEV site) and *Sa*PLK C110A as well as *Ef*PLK wt (*EF*_0202, *E. faecalis* V583) and *Ef*PLK C110A were prepared as previously described.[4]

8.1.7 Biological assays

Intact protein mass spectrometry (IPMS)

Recombinant protein was diluted in 49 µL K-buffer to a concentration of 5 µM, and compound was added to a final concentration of 500 µM and samples were incubated for 24 h (if not stated differently) at r. t. without shaking. Proteins were analyzed on a LTQ FT Ultra™ mass spectrometer (*Thermo Scientific*) equipped with electrospray ionization (ESI) source operated in positive ionization mode coupled to a Dionex Ultimate 3000 HPLC system (*Thermo Scientific*). Intact protein spectra were deconvoluted by the Thermo Xcalibur software 2.2 (*Thermo Scientific*).

PLK inhibition assay

A previously published kinase activity assay was performed with slight modifications.[5] Briefly, 110 µL K-Buffer containing 2 µM recombinant protein (*Sa*PLK wt and *Ef*PLK wt) was pre-incubated (2 h, 25 °C, 200 rpm) with 1.1 µL compound (final concentration: 1 µM – 1 mM, final concentration of DMSO 1% (v/v)) or DMSO in a 96-well flat bottom transparent plate. To start the activity assay, 98 µL of the pre-incubated samples were added to 1 µL ATP (250 mM in K-buffer, final concentration 2.5 mM) and 1 µL PL (200 mM in K-buffer, final concentration 2 mM) and the absorption at 388 nm was recorded (45 minutes, 25 °C, intervals of 75 seconds) using an Infinite® M200 Pro plate reader (*Tecan Group Ltd.*). The slope of the curve in the linear range was obtained *via* linear regression using *Prism* 5.03 (*GraphPad*). Values were normalized to DMSO-treated samples (100% activity) and samples without recombinant protein (negative controls, 0% activity). The assay was performed in three independent experiments with three technical replicates each.

PLK activity assay in Lysate

Kinase activity was determined in lysate of expression strains for *E. coli* and *P. aeruginosa* PLK wild types and mutants. BL21 (DE3) without plasmid was used as a negative control to identify the basal PLK activity level. For overexpression, LB medium containing 100 µg mL^{-1} ampicillin (for negative control without antibiotic) was inoculated (1:100) with overnight cultures of the corresponding expression strains and grown to an OD_{600} of 0.6 (37 °C, 200 rpm). To induce protein overexpression,

IPTG was added to a final concentration of 10 µM and bacteria were incubated under the following conditions: BL21 (DE3): 3 h, 37 °C, *Ec*PLK (wt and C122A): 3 h, 37 °C, *Pa*PLK (wt and C124A): 22h, 18 °C. Cultures were harvested (6,000 g, 10 min, 4 °C), washed with PBS and resuspended in K-buffer to a calculated OD_{600} of 40. Lysis was performed by sonication (3 min, 80%, Sonopuls HD 2070 ultrasonic rod, *Bandelin electronic GmbH*) on ice. The supernatant was cleared by centrifugation (18,000 g, 30 min, 4 °C), aliquoted and stored at –80 °C. The concentration of overexpressed PLK in lysate was determined semi-quantitatively. For that, varying concentrations of recombinant *E. coli* PLK wt were loaded on a gel and gray values of protein bands were measured using ImageJ. A calibration curve was calculated, which was used to determine the concentration of overexpressed PLK in lysates.

For the assay, lysates were diluted in K-buffer to a final concentration of 5 µM overexpressed PLK (98 µL final volume) and were incubated with 1 µL ATP (250 mM in K-buffer, final concentration 2.5 mM) and 1 µL PL (100 mM in K-buffer, final concentration 1 mM) at 37 °C. Over a time period of 16 h, the absorption at 388 nm was recorded every 15 minutes on a Tecan Infinite M200Pro plate reader (*Thermo Fisher*). The slopes of the curves in the linear range was determined *via* linear regression using *Prism* 5.03 (*GraphPad*). Using the PLP extinction coefficient (ε = 5444 M^{-1} cm^{-1}), slope values were transformed into PLP formation rates per hour. Samples containing lysate of untransformed BL21 (DE3) were included as negative controls and values were subtracted from the formation rates of PLK overexpression strains. The obtained rates indicate the in-lysate PLK phosphorylation activity of 5 µM overexpressed PLK as PLP formation rate per hour. The assay was performed in three independent experiments with three technical replicates each.

Labeling of recombinant PLK

Recombinant PLK was diluted in 50 µL K-buffer or *S. aureus* lysate (1 mg mL^{-1} protein in PBS) as background to a final concentration of 1 µM. For heat control samples, SDS was added to a final concentration of 0.4% (w/v) and the solution was heated (95 °C, 30 min). All solutions were incubated with 1 µL probe (50× stock) in varying concentrations or DMSO at r. t. for 24 h (if not stated differently) without shaking. Afterwards, the samples were subjected to click-reaction by adding 1 µL rhodamine azide (5 mM in DMSO), 1 µL tris(2-carboxyethyl)posphine (TCEP) (52 mM in ddH$_2$O), 3 µL 1 × tris(benzyltriazoyl-methyl)amine (TBTA) (1.67 mM stock) and 1 µL $CuSO_4$ (50 mM in ddH$_2$O). After incubation at r. t. for 1 h, 50 µL loading buffer (2×) was added. Samples were analyzed by SDS-PAGE.

SDS-PAGE. For sodium dodecylsulfate polyacrylamide gel electrophoresis (SDS-PAGE), gels containing 12.5% (v/v) acrylamide were used. 20 to 50 µL sample, protein marker Roti®-Mark Standard (*Carl Roth*) and fluorescent marker BenchMark™ Fluorescent Protein Standard (*Thermo Fisher*) were added to the gel. The gels were run at 150 V for 2.5 h in an EV265 Consort (*Hoefer*). Fluoresence images were recorded on a LAS-4000 (*Fujifilm*) equipped with a Fujinon VRF43LMD3 lens and a 575DF20 filter (*Fujifilm*). For coomassie staining, gels were incubated in coomassie staining solution overnight at r. t. under gentle mixing before destaining in destaining solution.

Bacterial growth assay

For identification of antibacterial properties of **Cl-PM-I** and **A-PM-I** in *Enterococci* spp., bacterial overnight cultures of *E. faecalis* and *E. faecium* were diluted 1:10,000 into fresh BHI medium. 99 µL of this solution were added in a sterile 96-well plate to 1 µL DMSO or to 1 µL of a 100× compound-stock in DMSO in triplicates. Sterile controls with 1 µL DMSO in 99 µL medium without inoculum were included. The plate was incubated for 20h at 37 °C, 350 rpm prior to optical inspection of turbidity

inside the wells. No reduction of bacterial growth was identified up to 100 µM compound (results not shown).

8.2 Computational modeling

Atomic models for **A-PM-P1** and **A-PM-P2** were generated with JLigand[6] and regularized with AceDRG.[7] Modeling of **A-PM-P1** and **A-PM-P2** in the **PL** binding site in the *Sa*PLK[4] and *Ec*PLK[8] X-ray crystal structures using the **PL** atoms of the pyridine ring as reference was carried out in Coot.[9] Structural figures were prepared in PyMOL (*Schrödinger*).

8.3 Chemical synthesis

Chemicals with reagent or higher grade as well as dry solvents were purchased from *Sigma Aldrich, TCI Europe, VWR, Roth* and *Alfa Aesar*, and were used without any further purification. Solvents of technical grade were distilled prior to use. Air- or moisture-sensitive reactions were carried out in flame-dried reaction flasks under an argon atmosphere (Argon 4.6, 99.996 Vol. % Ar, Westfalen).

Analytical thin layer chromatography was performed on aluminium-coated TLC silica gel plates (silica gel 60, F_{254}, *Merck KGaA*). For visualization, UV light (λ = 254 nm), $KMnO_4$-stain (3.0 g $KMnO_4$, 20.0 g K_2CO_3 and 5 mL 5% NaOH in 300 mL ddH_2O), CAM (5.00 g Cer-(IV)-sulfate, 25.0 g ammoniummolybdate and 50.0 mL concentrated sulphuric acid in 450 mL water) or ninhydrine (10 g ninhydrine in 300 mL ethanol) with subsequent heat treatment (ca. 250 °C) were used. Column chromatography was carried out using silica gel [40-63 µm (Si 60), *Merck KGaA*].

High performance liquid chromatography. Purification by preparative, reversed-phase HPLC was performed using a *Waters* 2545 quaternary gradient module equipped with a *Waters* 2998 photodiode array detector and fraction collector on a *YMC* Triart C18 column (250×10 mm, 5 µm). Gradients were run using ddH_2O and HPLC-grade acetonitrile as the mobile phase (Table 8.5).

Table 8.5. Gradients used for HPLC purifications.

Method A			Method B		
t [min]	%-H_2O	%-ACN	t [min]	%-H_2O	%-ACN
0	98	2	0	98	2
1	80	20	1	98	2
7	60	40	12	60	40
8	2	98	13	2	98
9	2	98	14	2	98
11	98	2	15	98	2
13	98	2	17	98	2

Mass-spectrometry. High-resolution mass spectra (HRMS) were obtained using an LTQ-FT Ultra (*Thermo Fisher*) equipped with an ESI ion source. Data were visualized and processed using Xcalibur 2.2 (*Thermo Fisher*). Low-resolution mass spectra were recorded on an MSQ Plus instrument (*Thermo Fisher*) equipped with a Dionex Ultimate 3000 separation module (*Thermo Fisher*). Data were visualized and processed using Chromeleon 7.2.7 (*Thermo Fisher*).

NMR-spectroscopy. ^{1}H-NMR experiments were conducted on Avance-III HD (300, 400 or 500 MHz) NMR systems (*Bruker Co.*) at r. t. using deuterated solvents. Chemical shifts are given in parts per million (ppm) and residual proton signals of deuterated solvents (CDCl$_3$ δ = 7.26 ppm, MeOD-d_4 δ = 4.87 ppm, DMSO-d_6 δ = 2.50 ppm, D$_2$O δ = 4.79 ppm) were used as internal reference. Coupling constants (*J*) are given in Hertz (Hz). For assignment of signal multiplicities, the following abbreviations were used: *br* s – broad singlet, s – singlet, d – doublet, dd – doublet of doublets, ddd – doublet of doublet of doublets, t – triplet, td – triplet of doublets, q – quadruplet and m – multiplet. ^{13}C-NMR spectra were measured on Avance-III HD NMR systems (*Bruker Co.*) with deuterated solvents. Chemical shifts were referenced to the residual solvent peak as an internal standard (CDCl$_3$ δ = 77.16 ppm, MeOD-d_4 δ = 49.00 ppm, DMSO-d_6 δ = 39.52 ppm). Spectra were processed using MestReNova *(Mestrelab Research).*

8.3.1 Synthetic procedures

4-(*N*-Acryloylaminomethyl)-3-hydroxy-5-hydroxymethyl-2-methylpyridine (A-PM-I)
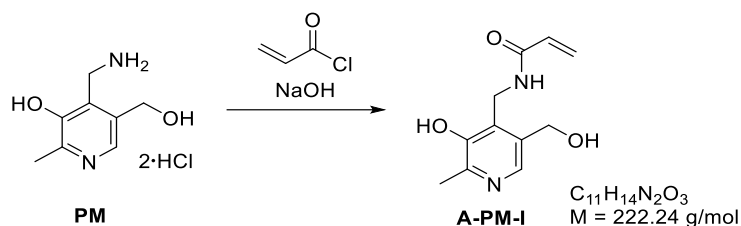
This synthesis was performed according to the protocol published by *Ueda et al.*[10] Briefly, pyridoxamine dihydrochloride (350 mg, 1.45 mmol, 1.0 eq.) was dissolved in 5 mL of water. Next, NaOH (480 µL, 30% in H$_2$O) was added slowly and the solution was stirred for 5 min. Afterwards, acryloyl chloride (140 µL, 157 mg, 1.74 mmol,1.2 eq.) was added and the reaction mixture was stirred for 4 h at r. t. followed by extraction with EtOAc (3×10 mL). The aqueous phase was neutralized using 2 N HCl and extracted with EtOAc (3×10 mL). The combined organic layers were dried over MgSO$_4$ and the solvent was removed under reduced pressure. The residue was dissolved in 5 mL of dry EtOH, HCl$_{(g)}$ was passed through the solution and the product was precipitated by the addition of diethyl ether (20 mL). The product was washed with diethyl ether (2×10 mL) and the remaining solvent was removed under reduced pressure to obtain the product **A-PM-I** in 6% (25.7 mg, 90.0 µmol) yield.

^{1}H-NMR (500 MHz, D$_2$O): δ [ppm] = 8.12 (s, 1H), 6.31 – 6.25 (m, 2H), 5.81 (dd, *J* = 9.2 Hz, 2.3 Hz, 1H), 4.89 (s, 2H), 4.62 (s, 2H), 2.63 (s, 3H).

^{13}C-NMR (126 MHz, D$_2$O): δ [ppm] = 169.2, 153.4, 143.5, 139.5, 137.6, 129.6, 128.63, 128.6, 58.4, 34.8, 14.7.

HRMS (ESI) *m/z*: (C$_{11}$H$_{15}$N$_2$O$_3^+$ [M+H]$^+$) found: 223.1077, calc.: 223.1077.

**N-((5-(Hydroxymethyl)-2-methyl-3-(prop-2-yn-1-yloxy)pyridine-4-yl)methyl)acrylamide (A-PM-P1)**
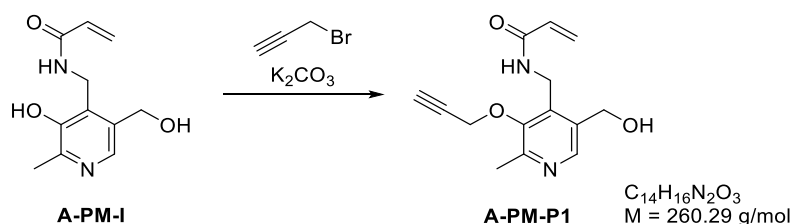
A-PM-I (87.0 mg, 400 µmol, 1.0 eq.) was dissolved in 4 mL of dry DMF and potassium carbonate (57.0 mg, 410 µmol, 1.0 eq.) was added. After stirring for 15 min at r. t., propargyl bromide (30 µL, 47.0 mg, 400 µmol, 1.0 eq.) was added dropwise. The mixture was stirred at r. t. for 9 h. The solvent was removed under reduced pressure and the crude product was purified by column chromatography (10% MeOH/DCM) yielding A-PM-P1 (63.9 mg, 245 µmol, 73%) as a yellow oil.

TLC: R_f = 0.34 (10% MeOH/DCM, UV).

^{1}H-NMR (500 MHz, DMSO-d_6): δ [ppm] = 8.26 (s, 1H), 6.23 (dd, J = 17.1 Hz, 10.1 Hz, 1H), 6.10 (dd, J = 17.1 Hz, 2.2 Hz, 1H), 5.59 (dd, J = 10.1 Hz, 2.3 Hz, 1H), 5.32 (t, J = 5.3 Hz, 1H), 4.67 (d, J = 2.4 Hz, 2H), 4.54 (d, J = 5.0 Hz, 2H), 4.44 (d, J = 5.2 Hz, 2H), 3.64 (t, J = 2.4 Hz, 1H), 2.54 (s, 1H), 2.46 (s, 3H).

^{13}C-NMR (126 MHz, DMSO-d_6): δ [ppm] = 164.4, 151.2, 150.8, 144.0, 137.2, 135.1, 131.3, 125.7, 79.2, 79.0, 61.0, 58.4, 33.9, 19.7.

HRMS (ESI) *m/z*: ($C_{14}H_{17}N_2O_3^+$ [M+H]$^+$) found: 261.1233, calc.: 261.1233.

2-Chloro-N-[3-hydroxy-5-(hydroxymethyl)-2-methylpyridin-4-yl]methyl-acetamide (Cl-PM-I)
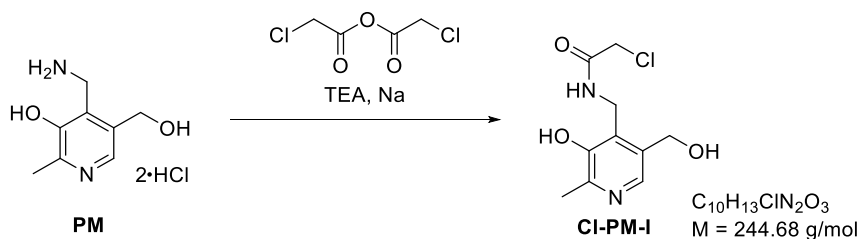
This synthesis was performed as previously published.[11] To a solution of pyridoxamine dihydrochloride (154 mg, 640 µmol, 1.0 equiv.) in anhydrous methanol (20 mL) at r. t., sodium metal (33.8 mg, 1.47 mmol, 2.3 equiv.) and triethylamine (232 µL, 1.66 mmol, 2.6 equiv.) were added. Next, chloroacetic anhydride (383 mg, 1.47 mmol, 2.3 equiv.) was added and the mixture was stirred at r. t. for 22 h. The crude reaction mixture was concentrated *in vacuo* and purified by preparative TLC (20×20 cm, UV$_{254}$, 2 mm) using EtOAc/hexane (10/1). Fractions detected by UV light were scratched from the glass surface and the product was dissolved in methanol. The suspension was cooled to 0 °C, filtered and concentrated *in vacuo* to obtain Cl-PM-I (29.9 mg, 122 µmol, 19 %) as an ocher-colored oil.

TLC: R_f = 0.08 (EtOAc/hexane = 10/1, UV).

^{1}H-NMR (500 MHz, CDCl$_3$): δ [ppm] = 9.26 (br s, 1H), 7.88 (s, 1H), 7.85 (br s, 1H), 4.76 (s, 2H), 4.50 (d, J = 6.7 Hz, 2H), 4.07 (s, 2H), 2.51 (s, 3H).

^{13}C-NMR (101 MHz, CDCl$_3$): δ[ppm] = 169.2, 150.9, 150.4, 139.5, 132.4, 130.1, 62.3, 42.2, 36.2, 19.8.

HRMS (ESI) *m/z*: ($C_{10}H_{14}ClN_2O_3^+$ [M+H]$^+$) found: 245.0687, calc.: 245.0687.

2-Chloro-*N*-[5-(hydroxymethyl)-2-methyl-3-(prop-2-yn-1-yloxy)pyridin-4-yl]methyl-acetamide (Cl-PM-P1)
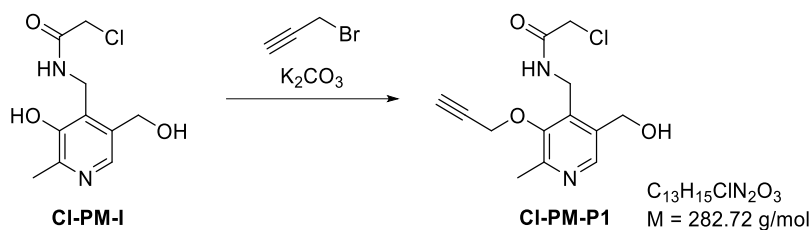
Cl-PM-I (19.3 mg, 78.9 μmol, 1.0 equiv.) was dissolved in anhydrous DMF (1 mL) before K_2CO_3 (10.9 mg, 78.9 μmol, 1.0 equiv.) was added. The suspension was stirred at r. t. for 15 min. Propargyl bromide (80% in toluene, 8.50 μL, 78.9 μmol, 1.0 equiv.) was added dropwise and the suspension was stirred at r. t. for 5 h. Brine (5 mL) was added and the aqueous phase was extracted with EtOAc (3×10 mL). The combined organic phases were washed with brine (5×30 mL), dried over Na_2SO_4 and concentrated *in vacuo*. The crude product was purified by column chromatography (EtOAc/hexane 10/1 → DCM/MeOH 10/1) to obtain **Cl-PM-P1** (5.30 mg, 19 μmol, 24%) as an ocher-colored solid.

TLC: R_f = 0.14 (DCM/MeOH = 10/1, UV).

^{1}H-NMR (500 MHz, CDCl$_3$): δ [ppm] = 8.29 (s, 1H), 7.61 (*br* s, 1H), 4.75 (s, 2H), 4.70 (d, *J* = 6.4 Hz, 2H), 4.69 (d, *J* = 2.4 Hz, 2H), 4.03 (s, 2H), 2.59 (t, *J* = 2.4 Hz, 1H), 2.55 (s, 3H).

^{13}C-NMR (126 MHz, Methanol-*d$_4$*): δ [ppm] = 168.8, 153.8, 153.0, 145.3, 140.4, 136.3, 79.3, 78.3, 62.1, 60.6, 43.1, 36.1, 19.6.

HRMS (ESI) *m/z*: ($C_{13}H_{16}ClN_2O_3^+$ [M+H]$^+$) found: 283.0843, calc.: 283.0844.

2-(But-3-yn-1-yl)-3-hydroxy-5-(hydroxymethyl)isonicotinaldehydeoxim (2)

Compound **1** was synthesized according to *Hoegl et al.*[12]
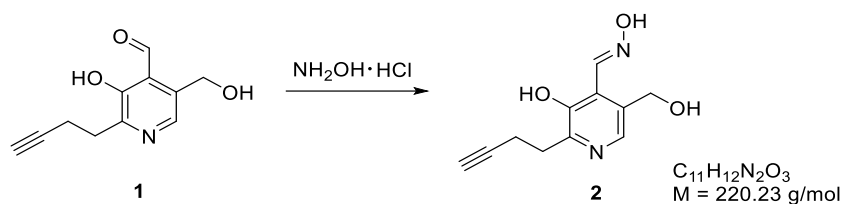
The formation of oxime **2** was adapted from *Dale et al.*[13] Compound **1** (126 mg, 420 µmol, 1.0 eq.) was dissolved in 18 mL of dry EtOH and hydroxylamine hydrochloride (115 mg, 1.66 mmol, 4.0 eq.) was added. The solution was stirred at r. t. for 49 h, the solvent was removed under reduced pressure and the crude compound was purified by HPLC using method A, yielding compound **2** (62.5 mg, 284 µmol, 68%) as a pale-yellow solid.

TLC: R_f = 0.45 (10% MeOH/DCM, UV).

HPLC: t_R = 6.4 min (Method A).

^{1}H-NMR (300 MHz, DMSO-d_6): δ [ppm] = 12.14 (*br* s, 1H), 10.80 (*br* s, 1H), 8.60 (s, 1H), 8.02 (s, 1H), 5.32 (s, 1H), 4.60 (d, *J* = 4.1 Hz, 2H), 2.97 (t, *J* = 7.6 Hz, 2H), 2.71 (t, *J* = 2.6 Hz, 1H), 2.57 (dt, *J* = 7.6 Hz, 2.6 Hz, 2H).

^{13}C-NMR (75 MHz, DMSO-d_6): δ [ppm] = 149.6, 148.2, 147.9, 139.1, 132.7, 120.2, 84.3, 71.1, 58.7, 30.5, 16.0.

HRMS (ESI) *m/z*: ($C_{11}H_{13}N_2O_3^+$ [M+H]$^+$) found: 221.0920, calc.: 221.0920.

N-((2-(But-3-yn-1-yl)-3-hydroxy-5-(hydroxymethyl)pyridine-4-yl)methyl) acrylamide (A-PM-P2)
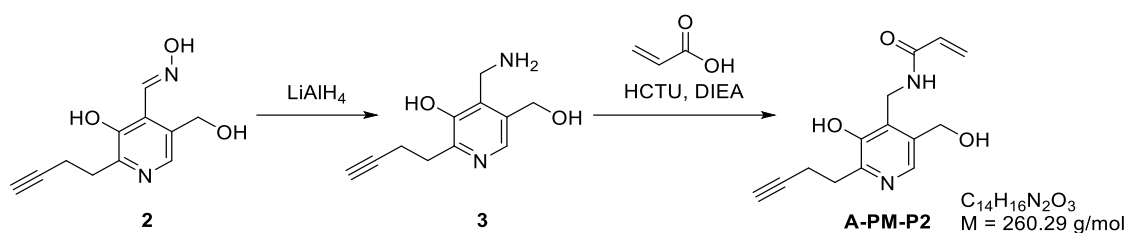
A protocol published by *Müller et al.* was used to reduce compound **2**.[14] Compound **2** (100 mg, 450 µmol, 1.0 eq.) was dissolved in 7 mL dry THF under argon and LiAlH₄ (320 µL, 2.4 M in THF, 29.2 mg, 770 µmol, 1.7 eq.) was added slowly at 0 °C. Upon stirring at r. t. for 1 h, the temperature was increased to 80 °C and the mixture was stirred for 5 h. Next, 1 N HCl (15 mL) was added, the solvent was removed under reduced pressure and crude amine **3** was directly used for the next step.

Acrylic acid (30.0 µL, 450 µmol, 1.0 eq.), DIEA (120 µL, 680 µmol, 1.5 eq.) and HCTU (281.3 mg, 680 µmol, 1.5 eq.) were dissolved in 2 mL DMF at 0 °C under argon and the solution was stirred for 2 h. Amine **3** dissolved in 7 mL DMF was slowly added at 0 °C and the mixture was stirred overnight. Next, the solvent was removed under reduced pressure and the residue was dissolved in EtOAc (30 mL). The organic phase was washed with 30 mL 1 N NaOH, 20 mL saturated NaHCO₃(aq) solution and 20 mL brine. The combined aqueous phases were neutralized and extracted with EtOAc (7×10 mL). The solvent of the combined organic phases was removed under reduced pressure. The crude product was purified by HPLC using method B followed by column chromatography (3% MeOH/DCM → 5% MeOH/DCM) yielding **A-PM-P2** (2.17 mg, 8.33 µmol, 2% over two steps) as a yellow oil.

TLC: R_f = 0.47 (10% MeOH/DCM, UV/KMnO₄).

HPLC: t_R = 5.4 min (Method B).

¹H-NMR (500 MHz, Methanol-d_4): δ [ppm] = 8.00 (s, 1H), 6.35 - 6.25 (m, 2H), 5.74 (dd, J = 9.5 Hz, 2.5 Hz, 1H), 4.76 (s, 2H), 4.55 (s, 2H), 3.07 (t, J = 7.6 Hz, 2H), 2.58 (td, J = 7.6 Hz, 2.6 Hz, 2H), 2.20 (t, J = 2.7 Hz, 1H).

¹³C-NMR (126 MHz, Methanol-d_4): δ [ppm] = 169.7, 152.8, 149.7, 138.2, 137.1, 134.7, 130.5, 128.6, 83.8, 70.3, 60.6, 35.6, 32.3, 17.8.

HRMS (ESI) *m/z*: ($C_{14}H_{17}N_2O_3^+$ [M+H]⁺) found: 261.1232, calc.: 261.1234.

8.3.2 NMR spectra

4-(*N*-Acryloylaminomethyl)-3-hydroxy-5-hydroxymethyl-2-methylpyridine (A-PM-I)

^{1}H-NMR (500 MHz, D$_2$O):
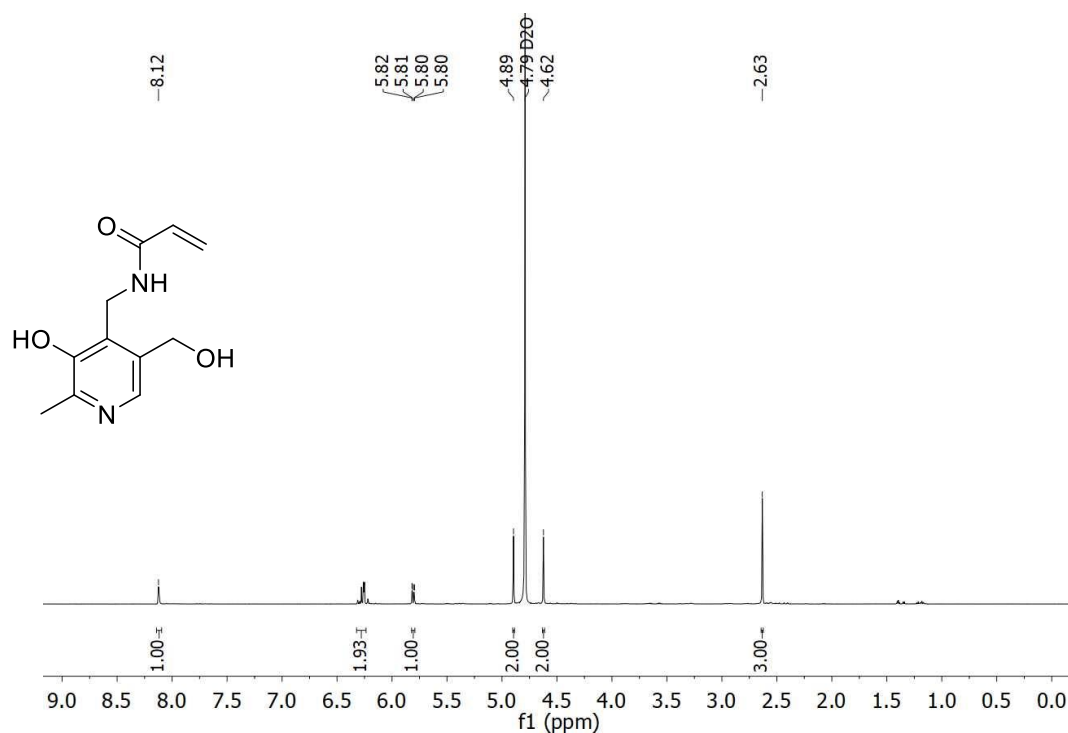
^{13}C-NMR (126 MHz, D$_2$O):
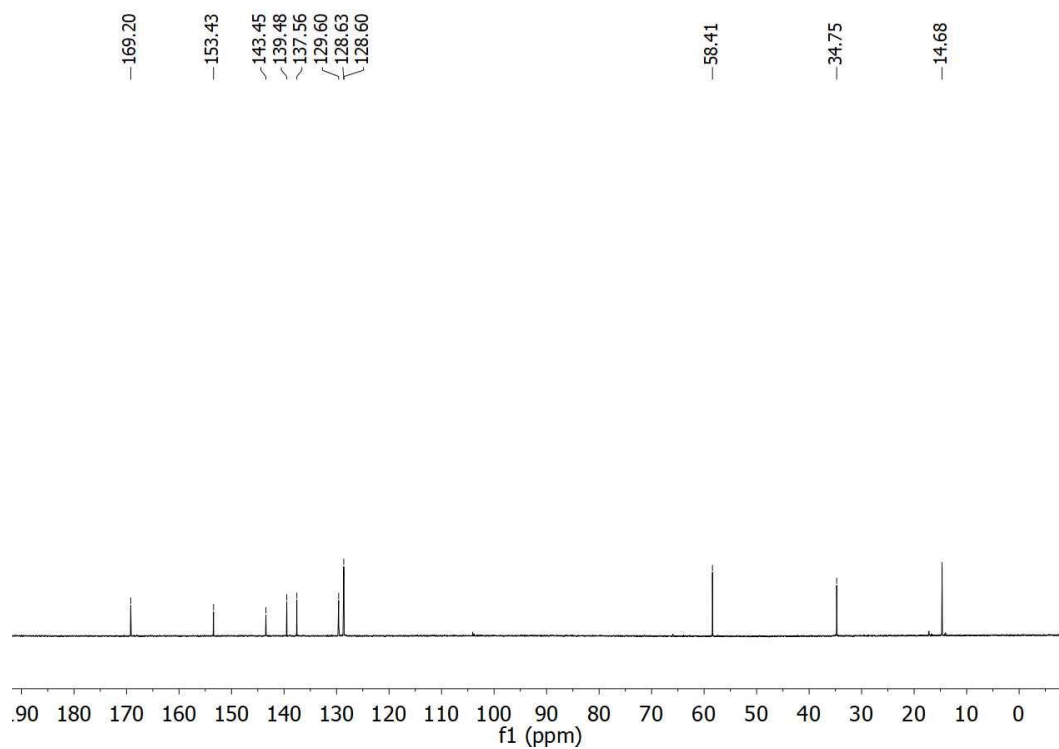
N-((5-(Hydroxymethyl)-2-methyl-3-(prop-2-yn-1-yloxy)pyridine-4-yl)methyl)acrylamide (A-PM-P1)

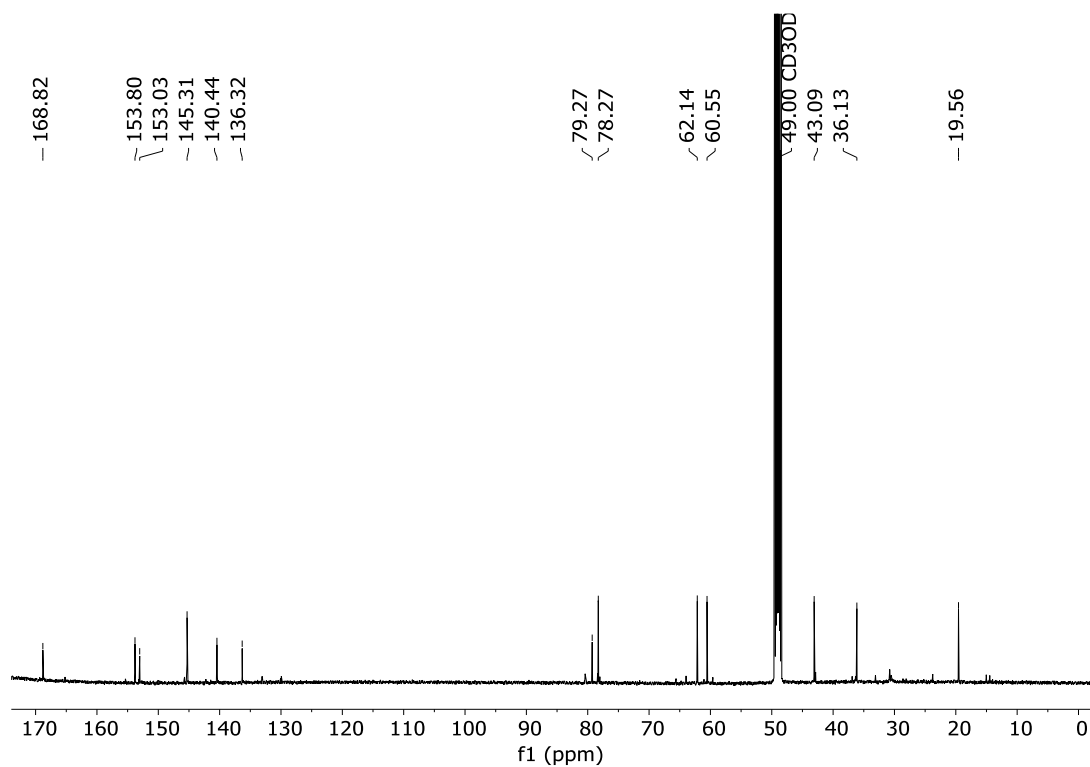**¹H-NMR** (500 MHz, DMSO-d_6):
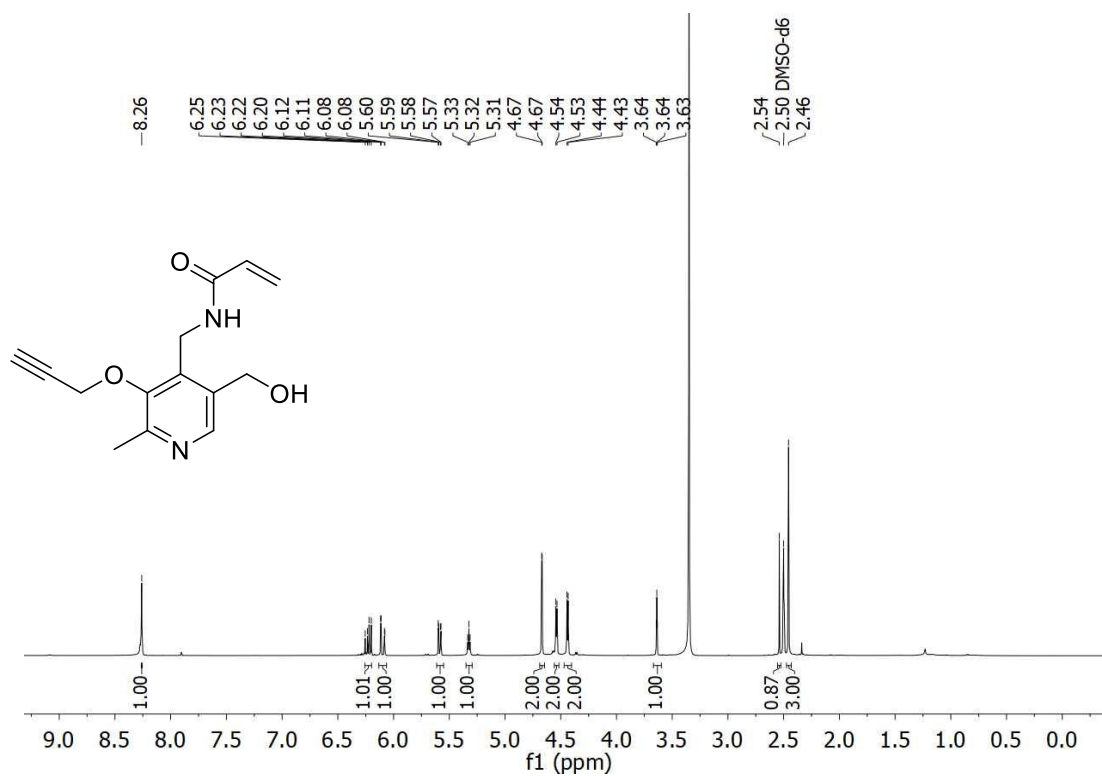
¹³C-NMR (126 MHz, DMSO-d_6):
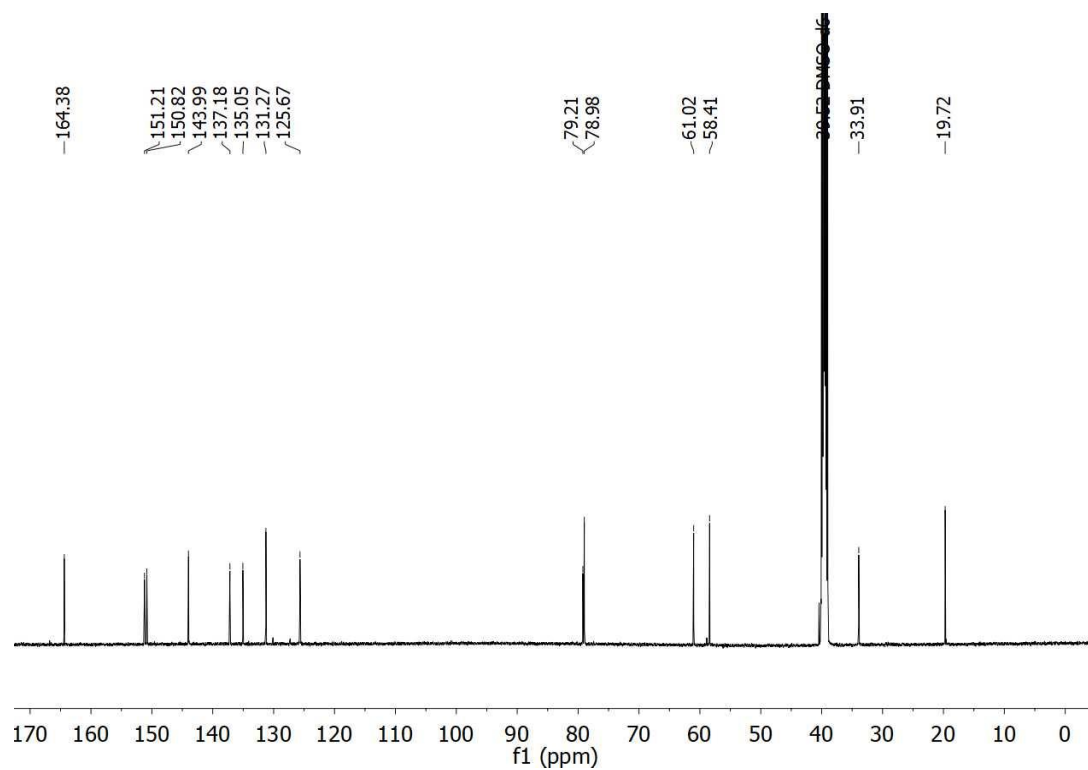
2-Chloro-*N*-[3-hydroxy-5-(hydroxymethyl)-2-methylpyridin-4-yl]methyl-acetamide (Cl-PM-I)

¹H-**NMR** (500 MHz, CDCl₃):
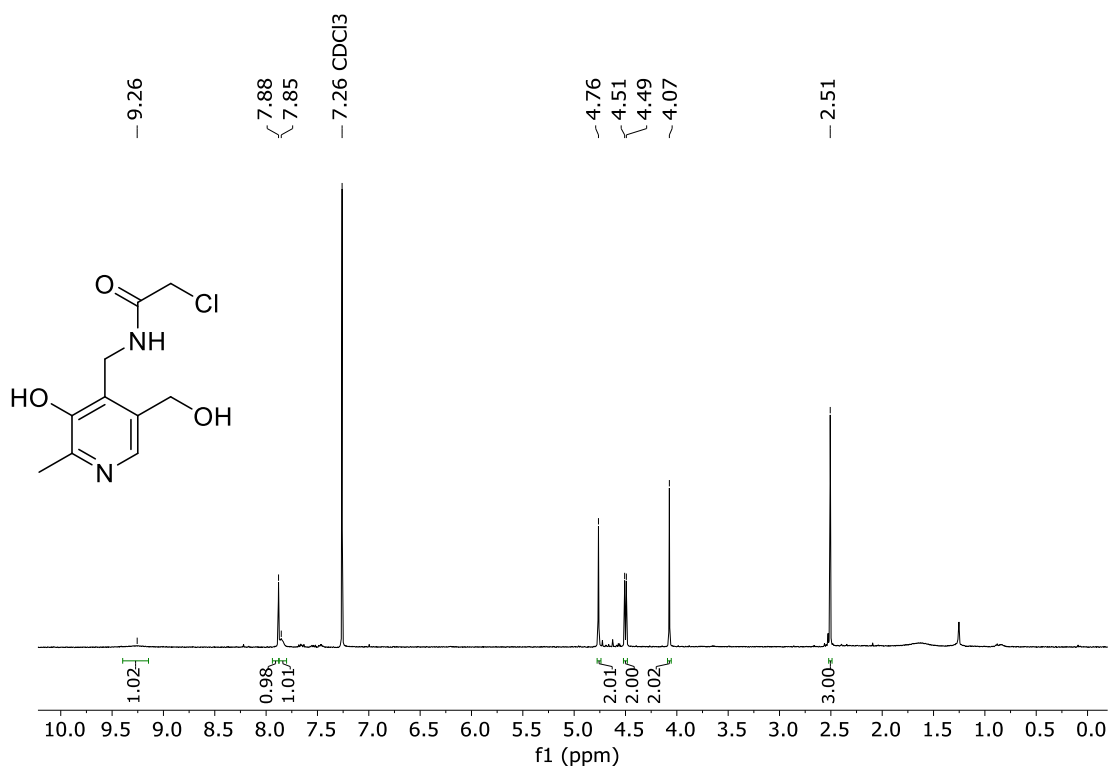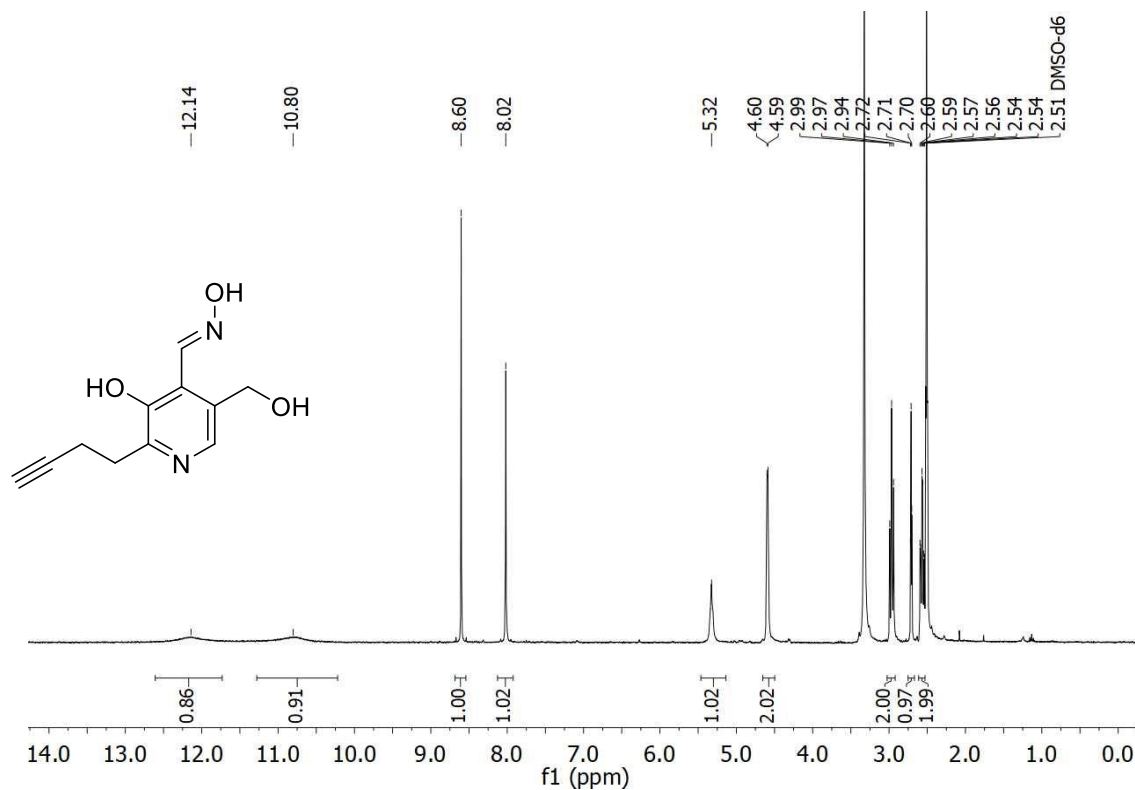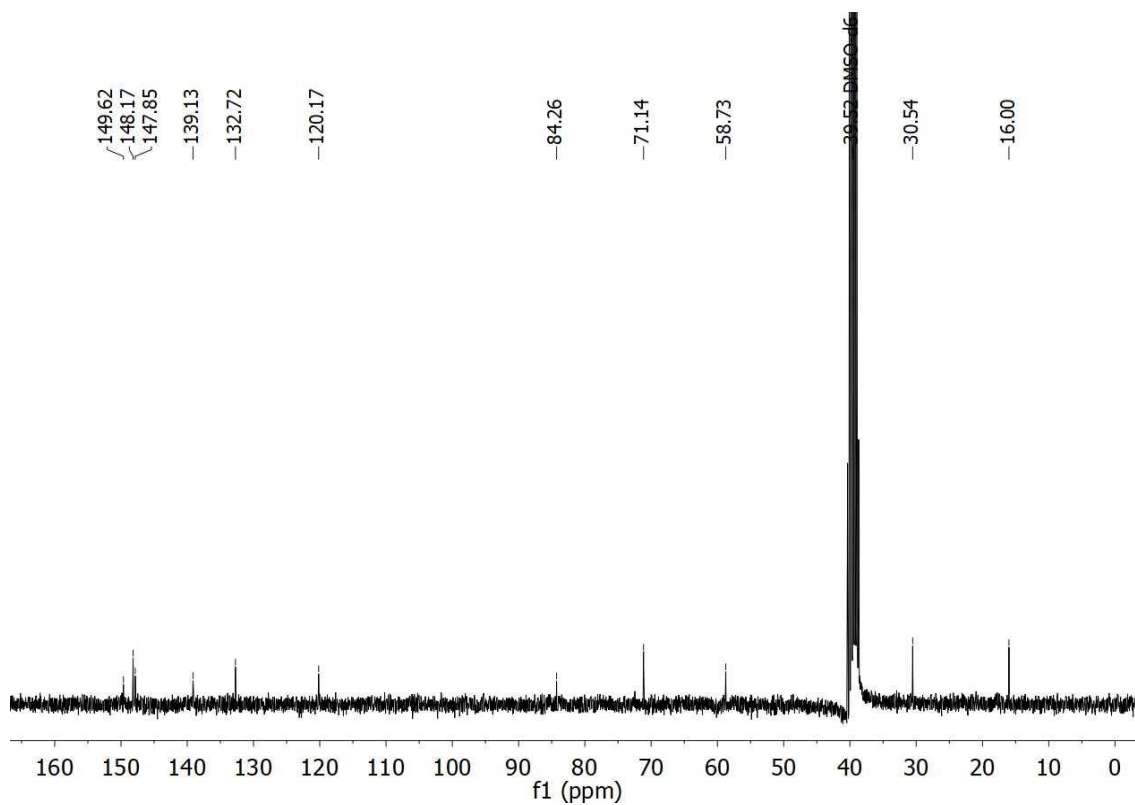

¹³C-**NMR** (101 MHz, CDCl₃):
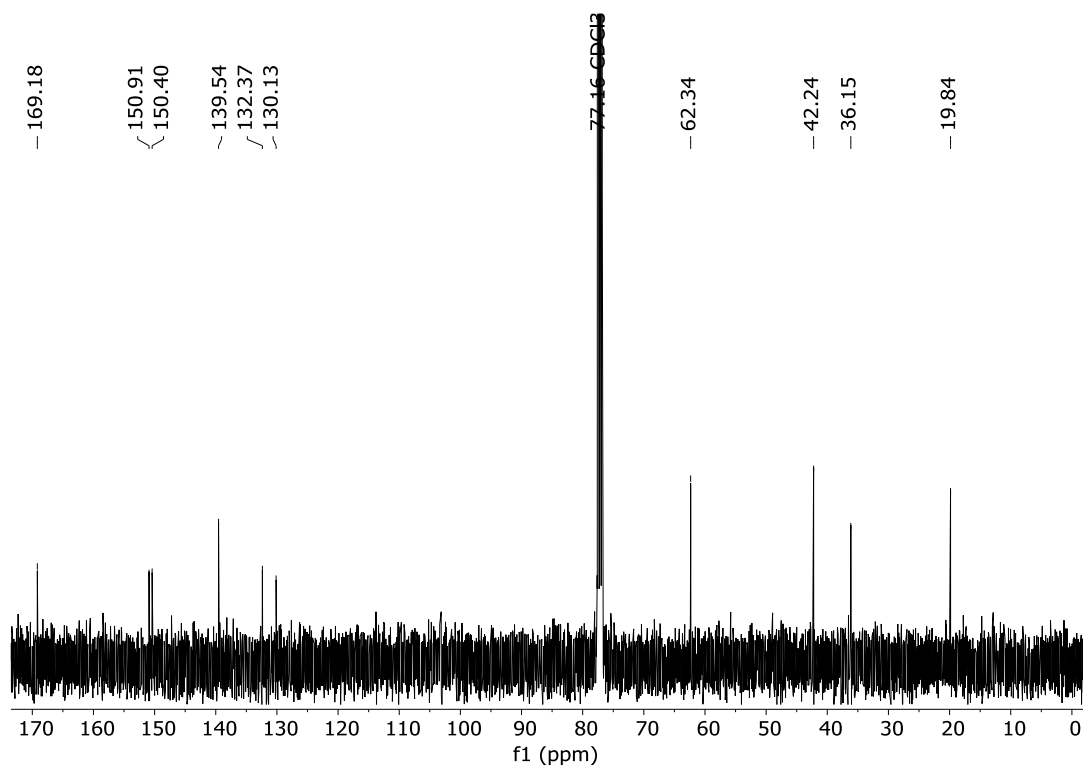
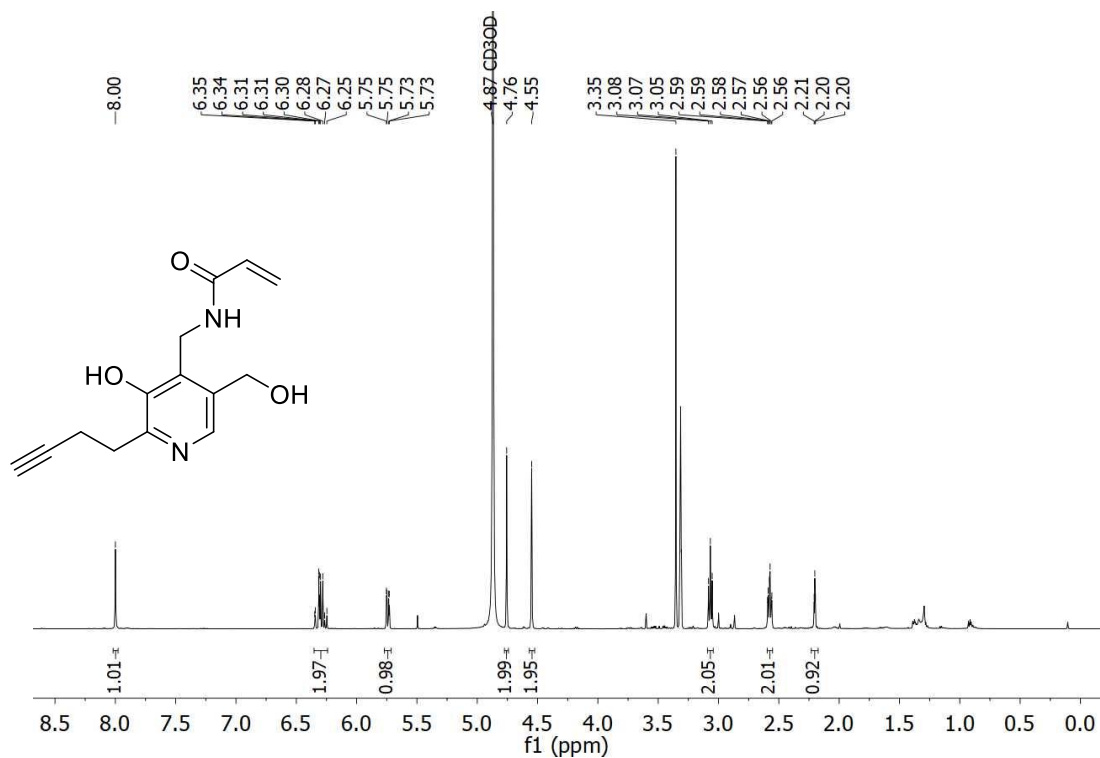**2-Chloro-*N*-[5-(hydroxymethyl)-2-methyl-3-(prop-2-yn-1-yloxy)pyridin-4-yl]methyl-acetamide (Cl-PM-P1)**

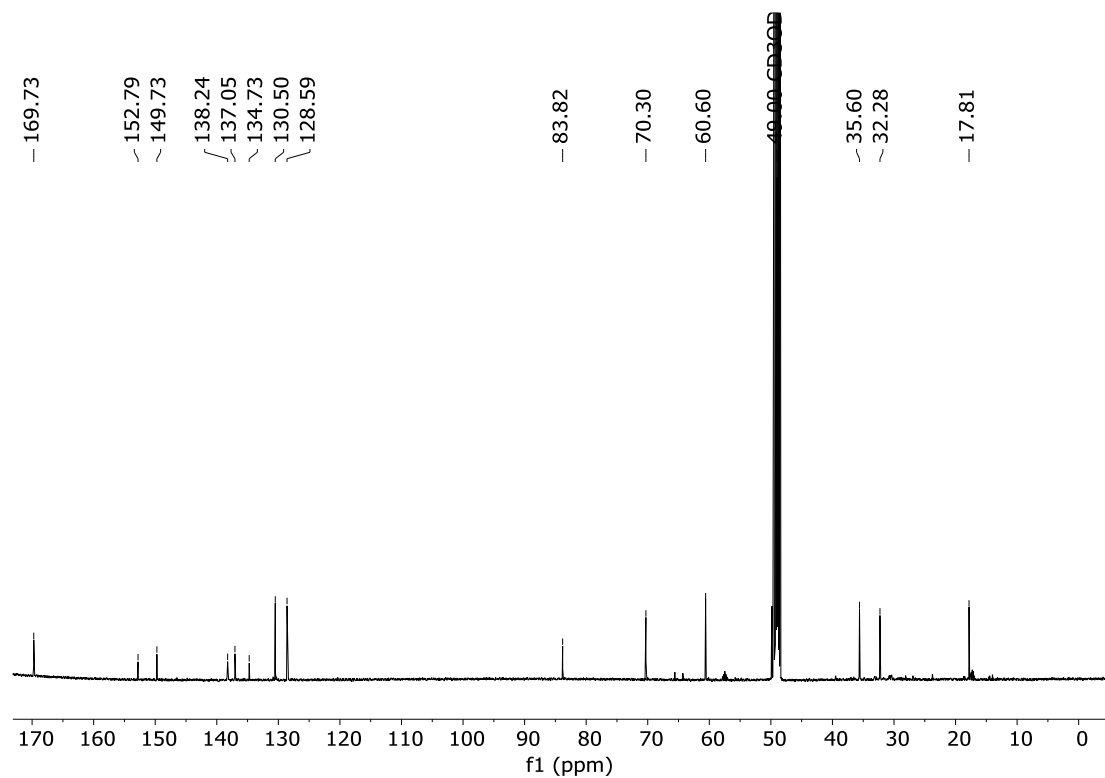**¹H**-**NMR** (500 MHz, CDCl₃):
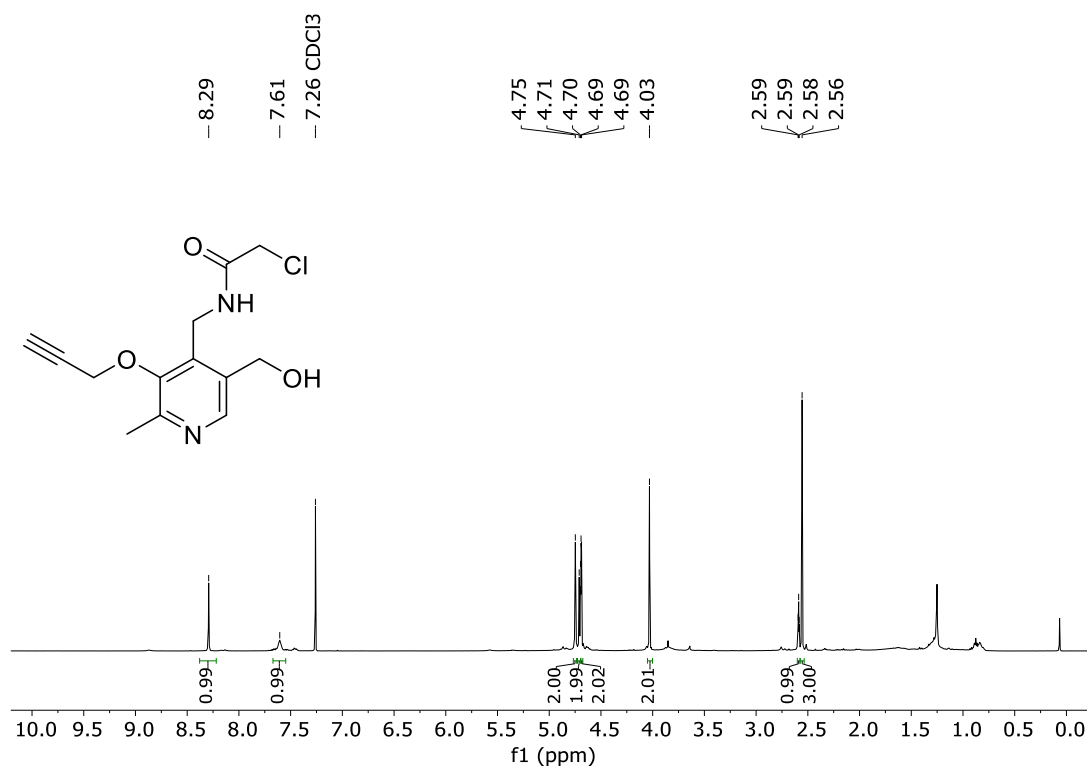
¹³C-**NMR** (126 MHz, Methanol-*d₄*):

2-(But-3-yn-1-yl)-3-hydroxy-5-(hydroxymethyl)isonicotinaldehydeoxim (2)

¹H-NMR (300 MHz, DMSO-*d*₆):

¹³C-NMR (75 MHz, DMSO-*d*₆):

N-((2-(But-3-yn-1-yl)-3-hydroxy-5-(hydroxymethyl)pyridine-4-yl)methyl) acrylamide (A-PM-P2)

¹H-NMR (500 MHz, Methanol-d_4):

¹³C-NMR (126 MHz, Methanol-d_4):

8.4 References

[1]   J. Cox, M. Mann, *Nature Biotechnology* **2008**, *26*, 1367-1372.

[2]   UniProtConsortium, *Nucleic Acids Research* **2023**, *51*, D523-D531.

[3]   S. Tyanova, T. Temu, P. Sinitcyn, A. Carlson, M. Y. Hein, T. Geiger, M. Mann, J. Cox, *Nature Methods* **2016**, *13*, 731-740.

[4]   M. B. Nodwell, M. F. Koch, F. Alte, S. Schneider, S. A. Sieber, *Journal of the American Chemical Society* **2014**, *136*, 4992-4999.

[5]   T. C. Scott, M. A. Phillips, *Molecular and Biochemical Parasitology* **1997**, *88*, 1-11.

[6]   A. A. Lebedev, P. Young, M. N. Isupov, O. V. Moroz, A. A. Vagin, G. N. Murshudov, *Acta Crystallographica Section D* **2012**, *68*, 431-440.

[7]   F. Long, R. A. Nicholls, P. Emsley, S. Grazulis, A. Merkys, A. Vaitkus, G. N. Murshudov, *Acta Crystallographica Section D* **2017**, *73*, 112-122.

[8]   M. K. Safo, F. N. Musayev, S. Hunt, M. L. di Salvo, N. Scarsdale, V. Schirch, *Journal of Bacteriology* **2004**, *186*, 8074-8082.

[9]   P. Emsley, B. Lohkamp, W. G. Scott, K. Cowtan, *Acta Crystallographica Section D* **2010**, *66*, 486-501.

[10]   T. Ueda, K. Nakaya, S.-i. Nagai, J. Sakakibara, M. Murata, *Chemical & Pharmaceutical Bulletin* **1990**, *38*, 19-22.

[11]   B. F. Cravatt, *WO2017210600A1,* **2017**.

[12]   A. Hoegl, M. B. Nodwell, V. C. Kirsch, N. C. Bach, M. Pfanzelt, M. Stahl, S. Schneider, S. A. Sieber, *Nature Chemistry* **2018**, *10*, 1234-1245.

[13]   T. J. Dale, A. C. Sather, J. Rebek, *Tetrahedron Letters* **2009**, *50*, 6173-6175.

[14]   T. E. Müller, A.-K. Pleier, *Journal of the Chemical Society, Dalton Transactions* **1999**, *n/a*, 583-588.

9|

Experimental section (chapter 5)

9.1 Biochemistry

9.1.1 Media and buffers

Table 9.1. Media and buffers.

	LB-Medium (1 L)	7H9-Medium (1 L)
Media	5 g Peptone 2.5 g yeast extract 2.5 g NaCl pH 7.5 in ddH$_2$O	4.7 g Middlebrook 7H9 broth + 900 mL ddH$_2$O, autoclave 10 min 121 °C Add sterile filtered to broth (ADC-Enrichment): 5.0 g bovine serum albumin fraction V 2.0 g glucose 3 mg catalase (beef) in 100 mL ddH$_2$O

	PBS	K-Buffer		Staining	Destaining
Protein - Buffers	10.0 mM Na$_2$HPO$_4$ 1.80 mM KH$_2$PO$_4$ 140 mM NaCl 2.70 mM KCl pH 7.4 in ddH$_2$O	50 mM HEPES 50 mM KCl 10 mM MgCl$_2$ pH 7.9 in ddH$_2$O	**Coomassie**	0.25% (w/v) Coomassie brilliant blue R250 10% (v/v) acetic acid 50% (v/v) ethanol abs. in ddH$_2$O	10% (v/v) acetic acid 20% (v/v) ethanol abs. in ddH$_2$O

	Seperation Gel	Stacking Gel	Running Gel (10×)	Loading Buffer (2×)
SDS-PAGE Buffer	3.00 M TRIS pH 8.8 in ddH$_2$0	0.50 M TRIS pH 6.8 in ddH$_2$O	24.8 mM TRIS/HCl 192 mM Glycine 3.5 mM SDS pH 8.3 in ddH$_2$O	63.0 mM TRIS/HCl 10% mM glycerol 0.25%$_{00}$ (w/v) Bromphenol blue 2% (w/v) SDS 5% (w/v) β-Mercaptoethanol in ddH$_2$O

9.1.2 Bacterial strains

Table 9.2. Handling of mycobacteria.

Species	Strain	Medium	Growth conditions
M. smegmatis	DSM 43756 (ATCC 19420)	7H9 + ADC enrichment	Baffled flask (250 mL) with glass beads and 0.05% (w/v) Tween-20
M. tuberculosis	---	7H9 + ADC enrichment	---

As *M. smegmatis* is classified as an S2 strain, living bacteria were handled under HeraSafe KS fumehoods (Thermo scientific). For inoculation, 5 µL bacterial solution from glycerol-cryostocks [50% (v/v), –80 °C] were added to 5 mL fresh medium (1:1,000, 37 °C, 200 rpm, Table 9.1, 9.2). After overnight growth, 500 µL culture were used to inoculate fresh medium (50 mL, 1:100) and cells were grown to stationary phase within 48h (OD$_{600}$ = 2.4) at 37 °C, 200 rpm. Experiments involving living *M. tuberculosis* cells were performed by Dr. Sönke Andres (Forschungszentrum Borstel).

9.1.3 Cloning

Recombinant ThiD proteins of *M. smegmatis* (UniProt ID: I7G2G7) and *M. tuberculosis* (UniProt ID: P9WG77) were constructed to carry an N-terminal His$_6$-tag followed by an additional maltose-binding protein (MBP) sequence for soluble protein expression, as previous unpublished in-house studies identified the N-terminal His$_6$-tags fusion-proteins as unstable. For plasmid construction, the Invitrogen™ Gateway™ cloning system (Thermo Scientific) was used with its manufacturer's protocol. Hence, wild-type (wt) primers were designed with *att*B1 or *att*B2 sequences (Table 9.3) in order to shuffle the respective PCR products into the donor vector pDONR207^{Gen} and destination vector pETG41K^{Kan} with transformation steps into *E. coli* Top10. The respective mutant plasmids, encoding for an alanine instead of a cysteine residue in the lid, were obtained by performing the QuikChange II site-directed mutagenesis protocol (Agilent) with pETG41K wt plasmids as templates. The respective primer sequences (Table 9.3) were designed with the QuikChange Primer Design tool (Agilent). After PCR, the wt plasmids were digested by DpnI and remaining mutant plasmids were transformed into chemically competent *E. coli* XL1-Blue cells prior to selection of colonies on LB agar plates with kanamycin.

After successful growth on plates with respective antibiotics, single colonies were selected and used to inoculate 5 mL LB medium, supplemented with appropriate antibiotics. Plasmid DNA was isolated with E.Z.N.A. Plasmid Mini Kit I (OMEGA Bio-Tek) according to the manufacturer's protocol on the next day and DNA concentration was assessed by an Infinite® M200 Pro plate reader equipped with a NanoQuant plate (Tecan Group Ltd.). Plasmid sequences were verified by DNA sequencing (Genewiz) prior to transformation into chemically competent *E. coli* BL21 (DE3) cells for ThiD fusion-protein expression.

Table 9.3. Primers for Gateway cloning and QuikChange site-directed mutagenesis. Lower cases encode *att*B1 and *att*B2 sequences and bold letters indicate TEV-protease recognition motif.

Primer name	DNA sequence (5´→3´)
*Mt*ThiD fwd TEV w/ *att*B1	ggggacaagtttgtacaaaaaagcaggcttt**gaaaacctgtattttcagggc**ACGCCGCCGCGGGTGTTGA
*Mt*ThiD rev w/ *att*B2	ggggaccactttgtacaagaaagctgggtgTCATGACAGCCGAAACAGCGGCG
*Mt*ThiD C109A 1st	TGCATGGATGCGGCTACCGGGTCGACGACG
*Mt*ThiD C109A 2nd	CGTCGTCGACCCGGTAGCCGCATCCGTGCA
*Ms*ThiD fwd w/ *att*B1	ggggacaagtttgtacaaaaaagcaggctttAAACTGCTACCGCTGACCCC
*Ms*ThiD rev w/ *att*B2	ggggaccactttgtacaagaaagctgggtgTCACGAGCCATGGTGCAACC
*Ms*ThiD C119A 1st	GTGCATCGACGCGGCCACCGGATCGACC
*Ms*ThiD C119A 2nd	GGTCGATCCGGTGGCCGCGTCGATGCAC

9.1.4 Overexpression and purification of mycobacterial ThiD fusion-proteins

For fusion protein overexpression, 2 L LB medium, supplemented with 25 μg mL^{-1} kanamycin, were inoculated (1:100) with an overnight culture of the respective ThiD wt or mutant fusion protein expression strain in order to grow cells at 37 °C, 200 rpm to an optical density of OD_{600} = 0.6. Protein expression was induced with 1 mM isopropyl-1-thio-β-D-galactopyranoside (IPTG) and cultures were incubated for 24h at 18 °C, 200 rpm. Bacterial cells were harvested (6,000 g, 10 min, 4 °C) and washed with PBS (50 mL). For lysis, the cell pellet was resuspended in 30 mL lysis buffer (50 mM HEPES, 150 mM NaCl, 0.2% (w/v) NP-40, 2 mM β-mercapto ethanol (BME), pH 8.0) and lysed by sonication (7 min 30% intensity, 3 min 70% intensity, 7 min 30% intensity) on ice. For affinity purification on an ÄKTA pure 25 FPLC protein purification system (GE Healthcare, software: unicorn 7.5) coupled to a fraction collector (F9-C, GE Healthcare), the lysed cells were centrifuged (18,000 g, 30 min, 4 °C). The cleared supernatant was filtered through a 0.45 μm PVDF filter (Whatman, GD/X25, Cytiva) before it was transferred via sample pump (S9, Cytiva) onto an equilibrated MBPTrap HP column (5 mL, Cytiva) with subsequent washing. The trapped and washed fusion protein was eluted with addition of 10 mM maltose in the lysis buffer. Fractions containing the protein based on UV-detection were pooled and concentrated in centrifugal filters (Amicon, 50 kDa cut-off, 5,000 rpm, 4 °C) while the buffer was exchanged to 50 mM HEPES, 150 mM NaCl, pH 8.0. The protein concentration was measured with an Infinite® M200 Pro plate reader equipped with a NanoQuant plate (Tecan Group Ltd.) at 280 nm (Table 9.4) and working stocks were flash frozen in liquid nitrogen and stored at –80°C.

Table 9.4. Amino acid sequence and characteristics of ThiD proteins. TEV-site is highlighted in grey.

Protein	Sequence (N→C)
*Ms*ThiD (UniProt ID: I7G2G7) m = 28,732.81 Da ε = 20,970 M^{-1} cm^{-1}	MKLLPLTPPGQTPTRVMTIAGTDSGGGAGIQADLRTFAMLGVHGCVAVAAVTVQNSVGVKGFHEVPVDIIAGQIQVV AEDIGIQAAKTGMLASAEIIGAVAETWRGLGTEAPLVVDPVCASMHGDPLLHPSALDSVRNELFPIASLVTPNLDEVRLIT GIEVVDEATQRDAAKALHALGPKWALVKGGHLRTSAQSPDLLYNGTDFYEFGAERIDTGHDHGAGDTLAAAAACALAH GMDMPDAVAFAKGWVTECLRAAYPLGHGHGPVSALFRLHHGS
*Ms*ThiD pETG41K wt m = 71,629.58 Da ε = 88,810 M^{-1} cm^{-1}	MKHHHHHHPMKIEEGKLVIWINGDKGYNGLAEVGKKFEKDTGIKVTVEHPDKLEEKFPQVAATGDGPDIIFWAHDRFG GYAQSGLLAEITPDKAFQDKLYPFTWDAVRYNGKLIAYPIAVEALSLIYNKDLLPNPPKTWEEIPALDKELKAKGKSALMFN LQEPYFTWPLIAADGGYAFKYENGKYDIKDVGVDNAGAKAGLTFLVDLIKNKHMNADTDYSIAEAAFNKGETAMTINGP WAWSNIDTSKVNYGVTVLPTFKGQPSKPFVGVLSAGINAASPNKELAKEFLENYLLTDEGLEAVNKDKPLGAVALKSYEE ELAKDPRIAATMENAQKGEIMPNIPQMSAFWYAVRTAVINAASGRQTVDEALKDAQTPGSGTMTSLYKKAGFKLLPLT PPGQTPTRVMTIAGTDSGGGAGIQADLRTFAMLGVHGCVAVAAVTVQNSVGVKGFHEVPVDIIAGQIQVVAEDIGIQA AKTGMLASAEIIGAVAETWRGLGTEAPLVVDPVCASMHGDPLLHPSALDSVRNELFPIASLVTPNLDEVRLITGIEVVDEA TQRDAAKALHALGPKWALVKGGHLRTSAQSPDLLYNGTDFYEFGAERIDTGHDHGAGDTLAAAAACALAHGMDMPD AVAFAKGWVTECLRAAYPLGHGHGPVSALFRLHHGS
*Ms*ThiD pETG41K mutant C119A m = 71,597.52 Da ε = 88,935 M^{-1} cm^{-1}	MKHHHHHHPMKIEEGKLVIWINGDKGYNGLAEVGKKFEKDTGIKVTVEHPDKLEEKFPQVAATGDGPDIIFWAHDRFG GYAQSGLLAEITPDKAFQDKLYPFTWDAVRYNGKLIAYPIAVEALSLIYNKDLLPNPPKTWEEIPALDKELKAKGKSALMFN LQEPYFTWPLIAADGGYAFKYENGKYDIKDVGVDNAGAKAGLTFLVDLIKNKHMNADTDYSIAEAAFNKGETAMTINGP WAWSNIDTSKVNYGVTVLPTFKGQPSKPFVGVLSAGINAASPNKELAKEFLENYLLTDEGLEAVNKDKPLGAVALKSYEE ELAKDPRIAATMENAQKGEIMPNIPQMSAFWYAVRTAVINAASGRQTVDEALKDAQTPGSGTMTSLYKKAGFKLLPLT PPGQTPTRVMTIAGTDSGGGAGIQADLRTFAMLGVHGCVAVAAVTVQNSVGVKGFHEVPVDIIAGQIQVVAEDIGIQA AKTGMLASAEIIGAVAETWRGLGTEAPLVVDPVAASMHGDPLLHPSALDSVRNELFPIASLVTPNLDEVRLITGIEVVDEA TQRDAAKALHALGPKWALVKGGHLRTSAQSPDLLYNGTDFYEFGAERIDTGHDHGAGDTLAAAAACALAHGMDMPD AVAFAKGWVTECLRAAYPLGHGHGPVSALFRLHHGS
*Mt*ThiD (UniProt ID: P9WG77) m = 27,510.51 Da ε = 20,970 M^{-1} cm^{-1}	MTPPRVLSIAGSDSGGGAGIQADMRTMALLGVHACVAVTAVTVQNTLGVKDIHEVPNDVVAGQIEAVVTDIGVQAAK TGMLASSRIVATVAATWRRLELSVPLVVDPVCASMHGDPLLAPSALDSLRGQLFPLATLLTPNLDEARLLVDIEVVDAESQ RAAAKALHALGPQWVLVKGGHLRSSDGSCDLLYDGVSCYQFDAQRLPTGDDHGGGDTLATAIAAALAHGFTVPDAVD FGKRWVTECLRAAYPLGRGHGPVSPLFRLS
*Mt*ThiD pETG41K wt m = 71,259.20 Da ε = 90,300 M^{-1} cm^{-1}	MKHHHHHHPMKIEEGKLVIWINGDKGYNGLAEVGKKFEKDTGIKVTVEHPDKLEEKFPQVAATGDGPDIIFWAHDRFG GYAQSGLLAEITPDKAFQDKLYPFTWDAVRYNGKLIAYPIAVEALSLIYNKDLLPNPPKTWEEIPALDKELKAKGKSALMFN LQEPYFTWPLIAADGGYAFKYENGKYDIKDVGVDNAGAKAGLTFLVDLIKNKHMNADTDYSIAEAAFNKGETAMTINGP WAWSNIDTSKVNYGVTVLPTFKGQPSKPFVGVLSAGINAASPNKELAKEFLENYLLTDEGLEAVNKDKPLGAVALKSYEE ELAKDPRIAATMENAQKGEIMPNIPQMSAFWYAVRTAVINAASGRQTVDEALKDAQTPGSGTMTSLYKKAGF<mark>ENLYFQ G</mark>TPPRVLSIAGSDSGGGAGIQADMRTMALLGVHACVAVTAVTVQNTLGVKDIHEVPNDVVAGQIEAVVTDIGVQAAK TGMLASSRIVATVAATWRRLELSVPLVVDPVCASMHGDPLLAPSALDSLRGQLFPLATLLTPNLDEARLLVDIEVVDAESQ RAAAKALHALGPQWVLVKGGHLRSSDGSCDLLYDGVSCYQFDAQRLPTGDDHGGGDTLATAIAAALAHGFTVPDAVD FGKRWVTECLRAAYPLGRGHGPVSPLFRLS
*Mt*ThiD pETG41K mutant C119A m = 71,227.14 Da ε = 90,300 M^{-1} cm^{-1}	MKHHHHHHPMKIEEGKLVIWINGDKGYNGLAEVGKKFEKDTGIKVTVEHPDKLEEKFPQVAATGDGPDIIFWAHDRFG GYAQSGLLAEITPDKAFQDKLYPFTWDAVRYNGKLIAYPIAVEALSLIYNKDLLPNPPKTWEEIPALDKELKAKGKSALMFN LQEPYFTWPLIAADGGYAFKYENGKYDIKDVGVDNAGAKAGLTFLVDLIKNKHMNADTDYSIAEAAFNKGETAMTINGP WAWSNIDTSKVNYGVTVLPTFKGQPSKPFVGVLSAGINAASPNKELAKEFLENYLLTDEGLEAVNKDKPLGAVALKSYEE ELAKDPRIAATMENAQKGEIMPNIPQMSAFWYAVRTAVINAASGRQTVDEALKDAQTPGSGTMTSLYKKAGF<mark>ENLYFQ G</mark>TPPRVLSIAGSDSGGGAGIQADMRTMALLGVHACVAVTAVTVQNTLGVKDIHEVPNDVVAGQIEAVVTDIGVQAAK TGMLASSRIVATVAATWRRLELSVPLVVDPVAASMHGDPLLAPSALDSLRGQLFPLATLLTPNLDEARLLVDIEVVDAES QRAAAKALHALGPQWVLVKGGHLRSSDGSCDLLYDGVSCYQFDAQRLPTGDDHGGGDTLATAIAAALAHGFTVPDAV DFGKRWVTECLRAAYPLGRGHGPVSPLFRLS

9.1.5 Labeling of bacterial proteome and proteins

SDS-PAGE. Samples were applied with 20-30 µL volume and 10 µL of the protein marker Roti®-Mark Standard (Carl Roth) and the fluorescent marker BenchMark™ Fluorescent Protein Standard (Thermo Fisher) were used as protein reference size. Gels (containing 12.5 or 15% (w/v) acrylamide) were run for 2.5 – 4.5h at 60 mA in an EV265 Consort (Hoefer) instrument. Fluorescent bands were recorded with an LAS-4000 (Fujifilm) instrument equipped with a Fujinon VRF43LMD3 lens and a 575DF20 filter (Fujifilm) using 520 nm EPI excitation wavelength. Gels were stained and destained by Coomassie-solution and destaining solution for 24h at rt, respectively.

***In-situ* labeling.** For an analytical labeling procedure, *M. smegmatis* was grown to stationary phase and cells were harvested (6,000 g, 10 min, 4 °C). After washing the pellet with PBS (15 mL), it was resuspended in PBS to a bacterial culture of OD_{600} = 40 in order to perform analytical *in-situ* labeling: To 200 µL cell solution, 2 µL probe (100× stock in DMSO, varying concentrations) or DMSO were added. After incubation (24h, 25 °C), the labeled cells were harvested (6,000 rpm, 10 min, 4 °C) and washed with PBS (2 × 0.5 mL). The pellet was resuspended in 200 µL 0.4% (w/v) SDS in PBS for lysis by sonification (3× 10 sec pulses, 70% intensity) at room temperature (rt). Cell debris was removed by centrifugaton (21,000 g, 30 min, rt) and 50 µL supernatant were subjected to click-chemistry for 1h at rt: 1 µL rhodamine azide or alkyne (5 mM in DMSO, for alkyne-or azide probes, respectively), 1 µL tris(2-carboxyethyl)phosphine (TCEP, 52 mM in ddH_2O), 3 µL 1× tris(benzyltriazoyl-methyl)amine (TBTA, 1.67 mM in 80% *t*BuOH and 20% DMSO) and 1 µL $CuSO_4$ (50 mM in ddH_2O). After stopping the reaction with 50 µL loading buffer (2×), the samples were analyzed by SDS-PAGE.

Preparative labeling of intact *M. smegmatis* cells with **A-PM-P1** (10 µM, 50 µM), **A-PM-P2** (10 µM, 50 µM) and **Cl-PM-P1** (1 µM, 10 µM) was carried out and analyzed as previously described[1] after *M. smegmatis* cells were cultured and prepared for labeling as reported in the previous paragraph. For data analysis, the following FASTA file from UniProtKB was used: *M. smegmatis* (taxon identifier: 1772, downloaded: 11 November 2019).[2] Downstream statistical analysis was performed as previously reported.[1]

E. coli expression strains of mycobacterial ThiD wt fusion-proteins were cultured and induced as described in the previous section "overexpression and purification". After expression of ThiD wt fusion-proteins, cells were harvested, washed and labeled with **A/Cl-HMP-Azide** for 3h at 25 °C similarly to "*in-situ* labeling" of *M. smegmatis*. Subsequently, the exact same down-stream procedure was applied.

Recombinant proteins. *Sa*PLK was expressed and purified as previously described.[1, 3] Recombinant *Sa*PLK as well as mycobacterial ThiD wt and mutant fusion-proteins were diluted to 1 µM in either K-buffer (50 µL) or *S. aureus* lysate background (50 µL, 1 mg mL⁻¹). Heat control samples additionally contained 0.4% (w/v) SDS and were incubated at 95 °C for 30 min. Protein solutions were incubated with DMSO or 10, 100 or 200 equivalents of probes (1 µL, 50× stock) compared to protein at rt for 24h (*Sa*PLK) or 2h (ThiD). Subsequently, the labeled proteins were conjugated to rhodamine by click-chemistry and visualized by SDS-PAGE as described above.

9.1.6 Mycobacterial growth assay

To assess antimycobacterial activity of **HMP** mimics in 7H9 medium supplemented with ADC enrichment (medium is generally thiamine free), MIC assays were performed in *M. smegmatis* (in-house) and *M. tuberculosis* (Forschungszentrum Borstel, Dr. Sönke Andres) in triplicates. Hence, mycobacterial cultures were diluted into fresh medium and coincubated with a concentration range of **HMP-Azide**, **A-HMP-Azide** and **Cl-HMP-Azide** up to 100 µM (DMSO stocks) at 37 °C over 48h

(*M. smegmatis*) or up to three weeks (*M. tuberculosis*). Sterile controls contained medium and DMSO, and all samples contained 1% DMSO maximum. Mycobacterial growth was found in all samples except for sterile controls (results not shown).

9.2 Chemical synthesis

General remarks. Thiamine hydrochloride (CAS: 67-03-8, ≥ 98.5%) was ordered from Roth and Acryloyl chloride (CAS: 814-68-6, ≥ 97%) as well as chloroacetic anhydride (CAS: 541-88-8, 95%) were obtained from Sigma Aldrich. All other chemicals (reagent or higher grade) were purchased from Sigma Aldrich, VWR, TCI, Roth and Alfa Aesar. Moisture-sensitive reactions were carried out in flame-dried reaction flasks. For thin layer chromatography (TLC), aluminium-coated silica gel plates (silica gel 60, F_{254}, Merck KGaA) were used, and spots were visualized with UV light (λ = 254 nm) and $KMnO_4$-stain (3.0 g $KMnO_4$, 20.0 g K_2CO_3 and 5 mL 5% NaOH in 300 mL ddH_2O) with subsequent heat treatment at 250 °C. Silica gel Geduran® Si 60 (40-63 µm, Merck KGaA) was used for column chromatography.

Mass spectrometry. Low-resolution mass spectra (LRMS) were recorded on an MSQ Plus instrument (Thermo Fisher) that was equipped with a Dionex Ultimate 3000 separation module (Thermo Fisher). For visualization and processing, Chromeleon 7.2.7 (Thermo Fisher) was used.

Nuclear magnetic resonance (NMR) spectroscopy. ^{1}H-NMR (300, 400 MHz) and ^{13}C-NMR (75, 101 MHz) experiments were performed on Avance-I/III HD NMR systems (Bruker Co.) with Topspin software (V2. 1/3, Bruker Co.) at room temperature for purity and structural analysis. Residual proton (DMSO-d_6 δ = 2.50 ppm, acetone-d_6 δ = 2.05 ppm) and carbon (DMSO-d_6 δ = 39.52 ppm, acetone-d_6 δ = 206.68 ppm) signals of deuterated solvents served as internal reference and are given in parts per million (ppm). Coupling constants (*J*) are given in hertz (Hz) and signal multiplicities were assigned as follows: s – singlet, d – doublet, dd – doublet of doublets and m – multiplet, *br* – broad. Data was evaluated with MestReNova (Mestrelab Research).

9.2.1 Synthetic procedures

5-(azidomethyl)-2-methylpyrimidin-4-amine (HMP-Azide)
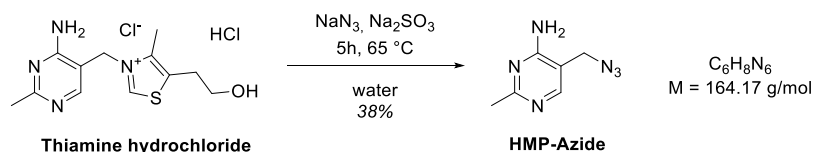
The compounds was synthesized as previously described.[4] In brief, thiamine hydrochloride (3.0 g, 8.9 mmol, 1.0 equiv.), sodium azide (1.5 g, 22.2 mmol, 2.5 equiv.) and sodium sulfite (112 mg, 889 μmol, 0.1 equiv.) were dissolved in water (30 mL) and stirred for 5h at 65 °C. After adjustment of the pH to 4 by adding citric acid (6.1 g, 31.6 mmol, 3.6 equiv.), the aqueous phase was washed with dichloromethane (3 × 15 mL). Then, the aqueous phase was adjusted to pH 10 with saturated potassium carbonate solution and subsequently extracted with ethyl acetate (3 × 20 mL). These merged organic phases were washed with brine (1 × 30 mL), dried over sodium sulfate and concentrated *in vacuo*. After recrystallization in hexane/ethyl acetate and filtration, 567 mg (38%) of the title compound were obtained as fine needles.
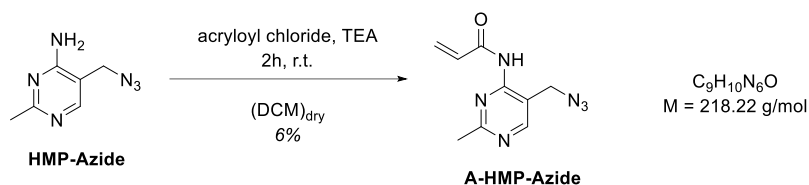
TLC: R_f = 0.03 (EtOAc, UV/KMnO$_4$).

^{1}H-NMR (400 MHz, DMSO-d_6): δ [ppm] = 2.31 (s, 3H, CH_3), 4.32 (s, 2H, CH_2-N$_3$), 6.89 (*br* s, 2H, NH_2), 8.00 (s, 1H, CH_{arom}).

^{13}C-NMR (101 MHz, DMSO-d_6): δ [ppm] = 25.3 (CH$_3$), 47.5 (N$_3$-CH$_2$), 107.7 (C_{arom}CH$_2$-N$_3$), 155.9 (C_{arom}H), 161.8 (C_{arom}NH$_2$), 167.0 (C_{arom}CH$_3$).

LR-MS (ESI, m/z): (C$_6$H$_9$N$_6^+$ [M+H]$^+$) found: 165.13; calc.: 165.09.

### *N*-(5-(azidomethyl)-2-methylpyrimidin-4-yl)acrylamide (A-HMP-Azide)

Triethylamine (167 µL, 1.22 mmol, 2.0 equiv.) and acryloyl chloride (59.1 µL, 731 µmol, 1.2 equiv.) were added to a stirred solution of HMP-Azide (100 mg, 609 µmol, 1.0 equiv.) in anhydrous dichloromethane (10 mL) at 0 °C. After stirring for 2h at room temperature, the reaction was stopped by addition of saturated sodium bicarbonate solution. The solution was extraction with DCM (3 × 5 mL) and the merged organic phases were washed with water (1 × 15 mL) and dried with brine (1 × 15 mL) and sodium sulfate. After filtration and concentration *in vacuo* at room temperature, the compound was purified by column chromatography (50% EtOAc in hexane) to obtain 7.5 mg (6%) of the title compound as temperature-sensitive pale yellow solid.

TLC: R_f = 0.63 (50% EtOAc/hexane, UV/KMnO$_4$).

^{1}H-NMR (400 MHz, acetone-d_6): δ [ppm] = 2.55 (s, 3H, CH_3), 4.60 (s, 2H, N$_3$-CH_2), 5.87 (dd, ^2J = 10.3 Hz, ^3J = 1.7 Hz, 1H, CHCH_2), 6.45 (dd, ^2J = 17.0 Hz, ^3J = 1.7 Hz, 1H, CHCH_2), 6.59 – 7.03 (m, 1H, CHCH$_2$), 8.67 (s, 1H, CH_{arom}), 9.71 (s, 1H, NH).

^{13}C-NMR (101 MHz, acetone-d_6): δ [ppm] = 25.6 (CH_3), 50.4 (N$_3$-CH_2), 119.9 (C$_{arom}$CH$_2$-N$_3$), 129.4 (COCHCH_2), 131.7 (COCHCH$_2$), 159.9(C$_{arom}$H), 164.9 (CO), 166.9 (C$_{arom}$NH$_2$), 168.3 (C$_{arom}$CH$_3$).

LR-MS (ESI, m/z): (C$_9$H$_{11}$N$_6$O$^+$ [M+H]$^+$) found: 219.28; calc.: 219.10.

N-(5-(azidomethyl)-2-methylpyrimidin-4-yl)-2-chloroacetamide (Cl-HMP-Azide)
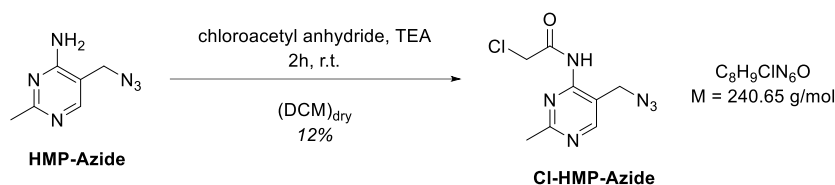
Triethylamine (50.9 µL, 364 µmol, 1.2 equiv.) and chloroacetic anhydride (62.5 mg, 365 µmol, 1.2 equiv.) were added to a stirred solution of HMP-Azide (50 mg, 304 µmol, 1.0 equiv.) in anhydrous dichloromethane (5 mL) at 0 °C. After stirring for 2h at room temperature, the reaction was stopped by addition of saturated sodium bicarbonate solution. The aqueous phase was extracted with DCM (3 × 5 mL) and the merged organic phases were washed with water (1 × 15 mL) and dried with brine (1 × 15 mL) and sodium sulfate. After filtration and concentration *in vacuo*, the compound was purified by column chromatography (50% EtOAc in hexane) to obtain 8.8 mg (12%) of the title compound as brown crystals.
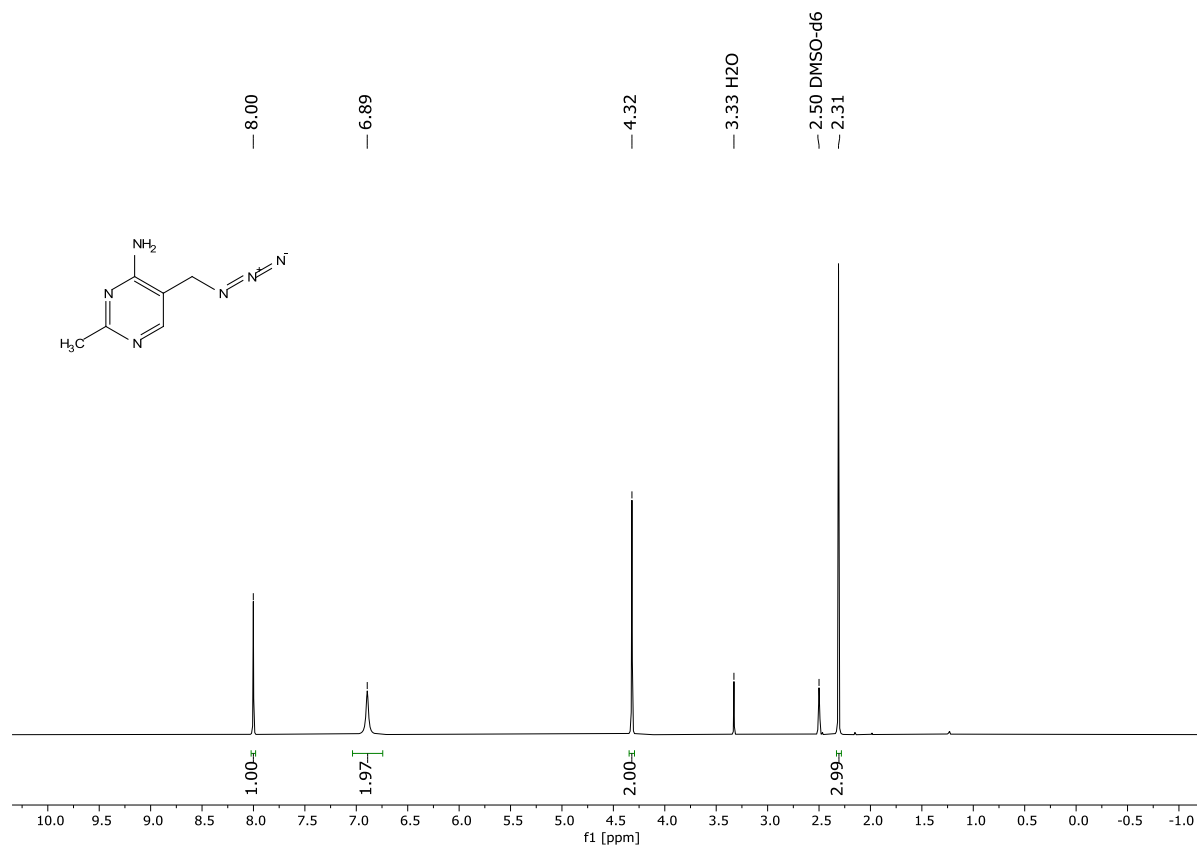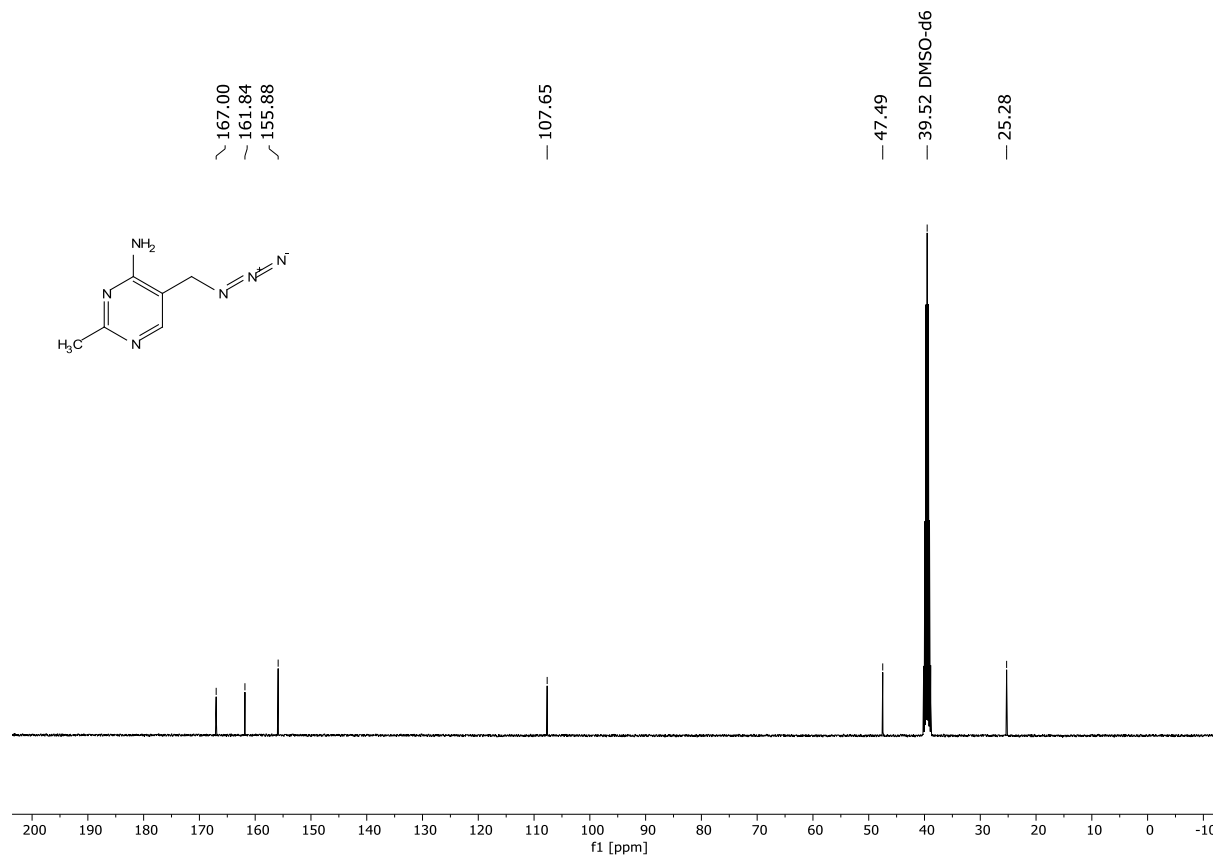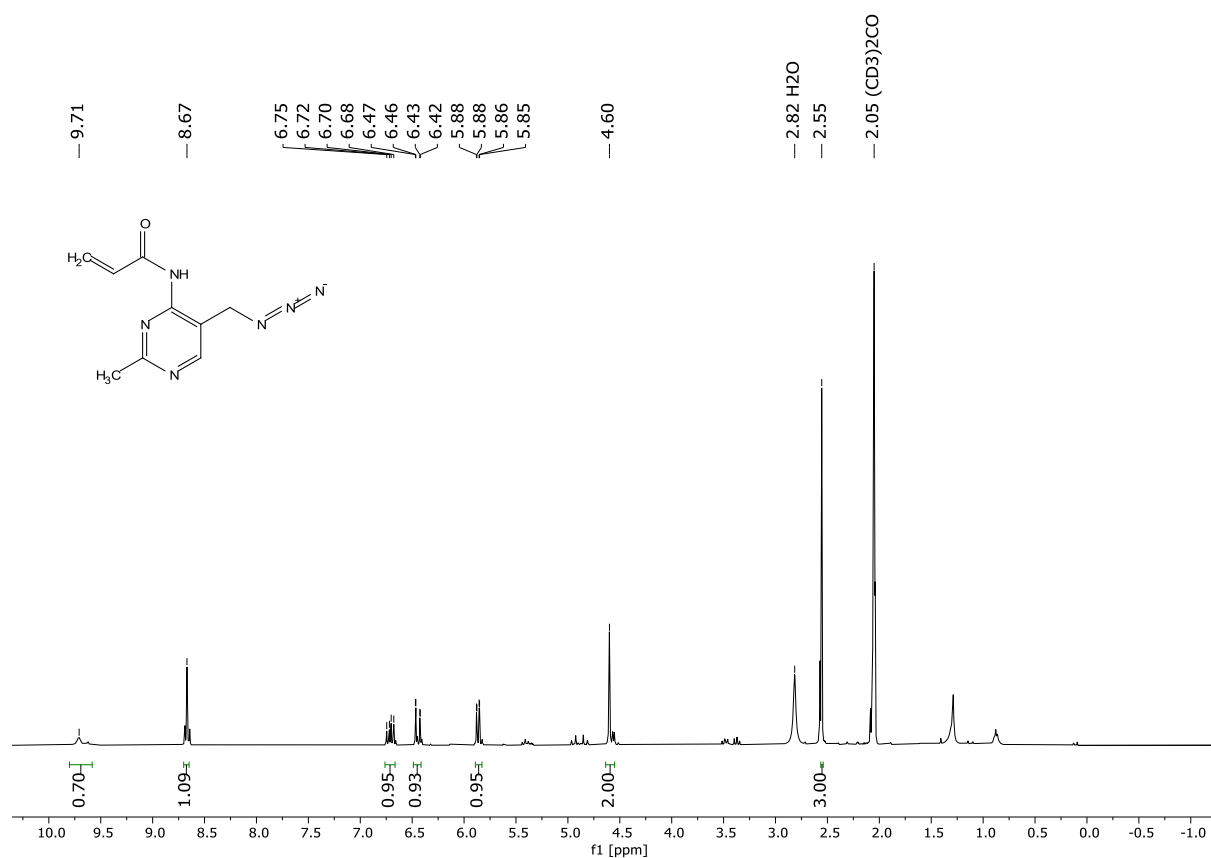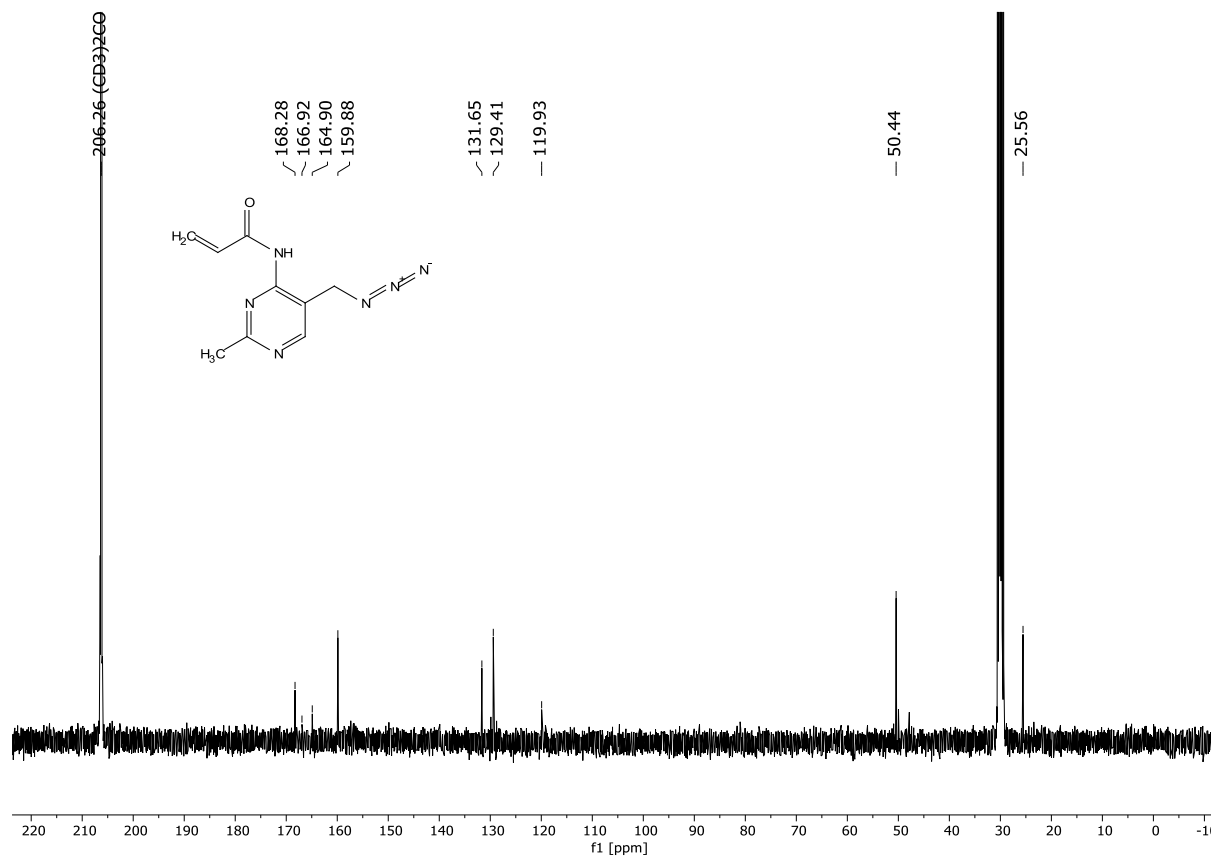
TLC: R_f = 0.27 (50% EtOAc/hexane, UV/KMnO$_4$).

^{1}H-NMR (400 MHz, acetone-d_6): δ [ppm] = 2.57 (s, 3H, CH_3), 4.58 (s, 2H, Cl-CH_2), 4.61 (s, 2H, N$_3$-CH_2), 8.66 (s, 1H, CH_{arom}), 9.62 (s, 1H, NH).

^{13}C-NMR (101 MHz, acetone-d_6): δ [ppm] = 25.5 (*C*H$_3$), 44.5 (Cl-*C*H$_2$), 49.5 (N$_3$-*C*H$_2$), 118.5 (*C*$_{arom}$CH$_2$-N$_3$), 156.3 (*C*$_{arom}$NH$_2$), 159.7 (*C*$_{arom}$H), 166.9 (*C*O), 168.3 (*C*$_{arom}$CH$_3$).

LR-MS (ESI, m/z): (C$_8$H$_{10}$ClN$_6$O$^+$ [M+H]$^+$) found: 241.23 (2/3) & 243.24 (1/3); calc.: 241.06 (2/3) & 243.06 (1/3).

9.2.2 NMR spectra

^{1}H-NMR (400 MHz, DMSO-d_6) of **HMP-Azide**:

^{13}C-NMR (101 MHz, DMSO-d_6) of **HMP-Azide**:

1H-NMR (400 MHz, acetone-d_6) of **A-HMP-Azide**:

9.71
8.67
6.75 6.72 6.70 6.68 6.47 6.46 6.43 6.42
5.88 5.86 5.85
4.60
2.82 H2O
2.55
2.05 (CD3)2CO

0.70
1.09
0.95
0.93
0.95
2.00
3.00

10.0 9.5 9.0 8.5 8.0 7.5 7.0 6.5 6.0 5.5 5.0 4.5 4.0 3.5 3.0 2.5 2.0 1.5 1.0 0.5 0.0 -0.5 -1.0
f1 [ppm]

13C-NMR (101 MHz, acetone-d_6) of **A-HMP-Azide**:

206.26 (CD3)2CO
168.28
166.92
164.90
159.88
131.65
129.41
119.93
50.44
25.56

220 210 200 190 180 170 160 150 140 130 120 110 100 90 80 70 60 50 40 30 20 10 0 -10
f1 [ppm]

¹H-NMR (400 MHz, acetone-*d*₆) of **Cl-HMP-Azide**:
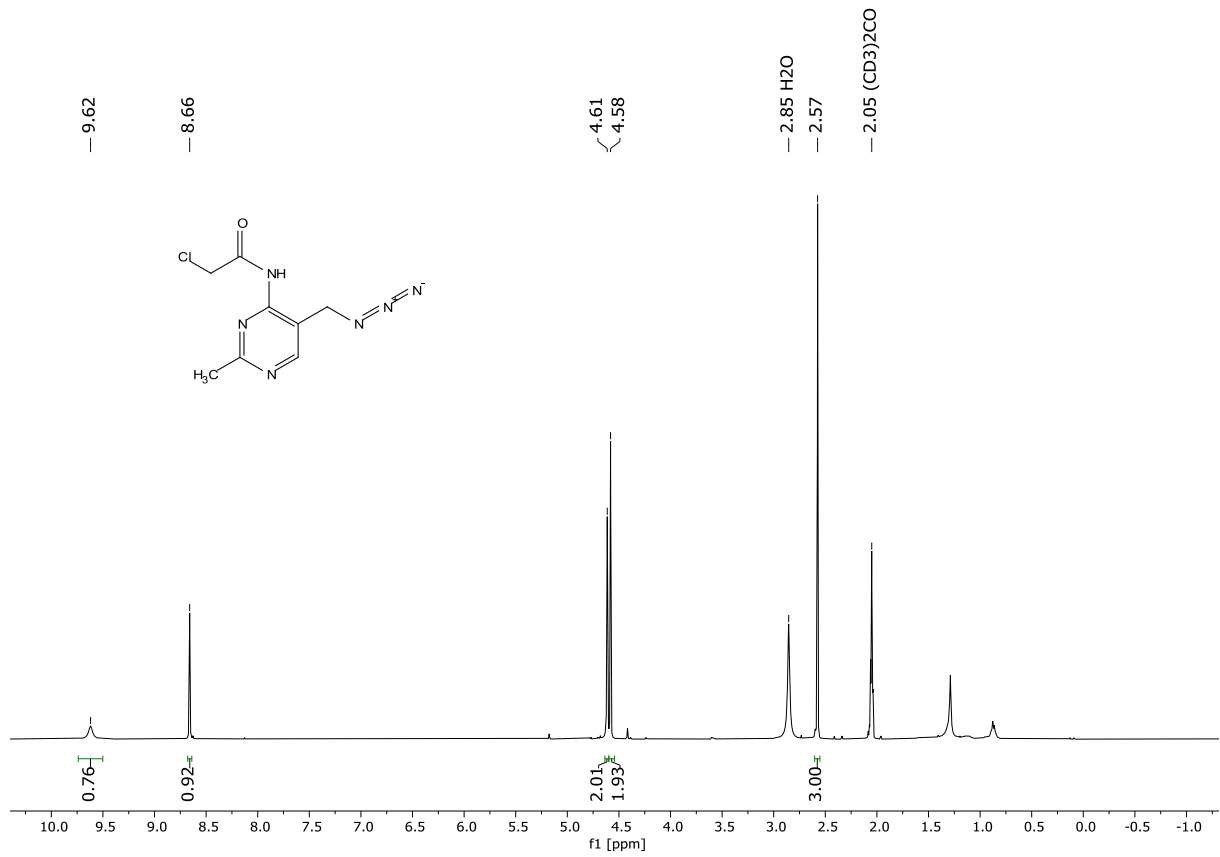
¹³C-NMR (101 MHz, acetone-*d*₆) of **Cl-HMP-Azide**:
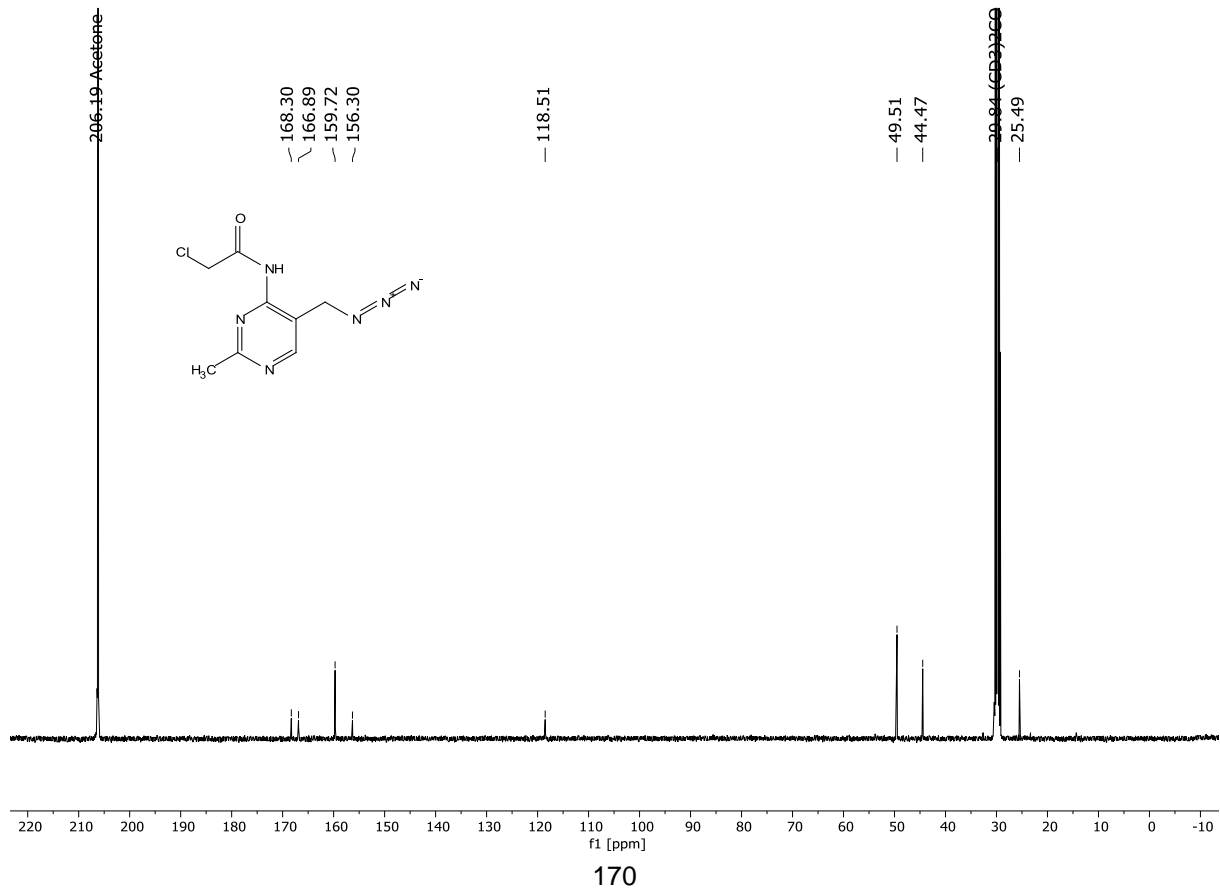
9.3 References

[1]   I. Hübner, J.-N. Dienemann, J. Friederich, S. Schneider, S. A. Sieber, *ACS Chemical Biology* **2020**, *15*, 3227-3234.

[2]   UniProtConsortium, *Nucleic Acids Research* **2023**, *51*, D523-D531.

[3]   M. B. Nodwell, M. F. Koch, F. Alte, S. Schneider, S. A. Sieber, *Journal of the American Chemical Society* **2014**, *136*, 4992-4999.

[4]   J.-B. He, Y.-L. Ren, Q.-S. Sun, G.-Y. You, L. Zhang, P. Zou, L.-L. Feng, J. Wan, H.-W. He, *Bioorganic & Medicinal Chemistry* **2014**, *22*, 3180-3186.

Danksagung

Ich möchte meinen ersten Dank an Konstantin Eckel und Dr. Pavel Kielkowski aussprechen, da sie mich an den AK Sieber gebracht haben. Konstantin war nicht nur mein Mitbewohner in Eching, sondern auch ein treuer Begleiter während meiner Promotion. Pavel, meinem Praktikumsbetreuer und Mentor für die Promotion, danke ich für die Anleitung und wertvollen Einblicke in die Biologische Chemie.

Ein aufrichtiges Dankeschön geht an Prof. Dr. Stephan Sieber für seine Betreuung und sein mir entgegengebrachtes Vertrauen während meiner Master- und Doktorarbeit im Bereich der Infektionsforschung und chemischen Proteomik. Seine Expertise und Unterstützung in allen Projekten haben maßgeblich zum wissenschaftlichen Erfolg beigetragen.

Für die Betreuung meiner Masterarbeit danke ich Dr. Ines Hübner, deren Ideen, Kritik und Einführungen den anfänglichen Grundstein für meine Promotionsarbeit legten. Zusätzlich möchte ich Julia Friederich, Sabine Schneider und Isabel Wilkinson für ihre wertvollen Beiträge, Überarbeitungen und Korrekturen im Zusammenhang mit der ersten Publikation in *ACS Chemical Biology* danken.

Mein großer Dank gilt auch Dr. Manuel Hitzenberger und Shu-Yu Chen aus der Gruppe von Prof. Dr. Martin Zacharias für ihre computergestützten Beiträge zur Veröffentlichung in der *Angewandten Chemie International Edition*, sowie Montana Sievert und Prof. Dr. Sean Prigge von der Johns Hopkins University in Baltimore, USA, für ihre erfolgreichen Experimente am Malariaparasiten. Ebenso danke ich Dr. Stephan Hacker für die Unterstützung bei der Auswertung proteomischer Daten und Prof. Dr. Michael Groll sowie Astrid König für ihre Kristallisationsarbeit und die Einblicke in Bereiche außerhalb meiner täglichen Arbeit.

Ein besonderer Dank geht an meine Praktikanten Lisa Klimper, Adrian Brunecker, Jonas Gellner, Lennart Brücher und Olga Kushnir, deren angeleitete Unterstützung in den verschiedenen Projekten von großem Wert war. Ebenso danke ich Markus Schwarz für das Korrekturlesen dieser Arbeit.

Ein herzliches Dankeschön möchte ich Josef Braun, Dr. Martin Pfanzelt, Till Reinhardt, Markus Schwarz, Michaela Fiedler, Alexandra Geißler, Dr. Vadim Korotkov, Martin Köllen, Michael Zollo, Max Bottlinger und Franziska Elsen aussprechen, die bei den Synthesen meiner Projekte ideelle und technische Unterstützung leisteten. Mein Dank gilt auch dem BioBioKommittee, bestehend aus Konstantin Eckel, Laura Eck, Dietrich Mostert, Michaela Fiedler, Alexandra Geißler, Till Reinhardt und Dominik Schum. Insbesondere Laura und Konstantin danke ich für ihre technische Hilfe bei den zahlreichen Äkta-Aufreinigungen. Ein herzliches Dankeschön geht auch an Mona Wolff, Katja Bäuml, Laura Meier, Katja Gliesche, Martin Köllen, Davide Boldini, Dr. Annina Steinbach, Barbara Seibold und Dr. Nina Bach für

ihre technische Unterstützung und administrative Hilfe. Dank gebührt auch Dr. Theresa Rauh, Dr. Martin Pfanzelt und Dr. Angela Weigert-Munoz vom Lab C für die tolle Atmosphäre im Chemie-Bunker.

Für die gemeinsame Teilnahme an Konferenzen und damit verbundenen wundervollen Reisen und Gesprächen danke ich Alexandra Geißler, Michaela Fiedler, Julia Hirschmann, Rachel Sonntag und Johanna Wallner.

Ein herzliches Dankeschön geht auch an meine Kollegen, die mittlerweile Freunde geworden sind, für die zahlreichen sozialen Veranstaltungen wie Partys, gemeinsame Mahlzeiten, sportliche Aktivitäten, Quiznächte, Konzerte, Eislaufen, Geburtstage und viele mehr. Durch Euch sind sie besonders spaßig geworden, auch wenn es für mich nicht immer so spät geworden ist wie für manche von Euch. Alex, Micha, Markus, Seppi, Domi, Konsti, Martin, Davide, Max, Wei, Laura, Katrin, Franziska, Yassmine, Didi, Till, Michael, Angela, Robert, Kora, Maxi, Ekatarina, Mary, Joshua, Thomas, Nina, Tao, sowie die ehemaligen Kollegen Martin, Theresa, Isabel, Thomas und Kyu: Ihr habt all diese Ereignisse zu etwas Besonderem gemacht und mich während meiner Promotionszeit unterstützt und für Heiterkeit sowie bleibende Erinnerungen gesorgt.

Am allerwichtigsten möchte ich jedoch meiner Familie und meinen Freunden von ganzem Herzen danken, die mich immer bedingungslos unterstützt und auch in schwierigen Zeiten begleitet haben. Meine Familie, meine Langzeit-Freunde aus der Schulzeit, meine Krefelder Bachelor-Freunde, sowie meine Münchner Freunde und natürlich auch Du Nick: Ihr seid für mich von unschätzbarem Wert in meinem Leben, und ich verspreche Euch von nun an nach Abschluss der Promotion wieder mehr verfügbar zu sein. Eure Unterstützung hat mir geholfen, niemals meine Hoffnungen und Ziele aus den Augen zu verlieren. Die gemeinsamen Erlebnisse und Erinnerungen mit Euch haben mich zu der Person gemacht, die ich heute bin. Mit größter Dankbarkeit widme ich Euch daher sehr gerne diese Arbeit!

Herzliche Grüße,

Euer Jan/ni <3